THE USE OF GROUND PENETRATING RADAR FOR TRACK SUBSTRUCTURE CHARACTERIZATION

DANIEL JACOBUS VORSTER

A dissertation submitted in fulfilment of the requirements for the degree of

MASTER OF ENGINEERING (TRANSPORTATION ENGINEERING)

In the

FACULTY OF ENGINEERING

UNIVERSITY OF PRETORIA

August 2012

DISSERTATION SUMMARY

THE USE OF GROUND PENETRATING RADAR FOR TRACK SUBSTRUCTURE CHARACTERIZATION

DJ VORSTER

Supervisor: Professor P. J. Gräbe

Department: Civil Engineering

University: University of Pretoria

Degree: Master of Engineering (Transportation Engineering)

Ground penetrating radar (GPR) has been used as a railway substructure investigation tool since the late 1990's and has seen significant development since then. To use GPR as a more effective tool for substructure investigation, a GPR substructure characterization model was developed. This dissertation provides a detailed description of railway track components, track geometry, soil properties and classification and substructure design. The historical background of GPR is discussed together with GPR principles, basic GPR equations, hardware and accessories as well as GPR data collection, processing and interpretation. Other in situ investigation techniques namely the dynamic cone penetrometer (DCP), light weight deflectometer (LWD) , Pencel pressuremeter, surface wave testing, remote video monitoring (RVM), multi-depth deflectometers (MDD) and continuous track modulus measurement techniques are also discussed. A comparison between the different track investigation techniques was also done, with reference to sample rate, cost, effectiveness and value.

Two sites in South Africa were selected for the investigation, one with good substructure conditions used for heavy haul coal export close to Vryheid (KN test section) and the other a general freight line with poor substructure conditions near Rustenburg (NT test section). These two sites were selected to develop a GPR substructure characterization model as they provided conditions ranging from poor to very good. This was supported by the analysis of the in situ soil sampling and testing. The calculation of the track substructure modulus from RVM deflection measurements showed three times higher values for the KN test section compared to the NT test section.

The subballast and subgrade thickness, the GPR ballast fouling (GBF) index as well as the GPR moisture condition index was used for the classification ranges used in the model. The subballast and subgrade layer roughness values were calculated and used for the substructure classification. The

GBF index and the GPR moisture condition roughness were used for the GPR fouling index classification. The GPR deliverables were divided into four classes (i.e. very good, good, moderate and poor). The evaluation of the characterization model showed that a traditional in situ investigation will cost approximately 3.7 times more than that of a GPR investigation. It would also take two thirds of the time to complete the GPR investigation compared to the traditional in situ investigation. The study showed that GPR can be used to develop a substructure characterization model and that it would be more cost effective and efficient than traditional in situ investigation techniques.

GPR surveys provide continuous measurements of the track structure condition and can therefore provide a continuous classification unlike the discreet and fragmented nature of in situ investigations. However, in situ tests can be done at certain intervals within the GPR survey or at point where the GPR classification is not clear. The best solution for railway track characterization can therefore be obtained by using GPR and in situ classification in combination.

DECLARATION

I, the undersigned hereby declare that:

I understand what plagiarism is and I am aware of the University's policy in this regard;

The work contained in this thesis is my own original work;

I did not refer to work of current or previous students, lecture notes, handbooks or any other study material without proper referencing;

Where other people's work has been used this has been properly acknowledged and referenced;

I have not allowed anyone to copy any part of my thesis;

I have not previously in its entirety or in part submitted this thesis at any university for a degree.

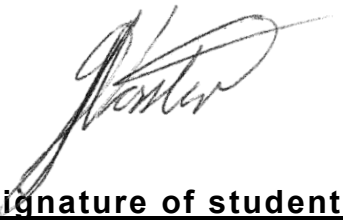

Signature of student

DJ Vorster

25012194

JULY 2012

ACKNOWLEDGEMENTS

This dissertation would not have been possible without the assistance and guidance from several individuals or organisations that in some way contributed in the preparation and completion of the study:

- First and foremost, I would like to express my sincere gratitude to my supervisor Professor Hannes Gräbe for his continuous support, enthusiasm, patience, motivation and his immense knowledge. Without his guidance this dissertation would not be possible. I could not have imagined having a better supervisor and mentor.
- My loving wife, Nelléne for her constant encouragement, love and support during the study.
- My Lord and Saviour for strength and wisdom.
- The Chair in Railway engineering at the University of Pretoria for financial support, the provision of data and the use of laboratory facilities during the course of the study.
- The following persons from Aurecon and Lennings Rail Services are gratefully acknowledged for organising and assisting with the GPR field investigation:

  Dr Terence Milne

  Mr Gerald du Randt
- The following persons from Roadscanners for the GPR field investigation and data acquisition:

  Mr Mika Silvast

  Mrs Dagmar Schmidtgen
- Mr Jerry Kae from Transnet Freight Rail's Track Technology Department for his assistance with the in situ investigation:
- The following persons from the University of Pretoria for their assistance in the lab and in the field:

  Mr Willie Bronkhorst

  Mr Johan Scholtz
- GEOSTRADA for the soil laboratory testing.
- Miss Sonja Theron for her assistance with the editing of the document.

TABLE OF CONTENTS

LIST OF TABLES

PAGE

LIST OF FIGURES

CHAPTER 1

1. INTRODUCTION

With the higher demand in freight transportation across the world, the need to upgrade and redesign old railway tracks is growing. To do this, the track substructure needs to be investigated. Traditional methods are expensive, time consuming and can only be conducted at single locations at a time. These methods include profiling of test pits, soil and ballast sampling, track and substructure deflection measurements. Other tests that are relatively inexpensive such as light weight deflectometer (LWD) tests and dynamic cone penetrometer (DCP) tests can also be used.

New methods of track investigation are more frequently used and include geophysical techniques like ground penetrating radar (GPR), continuous track modulus determination and infrared surveys. These methods provide a continuous evaluation of the track conditions. A method to continuously characterise the track substructure will provide a cost effective and efficient solution to railway investigations.

GPR provides the most deliverables as a single substructure investigation tool. These deliverables include subballast and subgrade thickness, GPR ballast fouling and GPR moisture condition. Using these deliverables, a track substructure characterization model was developed. The substructure characterization model would provide a continuous classification of the track substructure according to the substructure condition as well as the ballast fouling condition.

1.1 OBJECTIVES

The main objective of the study was to develop ground penetration radar (GPR) substructure characterization model using the subballast and subgrade thickness, the GPR ballast fouling and GPR moisture condition determined from a GPR line survey. The GPR substructure characterization model would then also be evaluated it against typical in situ substructure characterization methods.

Other objectives of the study included the following:

- To determine the dielectric permittivity for typical South African ballast materials in the field as well as in laboratory conditions.
- To compare the GPR field deliverables to in situ track substructure investigation techniques. These investigation techniques would include soil sampling, profiling, light weight deflectometer testing, dynamic come penetrometer testing and remote video monitoring.
- To use Remote Video Monitoring (RVM) to measure track and substructure deflections and comparing it to Multi-Depth Deflectometer (MDD) deflections and further comparing it to vertical axle loads. The deflections would also be used to determine the track substructure modulus.

1.2 SCOPE

The main focus of the study was to investigate the ballast, subballast and subgrade of a conventional track structure to a depth of 1.5 m below the bottom of the sleepers.

Superstructure components (rail, fastenings, and sleepers) were not included in the study as they are relatively easily maintainable. Ground Penetrating Radar (GPR) was the main investigation technology and the layer thickness, ballast fouling condition and moisture content was obtained from it. The results from the GPR survey were verified by using in situ testing techniques. The investigation techniques used were soil and ballast classification, profiling, Dynamic Cone Penetrometer (DCP) testing, Light Weight Deflectometer (LWD) testing, RVM and MDD. Laboratory testing was conducted for further verification of the GPR ballast and moisture conditions.

The substructure materials that were tested had a wide range. The ballast material tested was quartzite and dolerite and it was tested in the laboratory and in the field. The subballast and subgrade material ranged from granular material to clayey material and it was tested in the laboratory.

The characterization model was developed by using four classes for each of the input parameters (very good, good, moderate and poor). The use of a root mean squared formulation was used for ease of classification for some of the parameters. A broad classification of the substructure and ballast was attained for the characterization model. Analyses lengths were 200 m and longer for the purpose of easier maintenance strategies.

1.3 METHODOLOGY

The objectives of this study were achieved by following the points outlined below:

- A literature review of rail track components and terminology, soil properties and classification, substructure design and track modulus determination. This was followed by a description of track substructure investigation methods including the DCP, LWD, Pencel pressuremeter, continuous surface wave (CSW) testing, RVM and MDDs. Continuous track modulus measurement techniques, GPR history, principles and concepts were also discussed in detail. To conclude this chapter, a comparison between the different track investigation techniques was drawn.
- The preparation of GPR laboratory tests to evaluate the dielectric permittivity of the dolerite and quartzite followed by the execution of several GPR tests on the material.
- Conducting the two GPR surveys at the KN and NT test sites.
- Performing a substructure investigation at certain locations on the two test sections. DCP measurements, LWD tests, soil sampling and profiling and RVM tests were conducted at each of the test locations. MDD testing was also done at the KN test section.
- Analyses of the different site investigation measurements' results.
- Analyses of the GPR deliverables, subballast and subgrade surface roughness, GPR ballast fouling index and GPR moisture condition. Classification ranges were obtained for each of the deliverables.
- Finally, comparing the classification of the track substructure according to the GPR results with the classification of the traditional substructure investigation tools.

1.4 ORGANISATION OF THE REPORT

The report consists of the following chapters:

- **Chapter 1** gives background on the use of different site investigation techniques. It also provides the reasons why GPR can be used to classify track substructure condition. It introduces the topic of the report and outlines the objectives, methodology and scope of the report.
- **Chapter 2** is a literature review of rail track components and their functions, as well as field tests to investigate track substructure condition. The advantages and limitations of the test are discussed. The basic design models to calculate track modulus are discussed based on the principle of beam on elastic foundation and

foundation design models. The history, principles and basic concepts of GPR are discussed. Finally, different track investigation techniques are compared.

- **Chapter 3** describes the experimental work done. This includes laboratory tests conducted on the ballast material using GPR as well as tests done to calibrate RVM testing. Field tests done to determine the track modulus and track condition are described. The procedure of the GPR surveys is described for the two sections of track.
- **Chapter 4** presents the test measurement results and the comparisons between the different track investigation techniques. The procedure to obtain the classification ranges is also described. The differences between the different track classifications are also discussed. The evaluation of the GPR substructure characterization model concludes this chapter.
- **Chapter 5** contains the conclusions and recommendations of the report.
- **Chapter 6** includes references used in the report.
- **Appendix A** contains the measurement results from the GPR laboratory testing.
- **Appendix B** includes the measurement results and classification of the GPR field surveys.
- **Appendix C** contains the results from the soil sampling.

CHAPTER 2

2. LITERATURE STUDY

An in depth literature study was prepared on rail track components and the condition measurement of the railway track substructure. Knowledge and better understanding of the study field is used to develop a railway substructure condition monitoring model based on South African railways and to be used in future maintenance requirements. The classification and design of railway substructure as well as different test methods for the investigation there of, are discussed.

Rail track components and the condition measurement of the railway track substructure will are discussed. The classification and design of railway substructure as well as different test methods for the investigation thereof are discussed.

The development and use of GPR as a railway substructure investigation tool is described in detail. The basic principles, equations, GPR equipment and data collection, processing and interpretation are discussed to motivate the use of GPR for the development of a track substructure characterization model.

2.1 TRACK COMPONENTS AND TERMINOLOGY

To understand how the track functions and how the track components interact with one another, a description of the track components is needed. The functions of the different track components are discussed in this section. These components include the rails, fastening systems, sleepers, ballast and subballast, subgrade as well as drainage. Descriptions and figures of the track components are taken from *Track Geotechnology and Substructure Management* (Selig and Waters, 1994), unless stated otherwise.

The ballasted railway structure consists of two main components, the superstructure and the substructure. As indicated in Figure 2.1 and Figure 2.2, the superstructure consists of the rails, fastening systems and sleepers, while the substructure consists of the ballast and subgrade materials.

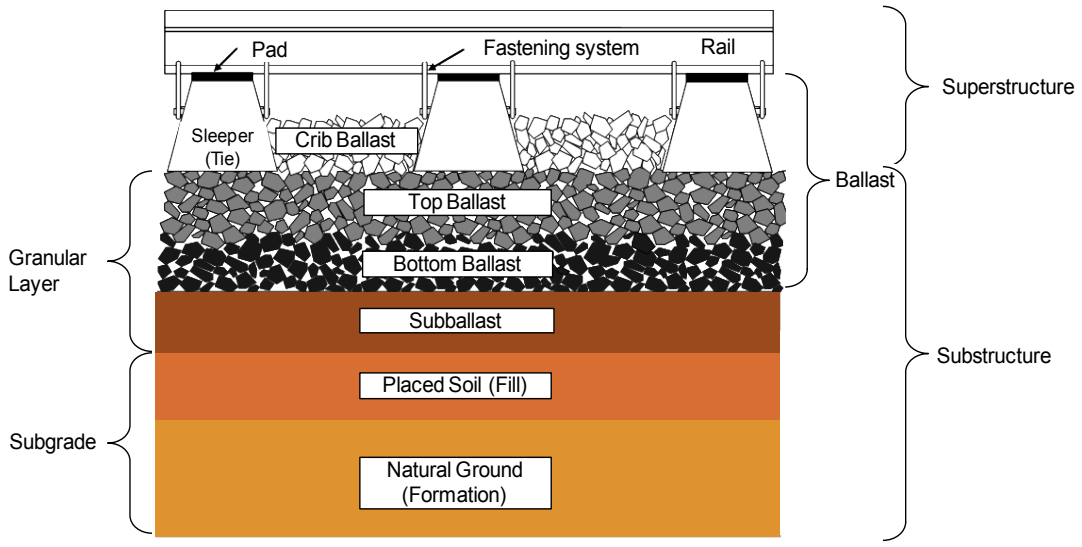

Figure 2.1: Track Components (side view), redrawn from Selig & Waters (1994).

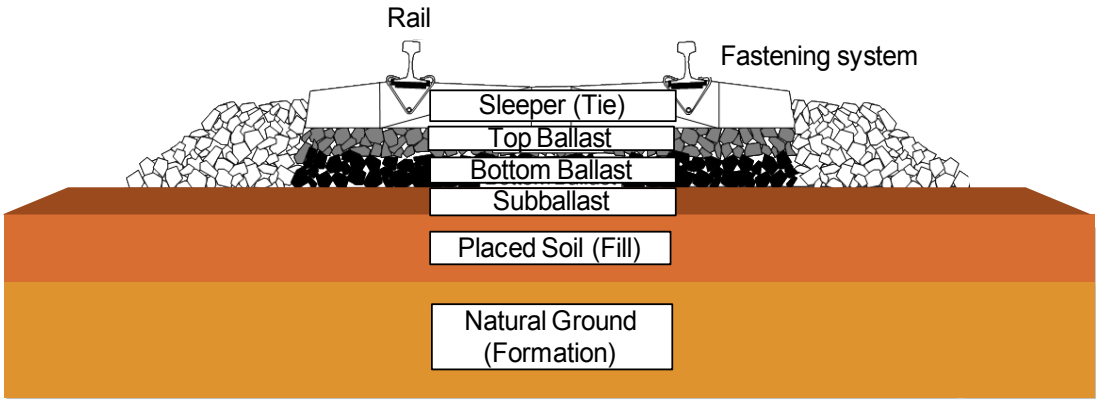

Figure 2.2: Track Components (cross section), redrawn from Selig and Waters (1994).

2.1.1 Rails

The first component of the superstructure is the rail. Rails are the longitudinal members stretching across the whole rail structure, guiding the train wheels. They act as beams to transfer the loads produced by the wheels, to the sleepers. This is done with sufficient stiffness so that excessive deflection between the sleepers does not occur. They also serve as electrical conductors and a ground line in the electrical locomotive power circuit.

The rail gauge is the spacing between the inside edges of the rail head. The importance of the gauge is to determine the design and spacing of all other track components. Both 1065 mm

and 1435 mm gauges are used in South Africa, but the 1065 mm is used predominantly (Gräbe, 2002).

Care also needs to be taken when constructing joints. Steel rail sections are connected by using bolts or different types of welds. As a result of the reduced stiffness of the rail at these joints, greater stresses are experienced in the ballast and subgrade. This adds to greater permanent settlement of the track, which produces an uneven track. Pumping action at joints is also responsible for accelerated rail failure, sleeper wear and fouling of ballast. Consequently, joints increase track deterioration and is an important consideration with respect to track maintenance.

To eliminate joints, continuous welded rail (CWR) is used. CWR is used on rail lines with high speed, high axle load or high traffic density. However, CWR has its own advantages and disadvantages. Benefits include extended rail life, reduced wear and tear of rolling stock and less damage to the substructure. Some disadvantages of CWR are difficulty in changing worn and defective rails and higher initial costs of welding, transportation and laying of longer rails.

2.1.2 Fastening System

The fastening system keeps the rails and sleepers against each other and provides resistance to movement due to vertical, lateral, longitudinal and overturning movements of the rail.

Concrete sleepers have spring fasteners. There are two main types of fasteners used, namely Fist fasteners and Pandrol fasteners. These are insulated electrically from the sleeper and the rail to minimize current leakage. Pads are also required between the rail and the sleeper. This provides resilience for the rail sleeper system, damping of wheel induced vibrations, electrical insulation for track circuits, and prevention of rail/sleeper contact attrition.

2.1.3 Sleeper (Tie)

Sleepers should fulfil the following functions:

- Transfer the train induced loads from the rail to the supporting track structure (ballast).
- Keep the fastening system in place to maintain the track gauge.
- Restrain movement of the rail by anchoring the superstructure in the ballast.

- Provide a cant to the rails for proper rail wheel contact in concrete sleepers.

Sleeper spacing can be responsible for vertical parametric oscillations of the moving wheels, by causing small variations in railway track vertical stiffness (Belotsserkovskiy, 2006). Therefore, care should be taken when placing the sleepers or the ballast.

Concrete sleepers are increasingly being used to replace wooden sleepers. These include pre-stressed concrete or twin block sleepers. The concrete variation of sleepers provides good rail stability because of their heavy weight. However, despite this advantage and their durability, concrete sleepers are difficult to handle and they require pads to provide resiliency (Ceney, 2001).

2.1.4 Ballast

The ballast structure consists of the top, bottom and crib ballast. Ballast is the crushed, granular material placed on the substructure. The ballast fulfils many functions. These include providing elasticity and resilience to the track structure as well as energy absorption and retaining the track in its required position by resisting vertical, lateral and longitudinal forces on the sleeper. In addition, the ballast transfers stresses from the sleeper to the underlying layers by reducing the pressure (Ceney, 2001).

The grade of the ballast (ballast fouling) may change as a result of:

- Mechanical particle degradation during construction, maintenance and under traffic loading.
- Chemical and mechanical weathering degradation.
- Subgrade attrition (particle migration to the bottom layers).
- Sleeper wear.

These processes cause fouling of the ballast, which then loses its open-graded characteristics and subsequently its functionality.

For the ballast to fulfil its structural functions, a sufficiently high resilient modulus is needed and a constant plastic strain is needed with repeated wheel loading. This is achieved by avoiding high positive pore pressure, with repeated loading, by using a permeable material. The ballast must not be susceptible to changes in moisture content and must be durable. Commonly ballast material is broadly-graded, naturally occurring or processed gravel, or broadly graded crushed natural aggregates.

2.1.5 Subballast

The subballast is the layer between the ballast and the subgrade. It has similar functions as that of the ballast layer. Some of the functions of subballast that distinguishes it from the other substructure layers are as follows:

- It reduces the stresses from the ballast to the subgrade.
- Prevents interpenetration of the ballast and subgrade layers.
- Prevent upward migration of fines into the ballast.
- Prevents subgrade attrition by ballast into the subgrade.
- Assists with drainage of water from the ballast.

For the subballast to achieve this, it should be designed to separate the ballast and subgrade particles. The material is designed as if it was a filter. Therefore, filter design criteria can be applied. However, the filter should not limit the structure to freely drain as saturation of the subballast will lead to poor performance and pore pressure development. The following criteria are suggested by Selig and Waters (1994) and are described by Cedegren (1977):

$$D_{15}(filter) \leq D_{85}(protected\ soil) \tag{2.1}$$

$$D_{50}(filter) \leq D_{25}(protected\ soil) \tag{2.2}$$

Where:

D_n = The size of which n percentage of particles is smaller than D_n

2.1.6 Subgrade

Subgrade can be divided into two section, prepared subgrade and natural ground and is the platform on which the track structure is constructed. The prepared subgrade forms part of the upper part of the subgrade and has a cross fall. It should provide a stable foundation for the railway track, ballast and subballast. A stable foundation is imperative since the influence of traffic induced stresses extends to a depth of more than five meters below the bottom of the sleeper, which is significantly deeper than the depth of the ballast and subballast layers.

The subgrade therefore influences the performance and maintenance of the track. It does this by contributing to the elastic deflection of the rail under the wheel load; this is part of the superstructure resiliency. Subgrade stiffness magnitude is also believed to influence ballast,

rail and sleeper deterioration. Two other subgrade failures, caused by large repetitive stresses, include progressive shear failure and excessive plastic deformation (Li, Selig and Chrismer, 1996; Li and Selig, 1998).

2.1.7 Drainage

Track drainage needs to be provided for water entering from the top of the track structure (precipitation), surface flow and subsurface seepage. A schematic of these water sources is shown in Figure 2.3.

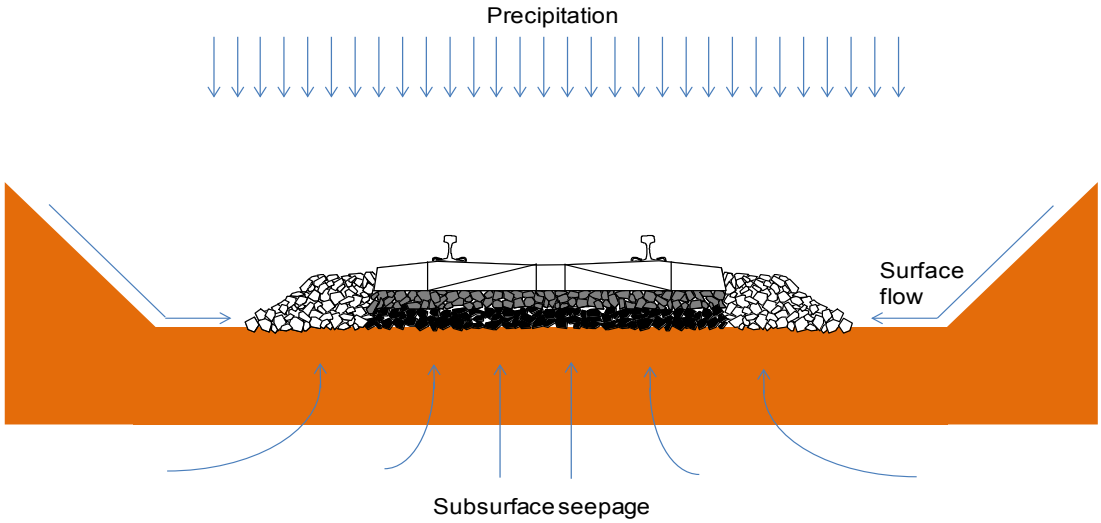

Figure 2.3: Water sources to the track structure, redrawn from Selig and Waters (1994).

The track structure deteriorates with excess water accumulation in the substructure. This is due to the decreasing strength of the soil with an increase of moisture content. Track maintenance costs subsequently increase and can be associated with the weakening of the track structure as a result of the following occurring:

- Increasing pore pressures from cyclic loading which causes plastic strain accumulation and a decrease in stiffness and strength.
- Subgrade attrition and slurry creation from ballast loading.
- Pumping of the fines.
- Change of volume in swelling clays.
- Chemical degradation of ballast from acidic water.

- Ballast and sleeper degradation from slurry formation.

2.2 TRACK GEOMETRY TERMINOLOGY

Track geometry refers to the alignment of the track in the vertical and horizontal planes and clearances around the track. The concept of alignment divides the three-dimensional track structure into its simpler, planar forms. The first of these is the horizontal alignment, which is a projection of each rail onto the horizontal plane (15 mm below the top of the rail). The second projection is the vertical profile. This projects the longitudinal vertical track geometry onto the vertical plane, using the top of the rail. The transverse vertical plane includes the cant, which is the distance between the two rails, and the twist, which is the difference in cant between two points in the longitudinal rail direction (usually about 2.75 m apart). Lastly, the gauge, referred to in the section on track components, is also part of the track geometry. Some of the geometry components are demonstrated in Figure 2.4 (Esveld, 2001).

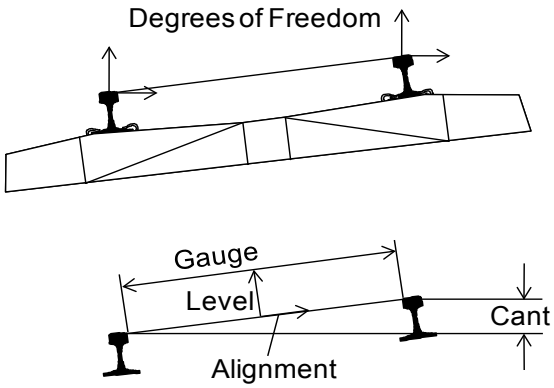

Figure 2.4: Track geometry components (Esveld, 2001).

The clearance is the space permitted for the train to have safe passage without any disturbances. The dimensions of normal clearance in South Africa are shown in Figure 2.5. This should be considered when doing testing on the track while trains are mobile on it.

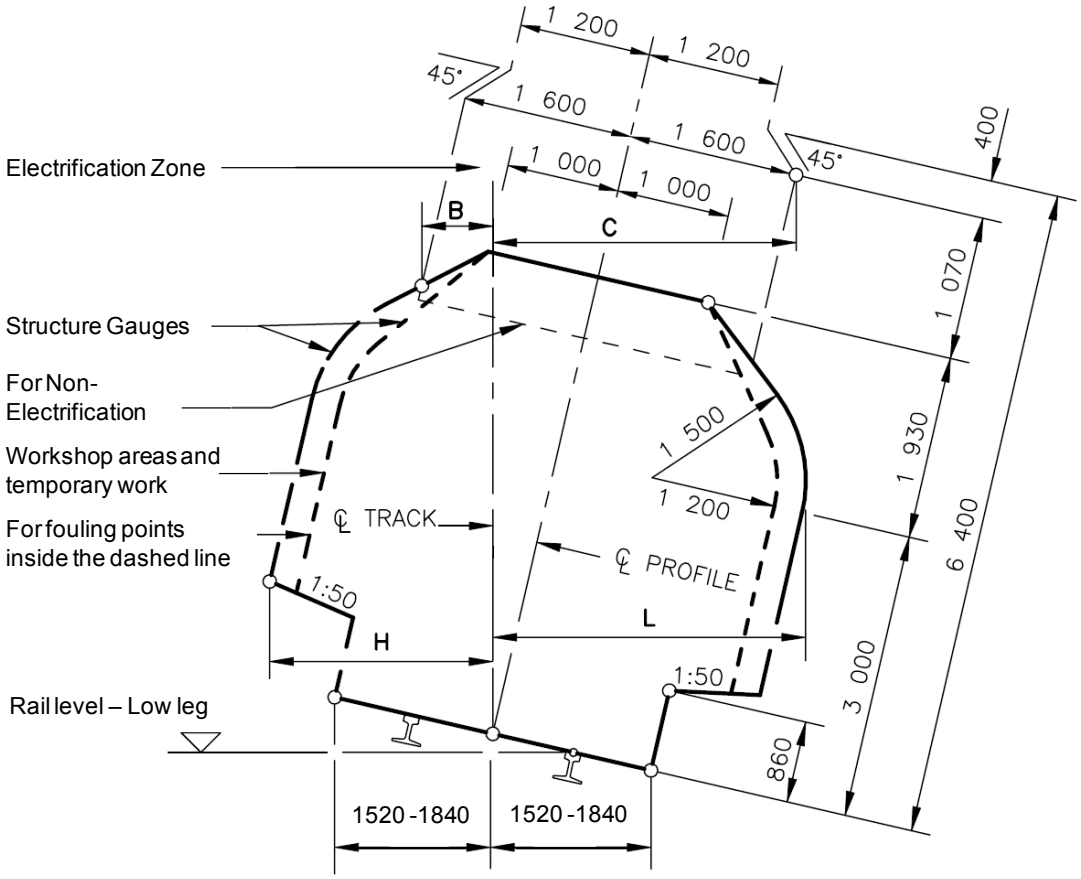

Figure 2.5: Track Clearance, from Transnet Track Maintenance Manual (2000).

2.3 SOIL PROPERTIES AND CLASSIFICATION

Soil and aggregate are defined by their properties and are distinguished from each other by classification methods. It is important to understand the different properties and classification methods for soil and aggregate within the railway environment which includes the ballast, subballast and subgrade, as well as placed soil or fill. Soil and aggregate parameters should be determined by adequate testing (Selig and Waters, 1994).

Selig and Waters (1994) describe the properties of both ballast and soil in detail. In South Africa, Transnet Freight Rail developed specifications for the ballast and foundation layer material. These can be found in *Transnet Freight Rail S410 (2006) Specification for railway Earthworks* and *Transnet Freight Rail S406 (1998) Specification for the supply of stone contents.* The tests used for determining the soil and aggregates parameters are listed in this section. Descriptions of the classification methods are also given. Detailed descriptions of these tests are given in *TMH1 (1986) Standard methods for testing road construction materials.*

2.3.1 Subballast / Subgrade parameters

The tests that define the parameters of the subballast and subgrade material are as follows:

- Grading analysis
- Atterberg limits
- Linear shrinkage
- California Bearing Ratio (CBR)

Strength, particle shape, moisture content and density tests are also conducted (Clayton, Matthews and Simons, 1995). Typical material classification and foundation designs according to the S410 (2006) are shown in Table 2.1.

Table 2.1 includes material classification for subballast (SSB and SB) and subgrade layers (A and B) and Table 2.2 shows typical foundation designs for 20t, 26t and 30t axle loading. The SAR index is the sum of the Liquid Limit (LL), the Plastic Limit (PL) and the material passing the 0.075 mm sieve. This value is expressed as a number. The Plasticity Index (PI) is the PL subtracted from the LL.

Table 2.1: Material properties according to the Transnet (2006).

Layer	Material Properties									Min. Compaction % of Modified AASHTO Density	Min. Strength after compaction CBR
	SAR Index	Minimum Grading Modulus	% By Mass Passing Sieve (mm)					PI	Max. CBR Swell %		
			75	13.2	2	0.425	0.075				
SSB	<50	2.0	100	60-85	20-50	10-30	5-15	3-10	0.5	98	60 (o) (1.5-3 MPa)
SB	<80	1.8	100	70-100	20-60	10-40	5-20	3-10	0.5	95	+ 30 (o) (1.5-3 MPa)
A	<110	1					<40	<12		95 100*	20
B	<155	0.5					<70	<17		93 98*	10
Bulk Earth Works								<25	2	90 95*	5

* These densities apply to non-cohesive soils

(o) Strengths in brackets apply in place of CBR values where sub-ballast is stabilised

\+ Increase to 45 in the absence of Layer SSB unless otherwise specified (Increase not normally required in dry areas.)

Table 2.2: Foundation designs according to the Transnet (2006).

Layer	Layer Thickness (mm)					
	Axle loading (t)					
	20		26		30	
SSB			200	150	250	200
SB	200	150	200	150	250	200
A	250	300	200	300	200	300
B	450	450	300	300	300	300
Total	900	900	900	900	1000	1000
Bulk Earthworks						

2.3.2 Ballast parameters

A detailed description of the tests that describe the properties of ballast material is given by Selig and Waters (1994). The S406 specification however recommends that the following tests be used to determine the ballast material parameters:

- The soundness of stone (Sodium Sulphate method),
- Durability tests:
  - Los Angeles Abrasion (LAA) test (ASTM C 131 - 89),
  - Mill Abrasion(MA) test (S406; Selig and Waters, 1994),
- Plasticity index from the fines obtained from the LA abrasion test (TMH1, 1986) ,
- Flakiness Index test (SABS 1083),
- Voids measured (SABS 1083),
- Relative density determination and
- Grading analysis.

The Abrasion Number (AN = LAA + 4MA) proposed by Klassen et al. (1987) provides an indication of both abrasion by fracture and wear. The amount of ballast fouling can also be determined. This can be done in situ or in a laboratory by means of a grading analysis (Selig and Waters, 1994). Figure 2.6 and Figure 2.7 show the grading of ballast for ordinary lines and heavy haul lines according to the S406 (1998) specification.

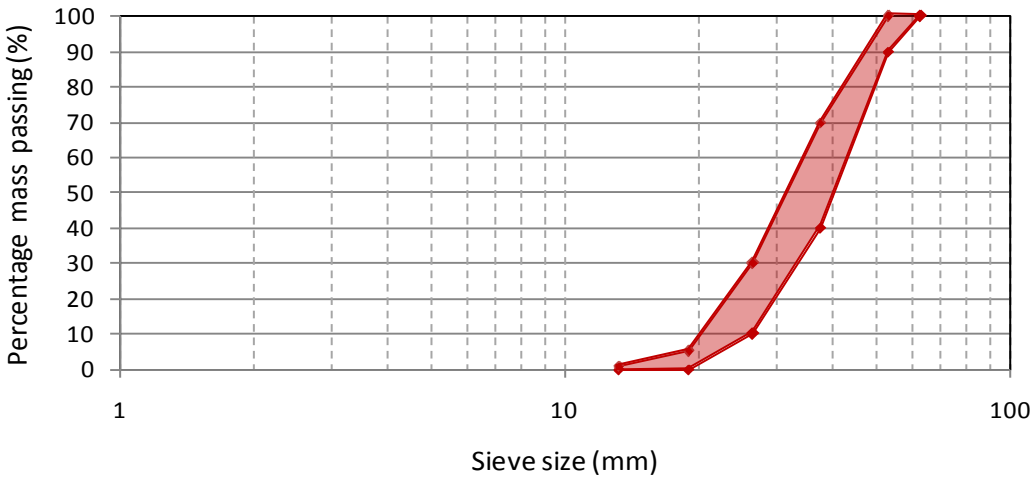

Figure 2.6: Grading of ordinary ballast according to Transnet (1998).

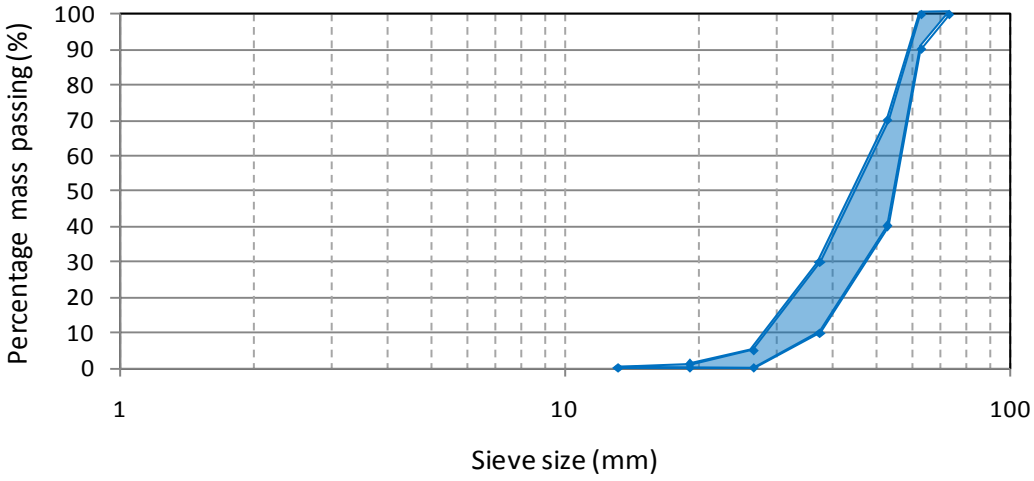

Figure 2.7: Grading of ballast for heavy haul conditions according to Transnet (1998).

2.3.3 Classification

Soils can be classified as gravel, sand, silt or clay and are classified by size as in the *ASTM D2488* standards, shown in Table 2.3. *ASTMD2487* also provides detailed information on a visual/manual soil identification procedure. The soil is classified in the same way as the Unified Soil Classification System (USCS) (ASTM 2487). The USCS and the American Association of State Highway and Transportation Officials (AASHTO) methods use soil particle size characteristics for classifying the soil. These methods provide no information on

the physical in-situ soil state as they are conducted on disturbed samples (Selig and Waters, 1994).

Table 2.3: Soil particle size

Soil Type	Size Range (mm)
GRAVEL (Coarse)	76 – 19
GRAVEL (Fine)	19 – 4.75
SAND (Coarse)	4.75 – 2
SAND (Medium)	2 – 0.425
SAND (Fine)	0.425 – 0.075
SILT and CLAY	0.075 – 0.002
CLAY	<0.002

Furthermore, the grading of the soil provides information on the uniformity as well as how well the soil is graded. A uniform soil consists of a narrow range of particle sizes whereas a well-graded soil has a wide range of particle sizes contained within it. This is defined by the coefficient of uniformity (Equation 2.3) and the coefficient of curvature (Equation 2.4). The coefficient of uniformity (C_U) defines the boundary between a well graded and uniform soil whereas the coefficient of curvature (C_Z) indicates how well a soil is graded. The soil is well graded if C_Z is between 1 and 3 (Craig, 2007).

$$C_U = \frac{D_{60}}{D_{10}} \tag{2.3}$$

and

$$C_Z = \frac{{D_{30}}^2}{D_{60}D_{10}} \tag{2.4}$$

Where:

C_U = Coefficient of uniformity

C_Z = Coefficient of curvature

D_n = The size of which n percentage of particles is smaller than D_n

A different soil classification method is the visual classification of soils in a test pit or borehole as developed by Jennings *et al.* (1973). This method was developed for the profiling of soil layers. The method uses the parameters in Table 2.4 to describe a soil profile layer. A full description of the method is given in Byrne and Berry (2008) and Jennings *et al.* (1973). Similarly, a method proposed by the ASTM D2488 based on the USCS method can be used.

Table 2.4: Parameters used for soil profiling (Jennings *et al.*, 1973)

Designation	Condition
M	Moisture
C	Colour
C	Consistency
S	Structure
S	Soil Type
O	Origin

2.4 SUBSTRUCTURE DESIGN

The design of the railway substructure is one of the most important aspects of a railway line (Burrow *et al.,* 2006). This is not only because it needs to effectively withstand the damaging effects of the railway traffic and climate, but also because of the difficulty of replacing it (Selig and Waters, 1994; Ebersöhn, 1995; Burrow *et al,*. 2006). Therefore, to fulfil the functions of the substructure, it should have adequate thickness, layer stiffness and resistance to plastic shear strain (Li and Selig, 1998a; Burrow *et al.,* 2006).

This section briefly describes the different substructure failures and different track substructure design methods to prevent these failures.

2.4.1 Track Substructure Failures

Progressive shear failure and excessive plastic deformation are the two most common types of failures caused by repetitive loading. The failure mechanisms are indicated in Figure 2.8 and

Figure 2.9 respectively. If the track fails in these ways, it requires extensive maintenance and rehabilitation (Selig and Waters, 1994; Li and Selig, 1998a; and Li and Selig, 1998b).

Progressive shear failure (Figure 2.8) develops at the surface of the subgrade. As a result of repeated overstressing, the soil is gradually sheared and remoulded. The subgrade surface is then replaced sideways, following the path of least resistance. The material fouls the ballast and water is prevented to drain freely from the track structure. This then allows moisture build-up which aggravates the failure.

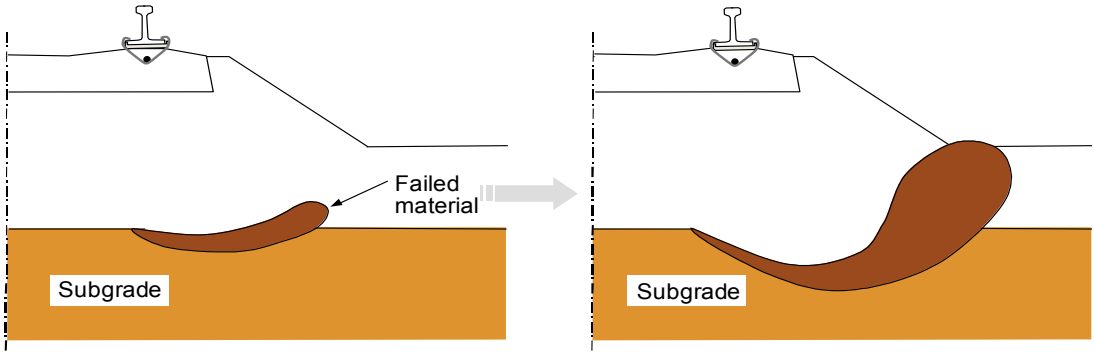

Figure 2.8: Subgrade progressive shear failure (Selig & Waters, 1994).

Excessive plastic deformation (Figure 2.9) is similar to progressive shear failure and is caused by repetitive loading from the rolling stock. However, it is the vertical component of the progressive shear failure that causes progressive compaction and consolidation of the subgrade. By only restoring the geometry of the track with ballast, this material will only create a ballast pocket and will not address the root cause of the failure.

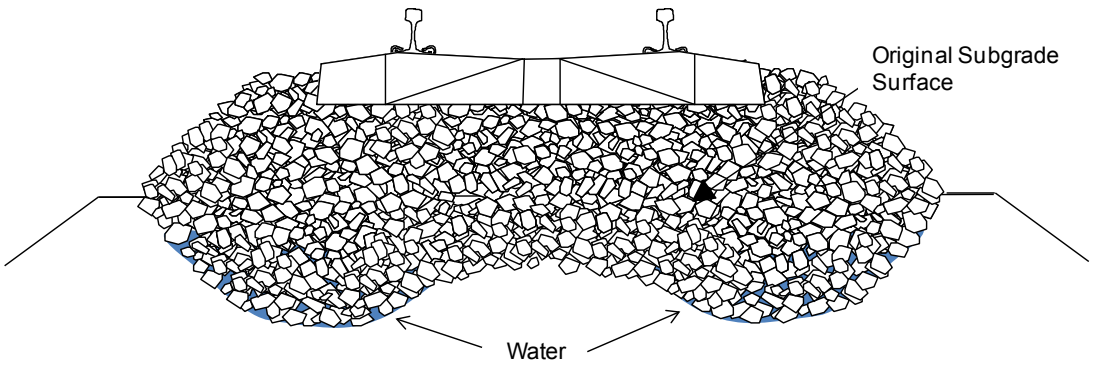

Figure 2.9: Excessive subgrade plastic deformation, redrawn from Li and Selig (1998a).

Two other failures that are not necessarily caused by repetitive loading is massive shear failure and consolidation settlement. Massive shear failure is caused by overloading of the foundation just after it is built or after major downpours. Consolidation settlement is caused by the dissipation of excess pore water in the soil (Selig and Waters, 1994).

2.4.2 Substructure Design Methods

Design methods have been developed by Network Rail (2005), West Japan Railway Standards (2002), Shahu *et al.* (2000), Li and Selig (1998a, 1998b), The International Union of Railways (1994), Heath *et al.,* (1972), and Raymond (1978). Burrow *et al.* (2006) compared some of these methods using variations in subgrade condition, axle load, speed and cumulative tonnage. The results showed varying recommended thicknesses and not all the design methods incorporated all the input parameters. Burrow *et al.* (2006) concluded that the method by Li and Selig (1998a, 1998b) presents the best analytical methodology. The methods by Shahu *et al.* (2000) and Raymond (1978) were not included in this study.

The method by Li and Selig (1998a, 1998b) uses two design criteria to determine the effective granular layer thickness. The first criterion is used to prevent progressive subgrade shear failure by limiting the total cumulative plastic strain at the subgrade surface to a maximum strain. This is done for a number of load repetitions over the railway's design period and is expressed by the following Equation 2.5.

$$\varepsilon_p \leq \varepsilon_{pa} \tag{2.5}$$

Where:

ε_p = total cumulative plastic strain at the subgrade surface for the design period

ε_{pa} = allowable plastic strain at the subgrade surface for the design period

The second criterion is used to prevent excessive plastic deformation of the subgrade by limiting the total cumulative plastic deformation of the subgrade over its design period and is expressed by the Equation 2.6.

$$\rho \leq \rho_a \tag{2.6}$$

Where:

ρ = total plastic deformation of the subgrade layer

ρ_a = allowable plastic deformation of the subgrade layer for the design period

Furthermore, to determine the total plastic deformation of all the subgrade layers, repeated load triaxial tests were conducted on various fine-grained soils (Li and Selig, 1996). From this, Equation 2.7 was established:

$$\varepsilon_p = a\left(\frac{\sigma_d}{\sigma_s}\right)^m N^b \tag{2.7}$$

Where:

σ_d = the soil's deviator stress

σ_s = compressive strength of the soil

N = number of repeated stress applications

a, b and m = parameters dependent on the soil type

By integrating the individual cumulative plastic strains of each subgrade layer over the total depth, the expected total deformation can be determined (Li and Selig, 1996). The following integral in Equation 2.8 is used:

$$\rho = \int_0^T \varepsilon_p dT \tag{2.8}$$

Where:

T = total subgrade thickness

Finally, using Equation 2.4, Equation 2.6 and a track model (GEOTRACK), design charts have been developed. These charts cover various soil conditions and granular layer conditions and it also takes into account untrained shear strength, soil type and resilient modulus.

However, according to Shahu *et al.* (2000), this method does not properly account for the soil type and drainage conditions and it does not propose a procedure for evaluating threshold stress.

Shahu *et al.* (2000) developed a rational method for estimating the threshold stress. This was done by conducting cyclic triaxial testing on the material under investigation. The focus of the design procedure was to keep the induced stresses on the subgrade surface below that of the threshold stress of the subgrade by providing a sufficiently thick formation. This method is an improvement on previous design methods, using laboratory testing of materials instead of relying on design charts. However, it still does not take into account the effect of principle stress rotation as suggested by Gräbe and Clayton (2009).

2.5 TRACK MODULUS

Track modulus is defined by the track deflection and the vertical contact pressure between the rail base and the supporting foundation. It combines the effects of all the track components below the rail in one parameter. This includes the sleepers, fasteners, ballast, subballast and subgrade (Cai *et al.*, 1994). Selig and Li (1994) define the track modulus as the supporting force per unit length of rail per unit rail deflection. The track stiffness defines the stiffness of the whole track whereas the track modulus defines the stiffness of the subgrade. The relationship is defined in Equation 2.9 and Equation 2.10.

$$k = \frac{P}{\delta_m} \tag{2.9}$$

$$u = \frac{(k)^{\frac{4}{3}}}{(64EI)^{\frac{1}{3}}} \tag{2.10}$$

Where:

k = Track stiffness

P = Vertical wheel load

δ_m = Vertical rail deflection

E = The rail Young's modulus of elasticity

I = The moment of inertia of the rail

u = Track modulus

Track modulus affects the track performance and maintenance conditions. Low track modulus values may cause differential settlement. This will cause an increase in maintenance needs (Ebersöhn, Trevizo, and Selig, 1993; Read *et al.*, 1994). Variations caused in track modulus often caused by changes in track support may increase dynamic loading (Davis *et al.*, 2003; Zarembski and Palese, 2003). Therefore, the performance of the track is critically related to that of track modulus (Selig and Li, 1994). When this occurs, the variation defies the premise on which the track modulus is based (beam on elastic foundation). In such a case, the measurement of a continuous track stiffness may provide an indication of poor track performance. Continuous track modulus measurement techniques as explained in Section 2.6.7 can be used for track performance characterization.

2.6 TRACK SUBSTRUCTURE INVESTIGATION METHODS

The investigation of substructure components is important for the design and maintenance thereof. Care should be taken when conducting a substructure investigation to establish the correct remedial action (Brough *et al.*, 2003). According to Selig and Waters (1994), to achieve this, a site investigation strategy has to be in place. This includes factors concerning technical and non-technical issues as well as economic considerations. These factors include soil type, equipment availability, time needed, difficulty of the test, amount of data obtained, data interpretation and test variability. Also, knowing what conditions need to be evaluated will determine the choice of investigation technique (Dunnicliff, 1988).

This section will briefly discuss various methods for the investigation of railway track substructures. These include the following:

- Dynamic Cone Penetrometer (DCP).
- Pencel Pressuremeter Test (PPT).
- Light Weight Drop Tester (LWD).
- Continuous Surface Waves (CSW).
- Remote Video Monitoring (RVM).
- Multi Depth Deflectometers (MDD).

2.6.1 Dynamic Cone Penetrometer (DCP)

The DCP is described in the *Standard Test Method for Use of the Dynamic Cone Penetrometer in Shallow Pavement Applications* in the ASTM standards (ASTM D6951 / D6951M – 09, 2009). The DCP is an apparatus that can be used to obtain an indirect measure of the strength or bearing capacity of flexible foundations. Multiple layer strength measurements can be done to a maximum depth of 1.5 m below the surface.

The DCP apparatus (Figure 2.10) consists of an 8 kg hammer that drops from a height of 575 mm and drives a 60° cone with a 20 mm diameter vertically into a layer of soil. A theoretical driving energy of 14.3 J/cm^2 is exerted by the hammer. The rod to which the cone is attached is of a smaller diameter (16 mm) to reduce skin friction.

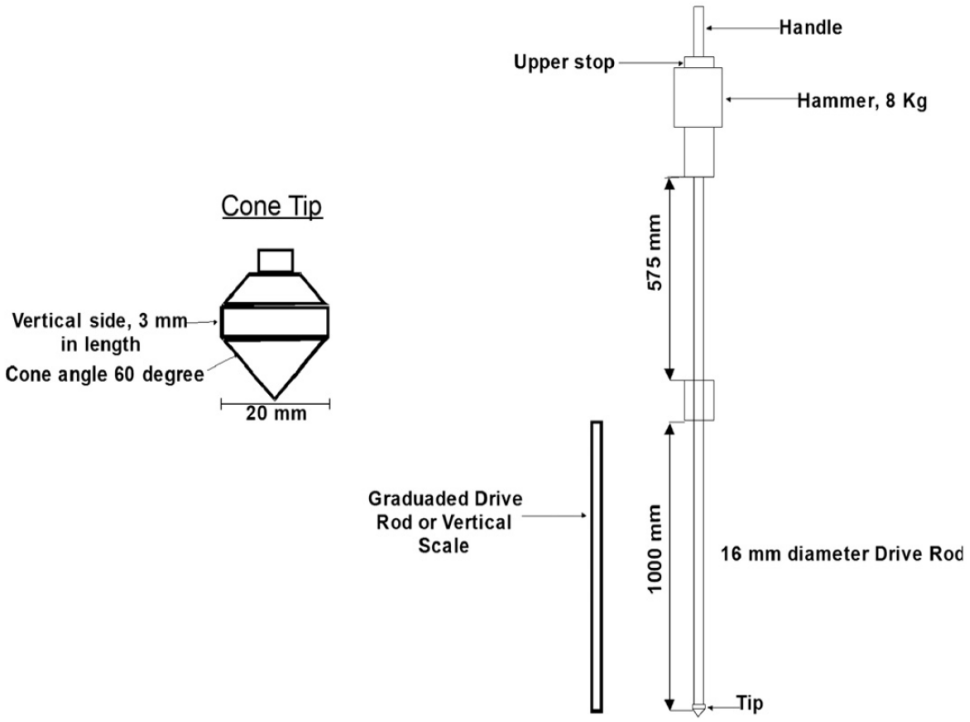

Figure 2.10: Dynamic Cone Penetrometer (DCP) (Mohammadi *et al.*, 2008).

The results of the DCP test are recorded using the number and the depth of penetration (in mm per blow). The DCP penetration index (DN) is the slope of the curve defining the relationship between the number of blows and the depth of penetration. The DN for individual layers can also be determined using the Equation 2.11 (Mohammadi *et al.*, 2008).

$$DN = \frac{P_{i+1} - P_i}{B_{i+1} - B_i} \tag{2.11}$$

Where:

DN = DCP Penetration Index (mm/blow)

P = Penetration at i or $i + 1$ hammer drops (mm)

B = blow count at i or $i + 1$ hammer drops

Relationships exist between the DCP penetration index (DN), California Bearing Ratio (CBR) and the Unconfined Compressive strength (UCS) (Paige-Green and Du Plessis, 2009; Kleyn, 1984).

2.6.2 Light Weight Deflectometer (LWD)

The LWD uses a dynamic loading plate that determines the dynamic load bearing capacity of substructure materials (Zorn, 2005). It can be used to measure elastic deformation of ground layers from the surface. An example of the apparatus being used for railway applications is shown in Figure 2.11.

Figure 2.11: Light weight drop tester used for railway foundations (Shaw, 2005).

A description on how to use the LWD follows. A 10 kg impact load is applied to a circular test area with a diameter of 300 mm. The operational depth of the LWD is 1.5 times the diameter of the load plate. The mass falls from a constant height down through a damping system that causes acceleration on the loading plate which is measured by an accelerometer. The acceleration is integrated twice to determine the settlement. The results are displayed on a portable electronic output device. Knowing the load applied and from the calculated settlement, the Deformation Modulus (E_{vd}) can be calculated shown in Equation 2.12:

$$E_{vd} = \frac{1.5(r\sigma)}{s} \tag{2.12}$$

Where:

E_{vd} = Dynamic Deformation Modulus (N/mm^2)

r = radius of load plate (mm)

σ = stress under load plate (N/mm^2)

1.5 = constant related to ground load from a circular plate

2.6.3 Pencel Pressuremeter Test (PPT)

The PPT was developed by Roctest, is based on the pavement Pressuremeter developed by Briaud and Shields (1979). The Pencel pressuremeter functions as a pre-boring pressuremeter and was modified from the original pressuremeter to suite pavement conditions. The Pencel pressuremeter's purpose is to determine the stiffness of pavement (formation) layers. In so doing, it determines the in situ conditions of track formation layers. It is an inflatable cylindrical probe that is inserted into a predrilled hole while expanding it with water and measuring the change in volume pressure in the probe (Briaud, 1992).

The Pencel pressuremeter consists of the following three main components:

- The Pencel (probe) that is placed within the pre-drilled hole, which consists of a cylindrical body. The cylinder contains an inflatable membrane, fluid inlet and saturation ports (see Figure 2.12).
- A connection pipe with two quick release shut-off valves on both sides. This allows the Pencel to be connected and disconnected without the loss of water or pressure.
- The control and measuring unit, which consists of control valves, a pressure transducer and a dial gauge, which measures the movement of a cylindrical piston to calculate the volume change.

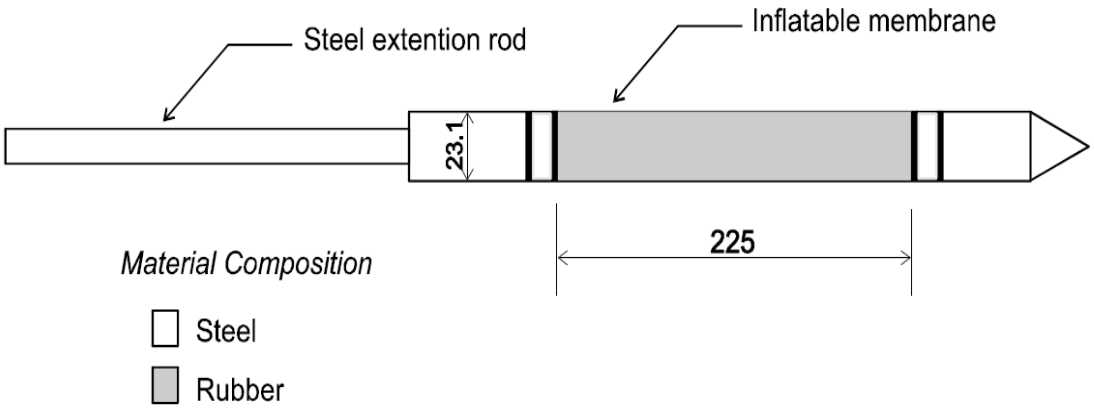

Figure 2.12: Schematic diagram of the Pencel Pressuremeter (Gräbe, 1997)

The test procedure used for the Pencel pressuremeter is described in detail as *Standard Test Method for Pressuremeter Testing in Soils* in the ASTM standard (ASTM D4719-87). A brief description of the test procedure is as follows:

- The Pencel (probe) is pushed into the drilled hole, either vertically or horizontally, to the desired position within the soil.
- The membrane is then inflated in the hole by increasing the volume of fluid incrementally.
- During the loading stage, a few the unload-reload cycles are done in the elastic range of the soil.
- The pressuremeter is then loaded to its maximum pressure (3 000 kPa) and unloaded.
- During the unloading stage, a few unload-reload cycles are done.

Typical test results obtained from the Pencel pressuremeter are presented in Figure 2.13.

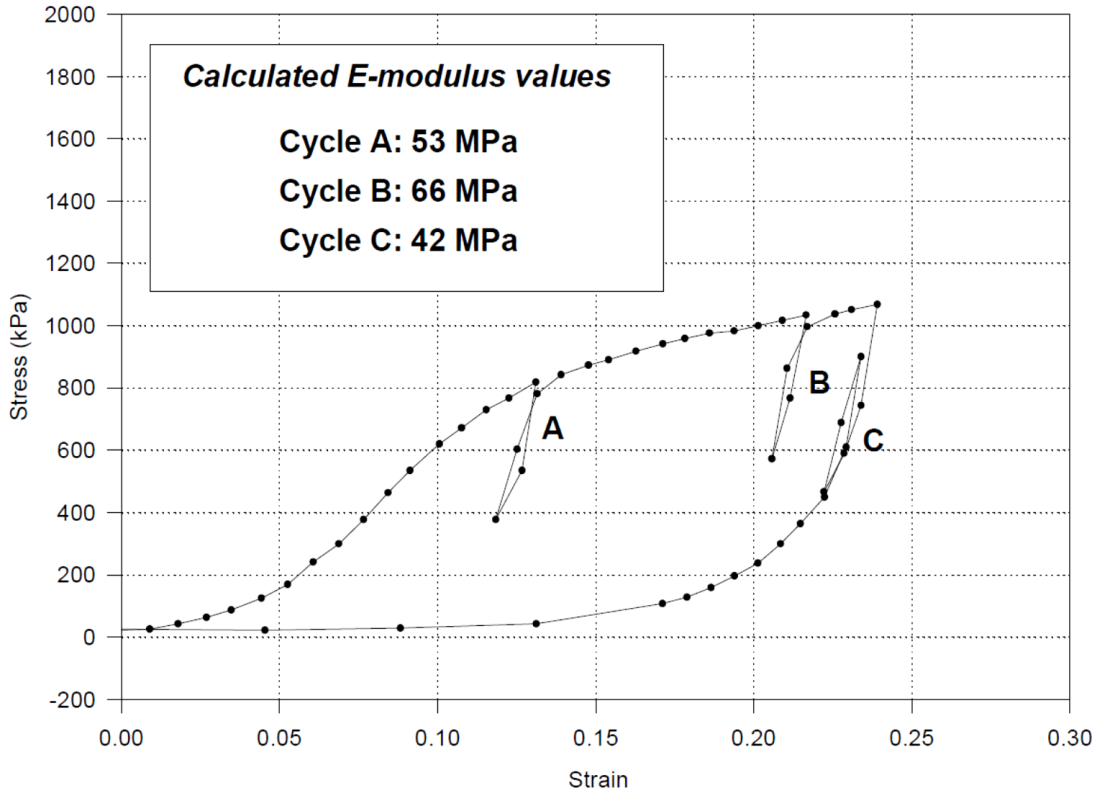

Figure 2.13: Typical test results from the Pencel pressuremeter (Gräbe, 1997).

The shear modulus is determined within the linear section of the stress-strain plot. It is given by Equation 2.13.

$$G = V \frac{dp}{dV} \tag{2.13}$$

Where:

G = shear modulus

V = current volume of the borehole cavity

p = corrected pressure

$\frac{dp}{dV}$ = the slope of the linear section

2.6.4 Surface wave testing

Seismic test methods rely on the velocity at which seismic (stress) waves move through the ground. These test methods were used for the characterization of the earth's interior, mineral exploration, geological stratigraphy of the subsurface and for obtaining engineering design parameters. When a seismic disturbance is induced at the ground surface, four seismic wave types will propagate at different velocities (Clayton, Matthews and Simons, 1995). These waves are as follows:

- Longitudinal waves (P-waves) are compression waves with the particle motion in the direction of the movement. They move the fastest of all the waves and are body waves. They move both in the soil skeleton and in the pore water.
- Traverse waves or shear waves (S-waves) are the second fastest waves, at 70% of P-wave velocity. The waves are body waves with particle motion perpendicular to the direction of movement. They only move through the soil skeleton. Therefore, because of the independence from pore water and from the elasticity theory, the relationship of shear wave velocity, bulk density and shear stiffness of the material is as follows (Equation 2.14):

$$G_0 = \rho V_s^{\,2} \tag{2.14}$$

Where:

G_0 = shear stiffness

ρ = bulk density

V_s = shear wave velocity

- Rayleigh waves (Rayleigh, 1885) travel on the ground surface. They include two thirds of the wave energy produced and attenuate slowly at a rate of $1/\sqrt{r}$ where r is the distance from the source. The particle movement caused by the wave is elliptical and parallel to the direction of movement. Rayleigh waves travel slower than shear waves. The relationship is presented by Equation 2.15:

$$\frac{V_r}{V_s} \cong \frac{0.874 + 1.117v}{1 + v} \tag{2.15}$$

Where:

V_r = Rayleigh wave velocity

v = Poisson's ratio

- Love waves (Love, 1927) are surface waves with particle motion parallel to the ground and perpendicular to the direction of the wave movement. They only account for a very small part of the energy produced.

Surface waves include the spectral analysis of surface waves (SASW) test, multi-channel analysis of surface waves (MASW) test, the frequency-wave (f-k) spectrum method and the continuous surface wave (CSW) test (Stokoe, Joh and Woods, 2004). These methods use Rayleigh waves to determine engineering parameters. The SASW, MASW and the f-k spectrum methods require an impact from hammer blows to the ground to generate seismic energy whereas the CSW test uses a shaker to generate vertical sinusoidal energy at the ground surface. The CSW test therefore has the advantage that the frequencies produced can be controlled. The Rayleigh wave propagation is detected by an array of geophones on the soil surface. Uni-axial geophones are used with the measurement axis perpendicular to the ground surface and they are placed in a line away from the shaker (Heymann, 2007).

The test setup for the CSW test described by Heymann (2007) is shown in Figure 2.14. The setup contains a signal generator, amplifier, shaker and geophones. The shaker is placed on the soil that will be tested and loose fine grained sand is placed beneath it for good contact with the ground. The geophones are placed in a straight line of three to six at equal distances from each other. The shaker is energized by a signal provided by an electronic signal generator and amplified by a linear power amplifier. The frequency range can be varied from 5 Hz to 9 kHz and is measured at different intervals. Geotechnical applications use frequencies of 15 Hz to 200 Hz (Heymann, 2007) and road pavements may require a frequency of up to 10 kHz for the uppermost layer (Svensson, 2001). Shaw (2005) used a similar setup for railway applications as shown in Figure 2.15.

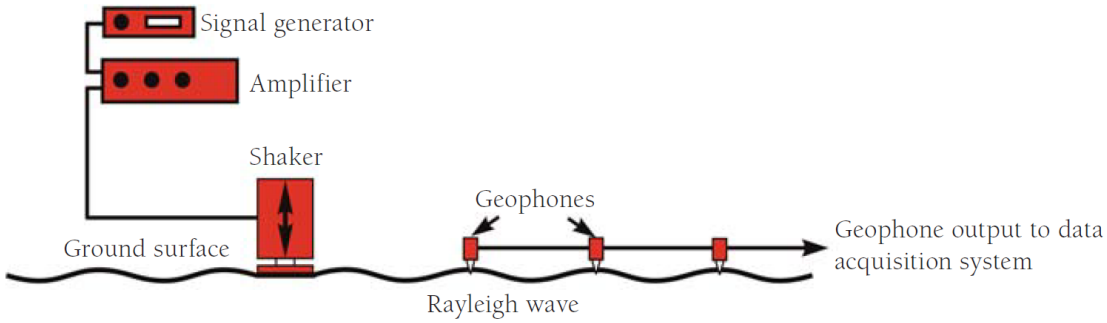

Figure 2.14: Layout of the continuous surface wave system (Heymann, 2007)

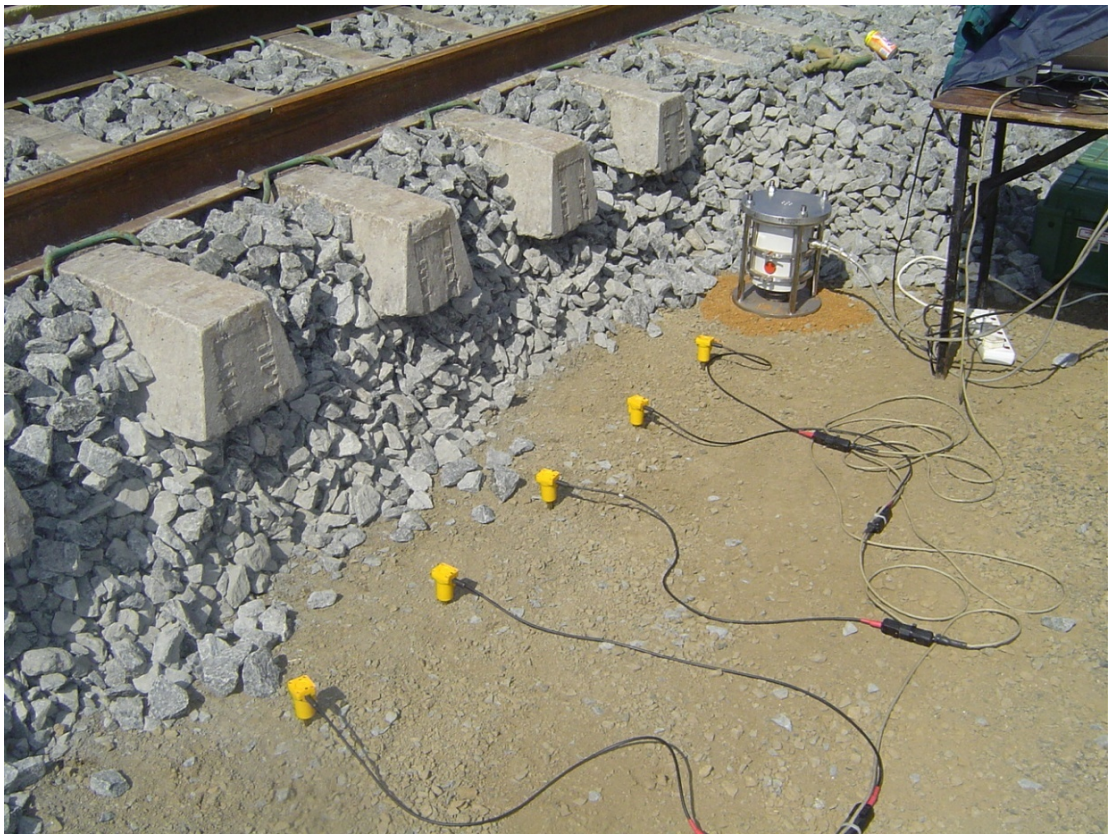

Figure 2.15: CSW test application on railway (Shaw, 2005)

To determine the phase of the generated signal at each geophone location, the signal is recorded by the geophones. The recorded signal is then converted by Fast Fourier Transform (FFT) from the time domain to the frequency domain. The wavelength of the Rayleigh wave as well as the Rayleigh wave velocity is determined by Equation 2.16 and Equation 2.17.

$$\lambda = \frac{d}{\left(n + \frac{\Delta\phi}{2\pi}\right)} \tag{2.16}$$

$$V_r = f\lambda \tag{2.17}$$

Where:

λ = wavelength of the Rayleigh wave

$\Delta\phi$ = Phase change from one geophone to the next

d = distance between two geophones

n = an integer that is dependent on the number of wavelengths between geophones

f = frequency

The shear modulus can also be determined by using elastic theory as assumed by Equation 2.16 and Equation 2.17. The characteristic dispersion curve for the soil section will be obtained by the Rayleigh wave velocities measured at the different excited frequencies. The dispersion curve needs to be inverted to obtain the velocity to depth profile form which the stiffness to depth profile can be estimated.

Advantages of the CSW system are as follows:

- Small strain stiffness can be measured.
- Stiffness measurements are done in situ with no disturbance to the soil.
- All soil types can be tested.

2.6.5 Remote Video Monitoring (RVM)

Remote video monitoring (RVM) is derived from particle image velocimetry. The particle image velocimetry (PIV) system is a velocity measuring technique originally used in the field of fluid mechanics (Adrian, 1991). The system is also used in the geotechnical field to measure the velocity around objects penetrating the ground (White, Take and Bolton, 2003). A similar system, remote video monitoring (RVM), is used to measure deflection in the railway track structure. This provides accurate readings of rail deflections without disruptions to the railway line (Bowness, Lock, Powrie, Priest and Richards, 2006).

Original use of the RVM system by Bowness *et al.* (2006) consisted of a webcam which directly captures the digital video image of a target onto a computer. The target is placed on any part of the track (rail, sleeper and formation). The typical target shape used for the system is shown in Figure 2.16. By attaching a telescope to the webcam, the monitoring system can be placed far enough from the target so that the vibrations and deflections of the ground caused by the train, do not affect it.

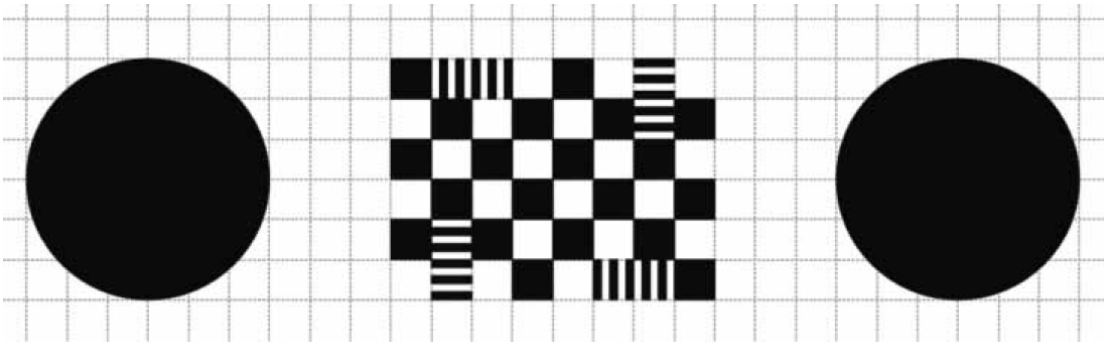

Figure 2.16: RVM target shape (Bowness *et al*., 2006).

Typical recording speeds for cameras vary from 25 frames per second (fps) for conventional video cameras to 500 fps for higher quality and more expensive cameras. The data is captured in audio video interleave (AVI) files at different resolutions. The target size in millimetres is converted to pixels in relation to the pixels in the AVI file.

A similar system was developed by Transnet Freight Rail (Track Technology) and TLC Engineering Solutions (Pty) Ltd. This system consists of a video camera from which the video data is transferred to a portable computer. With recent developments in video cameras, the recording speed can be between 25 fps and 600 fps but with a loss in resolution as the frame rate increases. The target is a 20 mm x 20 mm black square on a white background (Figure 2.17). The AVI video file is analysed by National Instruments Vision software. This is done by converting the pixels within the target into a measurable distance. The software then calculates both the horizontal and vertical displacement (Gräbe, 2008).

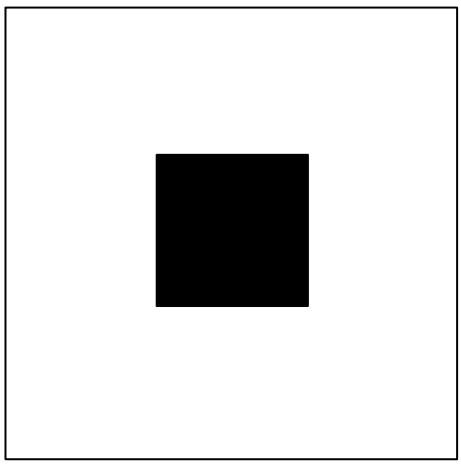

Figure 2.17: RVM target shape (Gräbe, 2008).

Advantages of the RVM system are as follows:

- The system is flexible and is easy to set up and move. Trains on the railway line need not be stopped for the setup of the system.
- The system is inexpensive due to the relatively low cost of components.

2.6.6 Multi Depth Deflectometers (MDD)

The CSIR developed the MDDs for the use in the Heavy Vehicle Simulator (HVS). MDDs are used to measure both the elastic and permanent in situ deformations of different pavement layers (Maree, 1993a).

The method consists of drilling a hole into the formation of the track structure. A series of Linear Variable Differential Transducer (LVDT) modules mounted in a string is the basis of the MDD system. The typical layout of the unit is indicated in Figure 2.18. Up to six of these units can be mounted in a string for different layers of the formation as shown in Figure 2.19. The reference rod is anchored about 3 m below the pavement surface and the modules are anchored to the soil by small metal balls forced into the sides of the hole. The top of the hole is sealed and it contains the connector to the data acquisition system (Maree, 1993a; Sussman and Selig, 2000; Shaw, 2005).

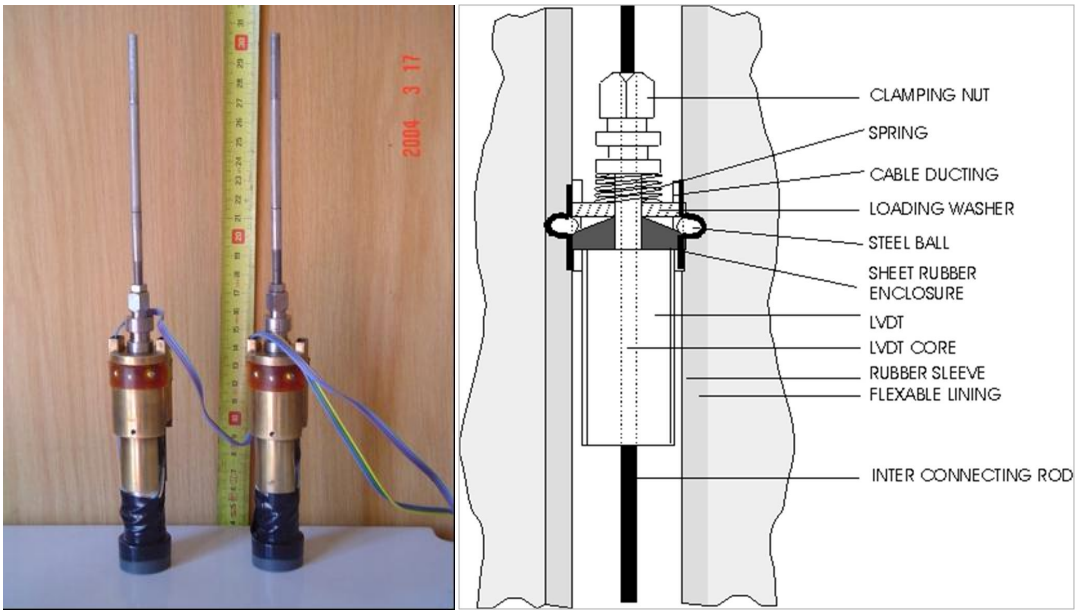

Figure 2.18: Layout of a MDD unit (Shaw, 2005).

Figure 2.19: MDD placement (Shaw, 2005).

Measuring both the permanent and elastic deformation of the in situ formation layers, the plastic deformation data can be used to formulate transfer functions. This includes functions relating load repetitions to plastic strain in the rail formation material layers. MDD data can be used for determining the effective elastic moduli or stiffness of each formation layer. The stiffness in terms of Young's Modulus (E) can be back-calculated with the use of linear elastic models (Sussman and Selig, 2000).

Advantages of MDDs (Sussman and Selig, 2000):

- No inherent stiffness is induced in the formation. The MDDs and their installation do not influence soil behaviour.
- Disturbance of material is minimal when drilling the hole.
- Due to the instrumentation technique, bedding errors is not a factor. Small strains can therefore be measured accurately.

2.6.7 Continuous track modulus measurements

The relationship between vertical track deflection and track loading provides the key for determining the track modulus and track stiffness as described in Section 2.5. Different methods of continuous track modulus measurement are described below.

Track Loading Vehicle (TLV) developed at the TTCI

The first on-board track modulus measurement systems were used in highway research (Carr, 1999). A long rigid straight truss that extends 30.48 m, supported by two unloaded wheels, was used. A third loaded wheel applied a load at the midpoint of the cord and the relative deflection between the wheels was measured. Two measurements are needed for this method, one light and one heavy load to distinguish between changes in geometry.

The TLV of the Transport Technology Centre (TTCI) uses a similar approach as mentioned above (Thompson and Li, 2002; Li, Thompson and Kalay, 2002). This vehicle can measure at speeds of up to 16 km/h and uses two cars that can vary the load. The vertical track deflection is measured by lasers. The system requires two passes over the track to determine the track modulus. The method poses problems with continuous long distance measurements and with track modulus measurements on curved track. This system was also used in combination with GPR measurements (Smekal, Berggren and Hrubec, 2003).

Rolling Stiffness Measurement Vehicle (RSMV)

A measuring car has also been developed to investigate track condition and is called the RSMV (Berggren, Jahlenius, Bengtsson and Berg, 2005; Berggran, Jahlenius and Dehlbom, 2010). The RSMV is a two axle freight wagon that is dynamically excited through two oscillating masses above each of the wheels (see Figure 2.20). The track stiffness is calculated by using the measured wheel force and by integrating measured accelerations. The system can operate at speeds of up to 50 km/h and an axle load of 180 kN can be applied.

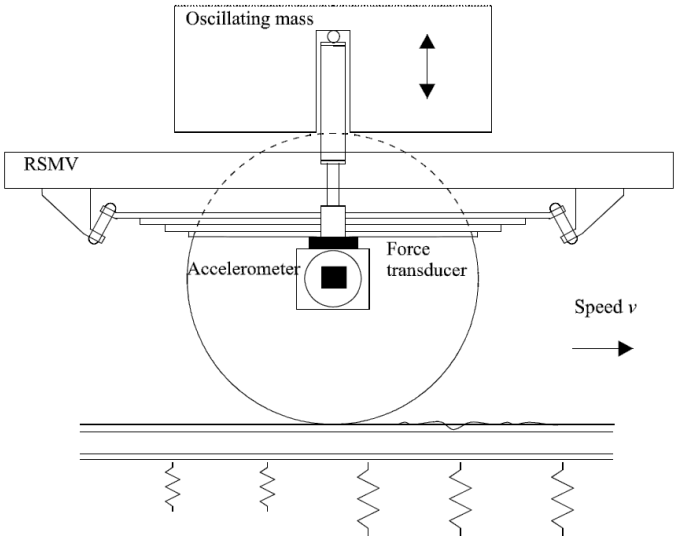

Figure 2.20: Measurement principle (one side only) of RSMV (Berggren *et al.*, 2010)

Line laser/camera system

Work done at the University of Nebraska allows the measurement of vertical track deflection from a moving rail car, thereby determining the track modulus (Lu *et al.*, 2008; Lu *et al.*, 2010). The system uses a beam attached to the side frame of a loaded hopper bogie that extends to the centre of the hopper. The deflection measurements of the rail are done approximately 1.3 metres from the inner wheel. This is achieved with a camera/laser system that determines the offset between the rail and the line established by two wheel rail contact points. The vertical measured deflection and the known load of the hopper wheels can be used to determine the track stiffness and track modulus. Using these continuous measurements the performance of the track can be characterized and possible poorly supported sections can be identified. A schematic of this system is shown in Figure 2.21.

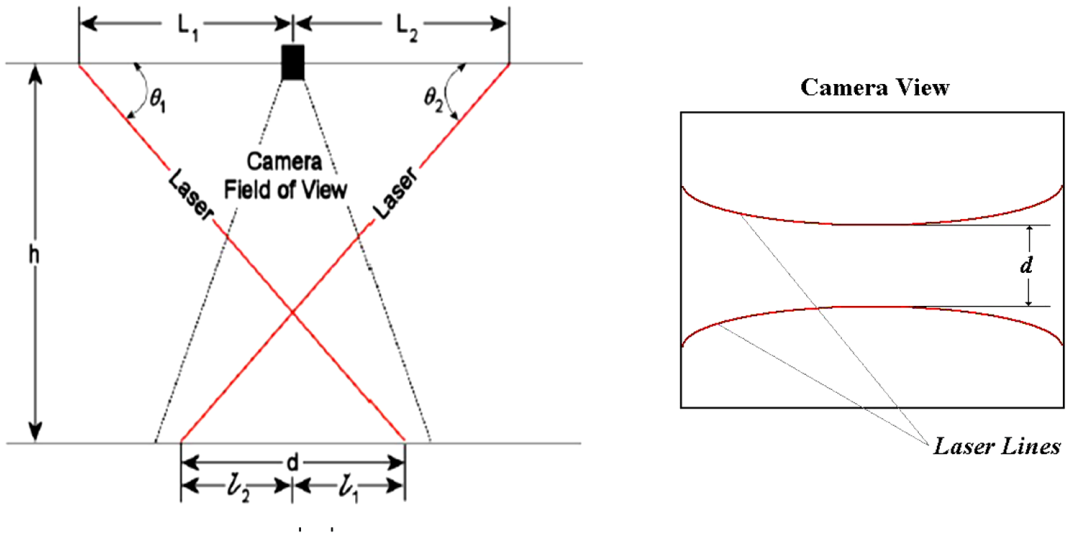

Figure 2.21: Continuous track modulus measurement system (Lu, *et al.*, 2008)

2.7 GROUND PENETRATING RADAR (GPR)

GPR is a non-destructive geophysical technique that uses electromagnetic waves to investigate nonconductive materials (Daniels, 1996). It is used in road, railway and geotechnical environments to detect concealed objects or to determine the internal structure of materials (Saarenketo, 2006).

This section includes the historical background and the development of GPR, GPR principles, electric properties of soil, equipment and processing of the results obtained from a GPR system. Unless otherwise stated, the information in this section was taken from *Ground Penetrating Radar* (Daniels, 2004) and *Ground Penetrating Radar Theory and Applications* (Jol, 2009).

2.7.1 Historical background of GPR

GPR has been used since the mid-1950's (El Said, 1956). Specifically in the 1970's it was used for transport infrastructure assessment. The first vehicle mounted systems were introduced in 1985. Also, in the 1990's GPR was used to determine layer thicknesses of road pavements (Morey, 1998). Initially, a high frequency air coupled antennae was used, followed by ground coupled antenna for road applications (Saarenketo, 2006).

GPR for railways was first used in Finland in the 1980's with discouraging results due to problems with data acquisition and processing (Saarenketo, 2006). It was then used again, with greater success, from mid-1990 until now (Galagher *et al.*1998, Jack and Jackson, 1999; Hugenschmidt, 2000; Sussman *et al.,* 2003; Saarenketo *et al.,* 2003). With respect to railway infrastructure it can be applied to ballast surveys (Clark *et al.,* 2001; Sussman *et al.,* 2002), geotechnical investigations (Saarenketo *et al.,* 2003; Sussman *et al.,* 2003; Carpenter *et al.,* 2004) and structural quality surveys (Maierhofer and Kind, 2002).

The development of GPR in the railway industry is as follows:

- Göbel, Hellman and Petzold (1994) first used GPR in Germany to determine ballast thickness, locate mudholes and ballast pockets and define subgrade soil boundaries.
- Hugenschmidt (1998, 2000) and Galagher *et al.* (1998, 1999) delivered the first successful reports on using GPR as a method for railway track inspection and ballast condition measurements in Switzerland and in the U.K. respectively. Jack and Jackson (1999) also evaluated GPR as a ballast and formation condition assessment tool.
- In the U.K., Clark *et al.* (2001) tested the electromagnetic properties of railway ballast. Clark *et al.* (2003a) used experimental and computer modelling to characterise ballast and Clark *et al.* (2003b) used GPR as a tool to characterize ballast. Brightwell and Thomas (2003) used GPR in the assessment of railway assets. Also, Clark *et al.* (2004) evaluated the use of GPR and infrared thermography as high speed non-invasive monitoring techniques.
- In Germany, Manacorda *et al.* (2002) used GPR for track verification.
- In North America, Olhoeft and Selig (2002) used GPR to evaluate railway track substructure conditions. Sussman *et al.* (2002) developed material properties for railway track materials for and Sussman *et al.* (2003) reported on railway track condition indicators using GPR.
- Staccone and De Haan (2003) explored the use of safe trackbed investigation using GPR in Austria, Switzerland, France, the Netherlands and Slovenia.
- In Sweden, Smekal *et al.* (2003) used GPR and a track loading vehicle for track substructure investigations and Berggren *et al.* (2006) used GPR for substructure condition assessment.
- In Finland, Saarenketo *et al.* (2003) used GPR to identify frost susceptible areas.
- Also, in North America, Narayanan *et al.* (2004) evaluated, by means of a multivariate linear regression analysis, that there is a relationship between railway track modulus and GPR reflectivities at specific depths.

- Eriksen *et al.* (2004) investigated the use of multi-channel GPR systems on road-rail vehicles to improve the productivity and reliability of ballast inspections.
- Silvast *et al.* (2006) investigated the use of GPR as a non-destructive technique (NDT).
- Al-Qadi *et al.* (2008) used scattering analysis to quantify railroad ballast contamination and Al-Qadi *et al.* (2010) investigated the use of multiple frequency GPR systems for the optimisation of railroad substructure investigation.
- Silvast *et al.* (2010) identified different GPR-based railway ballast degradation classes to establish a preventative maintenance system.
- Leng and Al Qadi (2010) evaluated the effects of ballast fouling in the laboratory with GPR and used short-time Fourier transform (STFT) to display the ballast fouling condition. This was validated with field trials.

2.7.2 GPR principles

GPR systems are used by transmitting a discrete pulse of ultra wideband radar energy, with a central frequency varying between 10 MHz and 2.5 GHz, into the ground surface. These short electromagnetic (EM) pulses are transmitted into the medium and are received when some of the energy is reflected off electrically distinctive interfaces between materials (Daniels, 1996). GPR originates from EM theory and can be described using the equations (Equation 2.18 to Equation 2.21) developed by Maxwell, that describes the physics of EM fields, and the constitutive relationship (Equation 2.22 and Equation 2.23) ,that describes material properties.

Maxwell's equations

$$\overline{\nabla} \times \overline{\mathrm{E}} = -\frac{\partial \overline{\mathrm{B}}}{\partial \mathrm{t}} \tag{2.18}$$

$$\overline{\nabla} \times \overline{\mathrm{H}} = \overline{\mathrm{J}} + \frac{\partial \overline{\mathrm{D}}}{\partial \mathrm{t}} \tag{2.19}$$

$$\overline{\nabla}.\overline{\mathrm{D}} = \mathrm{q} \tag{2.20}$$

$$\overline{\nabla}.\overline{\mathrm{B}} = 0 \tag{2.21}$$

Where:

$\bar{\nabla}$ = the divergence operator

$\bar{E}$ = electric field strength vector (V/m)

q = electric charge density (C/m^3)

$\bar{B}$ = magnetic flux density vector (T)

$\bar{J}$ = electric current density vector (A/m^2)

$\bar{D}$ = electric displacement vector (C/m^2)

$\bar{H}$ = magnetic field intensity (A/m)

t = time (s)

Constitutive relationships

$$\bar{J} = \tilde{\sigma}\bar{E} \tag{2.22}$$

$$\bar{D} = \tilde{\varepsilon}\bar{E} \tag{2.23}$$

$$\bar{B} = \tilde{\mu}\bar{E} \tag{2.24}$$

Where:

$\tilde{\sigma}$ = electric conductivity

$\tilde{\varepsilon}$ = dielectric permittivity

$\tilde{\mu}$ = magnetic permeability

The principles of the GPR technique are shown in Figure 2.22. A short EM pulse is generated and sent through the medium by the transmitting antenna. This pulse is then reflected back to the receiver when an electric interface is reached in the medium whilst the rest of the pulse proceeds. This reflected energy is displayed in waveform where the difference in amplitude shows the interfaces between wave pulses (Daniels, 1996; Saarenketo, 2006). A ground profile can be generated by repeating the measurements whilst moving the antenna across a target area with continuous series of radar pulses (Saarenketo, 2006; Sussman *et al.,* 2003; Hyslip *et al.*, 2003).

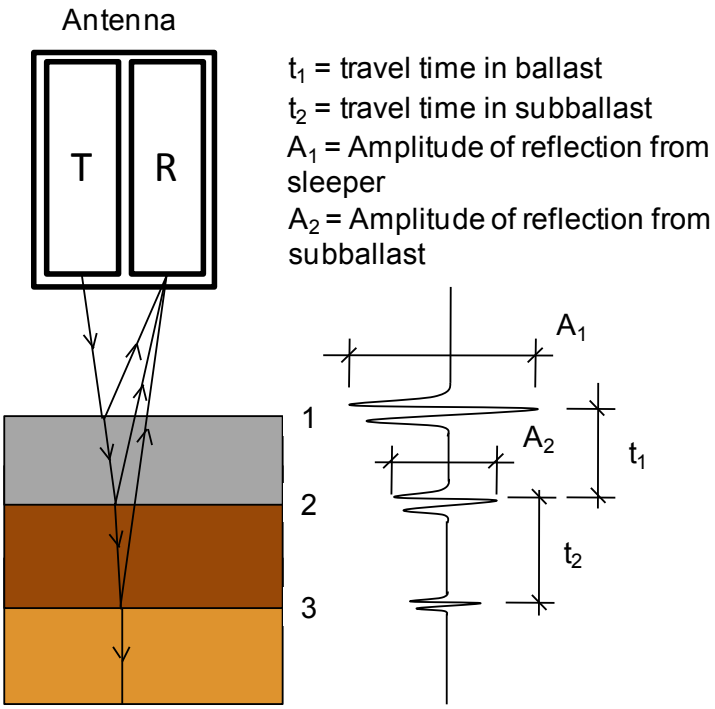

Figure 2.22: Basic principle of GPR redrawn from Saarenketo (2006).

The material properties that influence the propagation and reflection of the radar pulses are the dielectric permittivity, the electrical conductivity and the magnetic permeability as described by the constitutive relationships (Daniels, 2004; Jol, 2009). These parameters control the velocity of the radio pulses through the material layers and how fast the pulses' amplitude will decay. The pulse travels slower through material with a high dielectric permittivity and faster through material with a low dielectric permittivity. The radio pulses will decay faster in material with high electric conductivity and slower in material with low electric conductivity. Therefore it will penetrate deeper in material with low electric conductivity (Saarenketo, 2006; Hyslip *et al.,* 2003). Dielectric permittivity and its effect on GPR signal velocity in material are the most important properties that affect GPR survey results. It is important to know how the dielectric permittivity relates to the medium being tested in order to calculate the depth of the target (Saarenketo, 2006).

2.7.3 Dielectric Permittivity

The measure of a material to store charge at a given applied field strength is the dielectric value (Saarenketo, 1998). The complex dielectric permittivity value (ε), is a function of frequency. Relative dielectric permittivity $K^*(\omega)$ (dielectric value or dielectric constant) can

be expressed as shown in Equation 2.25. The $K^*(\omega)$ value is the ratio of complex dielectric permittivity to the dielectric permittivity of free space (ε_0). The dissipation term is defined by the imaginary part of the dielectric value (Hoekstra and Delaney, 1974; Davis and Annan, 1989). The relationship between the dissipation term (K'') and electrical conductivy (σ) is represented by Equation 2.26. The loss tangent ($\tan\delta$) is given in Equation 2.27 (Hoekstra and Delaney, 1974).

$$K^*(\omega) = K'(\omega) - iK''(\omega) \tag{2.25}$$

$$K''(\omega) = \frac{\sigma}{\varepsilon_0 \omega} \tag{2.26}$$

$$\tan\delta = \frac{K''(\omega)}{K'(\omega)} \tag{2.27}$$

Where:

ω = angular frequency

K' = real part of the dielectric value, varying between 1 (air) and 81 (free water)

K'' = imaginary part (the dissipation term) of the dielectric value

ε_0 = dielectric permittivity of free space, 8.85 x 10^{-12} F/m

The real part of the dielectric permittivity can range from 1 to 81 in soil; 1 for air and 81 for free polar water (Saarenketo, 2006). Table 2.5 provides dielectric permittivity values obtained from research. The dielectric permittivity of ballast and subgrade material varies between 3 and 38.5, from clean dry ballast to saturated fouled ballast respectively (Clark *et al.,* 2001). However, the effect of moisture on dielectric permittivity is greater than that of the material type itself (Clark *et al.,* 2001; Leng and Al Qadi, 2010).

Table 2.5: Typical dielectric permittivity values (Jol, 2009; Clark *et al.*, 2001).

Material	Relative dielectric permittivity ϵ_{ave}
Clay (dry)	2-20
Clay (wet)	15-40
Sand (dry)	3-6
Sand (wet)	10-30
Soil (sandy, dry)	4-6
Soil (sandy, wet)	15-30
Soil (clayey, dry)	4-6
Soil (clayey, wet)	10-15
Ballast (dry, clean)	3
Ballast (wet, clean) 5% water	3.5
Ballast (saturated, clean)	26.9
Ballast (dry, fouled)	4
Ballast (wet, fouled) 5% water	7.8
Ballast (saturated, fouled)	38.5
Concrete (dry)	4-10
Concrete (wet)	10-20

2.7.4 Basic equations for GPR surveys

The following formulae from Ground Penetrating Radar (1992) as explained by Saarenketo (2006) and Leng and Al-Qadi (2010) can be used in GPR surveys if it is assumed that magnetic susceptibility can be ignored. These equations can be used to determine different electromagnetic properties of materials. They are the combination and simplification of electromagnetic theory for use in GPR applications.

$$v = \frac{\mathrm{c}}{\sqrt{\epsilon_r}} \tag{2.28}$$

$$s = \frac{vt}{2} \tag{2.29}$$

$$k = \frac{(\sqrt{\epsilon_{r_2}} - \sqrt{\epsilon_{r_1}})}{(\sqrt{\epsilon_{r_2}} + \sqrt{\epsilon_{r_1}})} \tag{2.30}$$

$$R = 1 - k \tag{2.31}$$

$$A = \frac{1635\,\sigma}{\epsilon_r} \tag{2.32}$$

$$I = \frac{1000\,c}{f\sqrt{\epsilon_r}} \tag{2.33}$$

Where:

v = wave propagation speed (m/ns)

c = speed of light in a vacuum (0.3 m/ns)

s = interface depth (m) from the surface of the medium

t = two-way travel time from the soil surface to the interface depth (ns =10^{-9})

k = reflection coefficient

ϵ_r = relative dielectric permittivity of the soil

ϵ_{r_n} = relative dielectric permittivity of the nth layer

R = penetrating coefficient

A = attenuation in the medium (dB/m)

σ = electrical conductivity of the medium (S/m)

I = wavelength

f = frequency (MHz)

Using Equation 2.28 and Equation 2.29, the dielectric permittivity (ϵ_r) of the soil can be determined. With the determination of the ϵ_r of different layers, the reflection coefficient (k) and the penetration coefficient (R) can be determined by Equation 2.30 and Equation 2.31. From this, the attenuation (A) and the wavelength (I) can be determined with Equation 2.32

and Equation 2.33. The material quality information can be determined by using the time domain GPR data and converting it to the frequency domain with the use a Fourier transform (Silvast *et al*., 2006). This is used to determine the ballast fouling and the moisture condition and is calibrated with field measurements (Silvast *et al*., 2010).

2.7.5 GPR hardware and accessories

Both impulse radar systems and stepped frequency radar systems can be used for road and railway GPR surveys (Saarenketo, 2006). Typical GPR system components consist of the following:

- GPR antennae (ground coupled or air coupled, with transmitter/receiver electronics)
- Cables
- GPR control unit
- Pulse encoder with other positioning units
- Accessory equipment (This can include image capture equipment, global positioning systems (GPS) and three dimensional laser technology.)

A typical layout of the equipment used in railway surveys is given in Figure 2.23 below (Eriksen *et al*., 2004; Saarenketo, 2006; Al Qadi *et al*., 2008). The placement of the antennae may be in front or behind the vehicle.

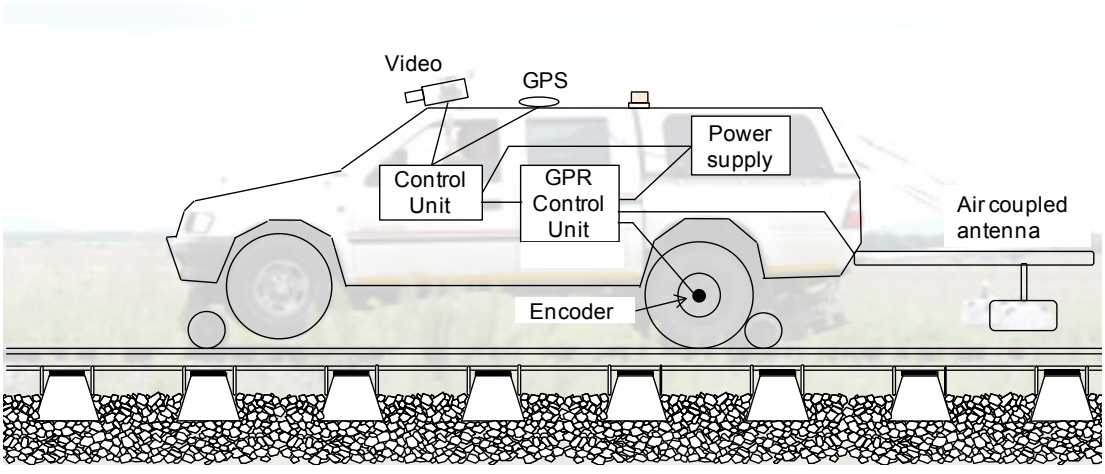

Figure 2.23: A GPR system for railroad surveys.

An antenna carries the radio frequency energy from a source into a transmitting medium. For GPR this is usually the ground. An antenna can transmit energy, receive energy or do both. Two types of GPR antenna systems are used, namely air coupled systems and ground coupled systems (Saarenketo, 2006). A comparison of the two systems is given in Table 2.6. Air coupled antennae are preferred for railway surveys as they are less easily damaged by the ballast compared to ground coupled antennae (Clark *et al.*, 2004; Saarenketo, 2006).

Table 2.6: Comparison of air coupled and ground coupled GPR systems.

Characteristic	Air coupled system	Ground coupled system
Radar	Pulse radar systems.	-
Frequency	500 MHz to 2.5 GHz	80 MHz to 1.5 GHz
Signal penetration	Signal penetration of 0.5 – 0.9 m.	Signal penetration of up to 20 – 30 m.
Antennae	Types: TEM horn antenna or hemispherical butterfly dipole (HAD) antenna.	-
Suspended height	During acquisition these antennae are suspended 0.3 – 0.5 m above the ground.	During acquisition these antennas are in contact with the surface or suspended just above it. However if this is done the suspended distance should stay constant.
Consistency	Repeatability, due to the antenna coupling method that stays consistent regardless of changes in the measured surface.	Rigging makes it difficult to repeat results and obtain near surface information
Operating speed	Can operate at traffic operating speed.	Operating speed of 5 – 30 km/h.
Signal quality	Cleaner signal.	Deeper signal penetration, but near surface signal needs processing.

Antennae used in GPR railway surveys are mostly bi-static meaning that both the transmitting antenna's as well as the receiving antenna's electronics are contained in the same antenna box (Saarenketo, 2006). Because of enhancements in technology as well as larger storage capabilities, multi-channel antenna systems are more readily available and allow for faster acquisition speeds (Clark *et al.*, 2004). Optimum antenna frequencies obtained are 1 GHz horn antennae (Olhoeft *et al.,* 2004) but due to EM emission rules by the FCC (Federal Communications Commission) , 400 MHz and 2 GHz antennae are used in North America

and 400 and 500 MHz antennae (Clark *et al*., 2003b; Saarenketo *et al.*, 2003) in the UK and Finland. Some advantages of multi-channel systems are as follows:

- Air coupled and ground coupled antenna systems can be used at the same time.
- Antenna array techniques can be used to determine signal velocities (Davis *et al.,* 1994; Mesher *et al.,* 1995)
- Multi-channel systems allow for the simultaneous measurement of different survey lines to create a 3D model of the surveyed line (Davidson and Chase, 1998; Manacorda *et al.,* 2002).

Due to the uniqueness of GPR systems, differences in signal readings are obtained. This, together with the performance deterioration of older antennas can affect the accuracy of systems (Saarenketo, 2006). Thus, performance comparison tests were developed to evaluate the performance of different antennas (Scullion *et al.,* 1996). Some of these tests are the noise to signal (N/S ratio) test, signal stability test, travel-time linearity test and the long-term stability test. Repeatability tests for different GPR systems or single GPR systems could also be done (Saarenketo, 2006).

Many other accessories can be used in conjunction with GPR systems. However, digital video and global positioning systems (GPS) are most commonly used. A sample drilling rig (Saarenketo, 2006) as well as infrared thermography (Clark *et al.*, 2003 b; Clark *et al.*, 2004) can also be integrated with GPR data. Smekal *et al.* (2003) used a track loading vehicle in conjunction with GPR results. Digital video allows the interpreter to evaluate the surroundings of the GPR survey after the initial survey (Clark *et al.,* 2004). By using these accessories together with the GPR survey data, a comprehensive understanding of the site can be established (Saarenketo, 2006).

2.7.6 GPR data collection

To carry out a thorough GPR survey, a detailed outline of the survey needs to be set up (Saarenketo, 2006). For a railway survey, the number of survey lines to be used needs to be determined as well as where they would be positioned. The primary survey line would be between the rails, but survey lines could also be taken on both sides of the railway track. If this data is combined, a cross section of the railway track can then be obtained (Saarenketo, 2006; Clark *et al.,* 2001; Morey, 1998).

GPR collection, however, has limitations. Typical examples are the difficulty of surveys in wet weather, due to the sensitivity of the dielectric constant to moisture and the survey speed.

The accuracy of data collection due to speed has been tested at 70 km/h and 80 km/h and errors of 5% and 9% of the dielectric values were obtained respectively (Hopman and Beuving, 2002).

Data collection for GPR surveys are site specific. A typical sampling density of 10 scans/m is used for railways (Saarenketo, 2006). Furthermore, gain and filter settings also need to be set. To determine the proper gain settings, calibration needs to be done and stored in the control unit. Filtering should be applied to remove noise and ringing and in such a way that it does not affect the actual data but rather makes it clearer. It should also be kept in mind that filtering can be done afterwards.

Care should be taken to accurately position the GPR data (Saarenketo, 2006). Some positioning methods are given below:

- Encoders that control the sampling interval
- Adding markers at known reference points to the GPR data
- GPS and video recording synchronized with the GPR data

2.7.7 GPR data processing and interpretation

GPR data processing, interpretation and visualisation are the time consuming phases of a GPR project. The GPR processing software is used to detect layer interfaces, individual objects within the ground from GPR data and transforming the GPR data from the time domain into depth scale (Saarenketo, 2006). Descriptions of GPR data processing is given by Daniels (1996), Daniels (2004) and Jol (2009). The phases of GPR processing are as follows:

- Pre-processing phase
- Data processing phase
- Interpretation phase
- Reporting phase

In the pre-processing phase, data editing is done in a way that ensures the data itself is not changed. Some of the tools used are file reversal, cutting and combining, scaling and linking of other GPR system data to the GPR survey data. Signal polarity should also be changed so that the colour scales are correct. GPR data processing is different for air coupled and ground coupled GPR survey methods. The signal processing methods are described in the GPR software manuals (Saarenketo, 2006).

Accurate estimates of layer dielectric values are important for GPR data processing. Traditionally, dielectric values are back-calculated from reference sampling. Another method in use is the surface reflection method (Maser and Scullion, 1991). If the dielectric values are not available for a GPR survey, general dielectric values can be used from Table 2.5. These values are required for the successful interpretation of the railway structure, defining the substructure layers and determining the moisture content. Also, estimates of moisture susceptibility, moisture sensitivity and compressibility of subgrade soils, homogeneity and ballast fouling can be made.

GPR survey data contains reflections from various components within the whole surveyed structure (Saarenketo, 2006). Therefore, to interpret GPR survey data, a thorough understanding of the surveyed structure is needed. In some cases reflection from components next to the track may influence the data. The interpreter should therefore interpret the main components first. For railways these are as follows:

- Ballast
- Subballast
- Thickness of the whole structure
- Embankment

It should also be noted that GPR survey data could be linked to other survey methods to get a better understanding of the GPR data itself (Clark *et al.*, 2003b; Clark *et al.*, 2004; Saarenketo, 2006).

2.8 TRACK INVESTIGATION TECHNIQUE COMPARISON

In order to understand which track investigation technique to use, a comparison in the form of a rating system is given in Table 2.7. The rating comprises the possible or the required sampling per kilometre, the cost effectiveness, the effectiveness and the value of the testing procedure. The sampling per kilometre is either for the required amount of samples needed to definitively describe the track condition or the possible sample rate. The cost effectiveness is related to the cost of the testing per kilometre. The effectiveness of the tests is attributed to the ease of obtaining parameters and the time taken after testing for obtaining parameters. The value provides an indication of what merit the test will have for a track engineer who needs to make design and maintenance decisions.

The rating is between 5 for a good and positive rating and 1 for a poor or negative rating. The values for the rating system were established by evaluating at the descriptions of the test methods within the literature study.

Table 2.7: Evaluation of track investigation techniques

Track Investigation technique	Sampling per kilometre (possible or required)	Cost Effectiveness (R/km)	Effectiveness (ease and parameters obtained)	Value (detail obtained from the testing)	TOTAL (Rating)
	Rating: High (5) - Low (1)				
CSW	1	2	1	3	7
MDD	1	1	3	5	10
DCP	3	5	2	1	11
Pencel Pressuremeter	2	3	2	4	11
Test Pits and soil sampling	2	3	4	4	13
LWD	3	5	3	3	14
RVM	3	4	3	5	15
Continuous track modulus measurements	5	4	3	5	17
GPR	5	4	3	5	17

Table 2.7 shows that the two continuous measurement techniques (GPR and track modulus measurements) are rated highest. Thereafter, RVM, LWD, test pits and sampling follow. The next group of tests are the DCP, Pencel pressuremeter, MDD and CSW. Each of the techniques has advantages and disadvantages for their use as part of track substructure evaluation.

GPR and continuous track modulus measurements provide continuous results with no need to disrupt train operations.

2.9 DISCUSSION

To develop a railway substructure characterization model, an understanding of the complete railway track structure is needed. The functions of each component provide an understanding of how the forces from the rolling stock are transferred to superstructure and then to the substructure of the track. It also provides insight into the difficulties of conducting tests at the substructure level.

Furthermore, understanding the geometry of the track provides an indication of track operating conditions as provided by the profile and versine roughness. It also gives the framework as to where track testing equipment is allowed during normal operating conditions on and off the track. This also includes the placement of equipment on locomotives and road rail vehicles.

Knowing how the different substructure layers are designed, classified and how their properties are measured, give an indication of what needs to be measured to determine the condition of a railway track substructure. This could also be used for the selection of the correct track testing equipment.

The track substructure can be evaluated using different track substructure investigation techniques, each providing different parameters. The parameters from each of these techniques can be used for the characterization of the track. However, the cost and the frequency of these techniques need to be evaluated and their use needs to be justified. The use of GPR as a non-invasive track condition measurement tool will therefore be evaluated for the characterization of the track substructure.

GPR has been used extensively as a substructure investigation tool across the world for the last two decades. A need therefore exists for more in depth GPR substructure investigations, especially in South Africa. GPR and other substructure investigation tools can be used to find correlations between the different characterization methods.

The GPR characterization of the track can be used as a non-invasive method for overall characterization of any length of track. This will result in a reduction of track substructure evaluation cost. Furthermore, a GPR characterization model would enable the identification of critical sections of track where more in-depth track substructure evaluation should be done using specialized testing equipment.

The literature discussed in this chapter highlights the need, which forms the purpose of this study, to evaluate the use of GPR as a track substructure characterization tool.

CHAPTER 3

3. FIELD AND LABORATORY TESTS

To develop a track substructure investigation tool or model from Ground Penetrating Radar (GPR), a comparative study needs to be conducted between GPR and other railway track substructure investigation tools. Two sites were selected in South Africa for this study. This included a section on the heavy haul Coal export line near Vryheid between Komvoorhoogte and Nhlazatshe (km 50 to km 70). A second site was selected on the railway line near Rustenburg between Northam and Thabazimbi (km 203 to km 223). The two railway lines are shown in Figure 3.1 with an overview of the two sites in Figure 3.2.

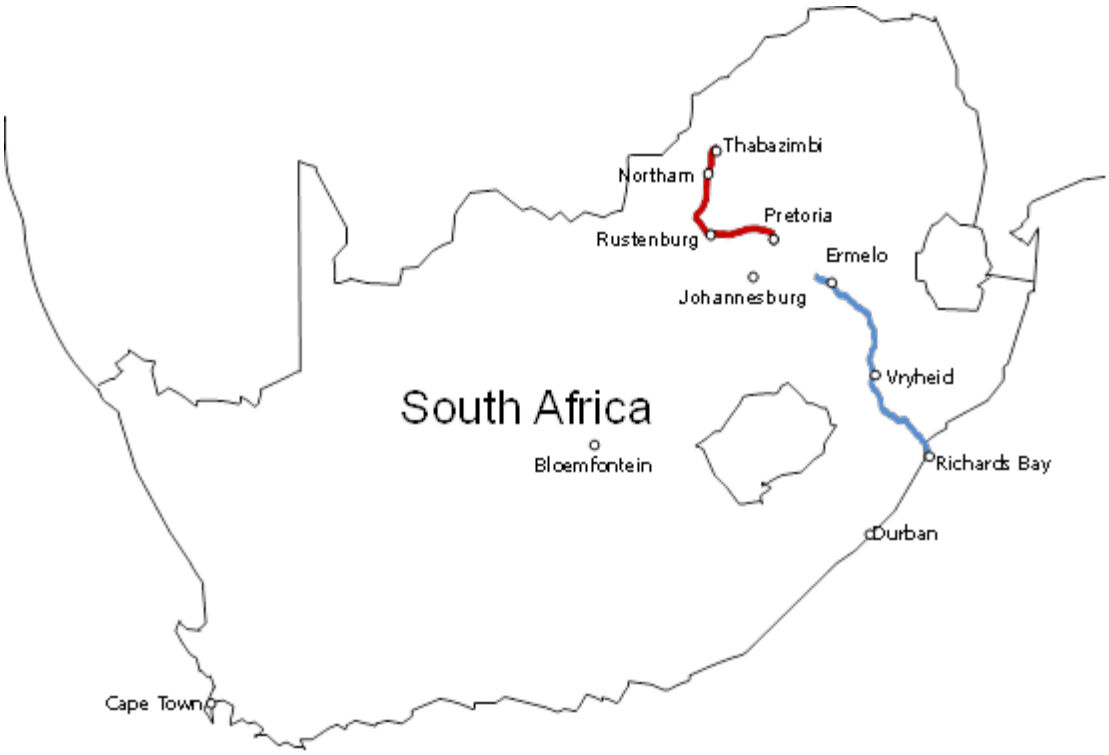

Figure 3.1: Location of the two test sections in South Africa.

a)

b)

Figure 3.2: Location of a) KN test section and b) NT test section (Google Earth, 2012).

Furthermore, laboratory tests using GPR equipment were conducted at the University of Pretoria on ballast materials typical of those found at the two track sections. The materials used was quartzite obtained from a Pretoria quarry and dolerite obtained from a Vryheid quarry. The ballast material was fouled using clay from the Bushveld Igneous complex near Thabazimbi. The fouling material was used only to provide an indication of the ballast fouling and is not typical at both test locations. Results obtained with GPR equipment were used for the comparison of the two ballast materials. A method similar to that of Leng (2010) was used. The main deliverable from this laboratory study was the dielectric permittivity of the ballast materials obtained from the GPR analysis.

For the model to be complete, geotechnical field testing methods needed to be compared to the GPR field results. Sampling and profiling of the layerworks would also be needed. The tests were done on both sections of track at the sites that were identified from the GPR results. Six test sites were investigated at each of the two test sections. The testing was limited to the most common tests used in the railway environment to evaluate the substructure. These included:

- LWD
- DCP
- MDD
- RVM

Sampling and profiling of the substructure layers were also needed. The following properties were obtained from the samples.

- Ballast fouling index
- California Bearing Ratio (CBR)
- Foundation indicators (FI)
- In situ moisture content

3.1 PURPOSE OF THE INVESTIGATION

The purpose of the investigation can be summarised as follows:

1. To obtain typical foundation condition parameters to characterize the foundation by using GPR.

2. Determine typical dielectric properties from GPR tests conducted on ballast material, including dolerite and quartzite, and evaluate the effect of moisture increase and fouling on these properties.
3. Determine in situ dielectric properties of the different foundation layers while also looking at the moisture content and ballast fouling index obtained from the in situ GPR testing.
4. Evaluate the use of RVM as a foundation condition assessment tool.
5. Evaluate the results obtained from LWD and RVM testing.
6. Obtain typical ground properties from the two selected sections of railway track.

3.1.1 Selection of the Tests

The selection of tests for the characterization of the track substructure was based on the parameters obtained from them. The ease of using the different test methods was also considered in the selection. GPR was used for continuous measurements and for the final characterization of the track substructure as it provides the most deliverables continuously. To effectively compare the deliverables from the GPR survey, test pits with soil sampling were used. Furthermore, for the ease of the testing method and for a more complete comparison of the characterization model, DCP, LWD and RVM measurements were also conducted. The geometry data obtained from the IM2000 and provided by Transnet, was also used as it is already used as a continuous track evaluation tool. The parameters provided by each of the measurement techniques are listed in Table 3.1 and are described in more detail in Chapter 3.

Table 3.1: Test selection and measurement parameters.

Test	Parameters
GPR Laboratory	Ballast dielectric permittivity
GPR Field	Substructure layer thickness Ballast fouling Index Moisture content In situ soil layer dielectric permittivity
DCP	Penetration (mm/blow) CBR
LWD	Foundation Modulus
RVM	Track and substructure deflection (mm) Track Modulus Substructure Modulus
MDD	Substructure deflection (mm) Track Modulus Substructure Modulus
Test Pits	CBR, FI and in situ moisture content

3.1.2 Methodology

The process followed to develop a foundation condition or characterization model with GPR was as follows:

Firstly, railway track sections with unique foundation conditions were identified. This was done to obtain a range of possible track substructure conditions. The types of ballast material used at the selected track sections were identified for the purpose of carrying out the GPR laboratory tests. Ballast samples were obtained at the relevant quarries and the necessary preparations were done to conduct the GPR tests.

Thereafter, the GPR equipment was attached to a road-rail vehicle to conduct the GPR survey at the two proposed sites. The GPR antennae were attached at the back to the left and to the centre of the vehicle. The survey was then conducted at each of the sites with the antennae kept in this position in one direction. Thereafter, the vehicle was turned around, keeping the antennae in the same position. This meant that four survey lines were obtained, one on the left side of the track, two in the middle and one on the right side of the track. The GPR data collected at the two testing sites were evaluated by Roadscanners in Finland.

After the processed GPR data was obtained, geometry and ground truth data had to be added. Using the GPR results (layer thickness, fouling index and moisture percentage) and geometry data obtained from the IM2000, a small number of verification sites were identified on each of the two test sections.

Standard as well as specialized tests were conducted at each of the selected verification sites. Firstly, LWD and DCP tests were done after clearing the ballast. A ballast sample was taken for laboratory testing. Where possible, a test pit was excavated to a depth of approximately 1m, followed by the collection of soil samples of the relevant layers.

To further evaluate the site conditions, RVM tests were done. One camera was positioned four sleepers to the left of the test pit and another camera four sleepers to the right of the test pit. At each of these locations, targets were placed on the side of the sleeper and on a rod cemented to the surface of the subgrade. Another target was placed on a rod driven 400 mm into the ground.

To complete the site experimentation, the site was restored as close as possible to its original condition.

3.2 SITE DESCRIPTION AND SELECTION

The two test sections were selected according to their substructure conditions. For the foundation condition model to be effectively calibrated, a data range ranging from poor substructure conditions to good substructure conditions was required. The one site was on Transnet Freight Rail's Coal export line near Vryheid and the other on a general freight railway line near Rustenburg. The tests sections selected for the study are described in Section 3.2.1 and Section 3.2.2.

3.2.1 Site Description: Komvoorhoogte to Nhlazatshe (KN)

The first section of track is located approximately 50 km from Vryheid in Kwazulu-Natal on Transnet Freight Rail's Coal export line in South Africa. The section of track used for the testing is situated between Komvoorhoogte and Nhlazatshe (km 50 to km 70). This section was selected because the substructure was reconstructed according to the S410 track substructure design standards in 2005. It could therefore be expected that this section would have a good substructure.

The dimensions and properties for the track design are shown in Figure 3.3 and Figure 3.4. As shown, the design differs for embankments and cuttings.

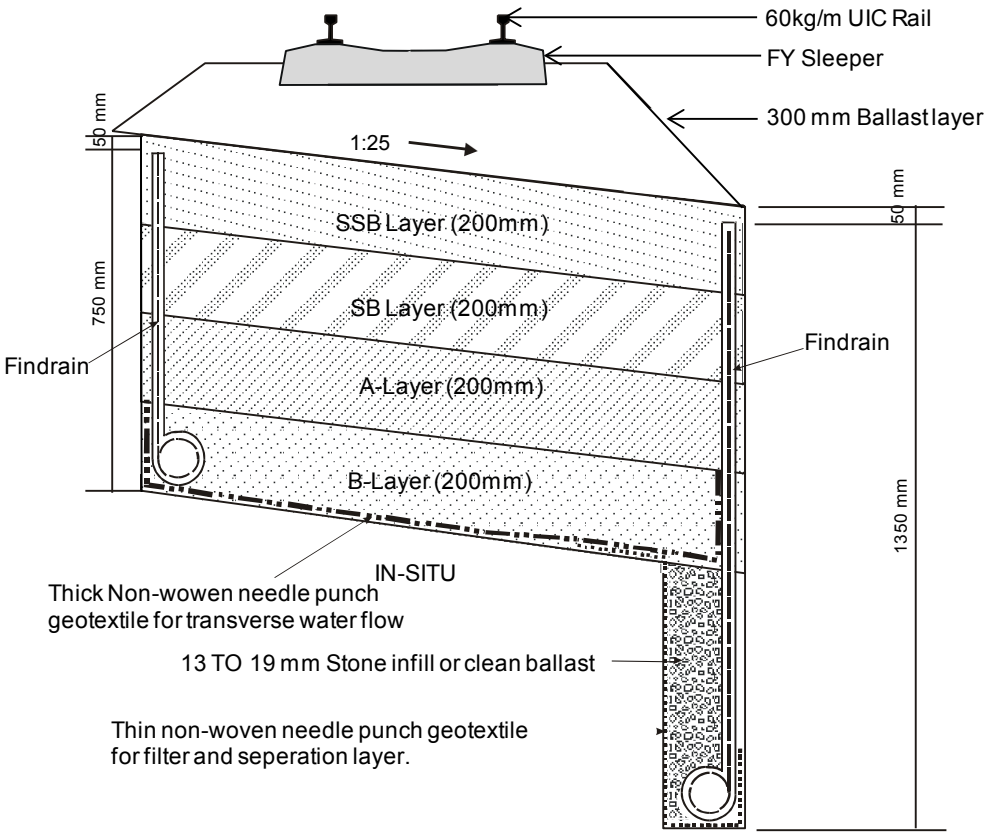

Figure 3.3: Coal line formation design for cuttings (26t/axle).

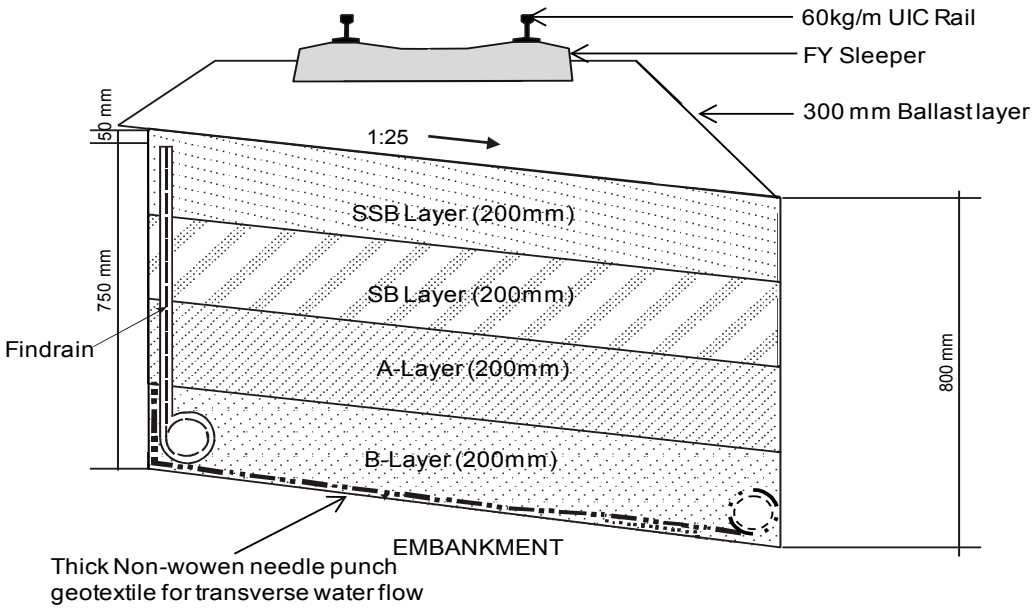

Figure 3.4: Coal line formation design for embankments (26t/axle).

3.2.2 Site Description: Northam to Thabazimbi (NT)

The second section of track located near Rustenburg between Northam and Thabazimbi (km 203 to km 248) was selected because of its poor substructure conditions. It is an old track, constructed in 1934 with a substructure consisting predominantly of clay.

The track properties for the track design are shown in Figure 3.5. There are no design parameters for the track substructure due to the age of the track. A fouled ballast layer of 100 mm has formed over the years from the interpenetration of the ballast and subgrade material.

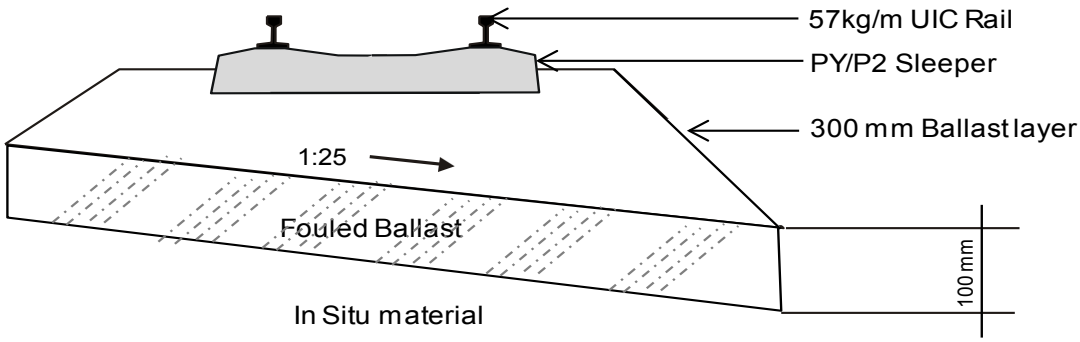

Figure 3.5: In situ substructure conditions for the Northam to Thabazimbi section.

3.3 GPR LABORATORY TESTING

The GPR laboratory testing procedure and typical results obtained from the tests are discussed in this section.

3.3.1 Testing procedure

To evaluate the dielectric properties of the ballast obtained at the two test sections, laboratory tests using GPR were conducted. The equipment used for these tests was as follows:

- GSSI SIR-20 amplifier
- Two GSSI 400 MHz antennae (model 5103A)
- 1 GHz antenna
- Railway Doctor Software developed by Roadscanners

Firstly, wooden boxes to hold the ballast had to be constructed. The size of each wooden box was 1.2 m x 1.2 m x 1 m. No metal nails were used in the construction to decrease the antenna noise that it could present to the GPR signal. This however created a challenge in keeping the boxes intact. To join the sides, the edges were cut to fit into each other (see Figure 3.6a). In addition, dowels were inserted in the opposite direction to further increase the strength of the sides. Plastic strapping was used for further reinforcement of the boxes as shown in Figure 3.6d.

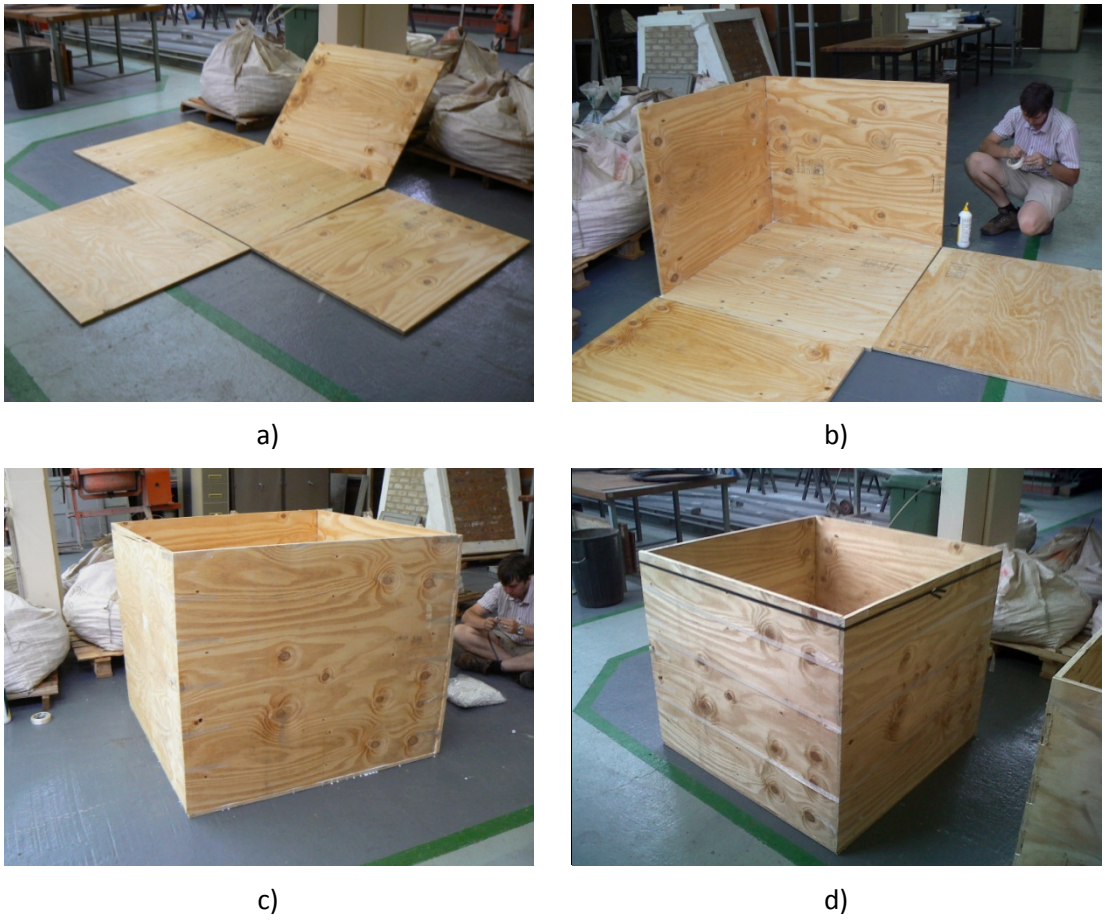

a) b)

c) d)

Figure 3.6: GPR laboratory tests box a) assembly, b) fixing, c) lifting and d) strapping.

The inside of the boxes were lined with plastic sheeting to improve waterproofing. After the sheeting was placed, each box was secured by strapping fibre glass tape around the sides. Four boxes were constructed using this method for the testing of the different ballast materials. The four constructed boxes with the lining and tape is shown in Figure 3.7.

Figure 3.7: The final constructed boxes for GPR laboratory tests

Two of the boxes contained dolerite and two boxes quartzite. One box of each type of ballast was fouled using weathered Norite (Black Turf). The relative density (RD) of the three materials was determined according to TMH1 (1986) and was as follows:

- Dolerite RD = 2.632
- Quartzite RD = 2.990
- Norite clay RD = 2.069

The fouling material was first air dried (see Figure 3.8a) and then oven dried for longer than a day (see Figure 3.8b). Once the material was removed from the oven, it was placed in a ball mill to remove the lumps (see Figure 3.8c). The dried material was weighed and placed in containers ready for placement in the boxes (see Figure 3.8d). The complete process of drying this material is shown in Figure 3.8. This material was added to two of the boxes after a layer of ballast was placed and before compaction.

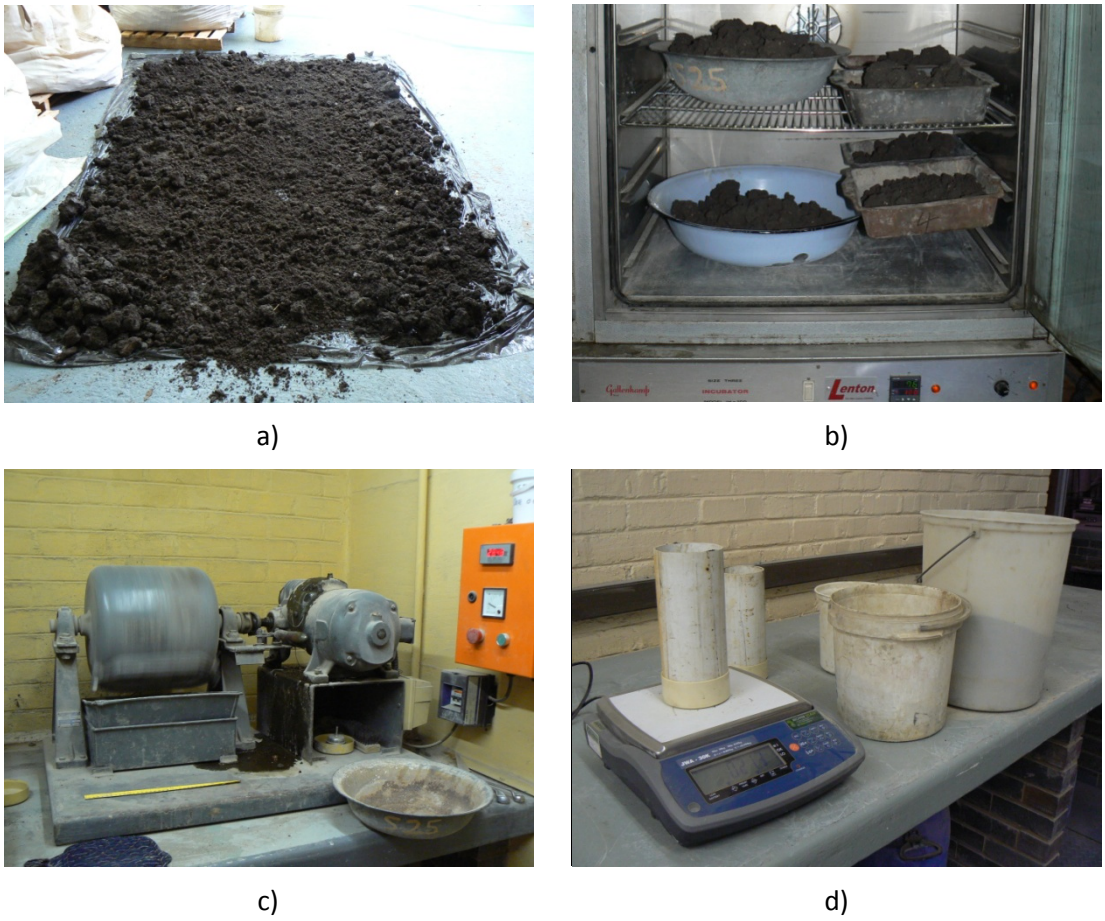

Figure 3.8: Material a) air drying, b) oven drying, c) milling and d) weighing for GPR lab testing.

The boxes were incrementally filled with the ballast material. This was done by constructing layers of 100 mm which were compacted. To place the ballast material in the boxes, the ballast material was first placed in bulk bags. These bags were hoisted above the boxes (see Figure 3.9a) and the ballast material dispensed from the bottom (see Figure 3.9b). To measure the amount of material disposed into each layer, a load cell was attached to the hoist (see Figure 3.9a). The difference in load was measured and shown on the load cell. This information was used to determine the relative density of material within the boxes. The material was levelled with a ballast fork as shown in Figure 3.9d.

a) b)

c) d)

Figure 3.9: Laying of ballast material in boxes.

The fouled material was added in a 3 x 3 grid (see Figure 3.10a, b). Equal amounts of fouled material were placed in each of the blocks and compacted (see Figure 3.10c). Thereafter, the next layer was placed (see Figure 3.10d).

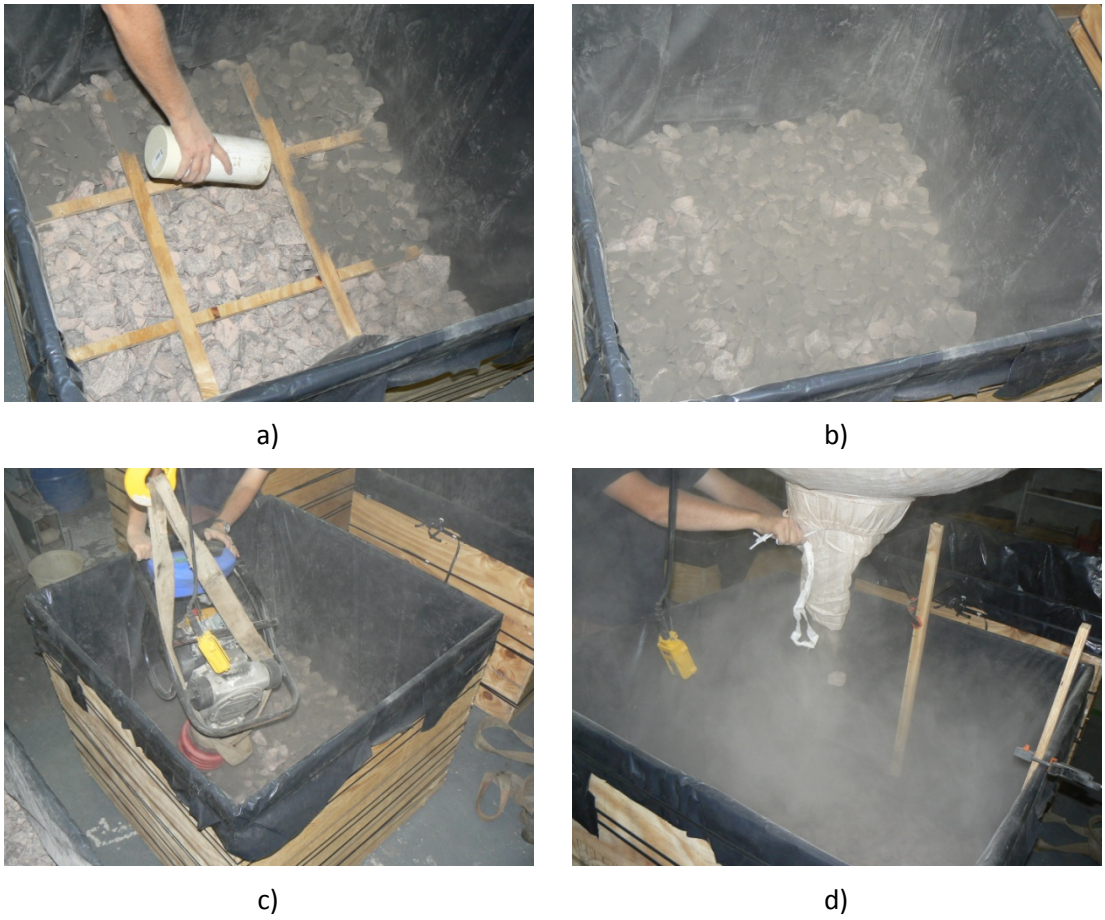

a) b)

c) d)

Figure 3.10: The a) distribution, b) spreading and c) compaction of the fouling material and d) placement of next layer of ballast

Detailed descriptions of these boxes are given in Table 3.2 and Table 3.2 and the completed boxes are shown in Figure 3.11.

Table 3.2: Details of the quartzite ballast box.

Box no. and Material Type		Layer Depth (from top of ballast) (mm)		Thickness (mm)	Mass (kg)/Volume (*l*)				Porosity (n)	% Fouled
					Total	Ballast	Fouled Material	Void		
1	Quartzite (Control)	1	282	282	588/ 382	588/ 223	0/0	0/ 159	41.52	0.00
2	Quartzite (Fouled ballast)	1	200	200	453/ 271	453/ 172	0	0/ 99	36.47	0.00
		2	380	180	416/ 244	407/ 155	9/4	0/ 85	34.80	5.12
		3	504	124	276/ 168	267/ 101	9/4	0/ 62	37.02	6.99
		Total		504	114/ 683	428	9	246	36.01	8.41

Table 3.3: Details of the dolerite ballast box

Box no. and Material Type		Layer Depth (from top of ballast) (mm)		Thickness (mm)	Mass (kg)/Volume (*l*)				Porosity (n)	% Fouled
					Total	Ballast	Fouled Material	Void		
3	Dolerite (Control)	1	272	272	644/ 369	644/ 215	0	0/ 153	41.57	0.00
4	Dolerite (Fouled ballast)	1	300	300	644/ 406	644/ 215	0	0/ 191	47.02	0.00
		2	470	170	444/ 230	435/ 145	9/4	0/ 81	34.96	5.40
		3	588	118	253/ 160	244/ 82	9/4	0/ 74	46.08	5.90
		Total		588	135/ 797	443	9	345	43.34	9.79

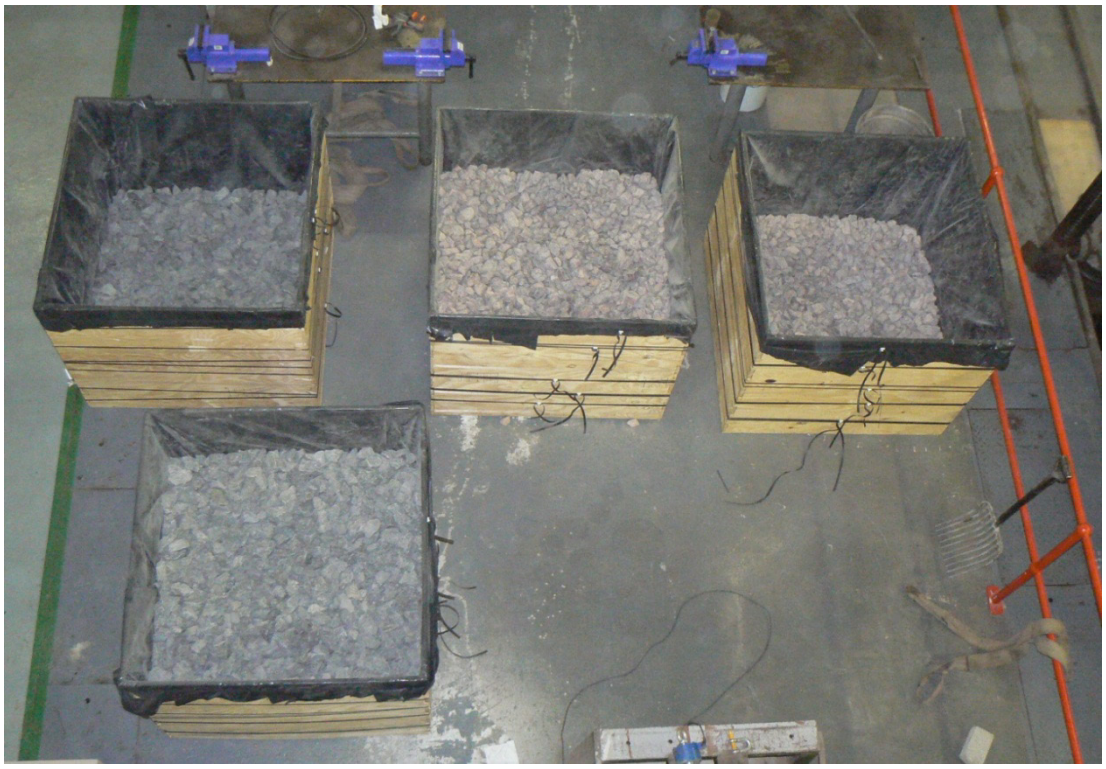

Figure 3.11: Completed boxes containing ballast material.

Testing in each of these boxes was conducted with both the 400 MHz antenna shown in Figure 3.12a and the 1 GHz antenna shown in Figure 3.12b. The first three tests were conducted with the 400 MHz airborne antenna.

a) b)

Figure 3.12: (a) 400 MHz and (b) 1 GHz antennae.

The first test was a static test whereby the 400 MHz antenna was kept stationary 300 mm above the surface of the ballast material (Figure 3.13a). The second test started with the

antenna 300 mm above the surface of the ballast where after the antenna was slowly lifted 1m above that point and brought down to its original position (Figure 3.13b). Both of these tests were conducted to remove background noise received by the antenna. The next test was a moving test where the antenna was 300 mm above the ballast surface at the side of the box and then moved slowly towards the other end (Figure 3.13c). The last test was done with the 1 GHz antenna and was on the surface of the ballast and started from the one side of the box and ended on the opposite side of the box (Figure 3.13d).

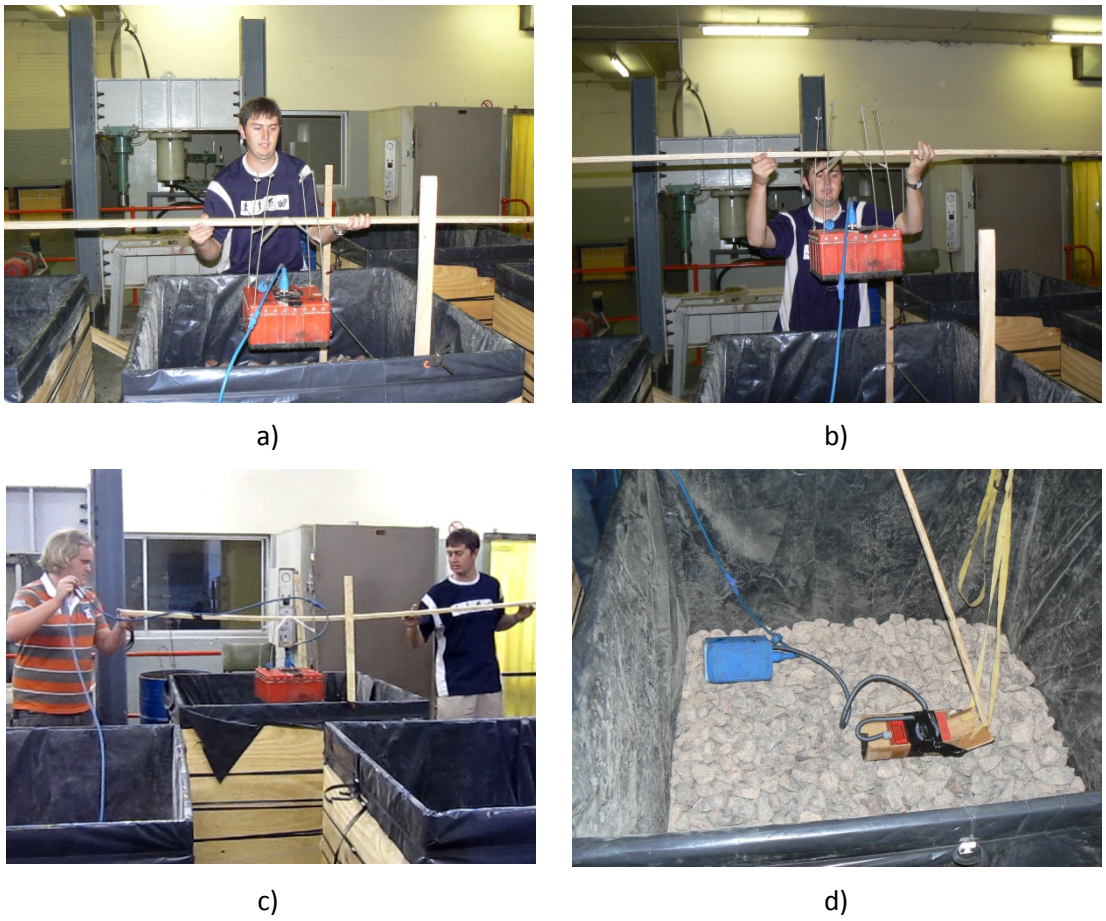

a) b)

c) d)

Figure 3.13: GPR laboratory tests; 400 MHz a) static, b) lifting, c) horizontal movement and 1 GHz d) horizontal movement.

The tests were first conducted when all four boxes were dry. This was done to determine a dielectric value for the materials that could be used as a control measurement. Thereafter, 20% moisture was added to the boxes according to the void ratio. This moisture was added after each hour and the GPR tests were done approximately 5 minutes after the water was added. The percentage of water added to each of the boxes is listed in Table 3.4. As a

precaution, piezometers were installed on all four sides of the boxes in the event of any leakages. The water levels from these piezometers were taken to determine the dissipation of water from the boxes. These measurements allowed for the correct amount of water retained in the boxes to be known at the time of the GPR measurements. The amount of water that retained is also shown Table 3.4.

Table 3.4: Water content of the GPR laboratory boxes.

Box	Water added (l) (% of voids)					
	Test 1 (20 %)		Test 2 (40 %)		Test 3 (60 %)	
	Proposed	Actual	Proposed	Actual	Proposed	Actual
1	31.8	15.9 (10%)	63.6	15.9 (10%)	95.4	15.9 (10%)
2	49.2	44.3 (18%)	98.4	54.12 (22%)	147.6	66.42 (27%)
3	30.6	15.3 (10%)	61.2	15.3 (10%)	91.8	15.3 (10%)
4	69	65.6 (19%)	138	90.7 (26.3%)	207	115.6 (33.5%)

3.3.2 Results

Typical results obtained from each of the four boxes are shown in Figure 3.14. The full set of results is available in Appendix A.

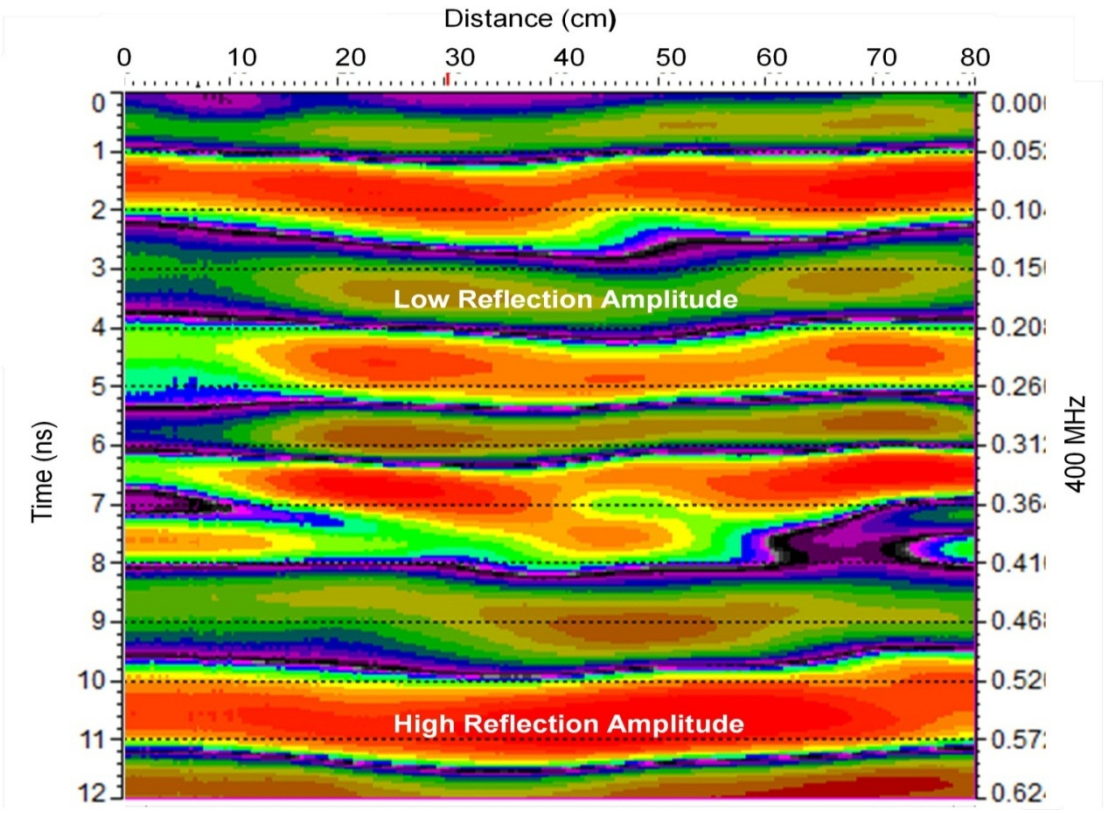

Figure 3.14: Typical GPR lab result.

The red colour across the whole length of the box shows high reflections amplitudes, typically at interface changes or high moisture content. The black is the negative part of the reflection amplitude. The faint colours are low reflection amplitudes. This is indicated by the sections where the red line is not across the whole length of the box.

3.4 GPR FIELD TESTING

GPR field testing was done at both of selected test sections. The GPR surveys were conducted along the full length of these sections. The process of the testing is described in Section 3.4.1 and Section 3.4.2.

3.4.1 Testing Procedure

The tests were conducted using a road-rail vehicle supplied by Lennings Rail Services. The GPR equipment was attached to the vehicle before testing. The equipment used for the GPR survey was as follows:

- GSSI SIR-20 amplifier
- Two GSSI 400 MHz antennae (model 5103A)
- Three industrial cameras (Firewire camera, resolution: 1024 x 768)
- RD Camlink software
- GPS system (used with RD Camlink)
- Distance measurement device

The GPR antennae were attached 1 m behind the vehicle with one antenna 300 mm above the edge of the sleeper and the other 300 mm above the centre of the sleeper. The three video cameras and the GPS antenna were placed on the roof of the vehicle. One camera faced directly in front of the vehicle and the other two faced to the two adjacent sides inclined to the front. The placement of the cameras therefore created a panoramic view of the track and its surroundings. In addition, the distance measurement device was attached to one of the rear wheels and was calibrated according to a known distance. The layout of the system is shown in Figure 3.15.

Figure 3.15: GPR system setup on vehicle.

The entire GPR system was taken apart and placed into storage while travelling between the two test sections. Upon arrival, the road-rail vehicle was manoeuvred onto the rails. The equipment was offloaded and attached to the relevant parts of the vehicle as described above. Final checks were done to make sure that all the test equipment was secure to prevent damage while travelling.

The GPR survey was carried out at a speed of 40 km/h. While the vehicle was travelling, datum points were taken at each kilometre interval. This was done to establish long and short chainages. At the end of the section, if possible, the vehicle was turned around facing the opposite direction. If this was not possible, the antenna on the left hand side was moved to the right hand side 300 mm above the edge of the sleeper. The position of the antennae is shown in Figure 3.16. The vehicle travelled back to the starting location at 40 km/h. After completion, the equipment was removed from the vehicle, packed away and the road-rail vehicle was manoeuvred off the tracks.

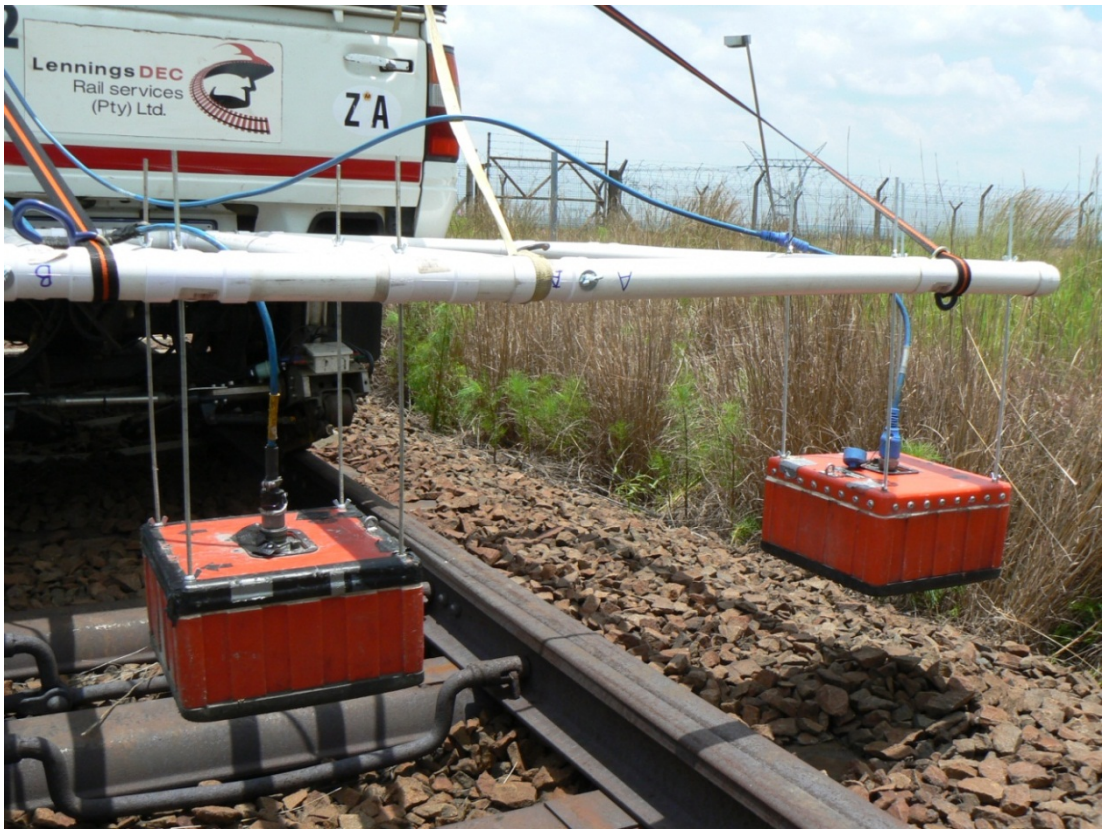

Figure 3.16: Placement of the GPR antennae on the testing frame behind the vehicle.

3.4.2 Results

The data obtained from the GPR system, GPR signal, video and GPS were combined using Railway Doctor 2.4 Software (Roadscanners, 2011). Typical results obtained from the GPR field testing are shown in Figure 3.17. The full set of results is available in Appendix B.

The data presented in Figure 3.17 contains the following plots and parameters:

1. GPR data and interpretation
2. GPR layer thickness interpretation
3. Ballast fouling
4. Relative moisture condition with depth
5. IM2000 Profile
6. IM2000 Profile Roughness
7. Survey inventory
8. Video feed
9. GPS placement

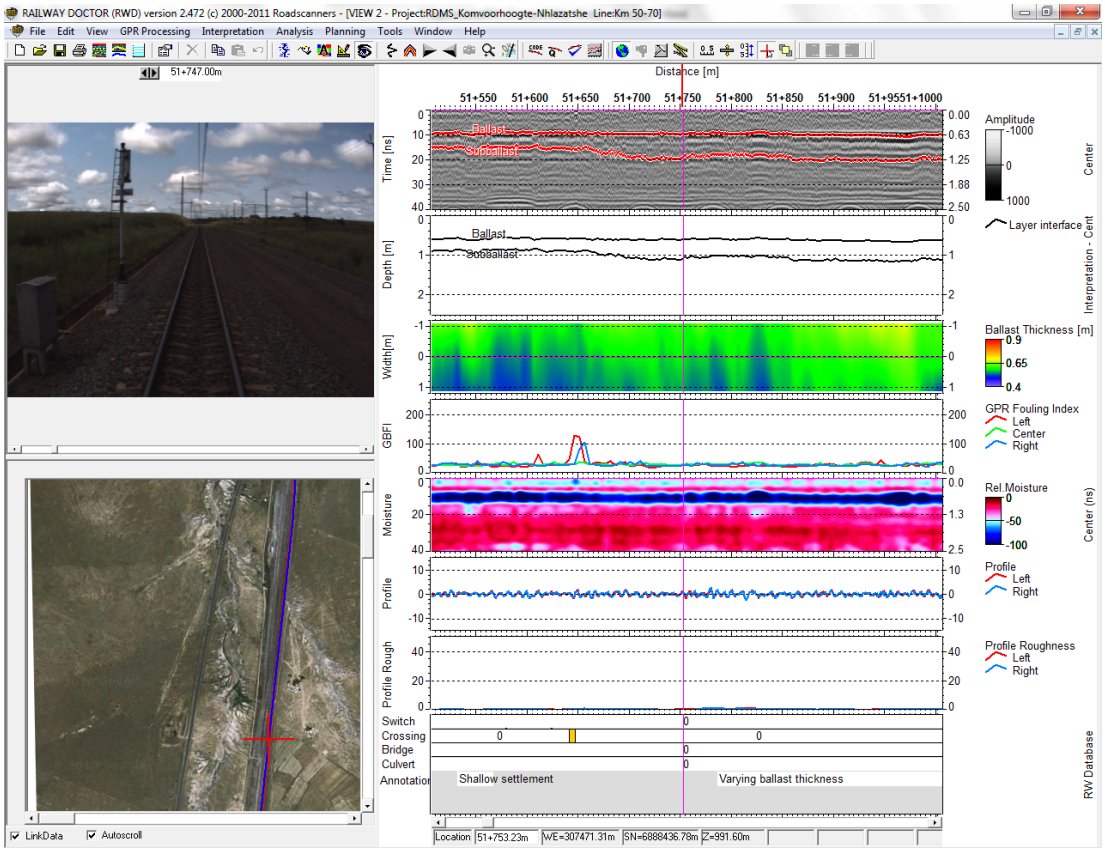

Figure 3.17: Railway doctor presentation of GPR survey data

3.5 FOUNDATION CONDITION MEASUREMENTS

The testing procedure and method for the in situ foundation condition measurements are discussed in this section.

3.5.1 Testing procedure and methods

The test procedures and methods for classifying and characterizing the substructure materials are described in this section. The verification test sites were selected visually from the GPR data as well as the geometry results from the IM2000. From this, six verification test sites were selected for each of the two test sections. Each of these locations represented a substructure condition range, from good to poor track conditions.

The testing procedure at each site was as follows:

1. Remove ballast material at the test position
2. Take a ballast sample for the determination of ballast fouling
3. Perform the LWD test
4. Perform the DCP test
5. Excavate the test pit to 1 m depth
6. Take soil and moisture samples of each distinctive layer
7. Profile the test pit
8. Close the test pit and compact it
9. Replace the ballast material

3.5.2 Ballast fouling

To determine what the ballast fouling was at each site, a ballast sample was taken. The sample was taken at the edge of the sleeper (Figure 3.18), from the bottom of the sleeper down to the surface of the formation layers. The sample was the same width as that of the sleeper and 100 mm deep in the direction of the sleeper.

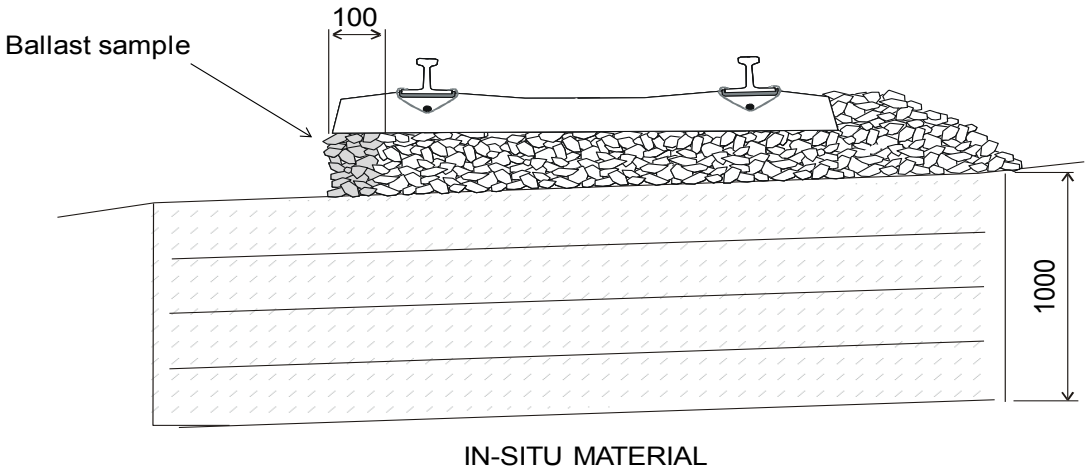

Figure 3.18: Ballast sampling location.

The depth of the ballast from the bottom of the sleeper to the top of the subgrade material was measured (see Figure 3.19a). A plastic sheet was placed at the edge of the ballast column that would be removed. This was done to ensure that all required material was obtained, including all the fines within the ballast. This allowed for a representative sample of the ballast and is shown in Figure 3.19b.

a) b)

Figure 3.19: a) Ballast depth measuring and b) ballast fouling sampling.

After the sample was obtained from the edge of the sleeper, it was placed into a plastic sample bag and taken to the laboratory. Once at the laboratory, the samples were sieved and the percentages passing the relevant sieve sizes were obtained. The grading results of the laboratory tests are shown in Figure 3.20 and Figure 3.21.

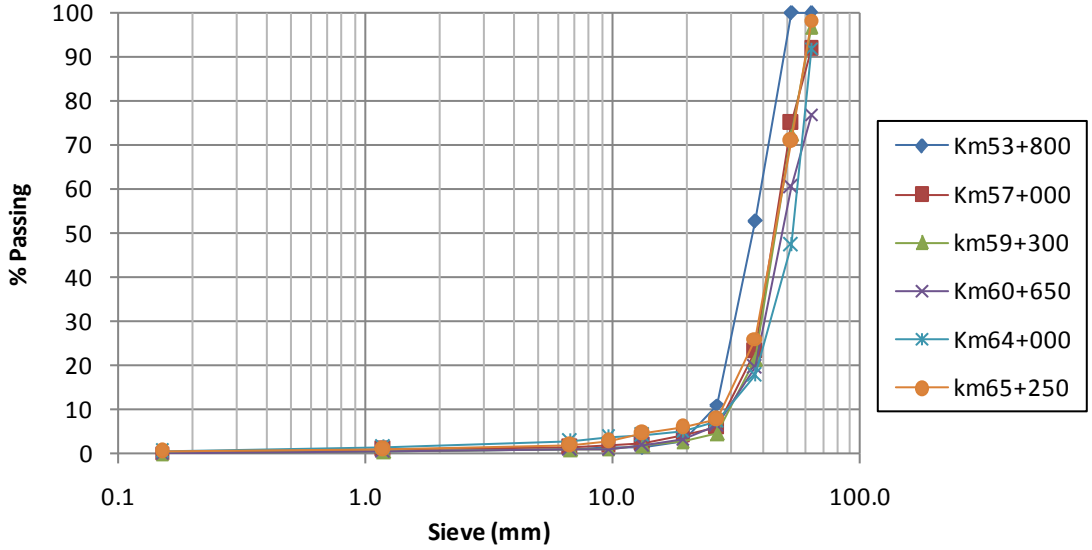

Figure 3.20: Ballast gradation of the Komvoorhoogte to Nhlazatshe test section.

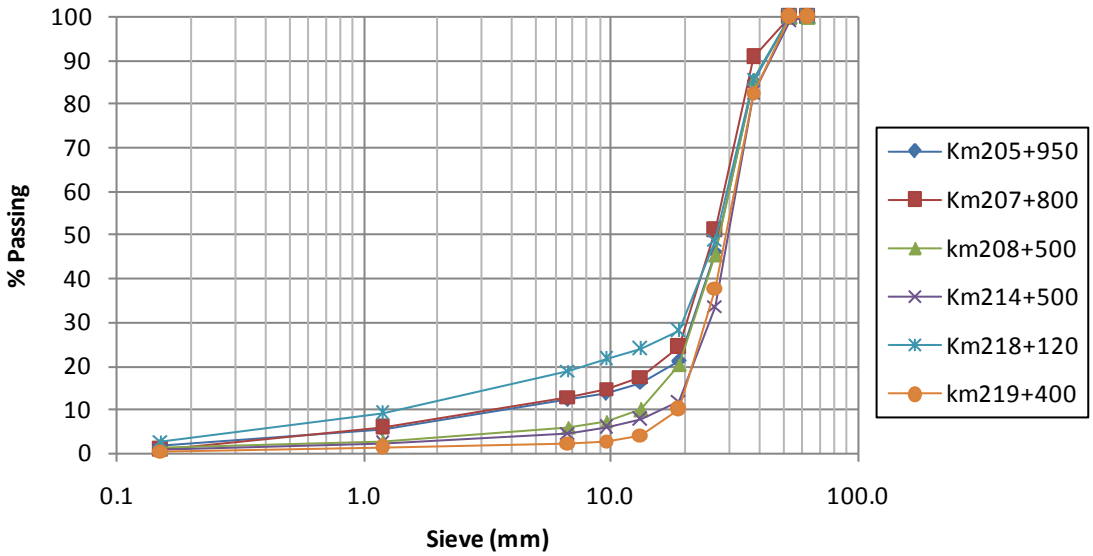

Figure 3.21: Ballast gradation of the Northam to Thabazimbi test section.

The ballast samples showed that the amount of fouling at the NT test section was more than that of the KN test section. The determination of the fouling percentages and the evaluation of the results are done in Section 4.2.2.

3.5.3 Light Weight Deflectometer (LWD)

The LWD test was conducted as close as possible to the edge of the sleeper directly on top of where the test pit would be excavated (Figure 3.22).

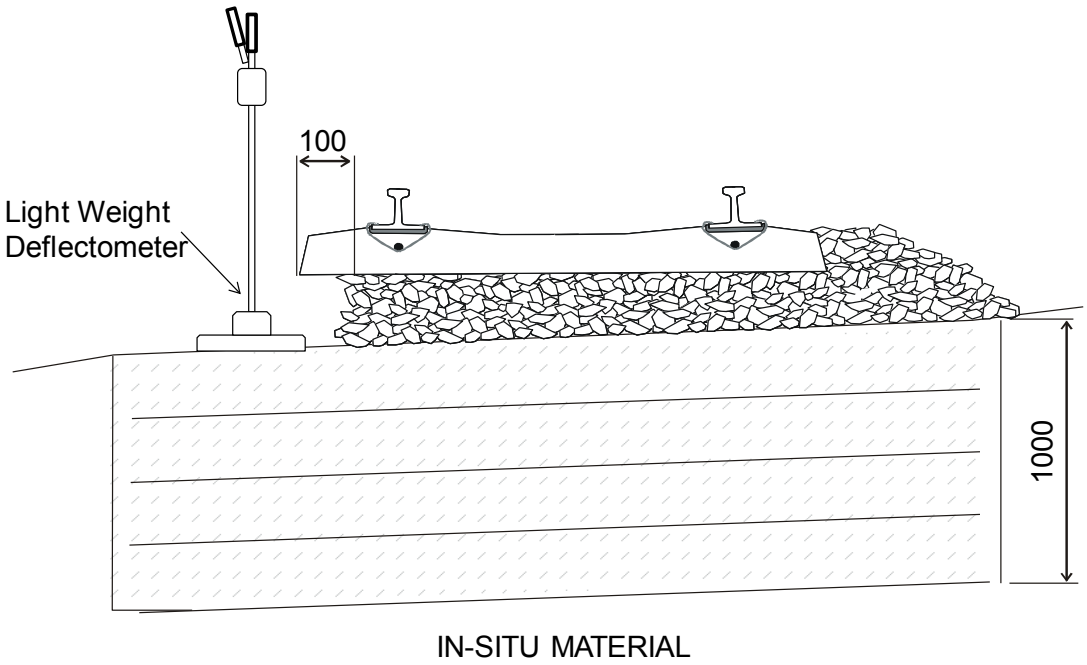

Figure 3.22: LWD test position.

The Zorn lightweight drop tester was used. After clearing the ballast material and levelling the ground (Figure 3.24a) a layer of fine sand was placed on the surface to smooth it out and to reduce bedding errors (Figure 3.24b). The base of the LWD was placed on top of this layer of sand and turned until the surface was evenly smoothed (Figure 3.24c). The second part containing the weight of the LWD was placed on the base. The weight was dropped without stopping it on the first bounce. This allowed for the soil to be compacted and to even out the surface below the base, further reducing bedding errors. It was important to do this consistently and to not change the conformance of the test. The LWD test preparation and

execution is shown in Figure 3.23d. The weight was dropped three times on the loading plate for the calculation of the stiffness. The results are displayed on the control unit shown in Figure 3.24. The data could be printed out or read off from the screen.

a) b) c) d)

Figure 3.23: The process followed to execute LWD tests.

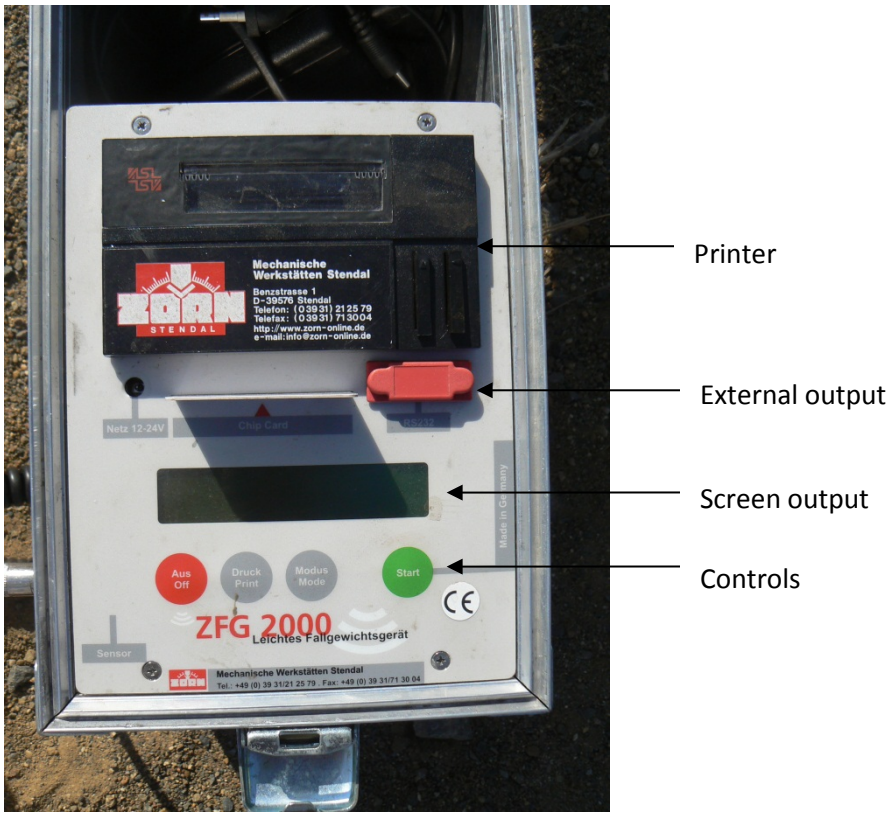

Figure 3.24: Zorn LWD control and display unit.

The results obtained from the LWD are presented, firstly as three deflection values in millimetre and then as a modulus in Mega Pascal. Typical results are shown in Table 3.5. The depth shown it the Table 3.5 shows the different depths at which the LWD test was conducted.

Table 3.5: Typical results from the Zorn LWD

Depth (mm)	LWD				
	Deflection (mm)				Modulus (MPa)
	1	2	3	Ave	
0	0.36	0.37	0.32	0.35	64.1
200	0.54	0.49	0.49	0.50	44.6
700	1.39	1.68	1.72	1.59	14.1

3.5.4 DCP

The DCP test was conducted next to the position of the LWD, that the compaction from the LWD did not affect the results as shown in Figure 3.25. The test depth for the purpose of this investigation was only 1 m.

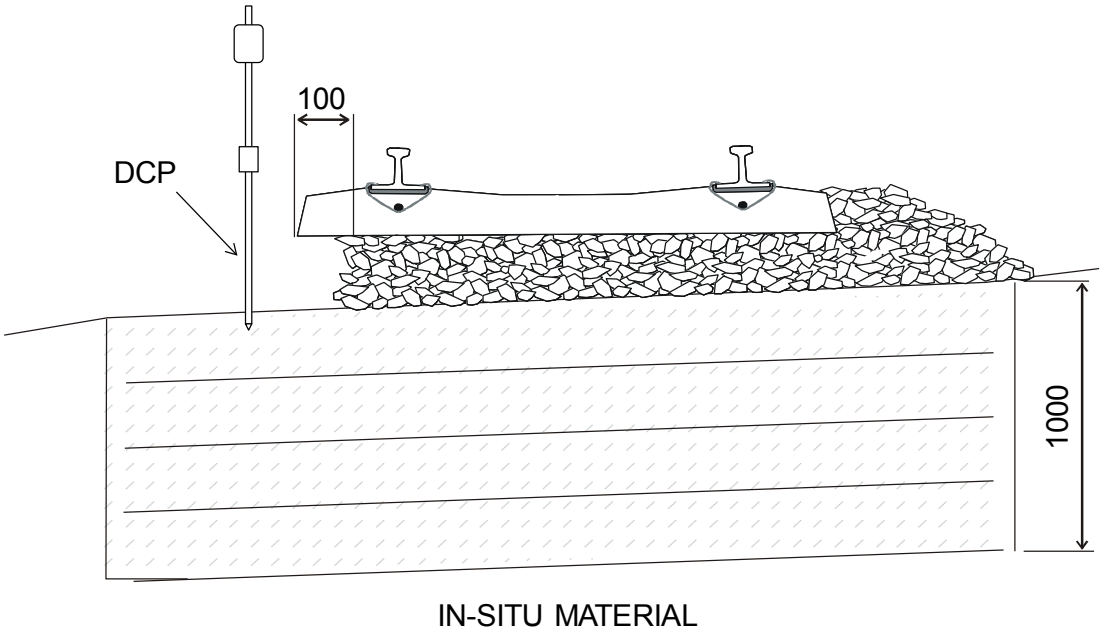

Figure 3.25: DCP test location.

The testing was conducted by dropping the weight from a height of 0.575 m (Figure 3.26a) and measuring the penetration (Figure 3.26b). For soft soil the penetration was measured after each blow and for harder soil the penetration was measured after every fifth blow. Refusal of the test was only agreed upon if the DCP did not penetrate the ground any further after 20 consecutive blows at three adjacent test locations. Comparing the number of blows taken to the depth of penetration, discernible layers can be identified as shown in Figure 3.27. The analysis of the DCP results is shown in Section 4.2.3.

a) b)

Figure 3.26: DCP Testing; a) dropping of weight and b) penetration.

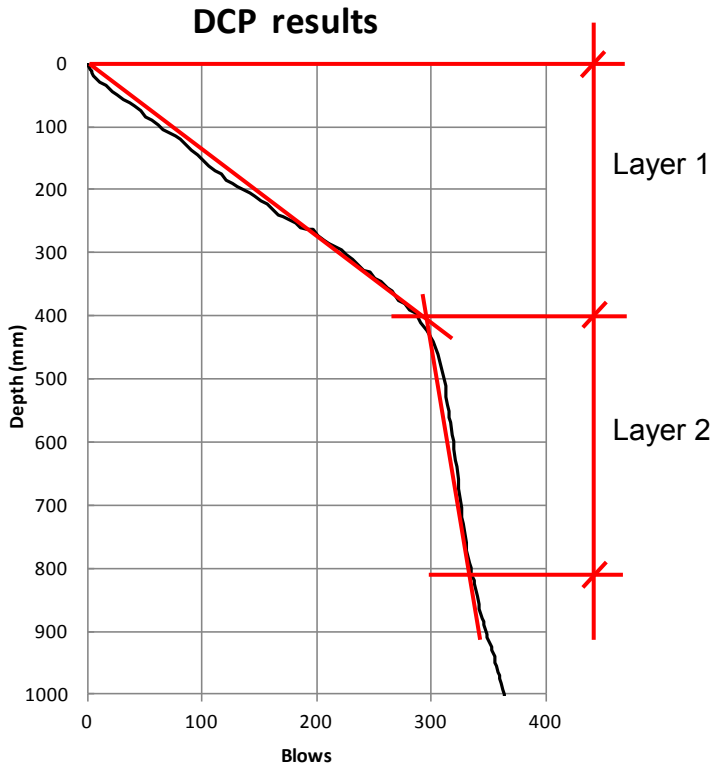

Figure 3.27: Typical DCP results.

3.6 SOIL CLASSIFICATION

Test pits were excavated to carry out the required soil classification. These test pits were then profiled and soil samples were taken from them. This section will discuss the process that was followed to excavate, profile and take samples at the respective test locations.

3.6.1 Excavation and profiling

A test pit of approximately 1 m deep, from the top of the formation, was excavated by hand (KN test section) or mechanically (NT test section). Where access to the test pit from the side of the track was possible, an excavator was used. The test pit was then profiled according to the method described in Section 2.4.3 by Jennings *et al*. (1973). A schematic of the test pit location with respect to the track is shown in Figure 3.28.

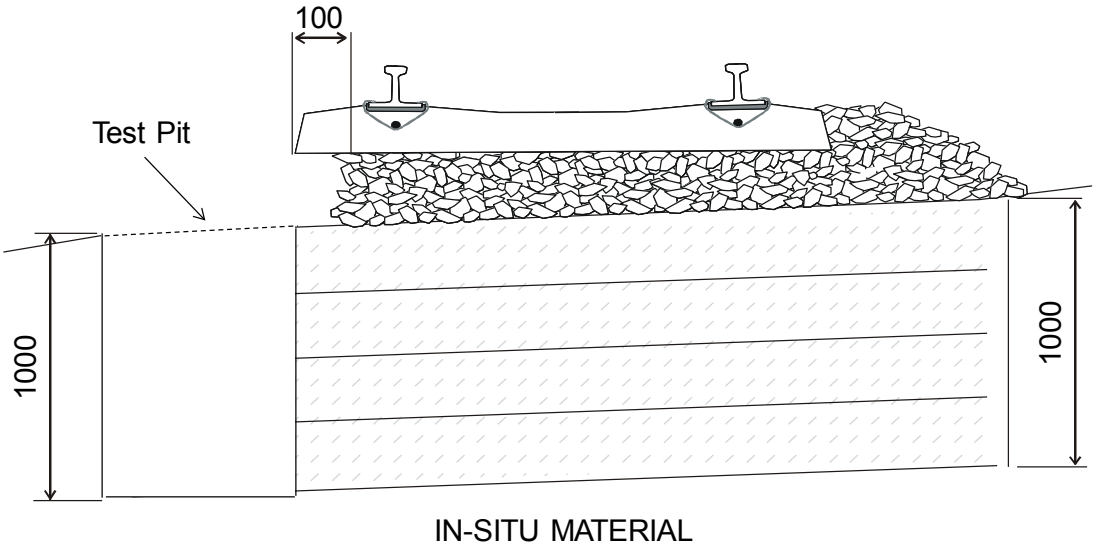

Figure 3.28: Test pit location.

3.6.2 Sampling for soil parameters

After the profiling was done, samples were taken from each of the discernible layers. The samples and the amount of material for each are given below.

- CBR (two bags of 50 kg each)
- Foundation indicators (FI) (one bag of 2 kg)

- Moisture content (one small sample placed in a jar)

The samples were taken from the ground that was excavated from the test pit and was heaped next to it. This was only done if the material from the different layers was not contaminated. If the layers were mixed, the material was gathered from inside the test pit. If the material from two different layers had similar properties according to the profiling results, only one CBR sample was taken and FI samples from both the test pits. The CBR and FI samples were supplied to a geotechnical laboratory for testing. The results of the laboratory testing are given in Appendix C.

Moisture samples were taken from all the different layers observed in the test pits. If the layers were more than 200 mm thick, a sample was taken at every 200 mm interval.

The moisture content was determined for each of samples. This was done by oven drying them at 105^{o}C for more than 24 hours. The mass of the sample was measured before and after the oven drying process, thereby determining the moisture content of each layer.

3.7 REMOTE VIDEO MONITORING (RVM)

RVM was used to determine the deflection of the track. Both the deflection of the sleeper and top of the substructure were determined. The apparatus, reduction of the data, laboratory calibration and testing procedure are discussed in this section.

3.7.1 Apparatus

The components of the RVM system are shown in Figure 3.29.

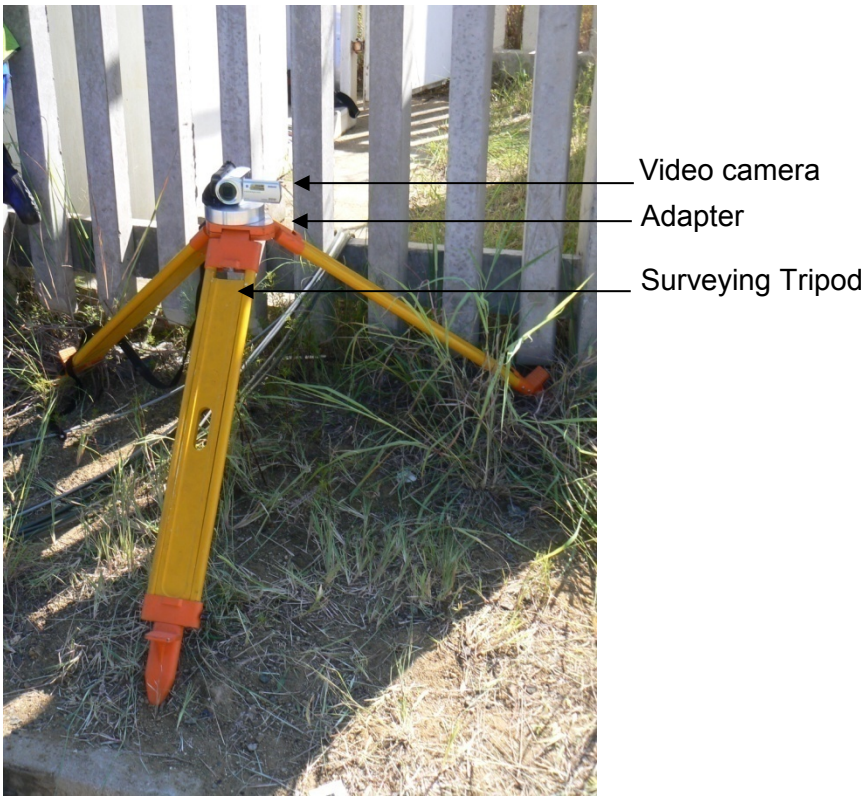

Figure 3.29: RVM video camera system.

Video cameras

A *SONY SR46E* digital video camera with 40 x optical zoom was used, allowing for it to be set up far enough away from the track so that the vibrations from the train would have minimal effect on the results. The camera also has a 40 Giga byte hard drive to store the data and to connect the system to a computer to do a real-time analysis. The camera effectively records 490 000 pixels when recording 16:9 aspect ratio video clips and it records at 25 frames per second (fps).

A *SANYO Xacti* high definition (HD) camera with 24 x optical zoom was also used. This camera could also be positioned far enough from the track to limit interference as described above because of the higher resolution. The camera uses an SD card as storage. It also has the option to record full HD video at 30 fps and 60 fps. In addition, the camera can effectively use 2.1 million pixels when recording at full HD.

Thread adapter

An aluminium adapter was designed for the surveying tripod to connect it to the video camera. This was necessary because the male screw from the surveying tripod (M16 x 2 mm thread) did not match the female thread from the camera (1/4" BSW). The adapter was machined out of a 300 mm diameter cylinder and was 30 mm thick for both male and female threads to fit properly. The technical drawing is given in Figure 3.30.

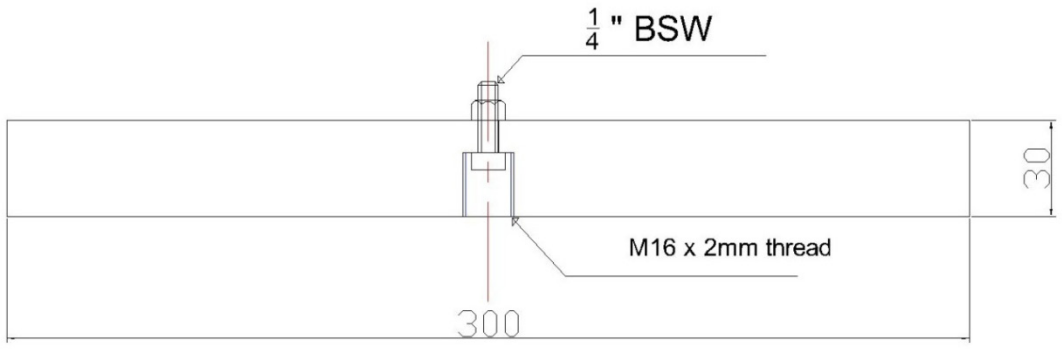

Figure 3.30: Schematic of the tripod adapter.

Surveying tripod

A surveying tripod was used because of its weight and stability. This decreased the effects of vibrations caused by the train. The reason for not using a conventional camera stand was that creep occurred when the camera was tightened to the rubber connection system. It was also too light and prone to vibrations caused by the train. More expensive camera tripods minimise both these effects.

Targets

The target is a 20 mm x 20 mm black circle (Figure 3.31a) or square (Figure 3.31b) printed on a 60 mm x 60 mm white piece of paper. The dimensions of the target block could be any size. It was found that with the specific cameras used, the 20 mm x 20 mm dimensions were sufficient once the camera was at full zoom at the required distance from the target. The target filled enough of the screen so that the deflections could be recorded at the required accuracy and resolution. The optimum distance for the target to be placed away from the camera, was between 3 m and 5 m.

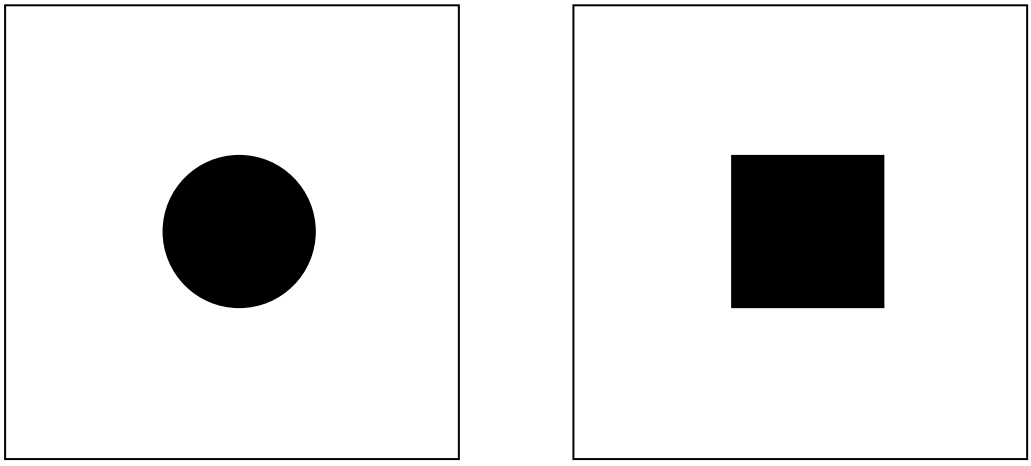

Figure 3.31: Targets used for RVM testing; a) circle and b) square.

Software

An analysis program developed by TLC Software, called Sleeper Tracker, which is based on National Instruments Lab View Vision Instrumentation software, was used to analyse the deflection caused by the train loading. The program only analyses audio video interleaved (AVI) files. This meant that the MPEG2 or MPEG4 files produced by the video cameras had to be converted. An MPEG to AVI converter was used to do this. It should be noted that a converter with 2-pass encoding was used for maximum quality encoding. An example of such a program is AVS video converter.

The analysis program, Sleeper Tracker, detects the amount of pixels that appears in the black part of the target and converts it to millimetres. The movement of the target can then be determined in millimetres. The software provides the results in a text file (*.txt) that is tab delimited. This program layout is indicated in Figure 3.32 and can be described as follows:

1. The number of frames per second (fps).
2. The width and height of the target.
3. The file directory.
4. File name.
5. The timer should be set longer than that of the AVI file in seconds.
6. The AVI file is displayed and the ROI (Region of interest) is chosen. It is chosen to be large enough so that the deflection does not exceed the frame dimensions.
7. The number of pixels in the black square.

8. A preliminary graph of the results.

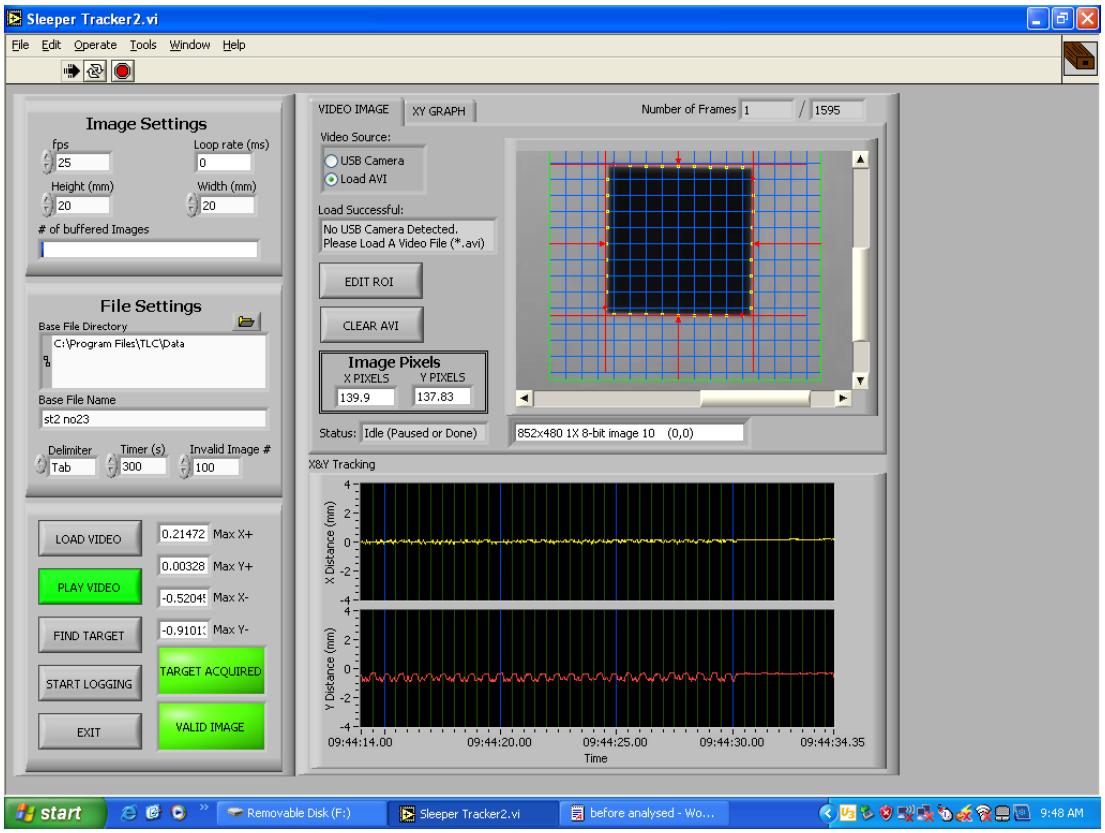

Figure 3.32: Sleeper tracker.

3.7.2 Methodology

The following method was used to convert the video files, analyse them and reduce the text files, generated from the analysis program, in Excel:

1. The camera was attached to the adapter and surveying tripod.
2. The target was placed on the object of which the deflection needed to be measured. The simplest method of attaching the target was the use of glue.
3. The camera system was positioned, focused and zoomed on the target. The camera needed to be on manual focus and the anti-vibration needed to be switched off. This was done so that the deflection that was recorded was not adjusted by the camera.
4. The next step was the recording of the video. The camera was started well before and stopped well after any movement, so that the data obtained could be zeroed at a later stage.

5. The video was converted from MPEG to AVI (2-pass encoding was used).
6. The AVI file was loaded into and analysed by Sleeper Tracker. The size of the target was specified as 20 mm x 20 mm. Also, the file name and directory needed to be indicated and the ROI range was specified. After this, the file could be started and the logging could commence.
7. The tab delimited *.txt file was then opened in Microsoft Excel. The fps was then converted to seconds. Once this was done, the vertical deflection was zeroed and corrected by both taking the average at the start or the end of the file and subtracting it from the rest of the data.

3.7.3 Laboratory calibration

The RVM system is still a new development in rail deflection analysis. This meant that tests needed to be conducted to determine the accuracy of the system. Other tests were also conducted. These include tests with relative angles, the effect of heat waves and the effect of shadows while analysing. A digimatic micrometer was used for the laboratory tests (Figure 3.33). The RVM results obtained were compared to the values obtained from the digimatic micrometer. For each test, a set of upward and downward readings were made by taking readings in 0.5 mm increments and maintained for two seconds, to a maximum of 3 mm and a minimum of -3 mm.

Figure 3.33: Digimatic micrometer.

The comparison of the RVM system and the digimatic micrometer results are shown in Figure 3.34. The average interval results from the RVM data are obtained by taking an average from the constant measurement at each increment. From these results it can be seen that the system has a minimal measurement error. The coefficient of indeterminacy (R^2), referring to the fraction of variation, is almost 1. The RVM system is therefore extremely accurate because of the R^2 value that is within 0.1% of 1, where 5% is usually accepted. In the repetition of the test, similar results were obtained, thus indicating that the system has good repeatability.

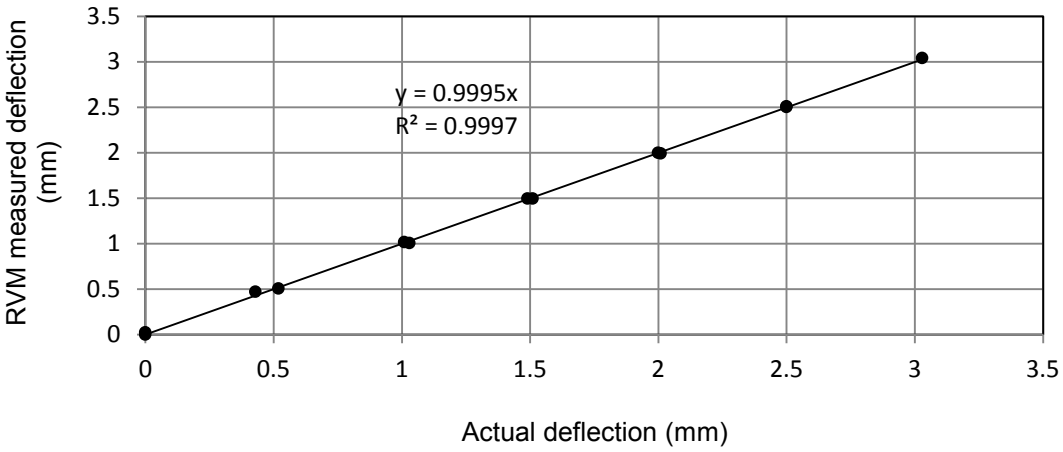

Figure 3.34: RVM calibration.

To determine the maximum relative error, the difference between the straight line obtained in Figure 3.34 and the actual values of the RVM system, was used. The results obtained are shown in Figure 3.35. From this, it was determined that the maximum relative error is 0.05 mm. The same results were obtained in the repetition of the test.

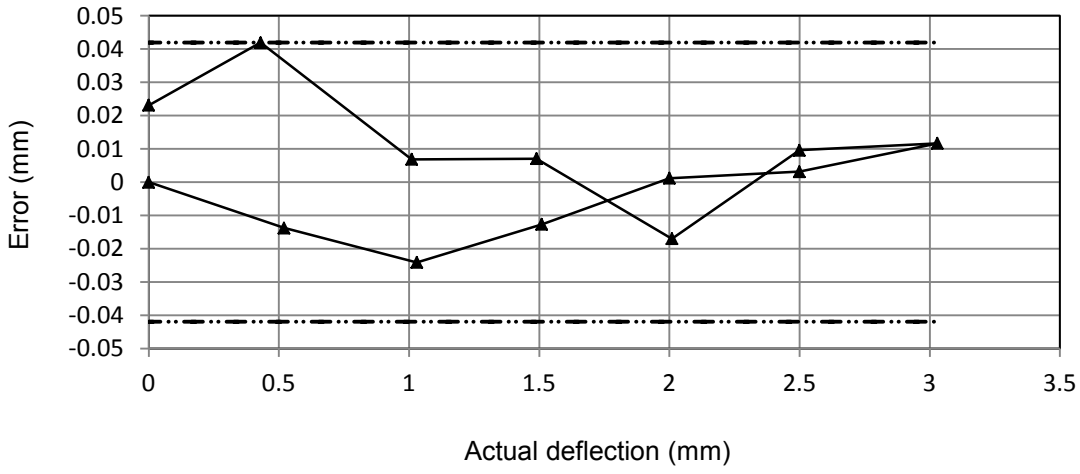

Figure 3.35: RVM system relative error.

The noise of the RVM system was determined by keeping the target stationary for more than 5 seconds. Figure 3.36 shows a representation of these results. The graph shows that the values vary over a range of less than 0.01mm. The standard deviation of the results is

0.00147 mm. The noise however, is dependent on other factors such as lighting and distance between target and camera.

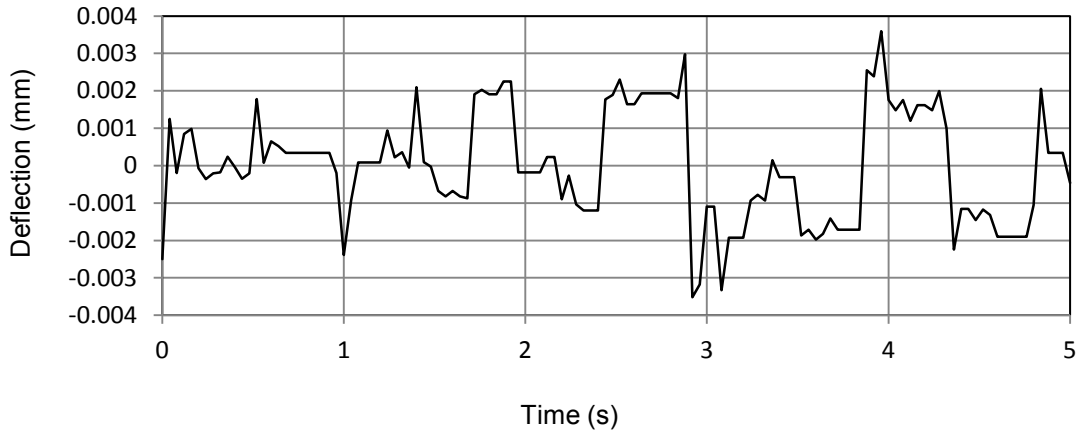

Figure 3.36: Noise in the RVM system.

Angle tests

For the angle tests, the target was placed at different angles relative to the camera. This was done to see what the effect of different measurement angles would be on the deflection measurements. The tests were carried out with a change in the horizontal axis, change in vertical axis and a change in both the horizontal and vertical axes. For the horizontal test, the distance between the camera and the target was 3 m and 3 m to the side, with both at the same height. For the vertical test the target was 3 m away from the camera while the camera was elevated to 1.405 m and the target to 0.235 m. In the combination test, the horizontal distance and the vertical difference of the two other tests were combined. The layouts of the tests are indicated in Figure 3.37.

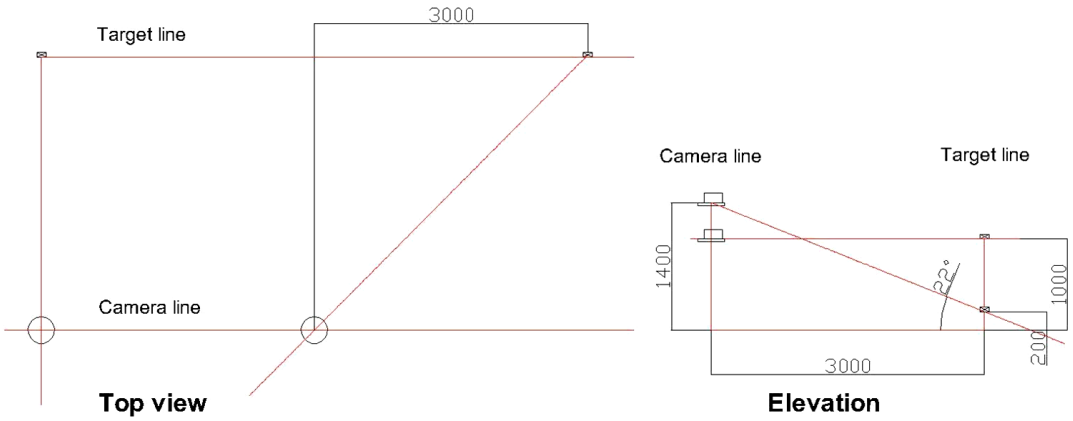

Figure 3.37: Layout of the RVM angle tests.

The analysis program, Sleeper Tracker, was designed in such a way that if the difference in horizontal and vertical pixels in the black square was more than 10%, the program would not analyse the file. This was built into the program as an accuracy control. Using trigonometry it was calculated that the maximum angle that the target could be positioned the camera at 3 m, was 25 degrees. Therefore, only the vertical angle test could be analysed. This could however be overcome by editing the aspect ratio of the video with the video converting software.

When setting up the vertical angle test, the tripod was at its highest and the target was at its lowest. This meant that the program restraints would not be a problem in the field testing. The accuracy and errors for these tests were also determined. The R^2 was the same as that in the calibration test (0.999) and the relative error was also similar with a maximum of 0.04 mm. This meant that the relative angle at which the test was done would have no effect on the accuracy.

Heat wave tests

For these tests a heater was placed under the target to simulate the effect of heat on the track causing heat waves. The camera and target was positioned at the same elevation and 3 m apart. An indication of the layout is given in Figure 3.38. An electronic heater with a filament was used and temperatures of 70 degrees Celsius were achieved. This was measured using an electronic thermometer.

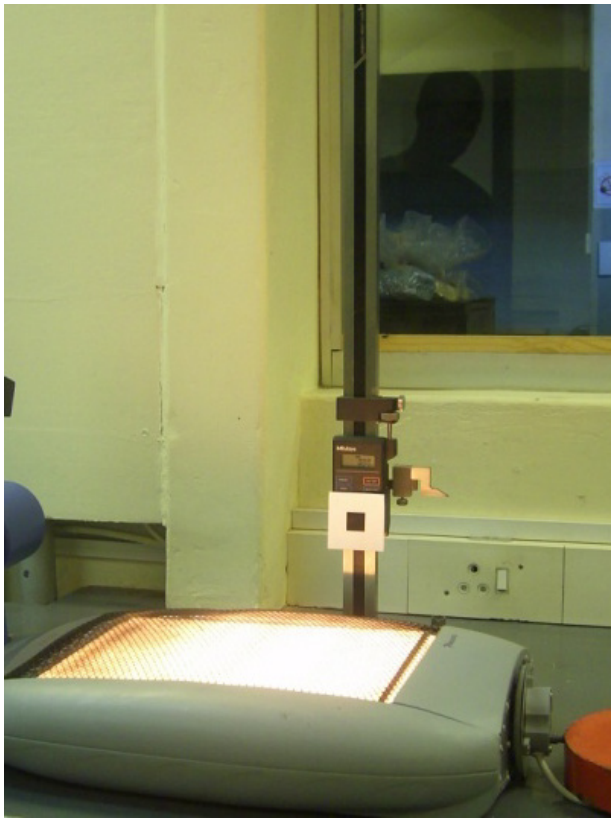

Figure 3.38: RVM heat wave test.

As before, the R^2 value and relative error were similar to that of the calibration tests. R^2 was 0.999 and the relative error was 0.05 mm. This meant that the heat waves did not have any real effect on the accuracy on the RVM system.

Light and shadow tests

In the lighting tests, the effect of shadows moving over the target while recording was analysed. This test was done outside in direct sunlight. A large piece of cardboard was moved back and forth over the target at both a rapid and slow rate. The setup was similar to that of the calibration test, with the target and camera 3 m apart and level. An indication of the setup is shown in Figure 3.39.

Figure 3.39: RVM lighting test setup.

For these tests, the main focus was the noise of the system. It was found that the sudden change in light causes a peak in the readings, as indicated in Figure 3.40. The maximum peak difference found throughout the tests was 0.7 mm. It was therefore established that provision should be made in the field to block out the effect of shadows.

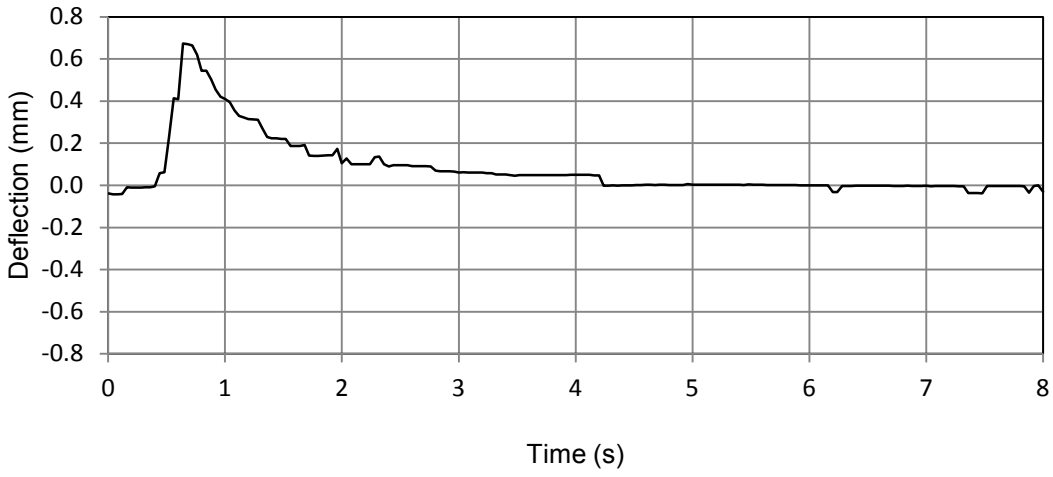

Figure 3.40: The effect of shadows on RVM tests.

Discussion of laboratory tests

From the tests described above, it was found that the RVM system is extremely accurate and would be adequate for track deflection measurement. Care should be taken when setting up the system so that the relative angle between the target and the camera is less than 25 degrees. Provision should also be made, in the form of shielding, to minimize the effect of shadows on the results. The use of protection of the RVM target against the effect of shadows is shown in Figure 3.41. Lastly, it was established that heat waves would have little effect on the accuracy.

3.7.4 Test procedure and schedule for in situ RVM tests

The RVM testing equipment is described in this section. The *SANYO Xacti* video camera was placed on a surveying tripod using the special adapter. The video camera was pointed at targets 3 m away. Three targets were placed, one on the edge of the sleeper, another on a metal rod cemented to the top of the subgrade and the third on a metal rod 400 mm into the subgrade. A black circular target, 20 mm in diameter, was placed on a white background 60 mm x 60 mm wide. The camera was zoomed in on these targets until the field of view was filled by the targets. The placement of the targets on the sleeper and formation is shown in Figure 3.41 and a schematic of the test setup is shown in Figure 3.42.

Figure 3.41: RVM shadow protection and target placement.

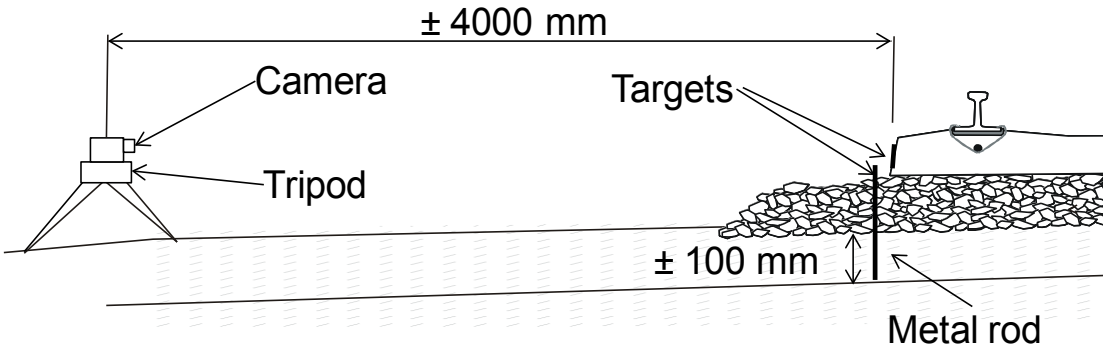

Figure 3.42: Schematic of RVM testing.

The RVM video cameras was positioned, one four sleepers to the left of the test pit and the other four sleepers to the right of the test pit, shown in Figure 3.43. They were left in position until a train approached. Once a train approached, the recording on the two cameras were started for the duration of the train passing the relevant points on the track. The recordings were stopped once the train's end has moved a significant distance past the test site. The video recording was started well before and stopped well after the train passed to obtain significant 0 lines before and after the data.

Figure 3.43: Placement of two RVM systems next to the track.

Typical results obtained from the RVM measurement system are shown in Figure 3.44.

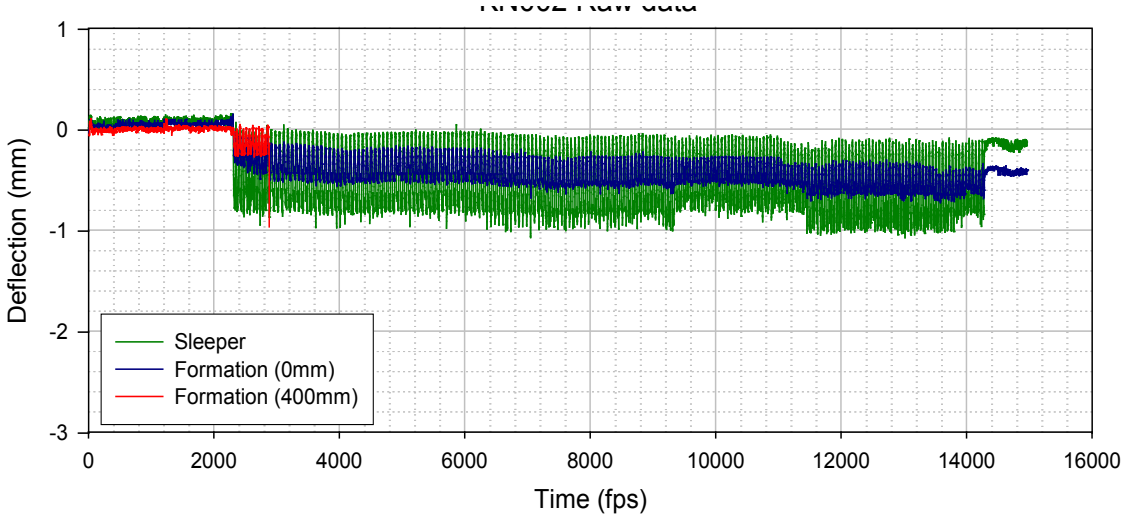

Figure 3.44: Typical RVM results

The deflections measurements from both test section were further analysed in Section 4.3

3.8 MULTI -DEPTH DEFLECTOMETERS (MDD)

MDD installations are very expensive and would not have been feasible to include in this study. However, on the Komvoorhoogte to Nhlazatshe test section, a previous MDD installation that was used to provide further insight into foundation condition assessment tools was available. The MDDs were used as part of a project to predict design life of a railway track presented by Gräbe and Shaw (2010). The instrumentation was installed during the reconstruction of the line in 2004. This test location coincides with the test location KN004 at km 60+650.

Three test sites, eight sleepers apart were instrumented. At each of the sites three holes were drilled into the ground into which a string of six MDD modules were installed (Figure 3.45). A schematic of one the test sites are shown in Figure 3.46. Only the second test site was used for the purpose of this study. Strain gauges to measure the vertical loads were also installed and calibrated. They were placed directly above the MDD modules on the left and the right rails. RVM deflection measurements were also conducted at this location for a comparison with the MDD deflection measurements. The vertical load strain gauges and the RVM targets are shown in Figure 3.47.

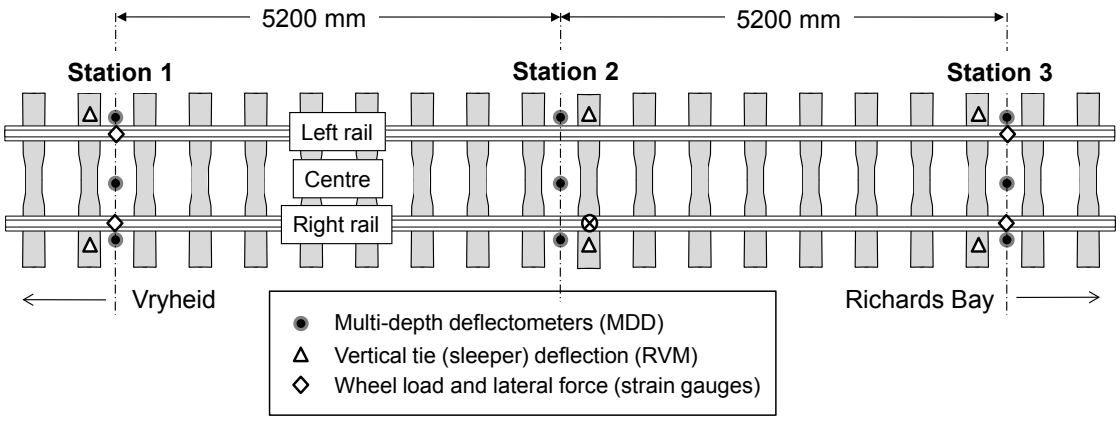

Figure 3.45: Instrumentation layout at KN004 (Bloubank).

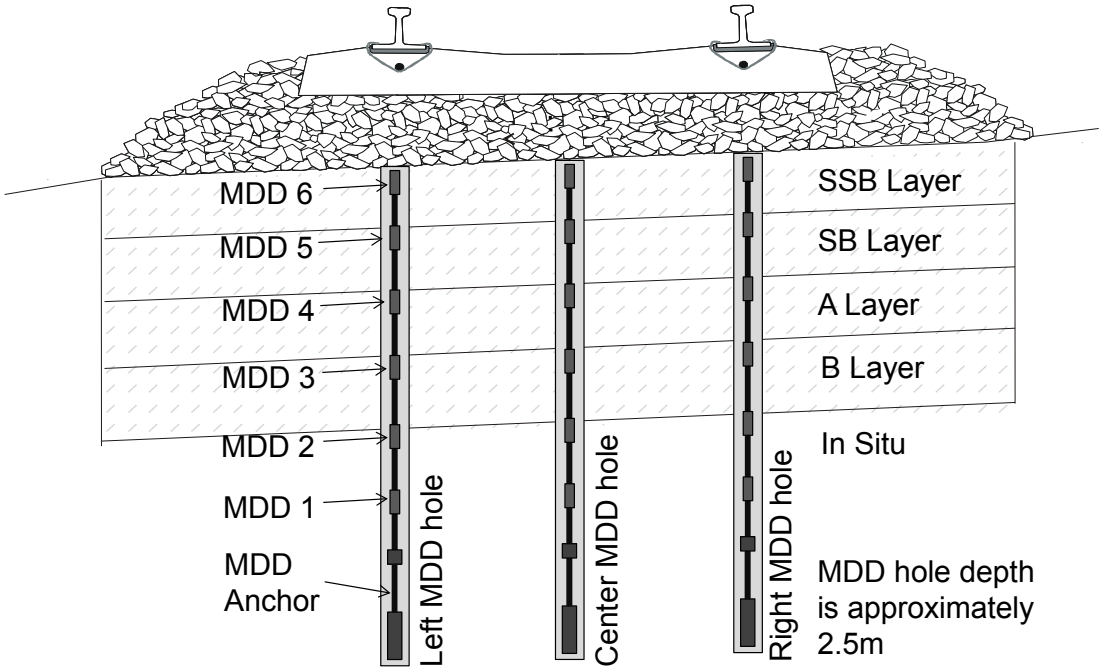

Figure 3.46: MDD module layout at KN004 (Bloubank).

Figure 3.47: Vertical load strain gauges and RVM target.

The software used to record the data from the vertical wheel load strain gauges and the MDD modules was CMSW, developed by TLC Software. The data are zeroed and then exported to Microsoft Excel for further analysis. A total of twenty five trains were recorded of which only four complied with the speed (35 km/h to45 km/h) required for the analysis. Typical results obtained for the vertical wheel loads and the MDD deflections are shown in Figure 3.48 and Figure 3.49 respectively.

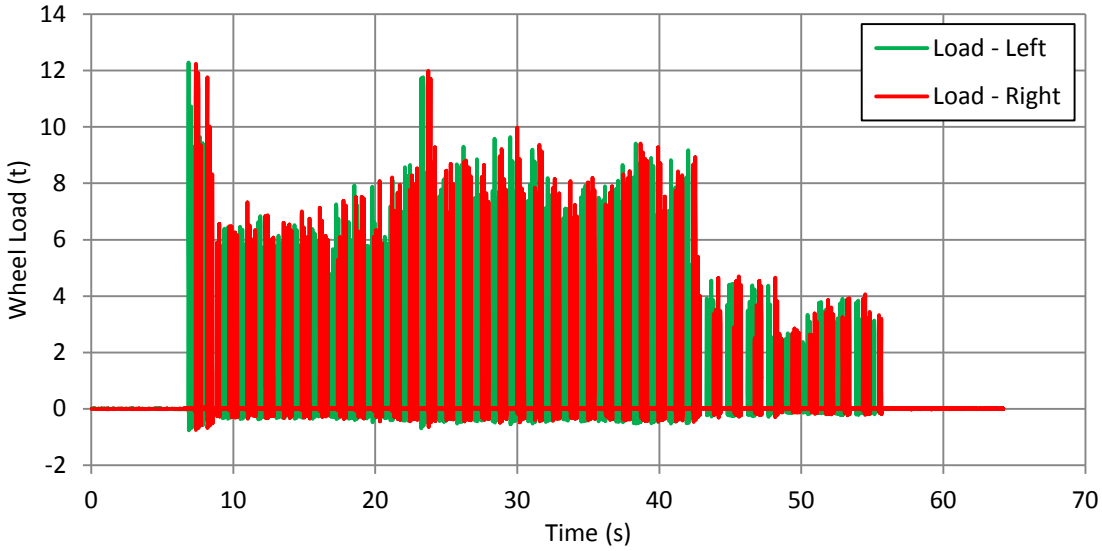

Figure 3.48: Vertical wheel load measurements at MDD test location.

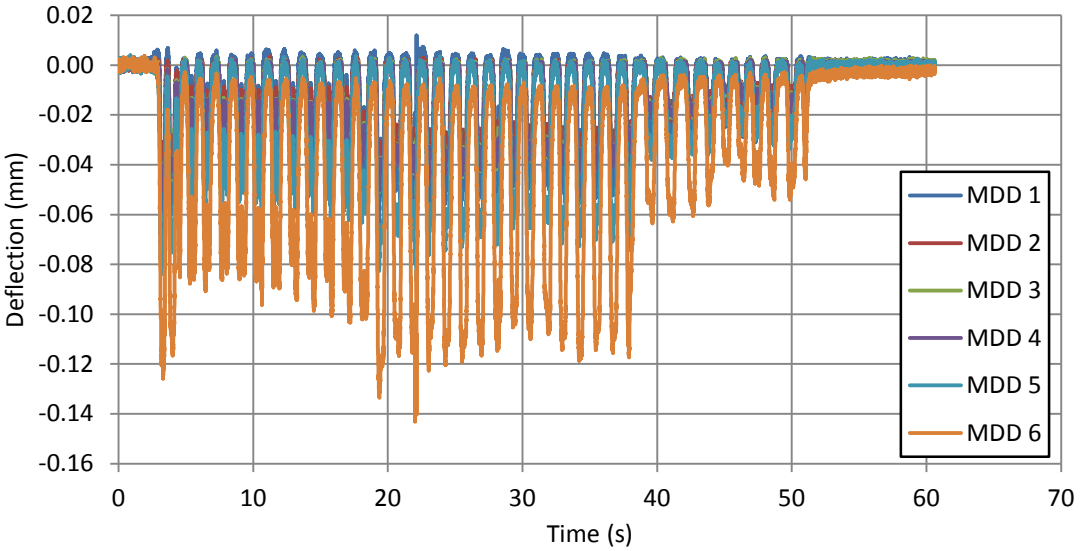

Figure 3.49: Typical results from MDD module string.

The MDD deflection measurement were further analysed and compared to the RVM deflection measurements in Section 4.3.

3.9 DISCUSSION

The field and laboratory tests that were conducted to develop the characterization model and to further verify the results were discussed in this section. The two test sections, between Komvoorhoogte and Nhlazatshe (KN) and Northam and Thabazimbi (NT), were described. GPR laboratory tests were conducted on the ballast material found at the two test sections to obtain their dielectric permittivity. The tests conducted to evaluate and calibrate the GPR field testing were test pits, soil sampling and DCP tests. RVM, LWD and MDD were also conducted and could be used for further investigation of track performance on a site specific basis where anomalies in the GPR data occur.

The laboratory tests were conducted on dolerite from the KN test section and quartzite from the NT test section. Four samples were prepared, two with 10 % fouling and two with no fouling. Tests were conducted with 400MHz GPR antennae before and after the samples moisture content was increased in increments of 20 %. Piezometers were used to measure dissipation of moisture from the boxes to obtain the exact moisture content at the time of the GPR measurements.

GPR field tests were conducted at both the KN test section and the NT test section over a distance of 20 km at both sections. Two 400 MHz antennae were suspended 500 mm above the top of the sleeper. Two passes were done to obtain surveys from the left, centre and right of the track. The layer thickness, GBF index and GPR moisture condition were obtained from the survey. This data was combined with video of the track, GPS coordinates and the survey inventory.

Twelve test locations were selected, six at each test section, at which ballast sampling, LWD and DCP testing, soil sampling, RVM and MDD testing were conducted. The ballast sampling, soil sampling and DCP data was used for the calibration and evaluation of the GPR results. The LWD, RVM and MDD tests were done for further evaluation of the substructure and to investigate possible anomalies within the GPR survey data. The RVM and MDD tests were conducted to evaluate other methods to determine the track stiffness and track modulus.

CHAPTER 4

4. ANALYSIS OF LABORATORY AND FIELD MEASUREMENTS

This chapter deals with the GPR laboratory and field tests as well as the substructure condition measurements discussed in Chapter 3. The GPR laboratory tests are evaluated and the results for the two different ballast materials are given. In addition, the soil parameters obtained from the test pits are compared against the S410 design specifications. The RVM deflection results are evaluated and two different methods of obtaining track and substructure moduli are displayed. The moduli obtained from the RVM measurements are shown in relation to the modulus measurements obtained from the LWD.

The GPR field measurements are evaluated and compared with the soil parameters obtained from sampling. The depth of the different foundation layers, ballast fouling index, moisture content and dielectric values are the parameters used for the characterization of the substructure.

4.1 ANALYSIS OF GPR LABORATORY MEASUREMENTS

The analysis of the GPR laboratory testing is discussed in this section. The test results of the four different boxes containing clean quartzite, fouled quartzite, dolerite and fouled dolerite were analysed with increasing moisture content. The ballast material used for the testing is identical to the ballast material used for the track construction at the two test sections. The dolerite ballast material was used at the Komvoorhoogte to Nhlazatshe test section (KN) and the quartzite ballast material was used at the Northam to Thabazimbi (NT) test section.

4.1.1 Data processing

To calculate the dielectric values for the different materials at the different stages of moisture addition, the GPR signals were processed. The following filters were applied to the signals before the interpretation was done:

- Horizontal Low Pass Filter (HFL) of 3 for horizontal smoothing
- Horizontal High Pass Filter (HFH) of 1500 to reduce noise levels
- Arithmetic Operation (ARI) of -1 for GPR signal correction, and

- Static Background Removal Filter (BGR) for removing background noise

For the use of the 400 MHz antenna, the BGR filter with a predefined background was used. This was obtained from the lifting test. The ARI filter was also applied with a multiplication factor of -1 to invert the GPR signal. The 1 500 MHz antenna had an HFL and HFH filter of 3 Hz and 1 500 Hz applied respectively. An ARI filter with a multiplication factor of -1 was also applied to invert the GPR signal.

4.1.2 Calculation of dielectric (ϵ_r) values

To calculate ϵ_r for each of the different materials at the different moisture contents, Equation 2.28 and Equation 2.29 were used. Combining the two equations, the following equation was obtained:

$$s = \frac{ct}{2\sqrt{\epsilon_r}} \tag{4.1}$$

Where:

c = speed of light in a vacuum (0.3 m/ns)

s = interface depth (m) from the surface of the medium

t = two-way travel time from the soil surface to the interface depth (ns =10^{-9})

ϵ_r = relative dielectric permittivity of the soil

The processed data from each of the boxes was visually inspected to determine the travel time of the signal between the antenna and the layer interfaces. This process was repeated three times to obtain an average. There was a clear distinction between the ballast rock and the concrete floor on which the ballast boxes were placed. Figure 4.1 shows where this interface is on one of these boxes. The colour scheme used for the interpretation shows the largest reflections as red or white and the smallest reflections as purple. The green lines are areas between large and small reflections.

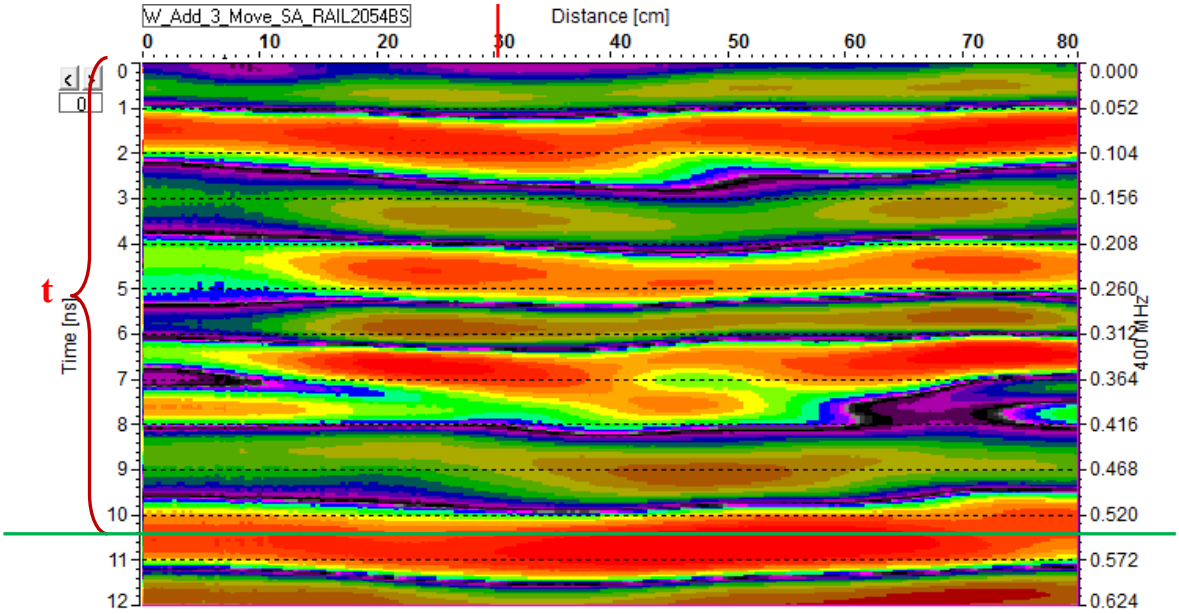

Figure 4.1: GPR laboratory testing, ϵ_r determination.

The dielectric permittivity values for each of the different moisture conditions and boxes are shown in Table 4.1. The three values calculated as described above as well as the average are shown.

Table 4.1: GPR Lab *t* and ϵ_r results

		Dry	Wet1	Wet2	Wet3 - after		
					30 min	60 min	90 min
Box1 (Quartzite) s = 0.282m	t (ns)	4.30	4.62	4.59	4.61	4.45	4.58
	ϵ_r	5.23	6.04	5.96	6.01	5.60	5.94
Box2 (Quartzite Fouled) s = 0.504m	t (ns)	10.14	10.50	10.36	10.72	10.88	10.72
	ϵ_r	9.11	9.77	9.52	10.19	10.49	10.19
Box3 (Dolerite) s = 0.272m	t (ns)	4.94	5.18	4.89	4.75	5.05	4.95
	ϵ_r	7.43	8.17	7.27	6.85	7.75	7.45
Box4 (Dolerite Fouled) s = 0.588m	t (ns)	10.85	12.34	No Result	No Result	12.14	12.05
	ϵ_r	7.66	9.91	No Result	No Result	9.59	9.45

From the lab testing results it was found that the dielectric permittivity of dolerite ($\epsilon_r = 5.23$) is higher than that of quartzite ($\epsilon_r = 7.43$). It was also determined that once the ballast material was moist, the dielectric permittivity would increase by about 0.8 to 2.2. Furthermore, when fouled, the quartzite ballast affected the dielectric permittivity more than with the dolerite. The results obtained compared well with literature stating that clean dry ballast has a dielectric permittivity of 3 and wet fouled ballast has a dielectric permittivity of 7.8.

4.2 ANALYSIS OF SOIL AND BALLAST PARAMETERS

This section describes the soil and ballast parameters obtained from the sampling of material at selected sites located at the two test sections. DCP tests conducted at the each of the sampling positions are also discussed. The differences between the two test sections are discussed to highlight the use of two sections for developing a GPR substructure condition model.

4.2.1 Soil Parameters

The soil parameters obtained from the test pits, shown in Appendix E, are summarised in Figure 4.2 to Figure 4.4. The parameters are classified in accordance with the railway earthworks specifications (S410, 1990) as shown in Section 2.4.1 in Table 2.1. The classification of the test pits are shown in Table 4.2.

The plots are divided into two different layers where Layer 1 contains parameters for the SSB and SB layers whereas Layer 2 contains parameters for the A and B layers at the Komvoorhoogte to Nhlazatshe (KN) test section. This is, however, not the case for the Northam to Thabazimbi (NT) test section as the substructure was not constructed in accordance with the railway earthworks specification. Yet, the data from this section are still displayed as two layers since two samples were taken at each test pit.

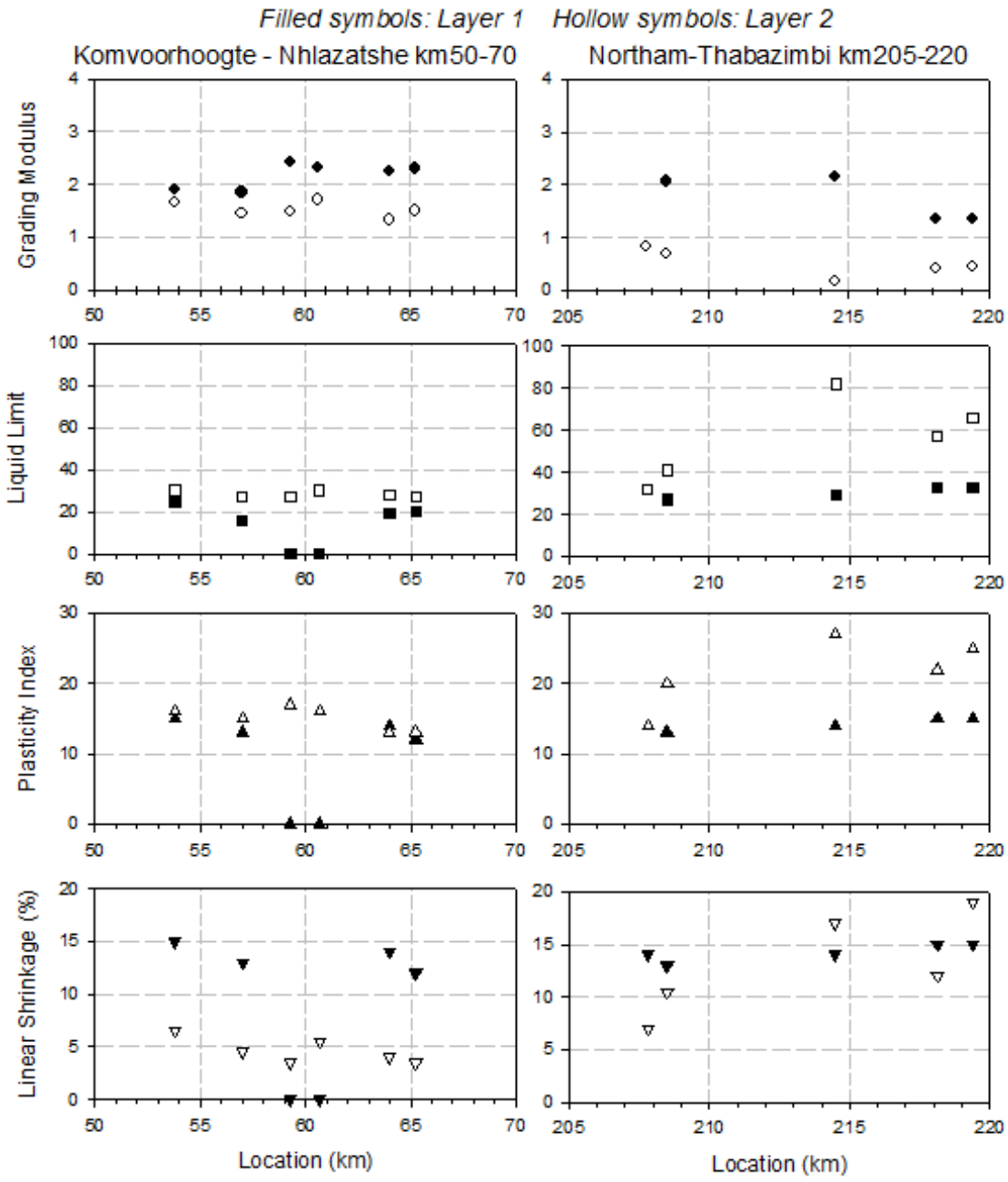

Figure 4.2: Soil parameter summary - Sheet A.

The results in Figure 4.2 show that the grading modulus for the KN test section is on average above 2 for Layer 1 and above 1 for Layer 2 and is in accordance with the specification. The grading modulus for the NT test section varies between 1.2 and 2.2 for Layer 1 and is 0.5 on average, for Layer 2. The plasticity index (PI) results show similar values for Layers 1 and 2 at the KN test section (12 to 18). The PI results at the NT test section are above 15 for both layers. Therefore, according to these results, the KN test section is in a better condition than the NT test section.

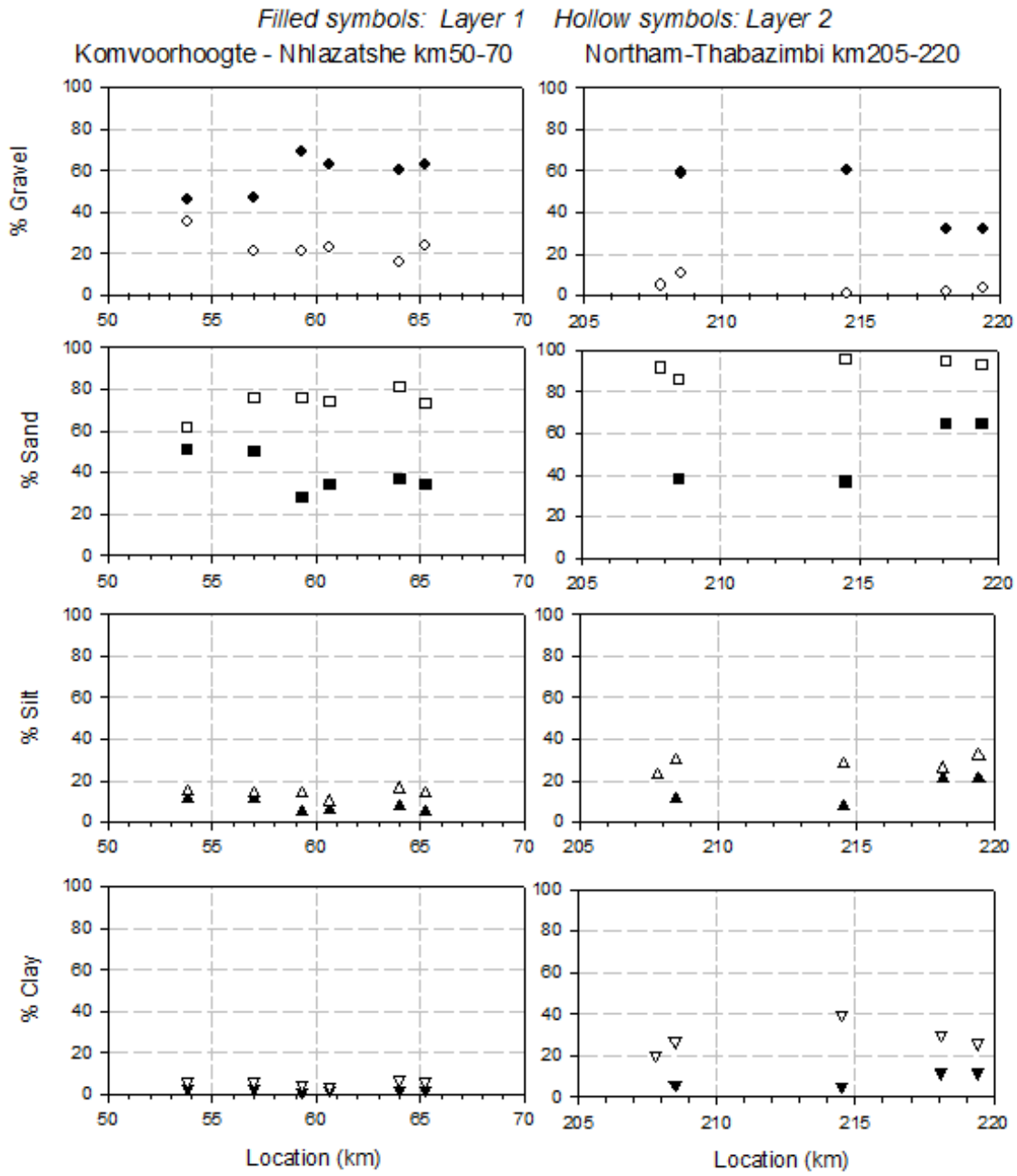

Figure 4.3: Soil parameter summary - Sheet B.

The material distribution in Figure 4.3 shows that the material from the two sections varies as follows: The material at the KN test section is more gravelly than that of the NT section. The silt and clay content of the NT test section is more than that of the KN test section. The sand content values of both sections are similar with the NT test section having significantly higher clay content in Layer 2.

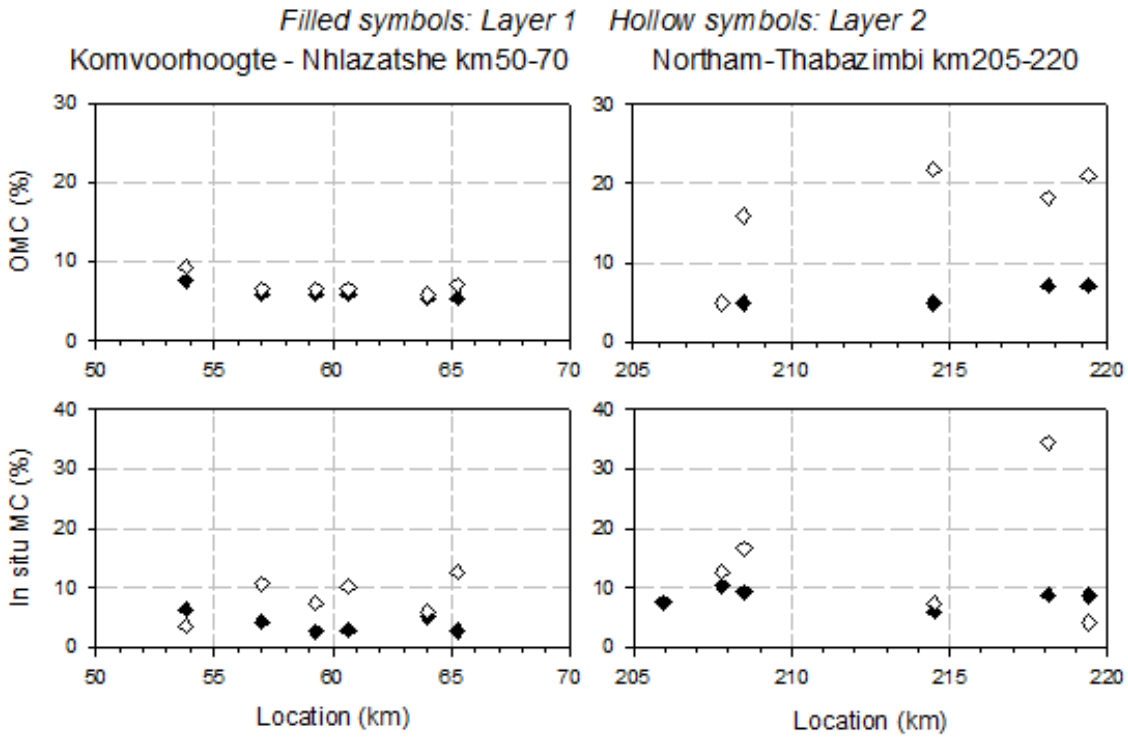

Figure 4.4: Soil parameter summary - Sheet C.

The moisture content for the KN test section is lower for both the Optimum Moisture Content (OMC) and the in situ moisture content compared to the NT test section. This could be attributed to the higher silt and clay content. The moisture content will influence the GPR dielectric permittivity as water has a higher dielectric permittivity than soil.

Table 4.2: S410 classification of soil parameters.

Test Site	Location (km)	Layer	SAR Index	Min. GM	Grading	PI	Max. CBR Swell	CBR	S410 Class
KN001	53+800	1	SB	SB	SB	SSB	SSB	SSB	SB
		2	SB	A	A	B	SSB	SSB	B
KN002	57+000	1	SB	SB	SB	SSB	SSB	SSB	SB
		2	SB	A	A	A	SSB	SSB	A
KN003	59+300	1	SSB	SSB	SSB	SSB	SSB	SSB	SSB
		2	SB	A	A	SSB	SSB	SSB	A
KN004	60+650	1	SSB	SSB	SB	SSB	SSB	SSB	SB
		2	SB	A	A	B	SSB	SSB	B
KN005	64+000	1	SSB	SSB	SSB	SSB	SSB	SSB	SSB
		2	SB	A	A	B	SSB	SSB	B
KN006	65+250	1	SSB	SSB	SSB	SSB	SSB	SSB	SSB
		2	SB	A	A	B	SSB	SSB	B
NT003	205+950	No sampling at this test location							
NT004	207+800	1	A	B	BE	BE	SSB	SSB	BE
		2	A	B	BE	BE	SSB	SSB	BE
NT006	208+500	1	SB	SSB	A	B	SSB	SSB	B
		2	B	B	B	BE	B	<BE	<BE
NT007	214+500	1	SB	SSB	A	B	SSB	SSB	B
		2	BE	BE	BE	<BE	<BE	<BE	<BE
NT010	218+120	1	A	A	A	BE	SSB	A	BE
		2	B	BE	B	<BE	<BE	<BE	<BE
NT012	219+400	1	B	A	A	BE	SSB	A	BE
		2	SB	A	B	BE	<BE	A	<BE

Using the S410 earthworks classification to classify the soil samples that were taken at the two test sections, the following was deduced:

- The material from Layer 1 at the Komvoorhoogte to Nhlazatshe (KN) test section was classified as either class SSB or SB which is in accordance with the design for subballast layers.

- The second layer of the KN test section was classified as either class A or B which is in accordance with the design of placed subgrade layers.
- At the Northam to Thabazimbi (NT) test section, both layers were predominantly classified as bulk earthworks or less. There were only two samples that were classified as class B.

Therefore, from the samples taken at the two test sections, it can be assumed that the Komvoorhoogte to Nhlazatshe test section will have better substructure conditions than the Northam to Thabazimbi test section.

4.2.2 Ballast parameters

The ballast fouling percentage was determined from the gradation of the ballast samples in Figure 3.20 and Figure 3.21. The percentage passing of the material through certain sieve sizes were used. Three methods were used to determine the ballast fouling percentage as summarised in Figure 4.5 by Arangie (1997).

The first method was developed by Pretorius (1993) and Equation 4.2 is used to determine the ballast fouling percentage. This method is used by Transnet Freight Rail for the determination of ballast condition.

$$F_e = (K_1 F_{19}) + (K_{21} F_{6.7}) + (K_3 F_{1.18}) + (K_4 F_{0.15}) \quad (4.2)$$

Where

F_e = effective degree of fouling

$F_{19} = \dfrac{[\%\ Pass(19mm) sieve] * 100}{27}$

$F_{6.7} = \dfrac{[\%\ Pass(6.7mm) sieve] * 100}{18}$

$F_{1.18} = \dfrac{[\%\ Pass(1.18mm) sieve] * 100}{11.5}$

$F_{0.15} = \dfrac{[\%\ Pass(0.15mm) sieve] * 100}{5.5}$

$K_1 = 0.4\ , K_2 = 0.3\ , K_3 = 0.2\ , K_4 = 0.1$

The second and third methods to determine ballast fouling percentage are as follows:

- % passing 22.4 mm sieve (ORE, 1991)
- % passing 4.75 mm plus 0.075 mm sieves (Tung, 1989)

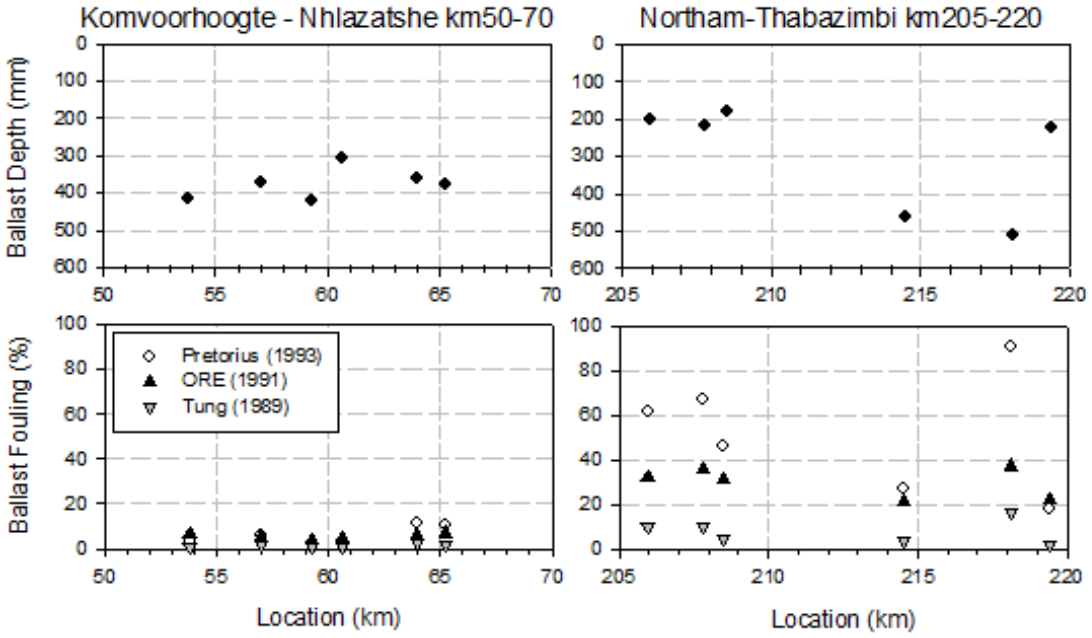

Figure 4.5: Ballast fouling parameters

The results show that the ballast fouling percentage is significantly less at the Komvoorhoogte to Nhlazatshe (KN) test section than the fouling percentage at the Northam to Thabazimbi (NT) test section. Using the first method of determining the ballast fouling percentage to compare the two sections, the following was observed:

- The average ballast fouling percentage was 5.8 % at the KN test section and 51.7 % at the NT test section. The ballast fouling percentage was therefore 8.8 times higher at the NT test section compared to the KN test section.
- Furthermore, the methods for determining ballast fouling percentage are sensitive to what particles size is regarded as fine material.
  - < 19.0 mm for Pretorius (1993)
  - < 22.4 mm for ORE (1991)
  - < 4.75 mm for Tung (1989)

Care should therefore be taken when deciding on the method used for ballast fouling percentage determination and it should coincide with the ballast material classification.

4.2.3 DCP

The DCP results were analysed by plotting the depth in millimetres against the number of blows it took to penetrate the soil for the 1 m long rod. A typical plot of this is shown in Figure 3.26. The layers were identified in accordance with the profiling of the test pits and correlated well with the DCP resistance of the layers. The layer thickness was then divided by the total number of blows required to give a value in mm/blow for each layer. The mm/blow was then converted to a CBR (%) value with Equation 4.3. Equation 4.3 is a summary of the work done by Kleyn (1975) and Kleyn (1984). This relationship was developed for typical road materials. These materials are similar to the SSB, SB, A and B layers recommended in the earthworks specifications. The results of the DCP tests for the two test sections are shown in Table 4.3 and Table 4.4.

$$CBR_{DCP} = 10^{(-1.30454 \log \mathrm{DN} + 2.60169)} \tag{4.3}$$

Where:

CBR_{DCP} = CBR calculated from DCP

DN = rate of DCP penetration for the layer in mm/blow

The CBR (%) values from the soil sampling are also included. Table 4.4 shows some samples where the soil was too weak to conduct the test. The first of which was a clayey material and the second a sandy clay.

Table 4.3: DCP results for Komvoorhoogte to Nhlazatshe.

Location (km)	Test depth (mm)	Layer (mm)	DCP		CBR @ 98 % Mod. AASHTO	CBR @ 95 % Mod. AASHTO	CBR @ 93 % Mod. AASHTO	CBR @ 90 % Mod. AASHTO
			mm/ blow	CBR				
53+800	635 - 855	220	5.74	40.94	85.0	69	66	62
53+800	855 - 1435	580	3.02	94.54	87.0	47	44	39
57+000	590 - 990	400	2.19	143.77	187.0	101	57	44
57+000	990 - 1390	400	4.77	52.02	65.0	39	29	18
59+300	640 - 1040	400	1.40	256.90	187.0	101	57	44
59+300	1040 - 1440	400	Refusal		65.0	39	29	18
60+650	525 - 1105	580	1.75	193.16	187.0	101	57	44
60+650	1105 - 1475	370	10.28	19.13	65.0	39	29	18
64+000	580 - 1040	460	1.34	272.43	134.0	91	62	35
64+000	1040 - 1580	540	Refusal		81.0	42	30	19
65+250	595 - 995	400	1.73	195.90	134.0	91	62	35
65+250	995 - 1395	400	1.86	177.81	55.0	32	23	14

Table 4.4: DCP results for Northam to Thabazimbi.

Location (km)	Test depth (mm)	Layer (mm)	DCP		CBR @ 98 % Mod. AASHTO	CBR @ 95 % Mod. AASHTO	CBR @ 93 % Mod. AASHTO	CBR @ 90 % Mod. AASHTO
			mm/ blow	CBR				
205+950	430 - 830	400	26.19	5.65	No sampling at this test location			
205+950	830 - 1230	400	25.00	6.00				
207+800	450 - 950	500	31.67	4.41	95.0	65	49	32
207+800	950 - 1450	500	35.38	3.81	95.0	65	49	32
208+500	410 - 860	450	15.32	11.36	95.0	65	49	32
208+500	860 - 1410	550	27.06	5.41	3.5	2.6	2.2	2.2
214+500	680 - 1280	600	4.13	62.88	95.0	65	49	32
214+500	1280 - 1680	400	13.33	13.62	Sample too weak for testing			
218+120	730 - 1130	400	20.00	8.02	48.0	29	25	21
218+120	1130 - 1530	400	Refusal		Sample too weak for testing			
219+400	445 - 845	400	17.50	9.55	48.0	29	25	21
219+400	845 - 1045	200	13.85	12.97	0.0	0.0	0.0	0.0
219+400	1045 - 1445	400	7.93	26.80	26.0	24	23	21

When comparing the CBR values from the DCP tests to the CBR laboratory tests, no significant correlation was found. The best correlation was between the DCP CBR results and the CBR at 98% of Mod. AASHTO density which had a correlation factor of 0.144. However, the DCP results provide a good indication of the layer thicknesses in places where different materials are found.

4.2.4 Conclusions

The results from the soils sampling, ballast sampling and the DCP testing provides a clear distinction between the two test sections. The substructure conditions of the KN test section are in accordance with the earthworks specification and the test section has distinct layers thicknesses. This section also has gravelly material in Layer 1 and sandy material in Layer 2. The conditions at the NT test section are variable and no distinct layer thicknesses are found. The material has some gravel but is predominantly sandy or silty clay. Therefore, the KN test section has a significantly better substructure condition than the NT test section.

4.3 ANALYSIS OF RVM AND MDD DEFLECTION MEASUREMENTS

The RVM deflection measurements at site KN004 on the Komvoorhoogte to Nhlazatshe test section (Appendix F) are analysed and compared to the MDD measurements (Appendix G). Firstly, the data from both the measurement techniques had to be reduced. A peak analysis was conducted on an entire train set's wheels. This made it possible to compare the deflection measurements from both the RVM and the MDD test results. The resilient deflections of the track components were compared with the axle loads. The measurements were presented and compared as follows:

- The comparison of axle load and substructure resilient deflections obtained from the RVM and MDD measurements.
- The comparison of the axle load, total track and substructure resilient deflection measurements.

4.3.1 General

For the evaluation of the measurement data, the following factors were considered for the selection of data:

Speed

It was decided that speeds between 35 km/h and 45 km/h would be used. This would reduce the effect that speed or dynamic impacts would have on the deflection on the respective track components. The speed was calculated by taking the distance between the wheels of two wagons and dividing it by the time it took to cross the measurement station. It was calculated at the start and end of each train.

Axle load

Axle loads ranged from 6 tons for empty wagons to 28 tons for full overloaded wagons. Axle loads were taken as the average of the axle load of a bogie axle pair as displayed in Figure 4.6.

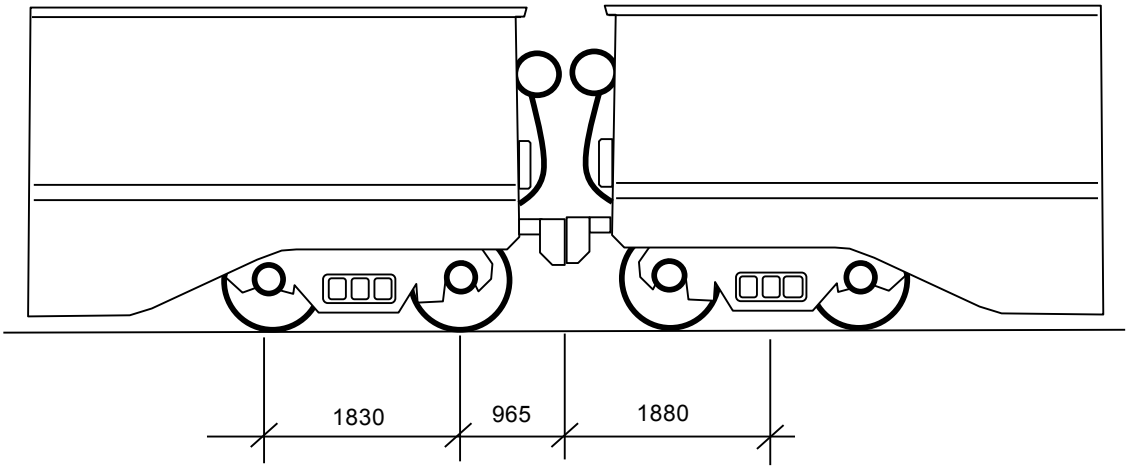

Figure 4.6: Typical wheel load configuration (based on 104 ton coal wagons – Transnet Freight Rail, South Africa).

RVM quality

After the measurement data with the required speed and axle loads were selected, the RVM data were analysed and zeroed. The quality of the measuring data was considered for the selection of the test site for the analysis. Station 2 provided the best quality measurement results. Although Station 3 also provided some good results, using two stations for the comparison would have delivered inconsistent results.

By using Station 2, it was found that only four runs complied with speed, axle load and quality. These included test runs 14, 16, 19 and 24. These test measurements still provided enough data points being collected for the comparison. A summary of the selected test runs is shown in Table 4.5.

Table 4.5: Summary of selected test runs at KN004.

	Train Consist					Speed		Axle Loads (ton)			
						(km/h)		Locomotives		Wagons	
Test run	Locos		Wagons		Direction	Start	End	Max	Min	Max	Min
14	1	7E	General freight		Down	37	39	20	16	18	8
16	2	7E	General freight		Down	37	39	22	18	18	12
19	4	11E	Jumbo	Smalls	Down	44	40	28	24	30	20
24	2	7E	Jumbo	Smalls	Down	40	39	24	20	22	14

4.3.2 Measurements at KN004

Similar to the axle load calculations, the deflection measurements would be the average of the peak deflections under each bogie axle pair. Maximum values were used for the analysis. A strand of six MDD modules measures the deflection of each individual layer and the individual deflections are added to obtain the total substructure deflection.

The deflection used for a typical load was taken as an average of the four deflections under the typical bogie load case represented in Figure 4.6. The test runs that complied with the speed conditions were analysed and all the typical load cases' deflections were obtained. After sufficient data was gathered for each of the selected test runs, the measurement results were compared. It should be noted that the number of data points from the RVM measurements (sampled at 25 Hz) are less than that of the MDD measurements (sampled at 500 Hz).

The deflection of each of the MDD modules under a typical load case (Figure 4.6) is shown in Figure 4.7. Typical results from the measurement data are shown in Figure 4.8 while the rest of the results are displayed in Appendix F.

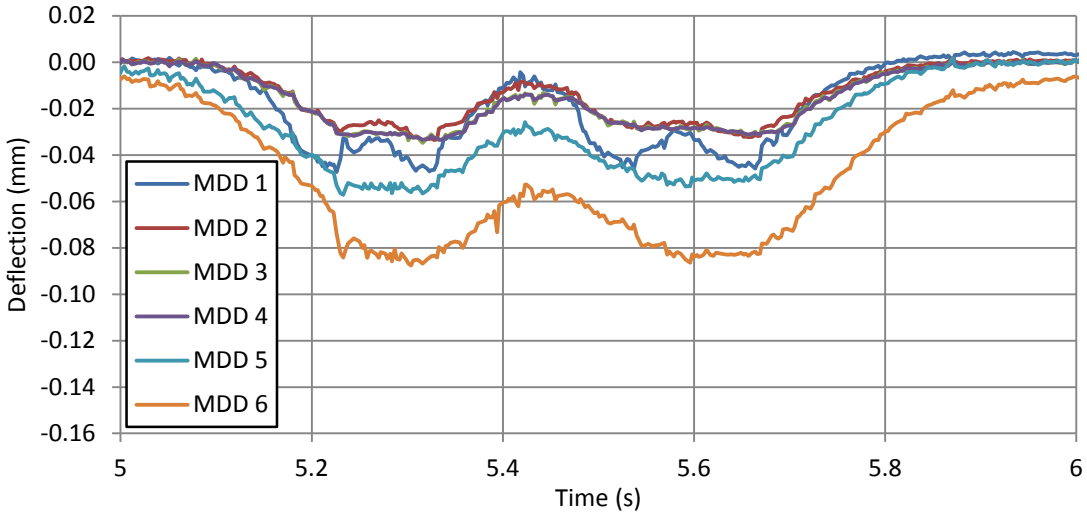

Figure 4.7: Individual MDD module deflections.

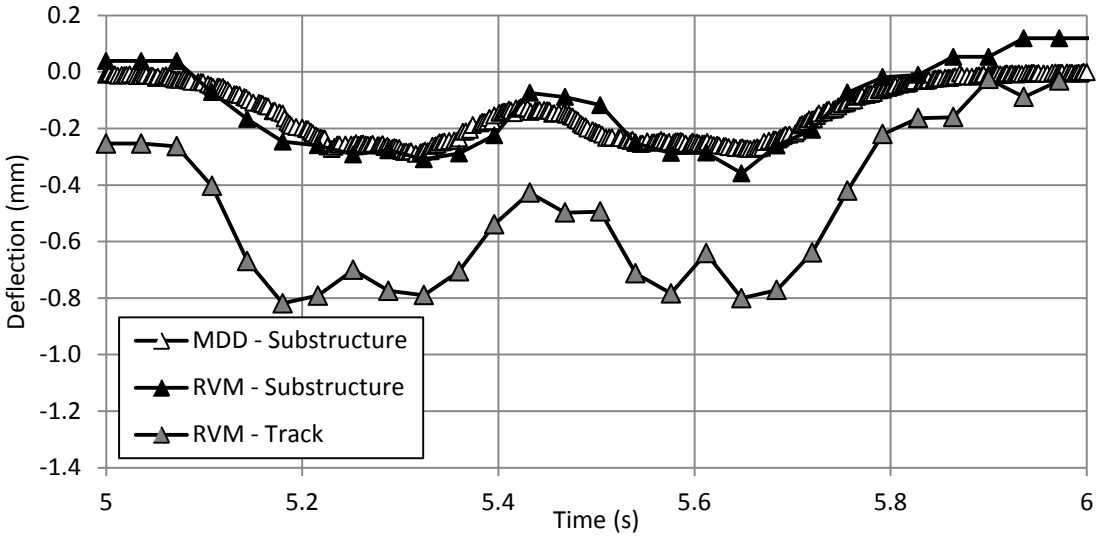

Figure 4.8: RVM and MDD deflection under typical load case.

4.3.3 Formation deformation (MDD and RVM) and axle load

To create a better understanding of the relationship between formation resilient deformation and axle load and how the RVM and MDD systems compare, the following relationships were established:

- A relationship between MDD formation deflection and axle load.
- A relationship between RVM formation deflection and axle load.

- A relationship between formation deflection and axle load.

The total deflection and substructure deflection from the MDDs and RVM system are displayed in Figure 4.9. The MDD substructure deflection was calculated by adding the deflection of all the substructure layer deflections obtained from the MDD measurement results. The RVM track and substructure deflections were obtained directly from the measurement system.

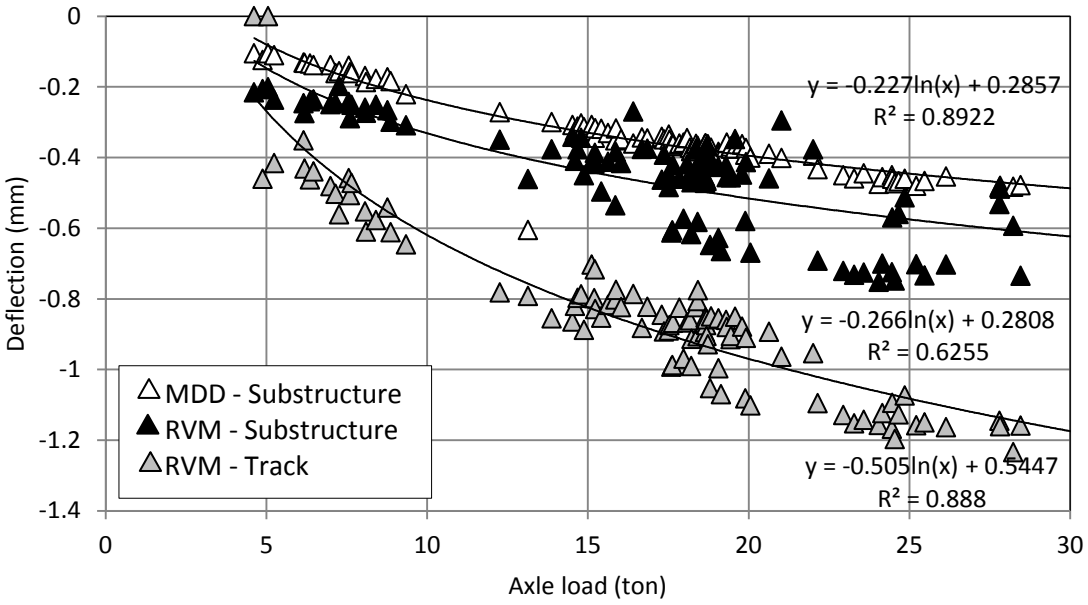

Figure 4.9: The relationship between total track and substructure deflection and axle load.

The general shape of the data was logarithmic and meant that the negative deflection increased less rapidly as the axle load increases towards 30 tons. A cause of the less rapid increase in resilient deflection could be the inherent stiffness of the materials. As the axle load increases, the soil particles compact and have less space to displace, causing a decrease in the resilient deflection. This is known as the strain hardening of soil (Craig, 2007).

The correlation coefficient for the MDD results and RVM track results were very good (R^2 = 0.89). For the RVM substructure results it was less with R^2 = 0.63 and could be attributed to the target being installed through the ballast. The rod, which was driven through the ballast into the top of the substructure, could be affected by the vibrations caused by the train. Even though the RVM substructure results are scattered more in comparison with the MDD results, larger negative deflections were recorded. The MDD results were 80% of that of the RVM

system. This was because of the fact that the MDD system did not measure from the top of the substructure layer. The uppermost MDD in the MDD string was not installed right at the top of the formation. Another explanation could be differential movement between the MDD system components. The RVM system therefore compares well with the MDD system and could be used for the measurement of formation deflections. However, care should be taken with the setup of the target. It was also found that the RVM formation deflection was 50% of total track deflection. This meant that the ballast resilient deflection was almost half of the total track deflection.

The comparison of the whole track structure deflection with respect to increasing axle load also illustrates the logarithmic relationship for axle loads (> 20 tons). This relationship does not relate to the linear relationship assumed by standard design models. These design models would lead to conservative and safe design of structures. They will, however cause higher capital cost expenditure.

To design for deflection with axle loads exceeding 28 tons, more research is required with different formations especially poor subgrade material subjected to higher axle loads.

4.4 RVM TRACK MODULUS DETERMINATION

The determination of the track modulus using RVM deflection measurements is discussed in this section. Two different methods were used for the determination thereof. In the first method, the total track deflection was used to determine the track modulus. From this track modulus, a substructure modulus was determined. In the second method, GEOTRACK was used with the formation deflection as a reference deflection to obtain substructure moduli. From this a proposed and actual track modulus was determined.

The total deflection and formation deflection obtained from the RVM measurements at the test locations used for the GPR analysis are shown in Figure 4.10. The two proposed methods are compared using these results.

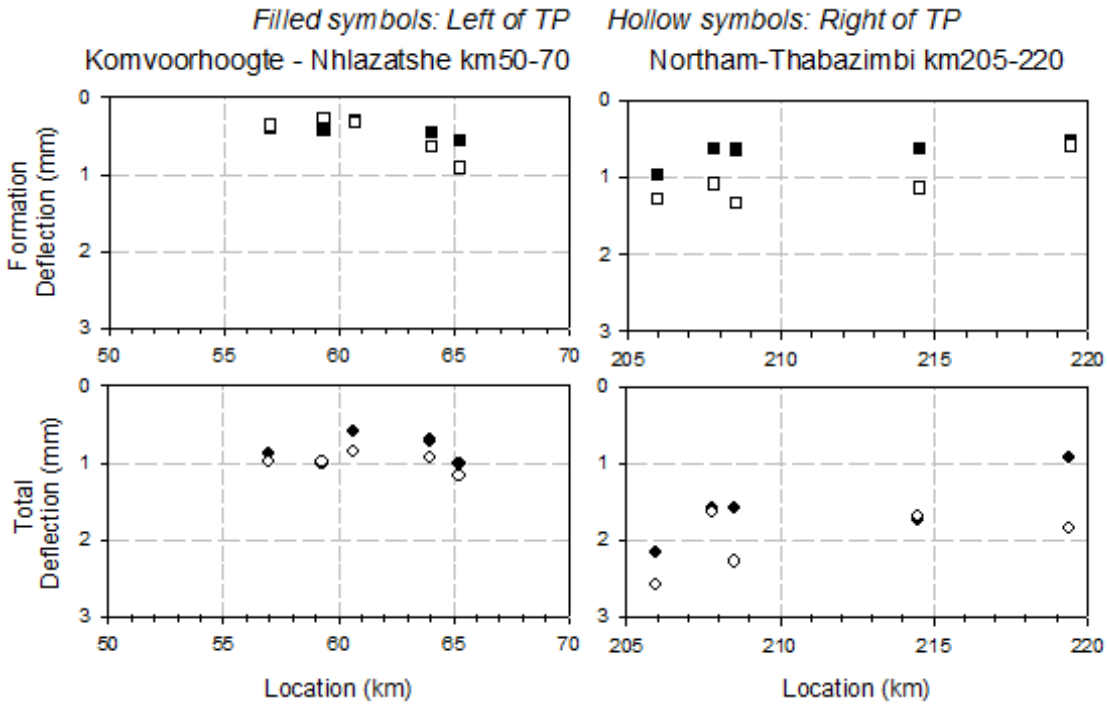

Figure 4.10: Total and formation deflection using RVM.

From the deflection measurements displayed in Figure 4.10, it can be seen that the formation and total deflection differ for the two track test sections. The total deflection for the first section ranges from 0.6 mm – 1.2 mm and the second section ranges from 0.9 – 2.6 mm. Furthermore, the formation deflection for the first section ranges from 0.3 mm – 0.9 mm and for the second section from 0.5 mm – 1.3 mm. This gives a clear indication that the substructure condition of the two sections of track vary in quality. This can be attributed both to the design and the type of material found in the track substructure. The material of the first test section are placed soil layers according to the track substructure specifications, whereas the foundation material of the second test section is predominantly in situ clay.

4.4.1 RVM Substructure and Track Modulus using deflection

Using the total deflection obtained from the RVM measurements and the load of a typical locomotive axle, the total track modulus was determined. The method proposed by Selig and Li (1994) for the determination of track modulus and substructure modulus was used. The track modulus Using the beam on elastic foundation model, Equation 4.4 and Equation 4.5 are used to determine deflections with given track moduli. The track modulus is a measure of the

vertical stiffness of the rail foundation and the track stiffness is a measure of the vertical stiffness of the entire track structure (Selig and Li, 1994).

$$k = \frac{P}{\delta_m} \tag{4.4}$$

$$u = \frac{(k)^{\frac{4}{3}}}{(64EI)^{\frac{1}{3}}} \tag{4.5}$$

Where:

k = Track stiffness (N/m)

P = Vertical wheel force (N)

δ_m = Maximum vertical rail deflection (m)

u = Track modulus (MPa)

E = Rail modulus of elasticity (GPa)

I = Rail moment of inertia (m^4)

By rearranging this formula, the track modulus can be determined from the maximum total deflection under a wheel. The maximum total deflection under a single wheel differs from that of the maximum total deflection under a locomotive bogie wheel set. Therefore, the beam on elastic foundation method was used to first determine the deflection bowl under a single wheel shown in Figure 4.11 (a). This deflection bowl was then superimposed according to the wheel load spacing of the locomotive bogie shown in Figure 4.11 (b).

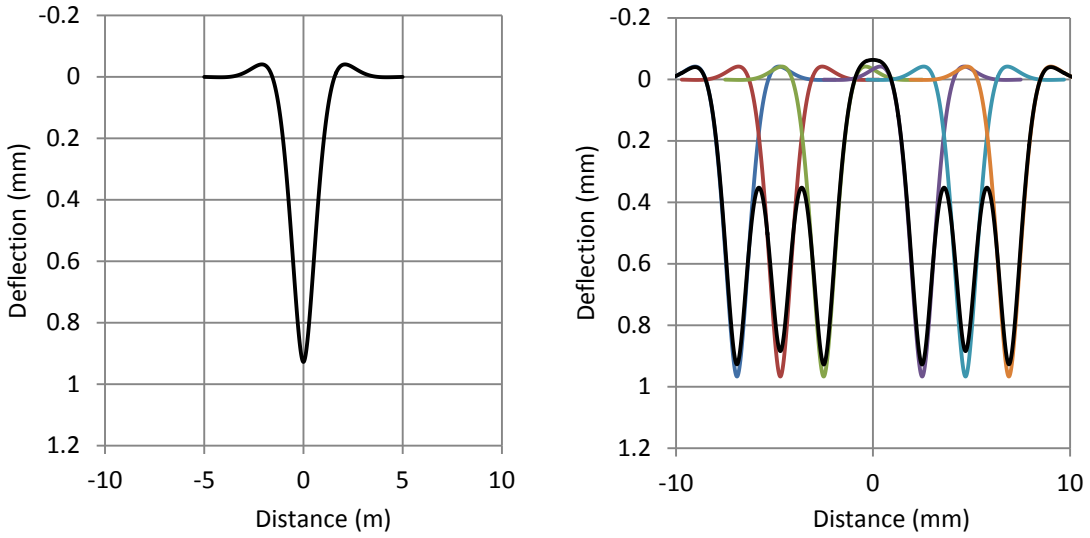

Figure 4.11: (a) Single and (b) Superimposed wheel load cases in beam on elastic foundation calculations.

To obtain the correct maximum deflection, the "solver" function within Microsoft Excel was used to change the deflection as a variable with respect to the true maximum deflection. The track modulus was determined from both the single wheel load as well as the superimposed wheel load. The substructure modulus was also determined from both these cases. The formulae used for this are Equation 4.6, Equation 4.7 and Equation 4.8. The substructure modulus is the vertical track stiffness per unit length of the track.

$$C = \frac{2us}{\kappa} \tag{4.6}$$

with

$$u = b_t C \tag{4.7}$$

$$\kappa = \frac{A_e \varsigma}{2} \tag{4.8}$$

Where:

C = substructure foundation modulus (MPa/m)

s = sleeper spacing

κ = characteristic value

b_t = transformation width of the sleeper (m)

A_e = effective sleeper area (m^2)

ς = fabrication material factor

= 1 for concrete sleepers

= 0.94 for timber sleepers (C< 60MPa/m)

= 0.91 for timber sleepers (C> 60MPa/m)

The results obtained from this analysis at both the Komvoorhoogte to Nhlazatshe (KN) and the Northam to Thabazimbi (NT) test sections are displayed in Table 4.6 and Table 4.7 below.

Table 4.6: RVM track stiffness, track modulus and track substructure modulus determination for the Komvoorhoogte to Nhlazatshe (KN) test section.

Location (km)	Load (t/axle)	Deflection (mm)		Track Stiffness (MN/m)		Track Modulus (MPa)		Substructure Modulus (MPa/m)	
		T*	F**	S***	SI****	S	SI	S	SI
57+000	21	0.876	0.389	129	124	89	84	175	166
		0.994	0.360	114	110	75	72	148	141
59+300	29	1.022	0.409	153	147	111	105	219	207
		0.993	0.265	158	151	115	109	227	215
60+650	21	0.598	0.296	189	182	148	140	291	276
		0.858	0.314	132	127	91	87	180	170
64+000	29	0.713	0.455	219	211	179	171	353	337
		0.928	0.636	169	162	126	120	249	236
65+250	21	1.024	0.562	111	107	72	69	142	135
		1.167	0.908	97	94	61	58	119	114

* T = Total track deflection (mm)
** F = Formation deflection (mm)
*** S = Single wheel load (t)
**** SI = Superimposed wheel loads (t)

Table 4.7: RVM track stiffness, track modulus and track substructure modulus determination for the Northam to Thabazimbi (NT) test section.

Location (km)	Load (t/axle)	Deflection (mm)		Track Stiffness (MN/m)		Track Modulus (MPa)		Substructure Modulus (MPa/m)	
		T*	F**	S***	SI****	S	SI	S	SI
205+950	21	2.158	0.956	53	54	27	28	53	55
		2.572	1.269	44	47	21	23	42	45
207+800	21	1.587	0.615	71	70	40	39	79	77
		1.637	1.080	69	68	39	38	76	75
208+500	21	1.584	0.629	72	70	40	39	79	78
		2.275	1.329	50	52	25	26	49	52
214+500	21	1.749	0.626	65	64	35	35	70	69
		1.692	1.131	67	66	37	36	73	72
219+400	21	0.918	0.510	123	119	83	79	164	156
		1.845	0.582	61	61	33	33	65	65

* T = Total track deflection (mm)
** F = Formation deflection (mm)
*** S = Single wheel load (t)
**** SI = Superimposed wheel loads (t)

A summary of the substructure modulus calculations for the two sections are also given in Figure 4.12. However, to compare the two sections, a classification system for substructure modulus used by Transnet Freight Rail was used. The classification of the substructure condition from substructure modulus (C) is as follows:

- Poor < 20 MPa/m
- Moderate 20 to 50 MPa/m
- Good 50 to 100 MPa/m
- Very Good >100 MPa/m

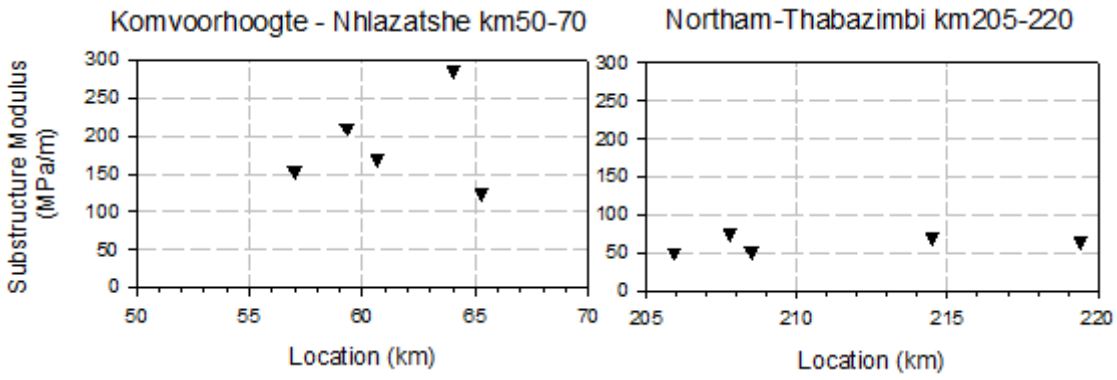

Figure 4.12: RVM Substructure Modulus.

The substructure condition for the Komvoorhoogte to Nhlazatshe (KN) test section falls in the "very good" category. This means that both the substructure foundation layers as well as the ballast were in very good condition. The substructure condition for the Northam to Thabazimbi (NT) test section falls in the "good" category with two "moderate" locations. This was the case even though the soil classification (Section 4.2.1) indicated that the foundation layers were not in good condition. It can therefore be assumed that with proper ballast and superstructure maintenance, the substructure condition can be improved. Furthermore, the average substructure modulus for the KN section was about three times higher than that of the NT section.

4.4.2 RVM Track Modulus determination using GEOTRACK

The methodology used to determine the track and substructure moduli using GEOTRACK and the RVM track and substructure deflection is described in this section. GEOTRACK is a track analysis software package that uses an analytical model to model the interactions between all the track components. The track modulus as well as maximum track deflection can be determined by entering the required design parameters. The software allows the user to determine deflections at different depths with respect to the top of the substructure (top of ballast). The substructure deflection could therefore be used to determine substructure moduli for the different substructure layers. Also, the total deflection measurement allows for the determination of the ballast modulus.

The track properties as discussed in Section 2.2 (rail, sleeper and substructure layers) were used for input parameters. The depth of the specific layers was in accordance with the test pits excavated at each site. Because the measurement of the deflection was done on the face of the

sleeper and at the top of the substructure layers, the layers assumed in GEOTRACK was that of the ballast, a single placed layer and an in situ layer. The layer profiles for the different test pits are summarised in Table 4.8 and Table 4.9.

Table 4.8: GEOTRACK layer inputs for Komvoorhoogte to Nhlazatshe.

Layer	Material	GEOTRACK Layer Thickness (mm)				
		KN002	KN003	KN004	KN005	KN006
1	Ballast	0 - 350	0 - 400	0 - 300	0 - 350	0 - 370
2	Subballast and Placed Layers	350 - 1150	400 - 1200	300 - 1250	350 - 1350	370 - 1170
3	In situ Material	> 1150	> 1200	> 1250	> 1350	> 1170

Table 4.9: GEOTRACK layer inputs for Northam to Thabazimbi.

Layer	Material	GEOTRACK Layer Thickness (mm)			
		NT004	NT006	NT007.1	NT012
1	Ballast	0 - 220	0 - 180	0 - 460	0 - 220
2	Subballast and Placed Layers	220 - 1220	180 - 1180	460 - 1460	220 - 1220
3	In situ Material	> 1220	> 1180	> 1460	> 1220

An iterative process was used to determine the track substructure and ballast moduli by varying the input values until the correct sleeper and substructure deflection was obtained. This was done, first keeping the ballast modulus constant at 220 MPa and the in situ modulus constant at 1 000 MPa for the Komvoorhoogte to Nhlazatshe (KN) test section. For the Northam to Thabazimbi (NT) test section, 300 MPa was used and by changing the subgrade soil modulus until the correct deflection was reached. These values were based on typical granular and clay materials (Byrne and Berry, 2008). Thereafter, the substructure and in situ moduli were kept constant and the ballast modulus was changed until the correct total deflection was reached. The results obtained from this analysis are shown in Figure 4.13. The input parameters and the results obtained from GEOTRACK are given in Appendix H.

The actual total deflection obtained from changing the ballast modulus was compared to a proposed total deflection where the ballast modulus was assumed to be 220 MPa. This was

done to highlight what the reduction in track modulus was due to slacks under the sleeper in the track. The actual elastic modulus values as well as the substructure modulus determination from the RVM results are shown in Figure 4.14.

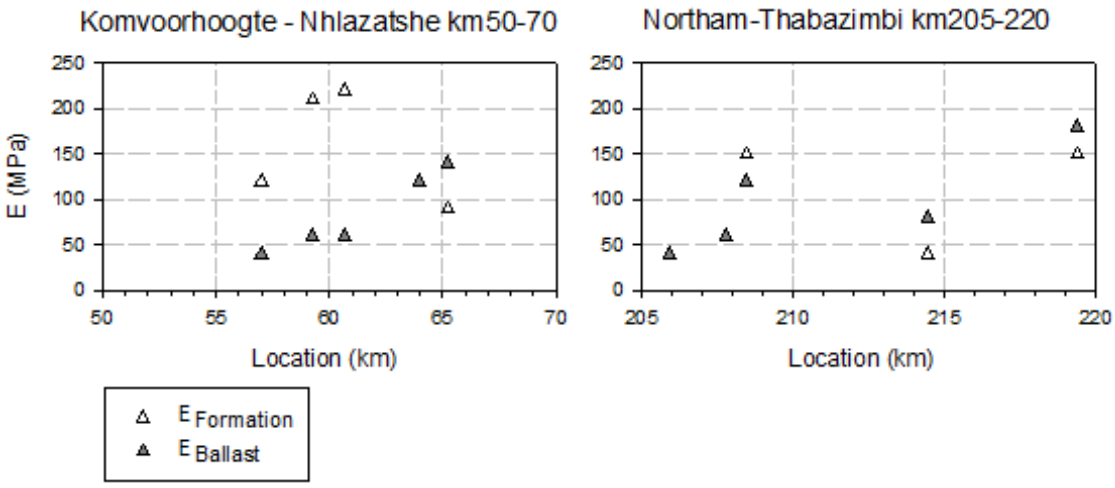

Figure 4.13: RVM substructure and layer Elastic moduli.

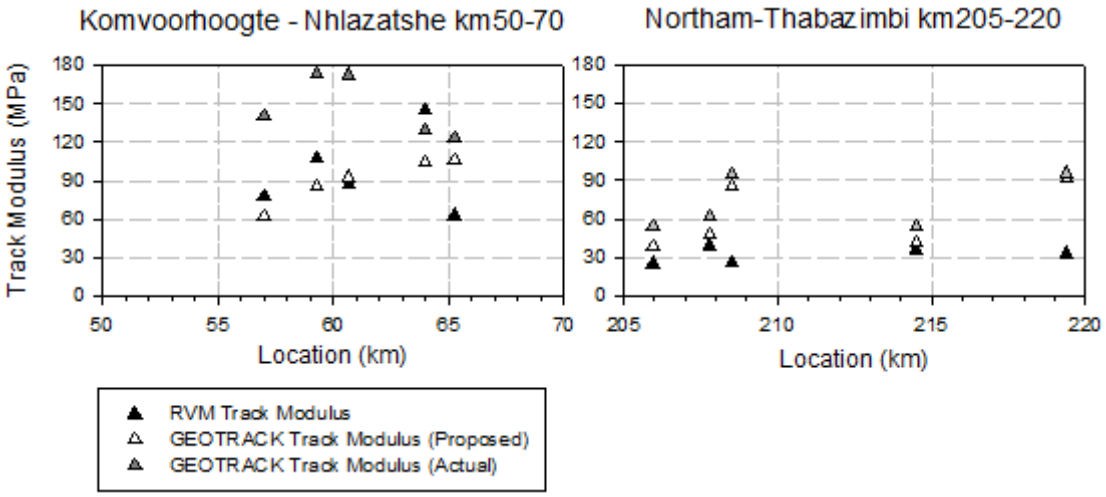

Figure 4.14: RVM Track Modulus Determination.

The different methods of determining track moduli show that the track modulus of the Komvoorhoogte to Nhlazatshe section is higher than that of the Northam to Thabazimbi section. The RVM track modulus for the first section is three times larger than that of the second section. The differences in RVM track modulus and the GEOTRACK track modulus

might originate from the assumptions made for the in situ elastic moduli in GEOTRACK. However, the GEOTRACK track moduli are mostly higher than the RVM track modulus for the Komvoorhoogte to Nhlazatshe section and lower for the Northam to Thabazimbi section. This means that the assumptions made for the placed soil and in situ modulus was conservative for the KN test section but too high for the NT test section.

4.5 LIGHT WEIGHT DEFLECTOMETER (LWD)

The LWD results as described in Section 3.7.3 is summarised and shown in Figure 4.15.

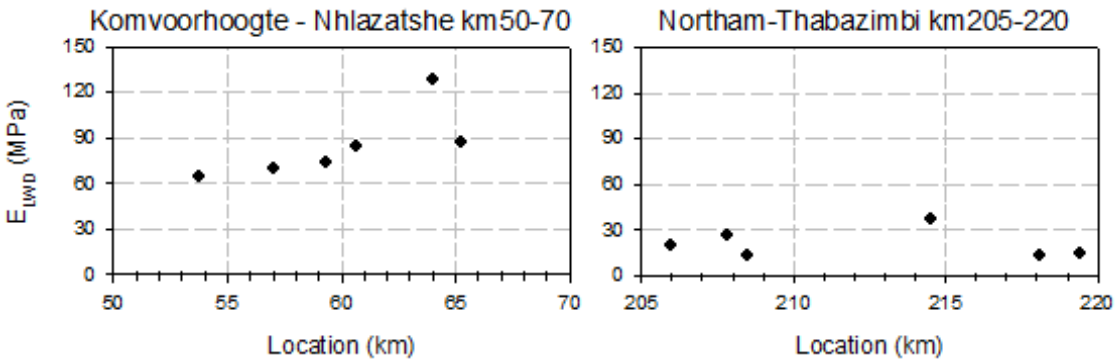

Figure 4.15: LWD Modulus for the two test sections.

The relationship between LWD modulus and the track substructure modulus is given in Figure 4.16. The relationship was linear and had a correlation coefficient of 0.864 which proved that the substructure modulus determination had a good correlation with geophysical moduli determinations.

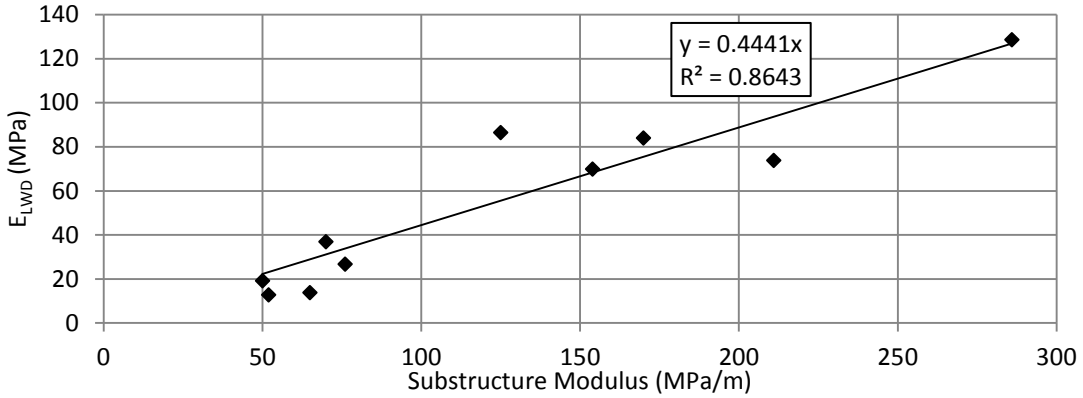

Figure 4.16: LWD modulus vs. Substructure modulus.

The substructure modulus, determined by the RVM deflections, for the KN test section is 3 times more than that of the NT test section. The substructure foundation modulus results were on average three times more than that of the LWD moduli for both the test sections.

4.6 ANALYSIS OF GPR FIELD MEASUREMENTS

This section deals with the determination of dielectric values from the known foundation layer depths. A comparison of in situ moisture conditions with GPR moisture condition as well as in situ ballast fouling and GPR ballast fouling index will also be done.

4.6.1 Dielectric values

The dielectric values at the test pit locations were determined by studying the profiled depths. Equation 4.1 as used in Section 4.1.2 was used to determine the dielectric values. The travel time (t) was determined by assessing a section of track at the test pit location stretching over a distance of more than 100 m. This allowed for continuity of the used GPR signals. The results of the Komvoorhoogte to Nhlazatshe section are displayed in Table 4.10.

Table 4.10: Dielectric permittivity of soil layers at Komvoorhoogte to Nhlazatshe.

Site	Distance (km)	Depth (mm)	Layer Thickness (mm)	Material Classification	t (ns)	ϵ_r
KN001	53+800	0 - 635	635	Sleeper + Ballast	9.7	5.8
		635 - 855	220	Silty Sand	5.6	5.6
		855 - 1435	580	Silty Sand	9.5	12.6
KN002	57+000	0 - 590	590	Sleeper + Ballast	9.4	5.7
		590 - 990	400	Silty Sand	6.6	6.1
		990 - 1390	400	Silty Sand	9.2	9.1
KN003	59+300	0 - 640	640	Sleeper + Ballast	9.2	5.0
		640 - 1040	400	Sand	9.0	11.4
		1040 - 1440	400	Silty Sand	9.0	11.4
KN004	60+650	0 - 525	525	Sleeper + Ballast	10.6	8.3
		525 - 1105	580	Silty Sand	9.8	6.4
		1105 - 1475	370	Sand	8.1	10.9
KN005	64+000	0 - 580	580	Sleeper + Ballast	9.2	5.7
		580 - 1040	460	Silty Sand	8.4	7.5
		1040 - 1580	540	Silty Sand	8.7	5.9
KN006	65+250	0 - 595	595	Sleeper + Ballast	9.5	5.7
		595 - 995	400	Sand	6.3	5.5
		995 - 1395	400	Silty	8.8	10.9

The results show that the average ϵ_r for the layers is as follows:

- ϵ_r(ballast) = 6.035
- ϵ_r(subballast) = 7.100
- ϵ_r(subgrade) = 10.131

This was in accordance with typical dielectric values as shown in Section 4.2.2. Therefore, the GPR dielectric permittivity for GPR analysis should give accurate layer thickness results.

Similarly, the $\epsilon_r$values for the Northam to Thabazimbi section were determined. The ϵ_r values of the ballast layer were determined, but the same was not possible for the other substructure layers. This was due to the variability in substructure layer thickness that is

caused by ballast penetration into the clayey substructure layers and subgrade attrition. The test pit profiling only provided the layer thickness of the substructure at individual points. With the variability in thickness, the alignment of the GPR survey data with the test pit locations was not precise. The variability of the layer thicknesses is depicted in Figure 4.17. The results of the ballast ϵ_r values are shown in Table 4.11. The average ϵ_r(ballast) value was 5.839 which were also in accordance with the literature.

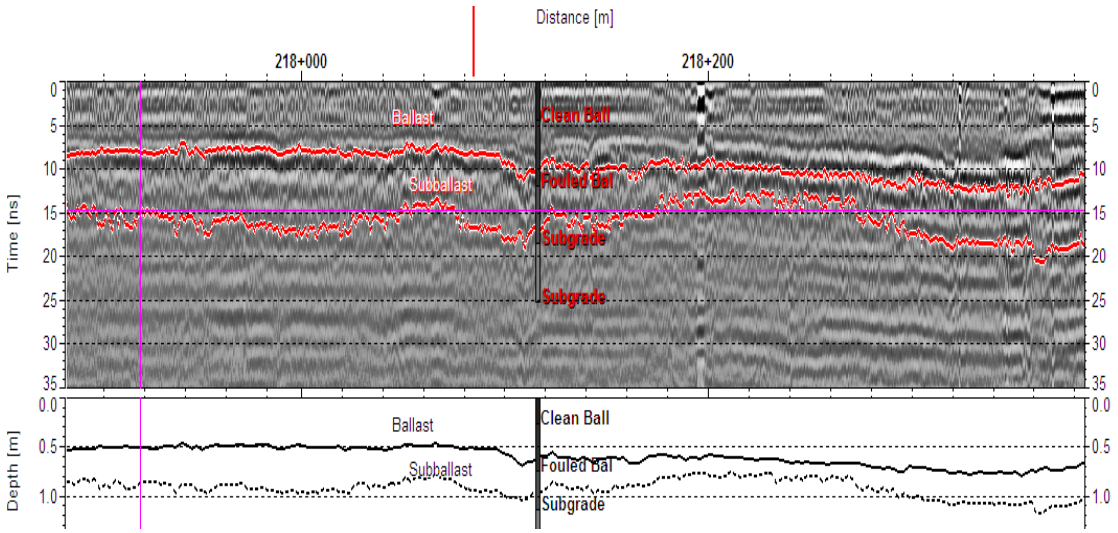

Figure 4.17: Substructure layer thickness variability at Northam to Thabazimbi.

Table 4.11: Dielectric permittivity of soil layers at Northam to Thabazimbi.

Test Site	Location (km)	Test depth	Layer Thickness (mm)	Material Classification	t (ns)	ϵ_r
NT004	207+800	0 - 450	450	Sleeper + Ballast	7.6	6.4
NT006	208+500	0 - 410	410	Sleeper + Ballast	6.8	6.2
NT007.1	214+500	0 - 680	680	Sleeper + Ballast	9.7	4.6
NT010	218+120	0 - 730	730	Sleeper + Ballast	11.0	5.1
NT012	219+400	0 - 445	445	Sleeper + Ballast	7.7	6.9

4.6.2 In situ moisture comparison

The GPR moisture index provides an indication of what material is found in the substructure layer. The higher the amount of moisture retained in the soil, the stronger the reflective signal

received by the GPR antennae. Knowing that clay and silty soil has a higher retention of water than sand and gravel, assumptions can be made of what material types are present in the substructure layers.

The in situ moisture samples taken can however not be compared to the GPR moisture index. This is because of the fact that the GPR signal strength decreases with depth and thus accurate moisture determination cannot be made for deeper depths. Also, the highest reflection occurs at the ballast and subballast interfaces. Therefore, the GPR moisture values should be used to indicate where moisture accumulates and to determine where possible mud holes and slacks in the track can occur.

Using the moisture as a substructure characterization tool will be discussed further in Section 4.7.3.

4.6.3 Ballast fouling comparison

The GPR ballast fouling (GBF) index provides an indication of the fouling condition on site. For the purpose of the comparison, the GBF index was calculated as an average over 200 m at the test locations. The average was used as the specific location of the GPR survey data could not accurately be determined. These values were compared to the traditional methods of determining ballast fouling percentage. The results are given in Table 4.12.

Table 4.12: Ballast fouling condition parameters.

Test Site	Location (km)	GBF Index	Fouling (%)		
			Pretorius (1993)	ORE (1991)	Tung (1989)
KN001	53+800	30.4	2.8	6.7	1.1
KN002	57+000	30.5	6.0	5.0	1.5
KN003	59+300	40.6	1.9	3.6	0.9
KN004	60+650	52.9	3.3	4.7	0.9
KN005	64+000	38.0	10.9	6.1	2.5
KN006	65+250	36.7	10.4	6.9	1.7
NT003	205+950	179.8	61.4	32.3	10.7
NT004	207+800	113.6	66.9	36.3	10.6
NT006	208+500	86.1	46.0	31.7	5.3
NT007	214+500	58.9	27.4	21.8	4.1
NT010	218+120	100.7	90.3	37.4	16.7
NT012	219+400	36.7	18.6	22.6	2.1

Using the ballast fouling results in Table 4.12, a linear regression analysis between the GBF index and the three methods were done. The results from the regression analysis are shown in Figure 4.18.

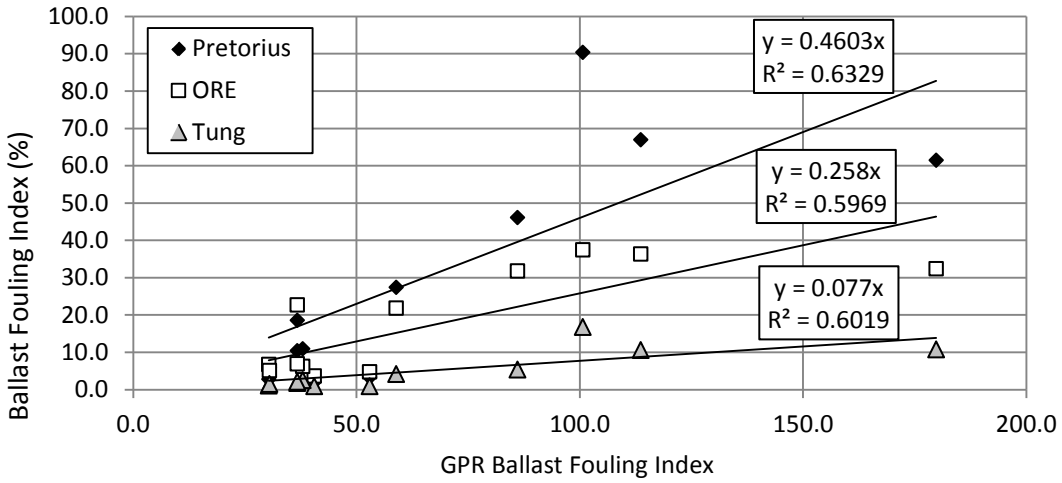

Figure 4.18: GPR Ballast Fouling Index comparison with traditional methods.

The linear regression analysis shows that the GBF index compares relatively well with all three methods with R^2 values of approximately 0.6 for all three ballast fouling determination methods. It should be noted that the GBF index can be calibrated according to the ballast fouling percentage results obtained in situ. For the purpose of this study, the characterization of good and bad sections of ballast was not done without using in situ testing.

4.7 GPR SUBSTRUCTURE CLASSIFICATION

This section describes the methodology followed to classify the GPR deliverables. The substructure layer profile roughness was determined and the ideal length for the root mean squared (RMS) method was also determined. The GPR substructure layer profile was then used for the classification. The GPR ballast fouling (GBF) index was also classified by using the results from the two surveyed sections.

4.7.1 Substructure roughness classification

The substructure roughness classification is described in this section. Firstly, the GPR substructure interpretation was extracted from the Railway Doctor GPR analysis software. The data are extracted as it was originally interpreted. This was done for ease of setting up a characterization model and so that the classification could be done without the field investigation.

The profile geometry of the subballast surface and the subgrade surface was used. The RMS method was used to determine the profile roughness of the layers (Equation 4.9) .This method was used because it exponentially increases the values and it simplifies the classification.

$$R^2 = \left(\frac{\sum_{i=1}^{n} {d_i}^2}{n}\right) \tag{4.9}$$

Where:

R^2 = Roughness (mm^2) route mean square calculation or variance

n = number of measurements in the length of track under consideration

d_i = difference between the elevation of the point being measured and mean filtered elevation

The roughness was calculated for 100 m, 200 m, 300 m and 400 m sections to determine what number of measurements would best suited the classification. The d_i values for the different n values were first calculated and are depicted in Figure 4.19, Figure 4.20, Figure 4.21 and Figure 4.22 for both the subballast and subgrade layers.

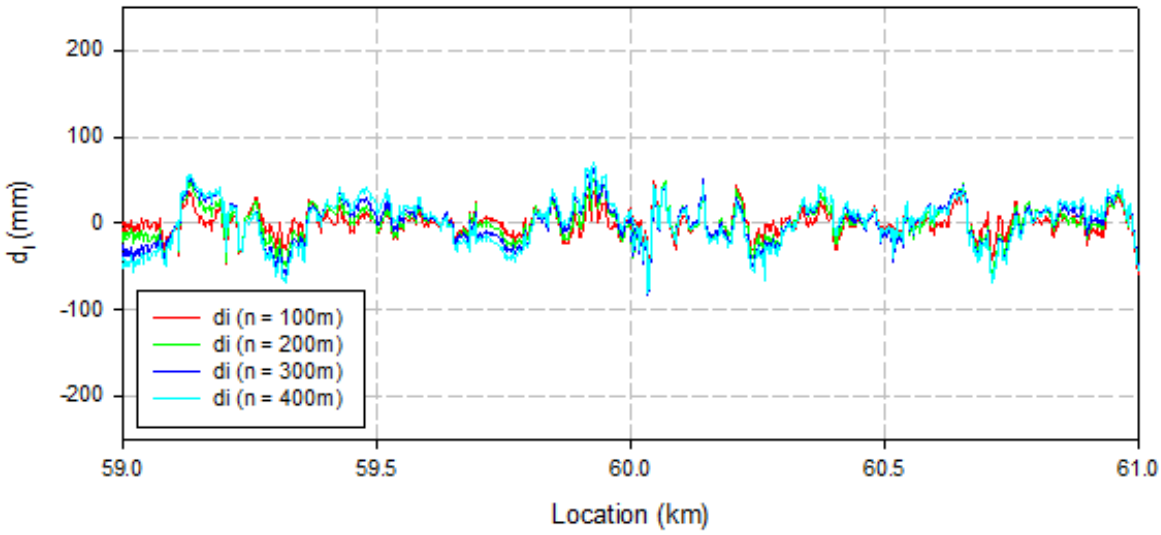

Figure 4.19: Typical subballast d_i values for Komvoorhoogte to Nhlazatshe.

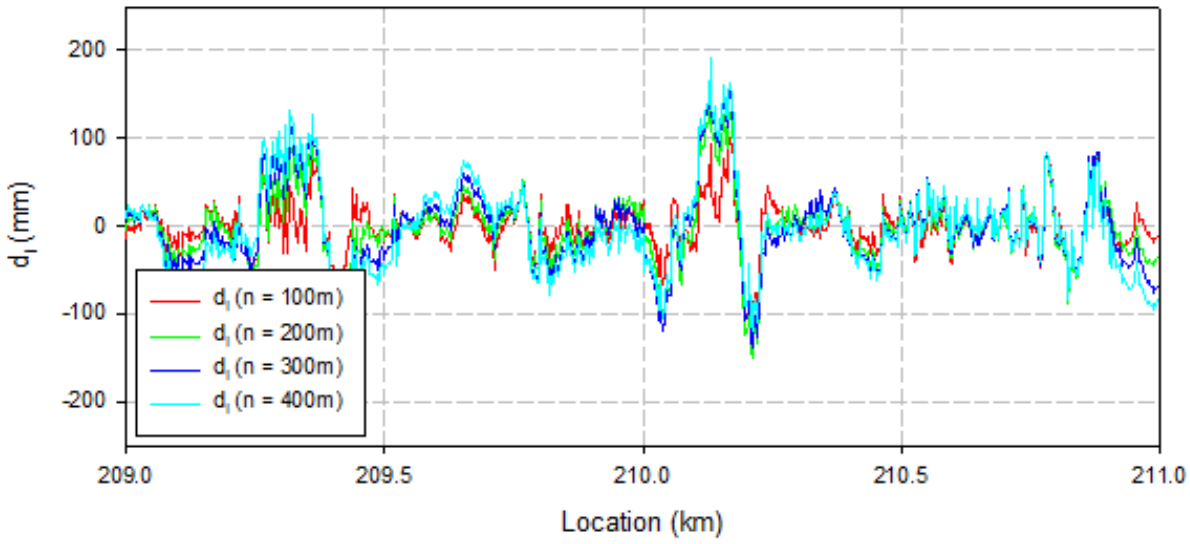

Figure 4.20: Typical subballast d_i values for Northam to Thabazimbi.

The results represented in Figure 4.19 and Figure 4.20 above shows that the d_i values for the subballast surface vary between -200 mm and 200 mm. The values at the Komvoorhoogte to Nhlazatshe (KN) test section vary between -100 mm and 100 mm (Figure 4.19). The values at the Northam to Thabazimbi (NT) test section vary between -200 mm and 200 mm.

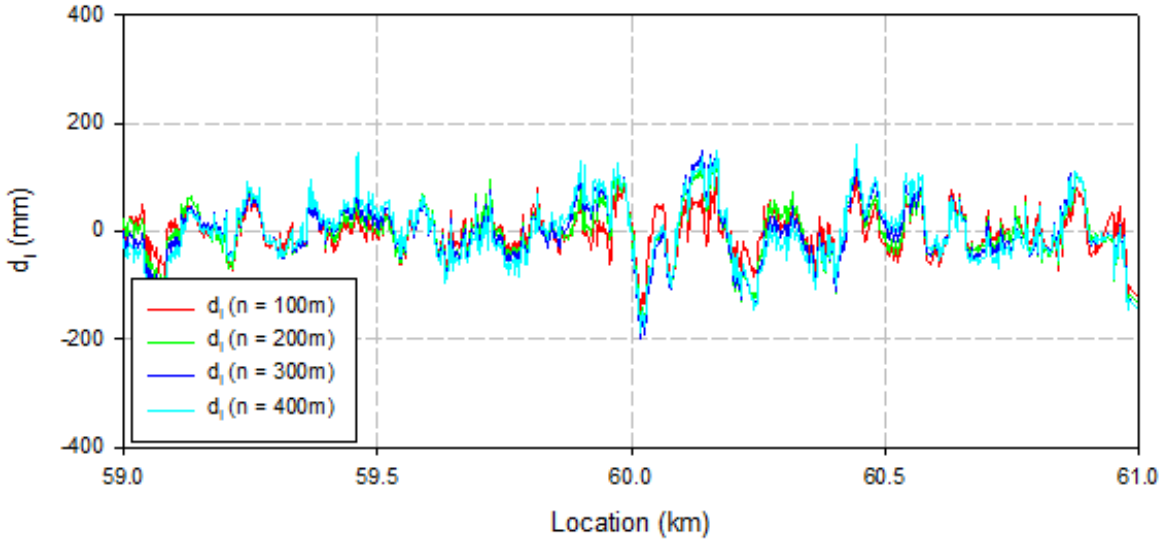

Figure 4.21: Typical subgrade d_i values for Komvoorhoogte to Nhlazatshe.

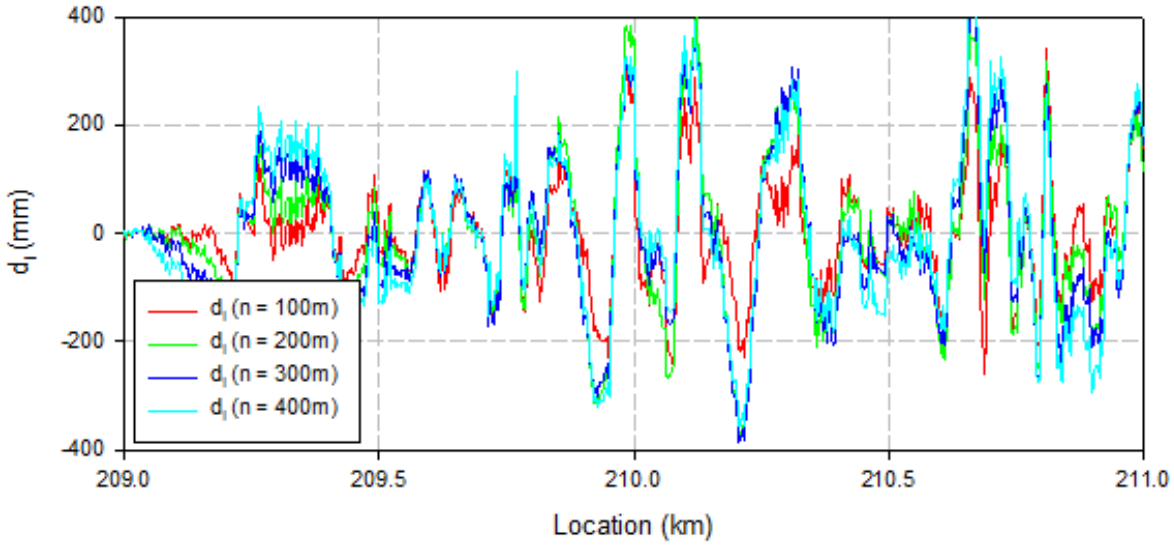

Figure 4.22: Typical subgrade d_i values for Northam to Thabazimbi.

For the subgrade surface (Figure 4.21 and Figure 4.22), typical d_i values obtained ranged between -400 mm and 400 mm with the KN test section range between -200 mm and 200 mm and the NT test section range between -400 mm and 400 mm. The figures above also show the difference in magnitude of the d_i values for the subballast and subgrade surfaces which are 200 mm and 400 mm respectively.

The d_i values were then used to calculate the R^2 values according to Equation 4.9. Typical results are shown in Figure 4.23, Figure 4.24, Figure 4.25 and Figure 4.26 for both the subballast and subgrade layers. The peaks shown on the graphs are position where possible deterioration within the track structure is occurring. It could also be instances where culvert, bridges or tunnels are located. These occurrences will be discussed further in Section 4.8.1.

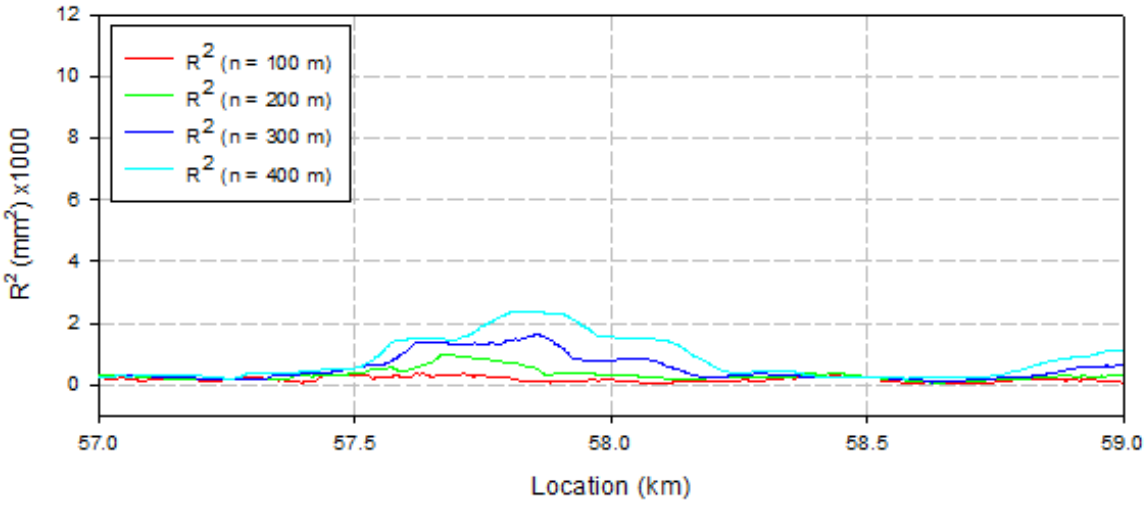

Figure 4.23: Typical subballast R^2values for Komvoorhoogte to Nhlazatshe.

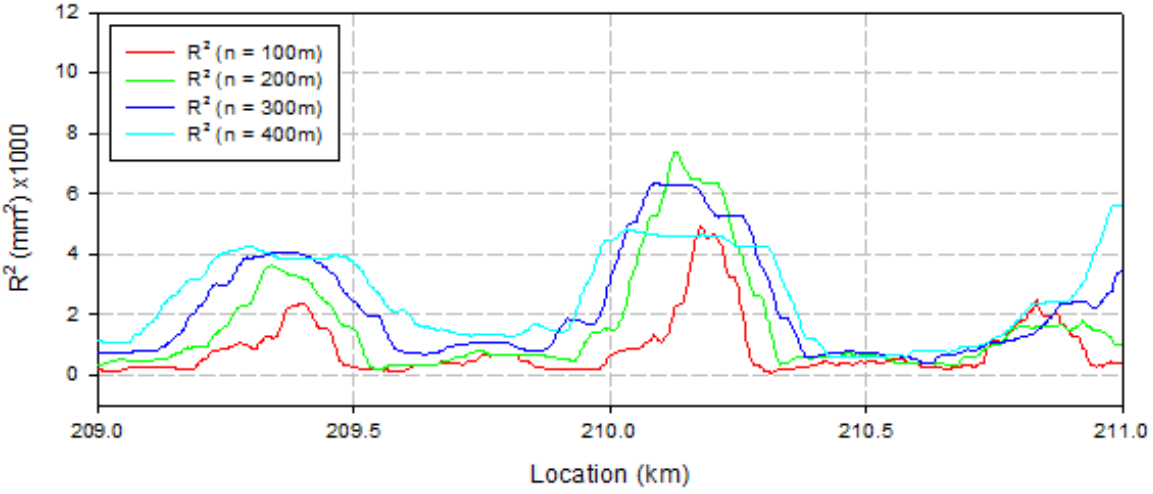

Figure 4.24: Typical subballast R^2values for Northam to Thabazimbi.

The maximum subballast roughness (R^2) obtained from the analysis was approximately 8 000 mm^2. Due to the large values and for the ease of characterization, the values were factored by a 1 000 (Figure 4.23 and Figure 4.24). The R^2 values at the KN test section ranged between zero and 4 000 mm^2 with most of the R^2 values below 500 mm^2. The values at NT test section were as high as 12 000 mm^2 with the R^2 values varying more than the results of the KN test section.

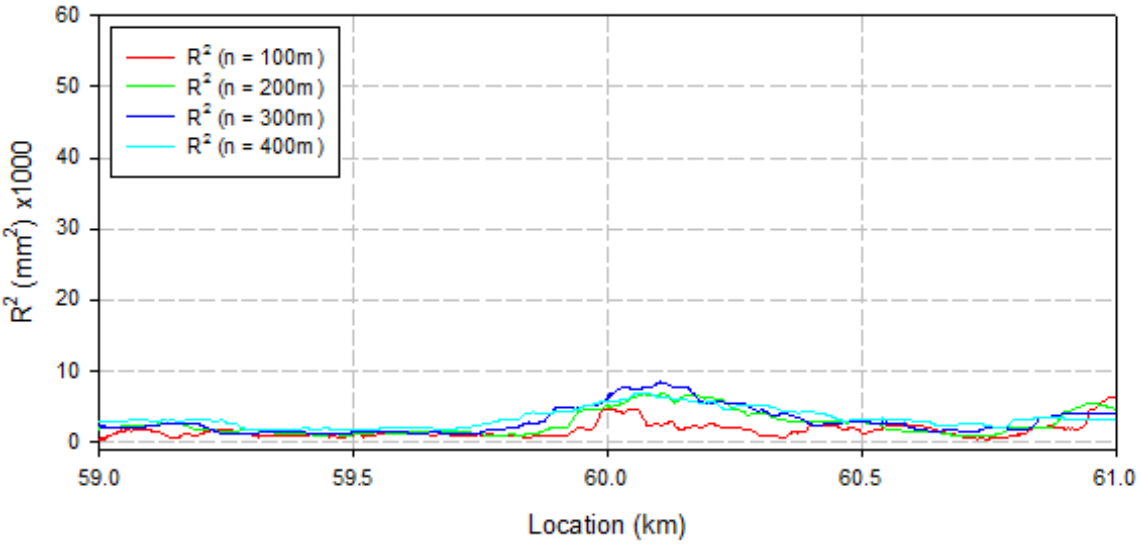

Figure 4.25: Typical subgrade R^2values for Komvoorhoogte to Nhlazatshe.

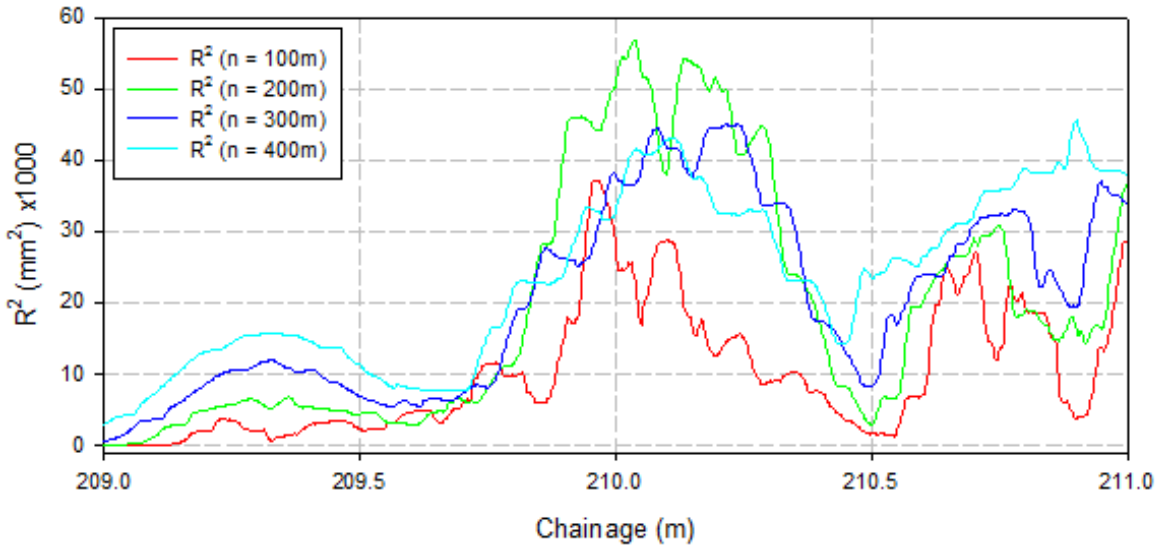

Figure 4.26: Typical subgrade R^2values for Northam to Thabazimbi.

The R^2 values of the subgrade (Figure 4.25 and Figure 4.26) were also higher and as with the subballast data, was factored by a 1 000. The R^2 values for the KN test section were less than 10 000 mm^2 and the values for the NT test section were as high as 60 000 mm^2.

The classification of the substructure surfaces was done using the values obtained from the RMS method with 200 m length intervals. The R^2 results of the subballast and subgrade layers used for the characterization model are shown in Figure 4.27, Figure 4.28, Figure 4.29 and Figure 4.30. The values used for the classification was obtained by assuming that typical R^2 values from the KN test section was of good condition and that of the NT test section was of poor condition based on the in situ tests and samples. The peaks in the data are section with poor quality or could be culverts, bridges or tunnels. These will be discussed in Section 4.8.1.

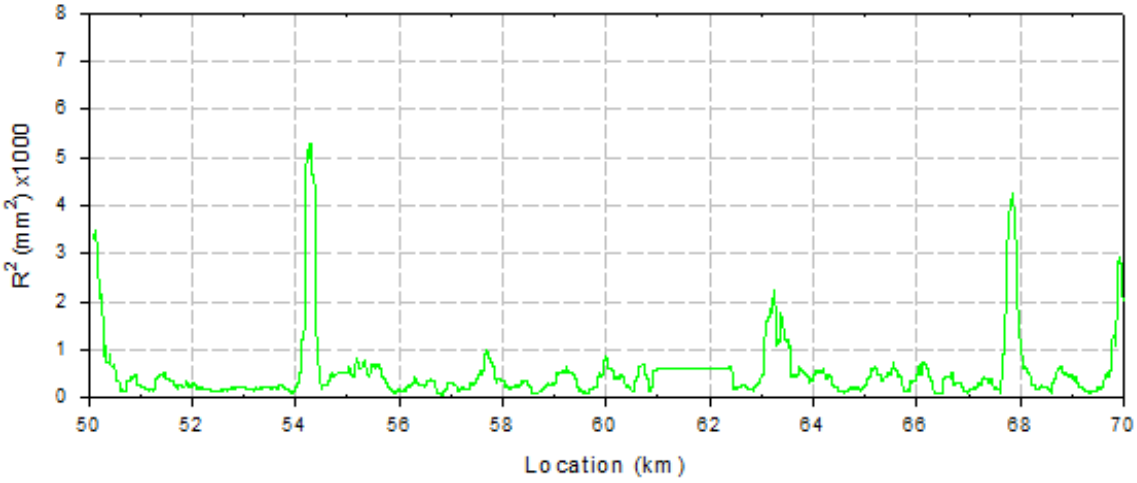

Figure 4.27: Subballast layer roughness for Komvoorhoogte to Nhlazatshe.

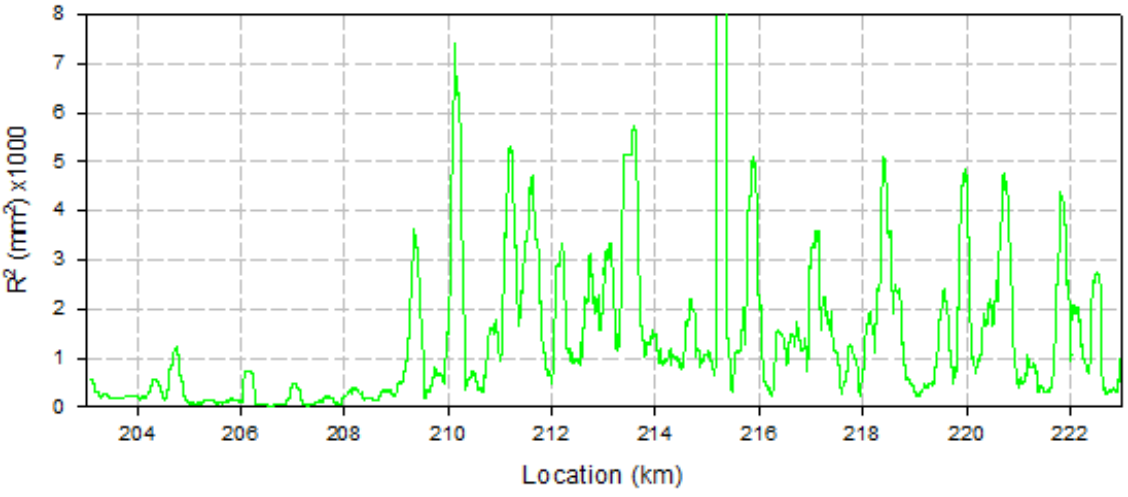

Figure 4.28: Subballast layer roughness for Northam to Thabazimbi.

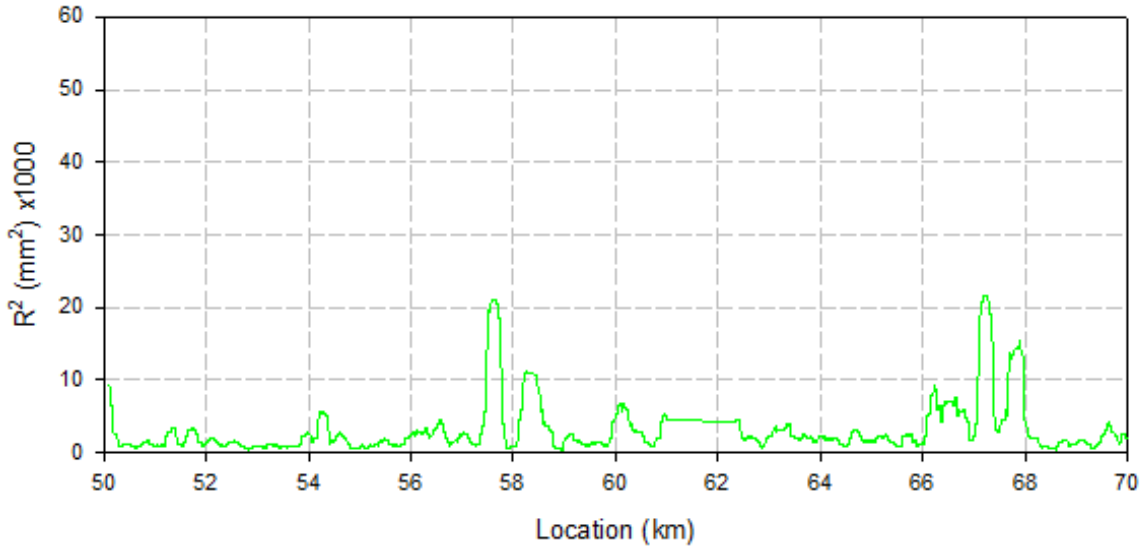

Figure 4.29: Subgrade layer roughness for Komvoorhoogte to Nhlazatshe.

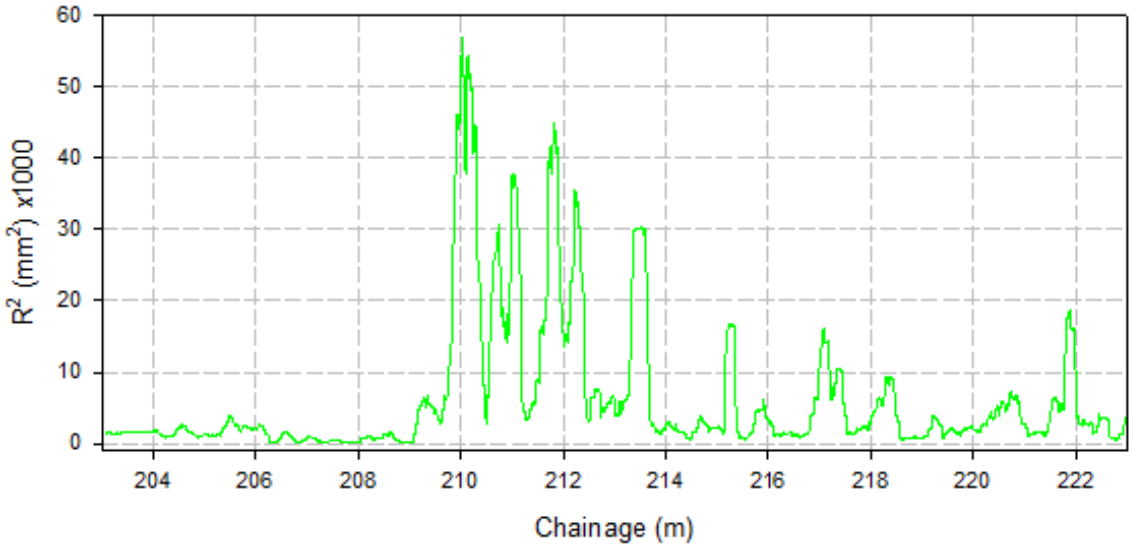

Figure 4.30: Subgrade layer roughness for Northam to Thabazimbi.

From the RMS analysis, almost all of the KN test section roughness values were below 1 000 mm^2 with three peaks above that. Furthermore, from all the roughness values below 1 000 mm^2, the majority was below 500 mm^2. Therefore, the first two classification ranges were selected to be from 0 mm^2 to 500 mm^2 and from 500 mm^2 to 1000 mm^2. The roughness of the NT test section's subballast varies over the whole section with values from 0 mm^2 to as high as 8 000 mm^2. It was decided to classify any values higher than 1 500 mm^2 as the worst condition of subballast roughness. The NT test section with poor foundation quality had

similar values and higher. The final characterization ranges for the subballast layer roughness factored by a 1 000 are defined as follows:

- Class 1: Very good = 0 to 0.5 mm^2 (x1 000)
- Class 2: Good = 0.5 to 1 mm^2 (x1 000)
- Class 3: Moderate = 1 to 1.5 mm^2 (x1 000)
- Class 4: Poor = > 1.5 mm^2 (x1 000)

The subgrade layer roughness of both test sections varied more than that of the subballast roughness. The roughness of the KN test section however still varied less than that of the NT test section. The roughness values for the KN test section were predominantly below 4 000 mm^2 and it was therefore decided to divide this into two classification ranges. Keeping to the same approach as that used for the subballast, using multiples of the first two ranges for the second two ranges. The final ranges for the subgrade surface characterization factored by a 1 000 are then as follows:

- Class 1: Very good = 0 to 2 mm^2 (x1 000)
- Class 2: Good = 2 to 4 mm^2 (x1 000)
- Class 3: Moderate = 4 to 6 mm^2 (x1 000)
- Class 4: Poor = > 6 mm^2 (x1 000)

4.7.2 GPR ballast fouling index characterization

The GPR ballast fouling (GBF) index was used for the characterization of the ballast condition. The results of the GBF index obtained for the left, centre and right survey lines were used for the analysis. The average of the three survey lines across the track was obtained. Typical results from both the test sections are displayed in Figure 4.31 and Figure 4.32.

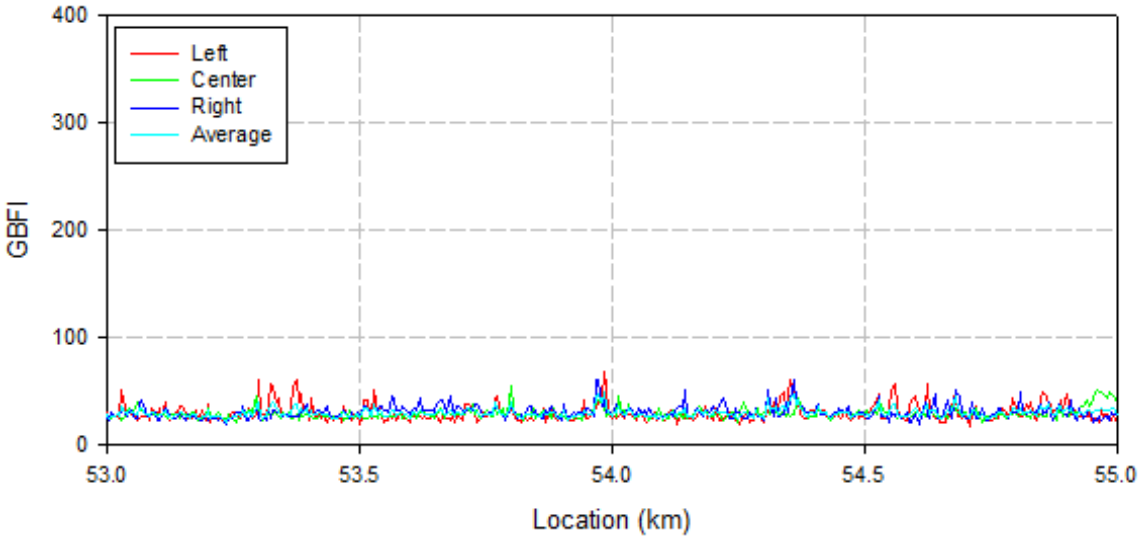

Figure 4.31: Typical GBF index results from Komvoorhoogte to Nhlazatshe.

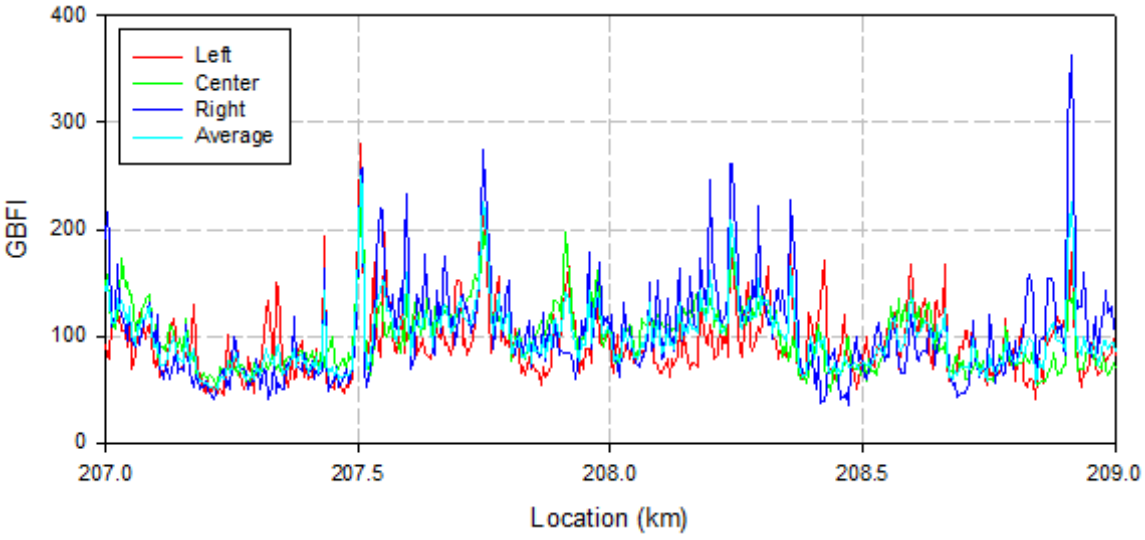

Figure 4.32: Typical GBF index results from Northam to Thabazimbi.

The results obtained shows that the GBF index can be as high as 400. However, the values at the KN test section were typically around 50 and the values at the NT test section were between 50 and 150.

The average GBF index values obtained from the two test sections were used for the classification of the ballast (Figure 4.33 and Figure 4.34). As for the substructure profile roughness, the GBF index at the KN test section was assumed to be of good condition while

that of the NT test section was of poor condition according to the ballast fouling index laboratory results.

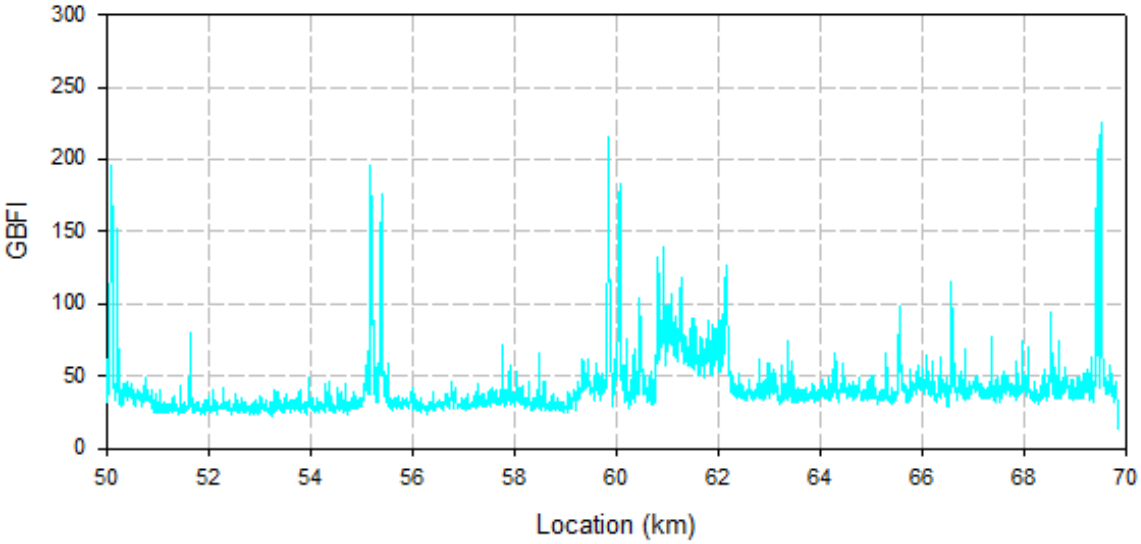

Figure 4.33: GBF index for Komvoorhoogte to Nhlazatshe.

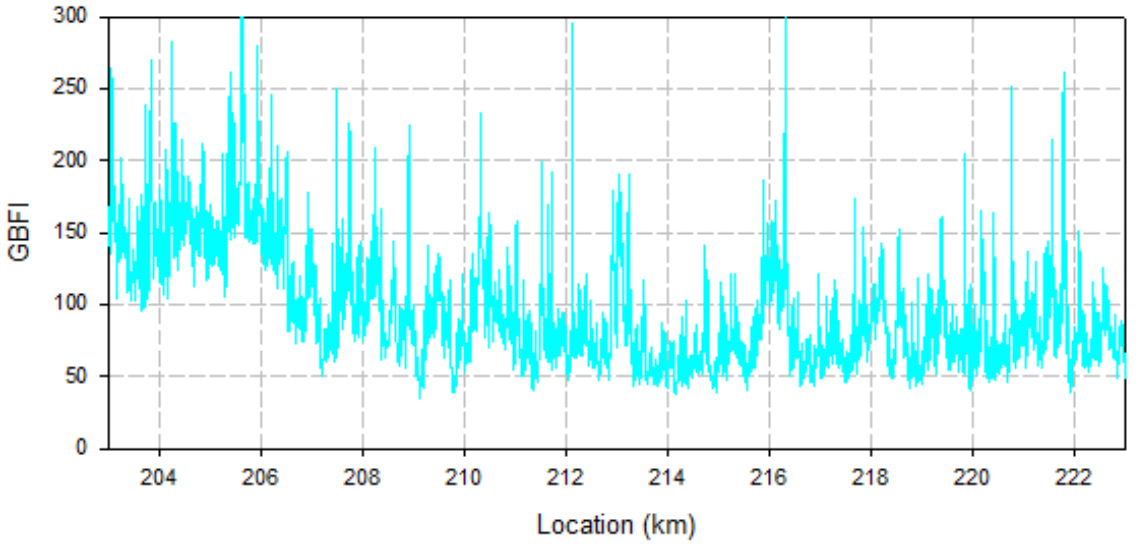

Figure 4.34: GBF index for Northam to Thabazimbi.

The GBF index values for the KN test section were mostly below 70 and that of the NT section below 140. The classification was also divided in four sections of which the last class was from 105 and higher. The characterization classes for the GBF index are listed below:

- Class 1: Very Good = 0 to 35

- Class 2: Good = 35 to 70
- Class 3: Moderate = 70 to 105
- Class 4: Poor = > 105

4.7.3 GPR moisture characterization

The GPR moisture condition with depth was also characterized. Because of the high variability in dielectric permittivity in materials with changing moisture conditions, a fixed range for classification would not have been possible. Therefore, the moisture condition at each location with depth was averaged to obtain one moisture value at each location. The results displayed in Figure 4.35 and Figure 4.36 was obtained.

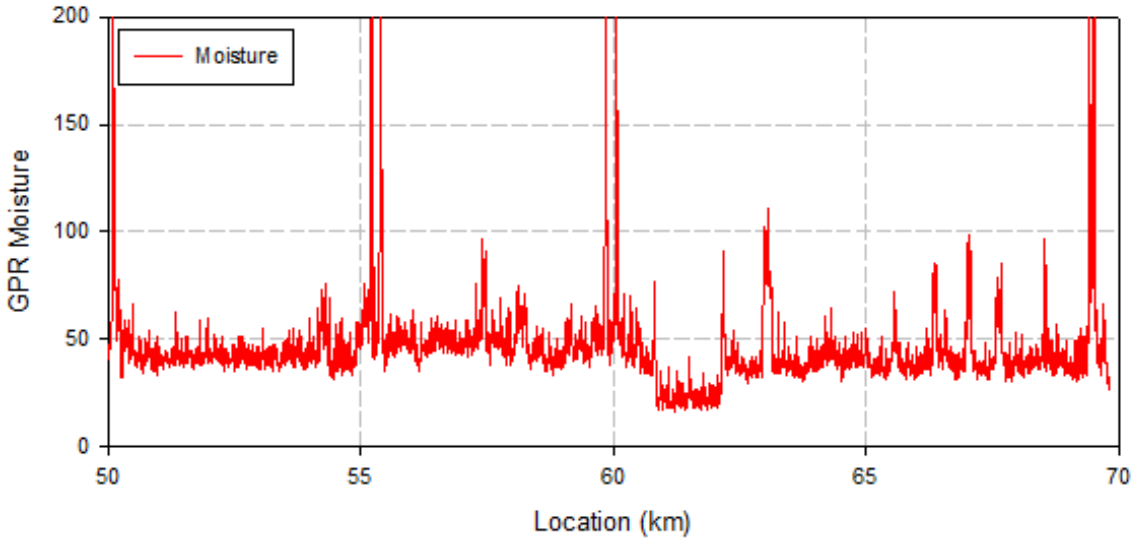

Figure 4.35: GPR moisture condition at Komvoorhoogte to Nhlazatshe.

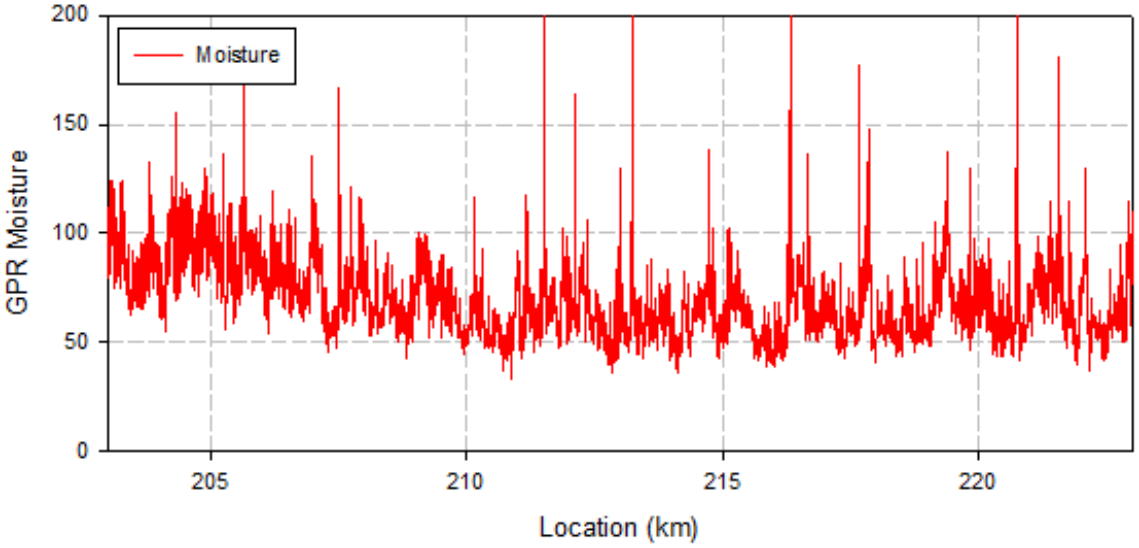

Figure 4.36: GPR moisture condition at Northam to Thabazimbi.

The results from the GPR moisture condition also did not provide a clear distinction between the two test sections. However, the results from the NT test section did have more variability than that of the KN test section. Therefore, an RMS analysis was conducted to emphasize the differences.

A similar RMS method was used as the one used for the substructure surface profiles. The d_i values were first calculated at 100 m, 200 m, 300 m and 400 m intervals. The R^2 values were then determined. Typical results obtained from the analysis are shown in Figure 4.37 and Figure 4.38.

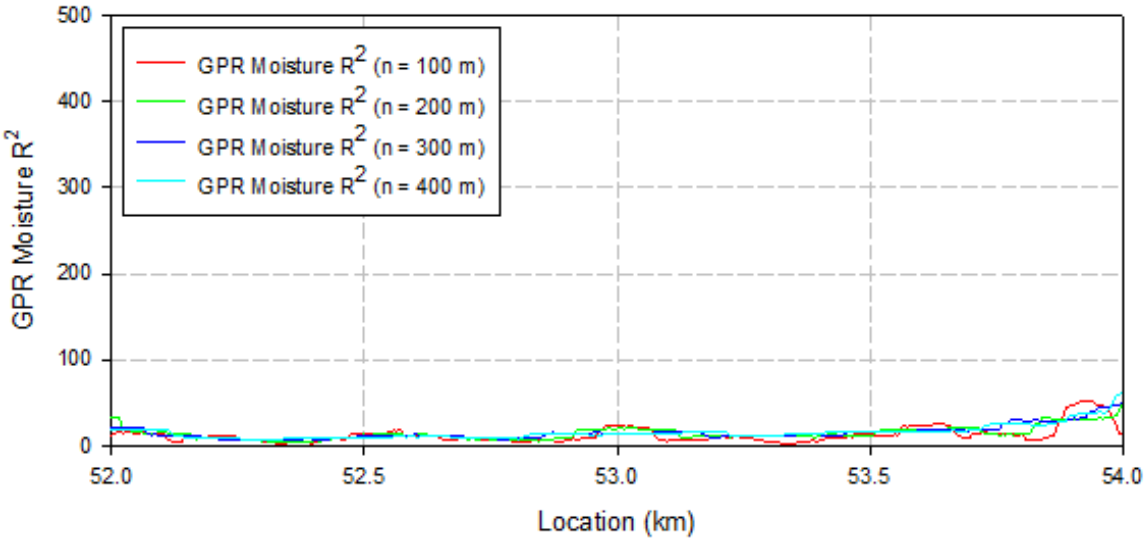

Figure 4.37: Typical GPR moisture R^2 for Komvoorhoogte to Nhlazatshe.

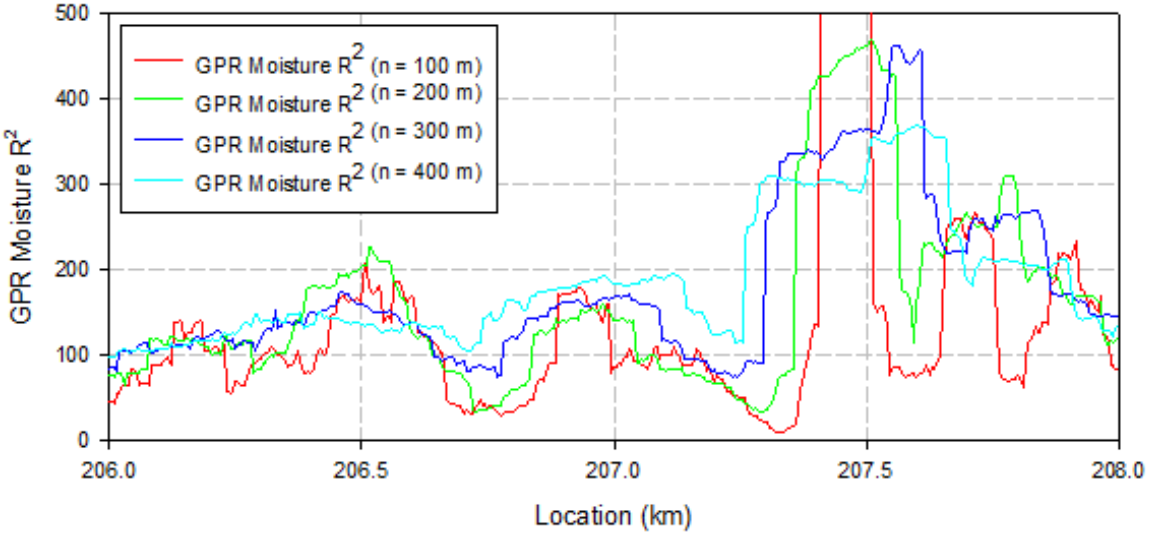

Figure 4.38: Typical GPR moisture R^2 for Northam to Thabazimbi.

The results from the RMS analysis provide a clear difference between the two test sections and could therefore be used for the classification. The results also clearly showed that at level crossings and at bridges, higher values were obtained than the rest of the track (Figure 4.39 and Figure 4.40). Therefore, the results at level crossings and bridges were not used for the characterization.

The remaining data showed that the R^2 values at the KN test section were typically below 50 and the R^2 values at the NT test section were typically below 200. The values from the RMS analysis with the interval length of 200 m were used for the classification of the GPR moisture condition (Figure 4.39 and Figure 4.40).

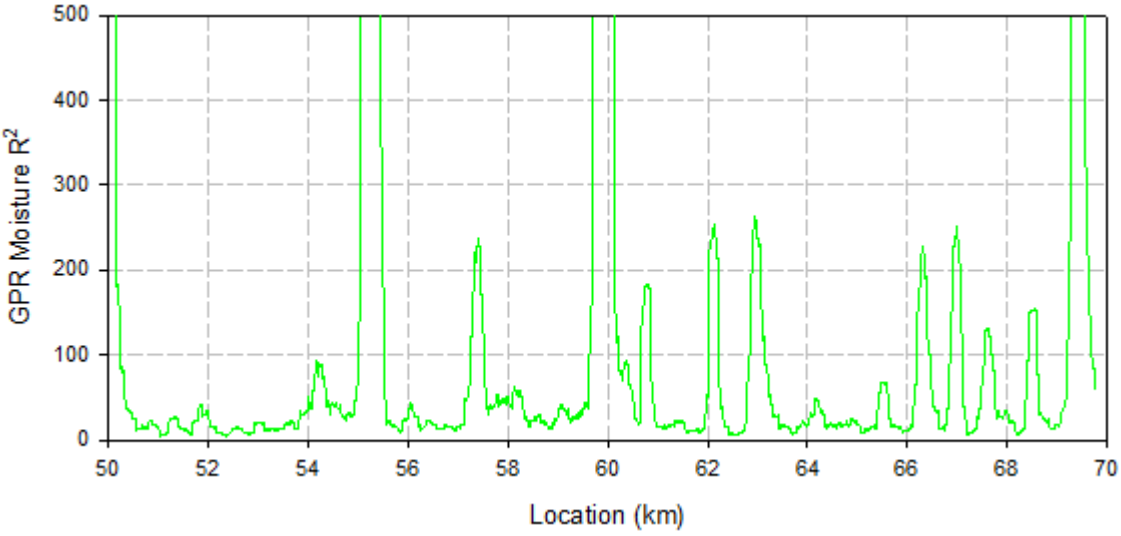

Figure 4.39: GPR moisture roughness for Komvoorhoogte to Nhlazatshe.

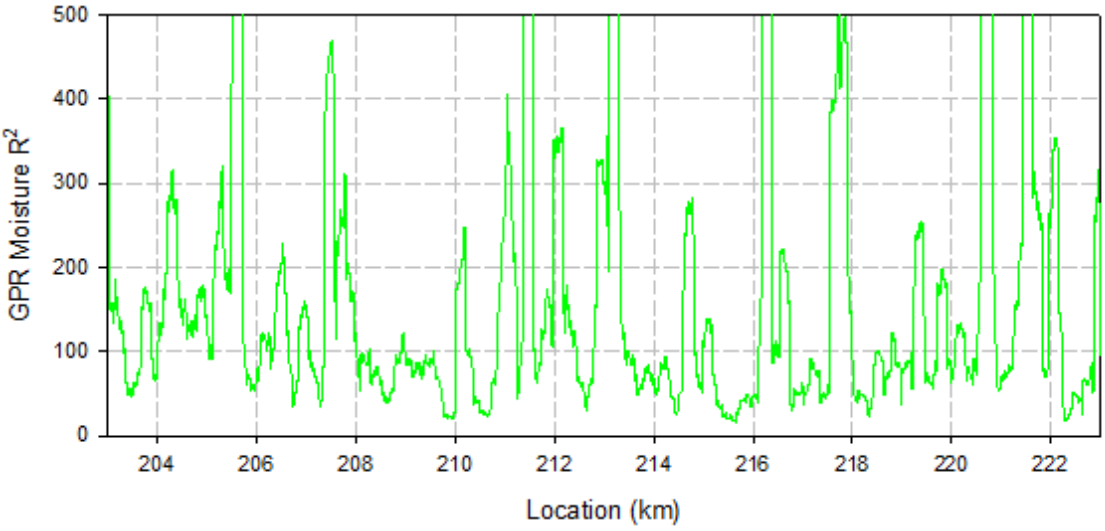

Figure 4.40: GPR moisture roughness for Northam to Thabazimbi.

The results from the GPR moisture roughness analysis of the two test sections show a clear difference between the two sections. The roughness of the KN test section is predominantly below 40 and the higher roughness values can be attributed to bridges, culverts and tunnels. The roughness of the NT test section varies a lot more and most of the values are between 80 and 200. The ranges for the GPR moisture roughness index classification were taken as multiples of 40 and are as follows:

- Class 1: Very good = 0 to 40

- Class 2: Good = 40 to 80
- Class 3: Moderate = 80 to 120
- Class 4: Poor = >120

4.8 GPR CHARACTERIZATION MODEL

The GPR characterization model was developed using the classes obtained from the subballast roughness, subgrade roughness, GBF index and the GPR moisture condition roughness classifications. The ranges for each of the classes are shown in the Table 4.13 below.

Table 4.13: GPR Substructure classifications.

	Class 1	Class 2	Class 3	Class 4
	Very Good	Good	Moderate	Poor
Subballast surface R^2	0 to 0.5	0.5 to 1	1 to 1.5	>1.5
Subgrade surface R^2	0 to 2	2 to 4	4 to 6	> 6
GBF index average	0 to 35	35 to 70	70 to 105	>105
GPR moisture R^2	0 to 40	40 to 80	80 to 120	>120

The characterization of the different GPR deliverables were done using Microsoft Excel and then transferred to the Railway Doctor GPR analysis software. The methodology followed to obtain the continuous classification is described in Section 4.8.1.

4.8.1 Classification

The same methodology was followed for the subballast surface roughness, subgrade surface roughness, GBF index average and GPR moisture condition roughness classification.

The frequency at which each of the data sets were recorded, were different and therefore different amounts of data points were recorded for the same length of track. The data sets were modified so that values from different data sets were contained in the same rows. This was done by creating a new set of track positions (in meters) that contain the smallest possible change in distance recorded, namely 0.5 m intervals. The track distance values that were not

taken in 0.5 m intervals were rounded to the nearest 0.5 m interval. The data sets were then lined up and where there were no values, the available values were equally distributed between positions.

The data sets were automatically classified by a function using the ranges in Table 4.13 that gave a numerical value for each of the classes (1 to 4). This was done for both the Komvoorhoogte to Nhlazatshe (KN) test section and the Northam to Thabazimbi (NT) test section. The characterized values were then imported into Railway Doctor and displayed with the line data to provide a continuous characterization of the track substructure. Furthermore, the classification of the subballast layer roughness and the subgrade layer roughness values were grouped together to provide one classification for the layer roughness. The GPR ballast fouling index and the GPR moisture index roughness values were also grouped together. The classification for the two test sections are displayed in Figure 4.41, Figure 4.42, Figure 4.43 and Figure 4.44. The results are extremely detailed and can be processed further. This made it possible for a direct comparison between the in situ test classification and the GPR substructure classification. It also allows for the data to be grouped according to different conditions and lengths.

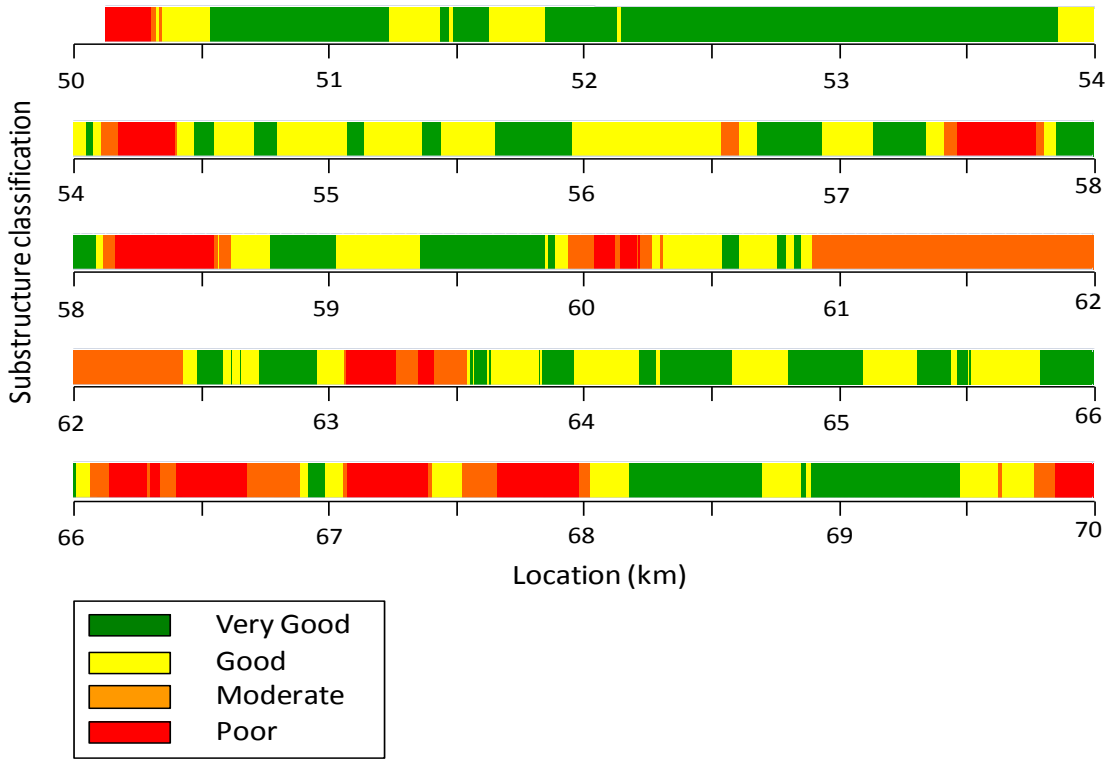

Figure 4.41: Substructure classification for KN test section.

The substructure classification at the KN test section showed that most of the track is in a good or very good condition. There are however sections with moderate and poor condition. After further investigation using the Railway Doctor software, it was determined that some of these sections were at turnouts, culverts, bridges and tunnels. A summary of the moderate and poor sections are as follows:

- km 50+000 to km 50+300 was at a station with turnouts
- km 54+200 to km 54+400 showed shallow settlements
- km 57+400 to km 58+000 was at the end of a bridge and cutting
- km 58+300 to km 58+800 was on a bridge and a fill
- km 60+200 to km 60+400 was at a station with two turnouts
- km 60+900 to km 62+400 was at a tunnel
- km 63+200 to km 63+600 was on a bridge and fill
- km 66+200 to km 66+900 was at a cut, bridge and cut
- km 67+100 to km 68+000 was at three cuts and two bridges
- km 69+900 to km 70+000 was at a station with turnouts

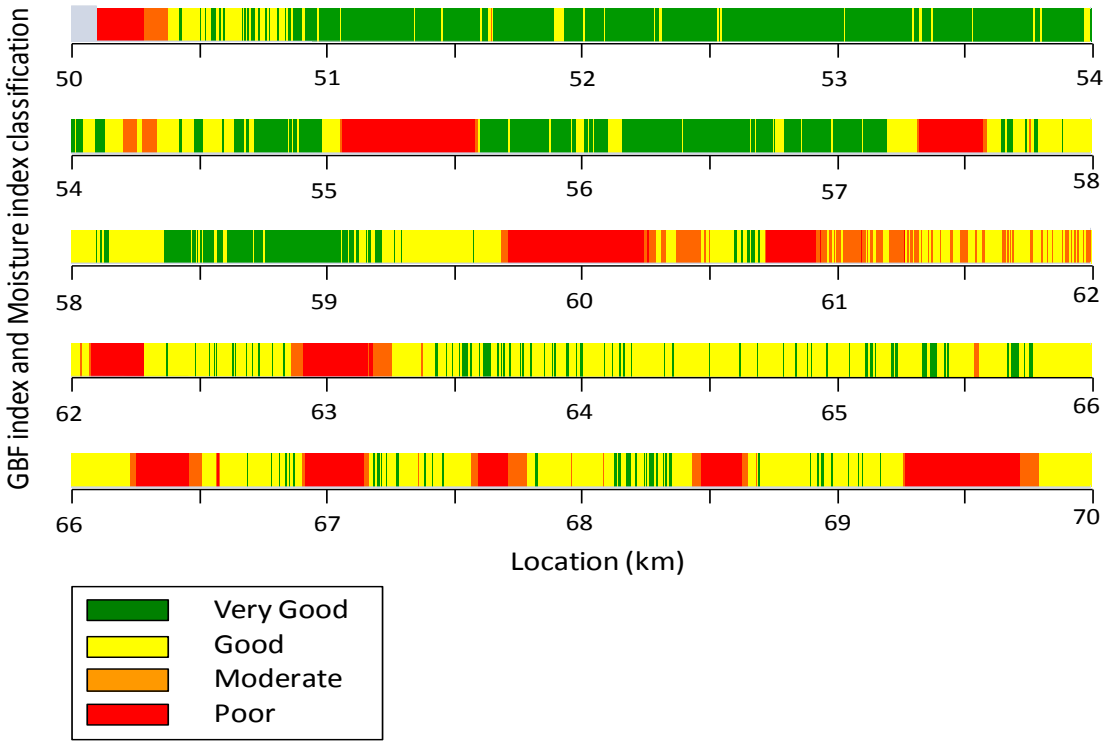

Figure 4.42: GBF index classification for KN test section.

The GBF index and GPR moisture condition index classification for the KN test section also showed that most of the section is in a good and very good condition. There were however more variability in the results with classification sections being much shorter. With further investigation of the moderate and poor sections, using the Railway Doctor software, the following was observed:

- km 50+000 to km 50+300 was at a station with turnouts
- km 54+200 to km 54+400 showed shallow settlements
- km 55+100 to km 55+600 was at two turnouts
- km 57+400 to km 58+000 was at the end of a bridge and cutting
- km 59+800 to km 60+400 was at a station with two turnouts
- km 60+900 to km 62+400 was at a tunnel
- km 62+900 to km 63+300 was on a bridge
- km 66+300 to km 66+500 was a bridge
- km 66+900 to km 67+100 was a bridge
- km 67+600 to km 67+800 was a bridge
- km 68+400 to km 68+600 was a fill
- km 69+400 to km 70+000 was at a station

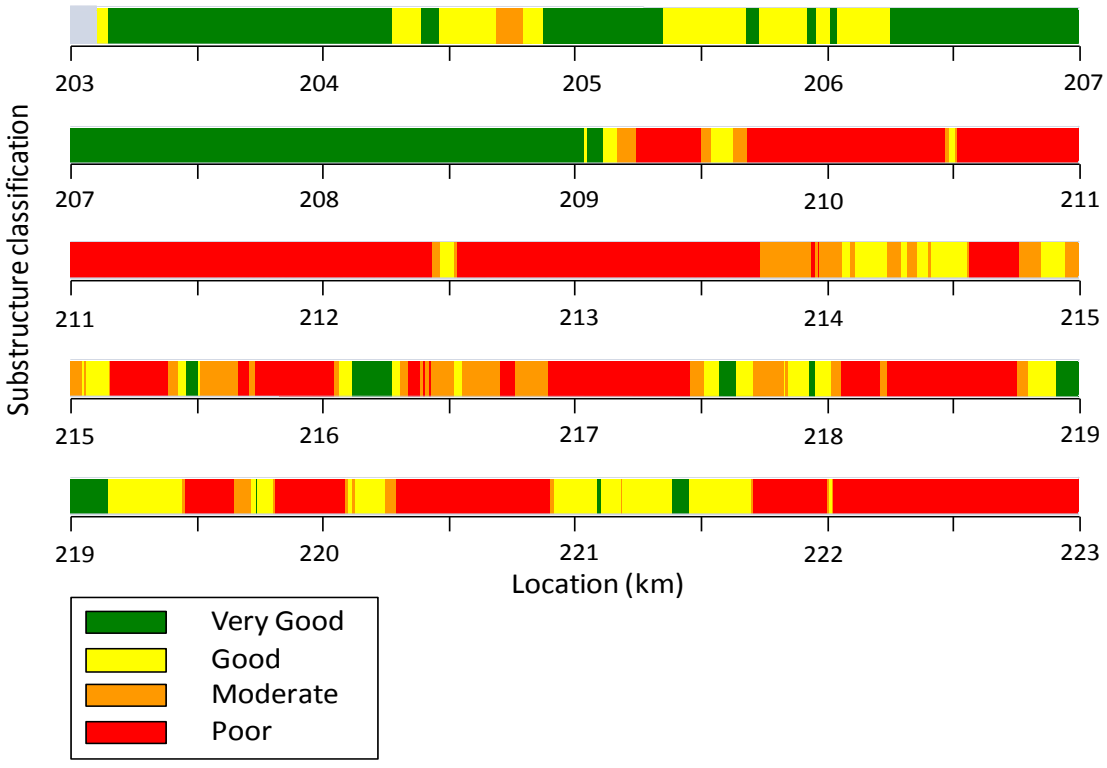

Figure 4.43: Substructure classification for NT test section.

The substructure classification at the NT tests section showed that most of the section is in a poor condition. This section did not show distinct reasons as to why the sections were poor. It can therefore be assumed that the substructure conditions are poor. There were however some turnouts and culverts that could have affected the classification of the track. It was assumed that these sections had negligible effect on the overall classification as the classification was the same before and after them.

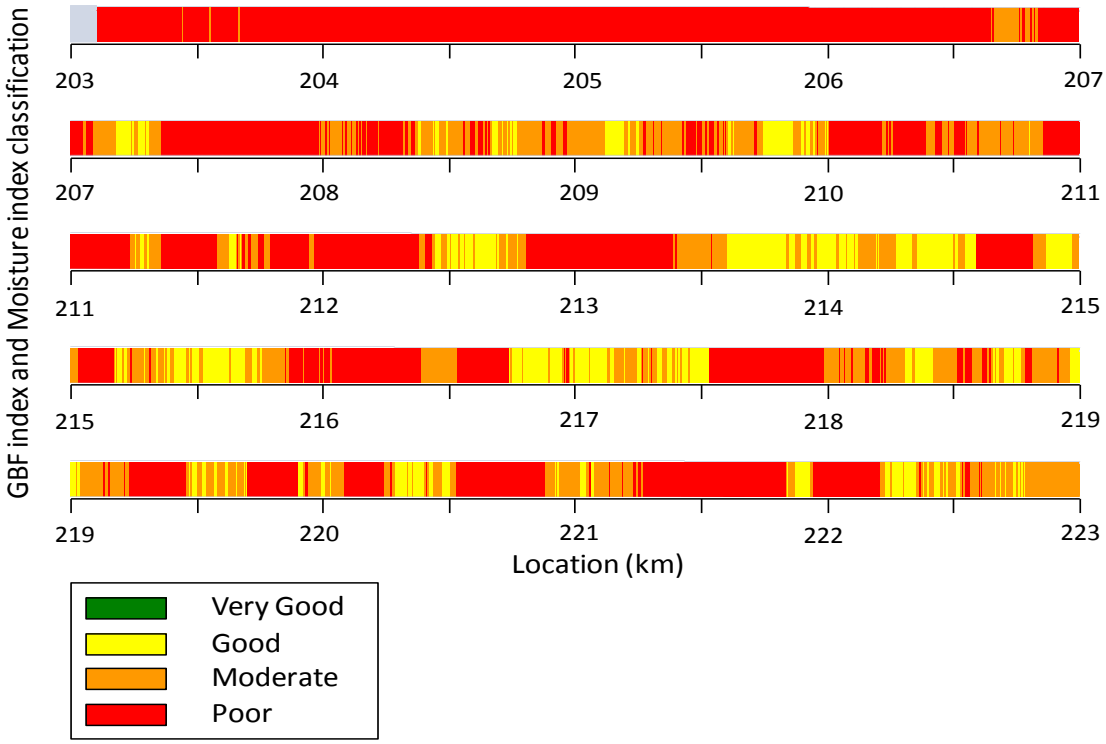

Figure 4.44: GBF index classification for NT test section.

The GBF index and GPR moisture condition index classification for the NT test section showed that most of the section has a poor condition. This meant that both the ballast fouling condition and the moisture condition was of poor quality.

A summary of the classification of the two track sections is given in Figure 4.45. This shows the percentages of the track that is classified as having very good, good, moderate and poor condition.

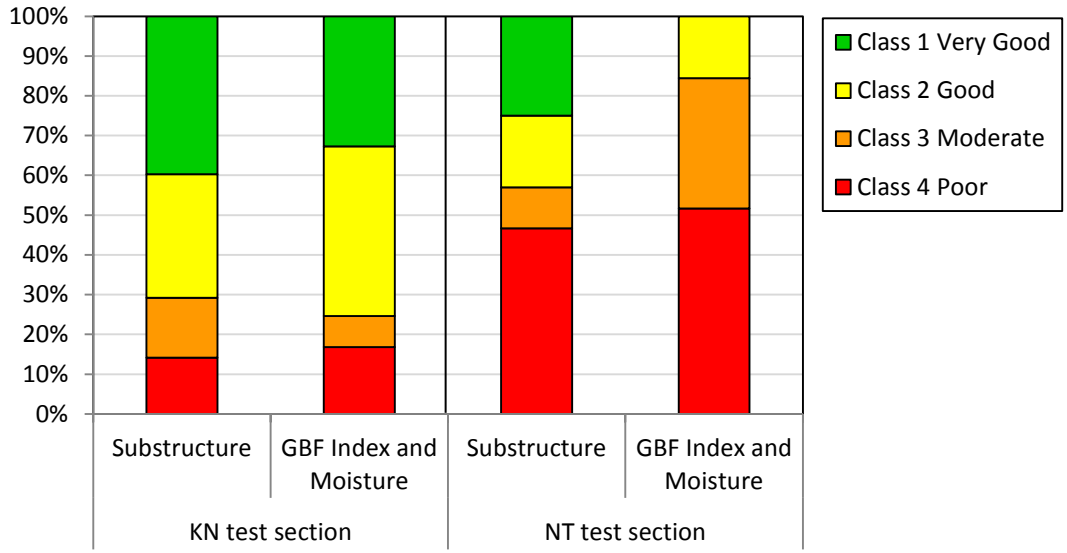

Figure 4.45: GPR classification percentages at the two test sections.

The percentages of the different classes for two sections once again highlight the difference in quality between them. The KN test section showed that 70.8 % and 75.4 % of the track was very good and good for the substructure and GBF index and GPR moisture index classification respectively. For the NT test section, 46.7 % and 51.7 % of the track was poor for the substructure and GBF index and GPR moisture index classification respectively.

4.9 COMPARISON OF SUBSTRUCTURE CLASSIFICATION

This section compares the different classifications obtained from the GPR survey data with the in situ classification methods. The GPR substructure classification will be compared to the earthworks classification and the GPR ballast fouling index and GPR moisture index will be compared to the ballast fouling classification.

4.9.1 Comparison of substructure classification

To compare the classification of the substructure layers, the layer classification according to the railway earthworks specification (see Section 4.3) was also divided into four classes, one for each layer. The subballast layers were grouped as one layer because they usually consist of similar material and it is therefore difficult to distinguish between them. Similarly, the subgrade materials were grouped together as one layer. The substructure foundation modulus

classification typically used by Transnet Freight rail was also used. Table 4.14 shows the classification of the layers.

Table 4.14: Railway earthworks classification.

Classification		Layer 1	Layer 2	Track Substructure Modulus
		Subballast	Subgrade	(MPa/m)
Class 1	Very Good	SSB	SSB, SB and A	>100
Class 2	Good	SB	B	50 to 100
Class 3	Moderate	A	BE	20 to 50
Class 4	Poor	B, BE and <BE	<BE	<20

A summary of the comparison between the GPR substructure classification and the bulk earthworks classification is given in Figure 4.46. The comparison is as follows:

- Exact match in class (green)
- Differed with 1 class (orange)
- Differed with 2 classes (red)

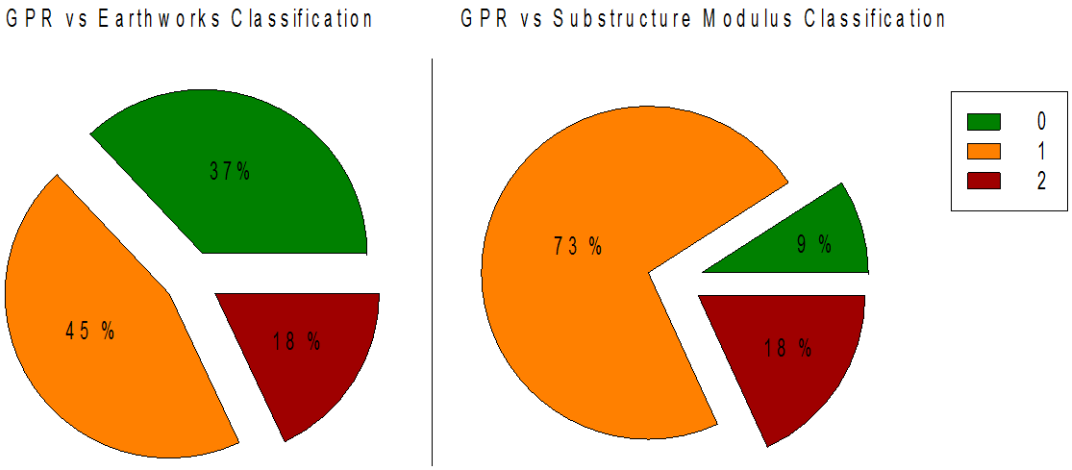

Figure 4.46: GPR classification class differences.

Comparing the railway earthworks classification with the GPR classification, it was found that 37 % of the classes matched exactly, 45 % differed with one class and only 18 % differed with two classes. In the comparison between the track substructure modulus classification and

the GPR classification, 9 % matches exactly, 73 % differed with one class and 18 % differed with two classes.

4.9.2 Comparison of ballast fouling classification

The classification of the GPR ballast fouling (GBF) index and the GPR moisture condition index was compared with the ballast fouling index. For the comparison, the classification used by Transnet Freight Rail for the ballast fouling index has five classes and had to be changed to four. The modified classes are shown in Table 4.15.

Table 4.15: Ballast fouling index classification.

Classification		Ballast fouling index (%)	
Class 1	Very Good	Clean	< 1
Class 2	Good	Moderately clean	1 to 10
		Moderately fouled	11 to 20
Class 3	Moderate	Fouled	21 to 40
Class 4	Poor	Highly fouled	> 40

A summary of the comparison of the GBF index and GPR moisture condition index classification and the ballast fouling index classification is given in Figure 4.47. The comparison is as follows:

- Exact match in class (green)
- Differed with 1 class (orange)
- Differed with 2 classed (red)

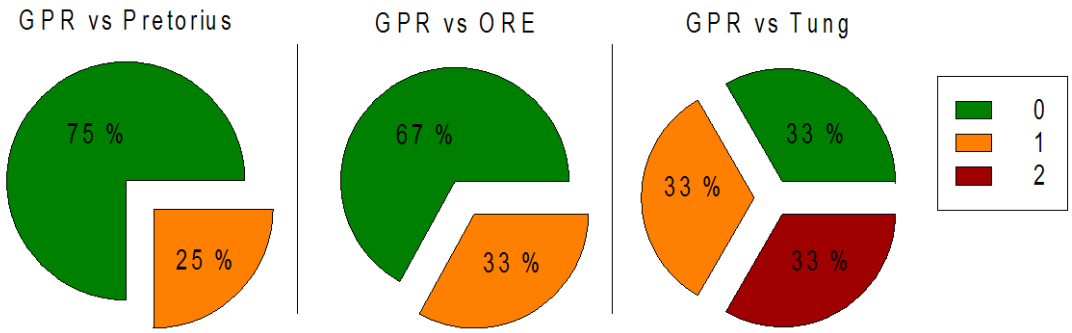

Figure 4.47: GPR ballast classification class difference.

The GBF index was compared to the different ballast fouling index method classifications. From this it was found that the method developed by Pretorius (1993) and the ORE (1991) compared best as 75 % and 67 % of the classification respectively matched exactly. The method proposed by Tung (1989) only had 33 % matching exactly, 33 % that differed with one class and 33 % that differed with two classes.

4.10 EVALUATION OF THE GPR SUBSTRUCTURE MODEL

The evaluation of the GPR characterization model is discussed in this section. The evaluation of the GPR substructure characterization model was done by comparing it to a typical rail line investigation used to characterize the track. The GPR substructure characterization was first consolidated so that the classification sections were long enough for investigation.

The GPR substructure characterization model was then compared to a typical rail line investigation used for characterizing the track substructure. The cost and efficiency of the two characterization methods were then evaluated.

4.10.1 Consolidation of the classification

To compare the GPR substructure characterization model with traditional track characterization, the GPR classification of the two sections was further evaluated and the data was consolidated for better interpretation. This was done by combining the classifications of the section so that there were less short sections. The minimum distance that the combination of the classification could have is 1 000 m. The combinations of the classes were done by giving a section the worst classification that was contained within the minimum distance. This

was done with the exception of bridges, large culverts, switches, stations and tunnels as all of these affect the GPR results. The consolidated classifications of the Komvoorhoogte to Nhlazatshe (KN) test section and the Northam to Thabazimbi (NT) test section are shown in Figure 4.48 and Figure 4.49 respectively.

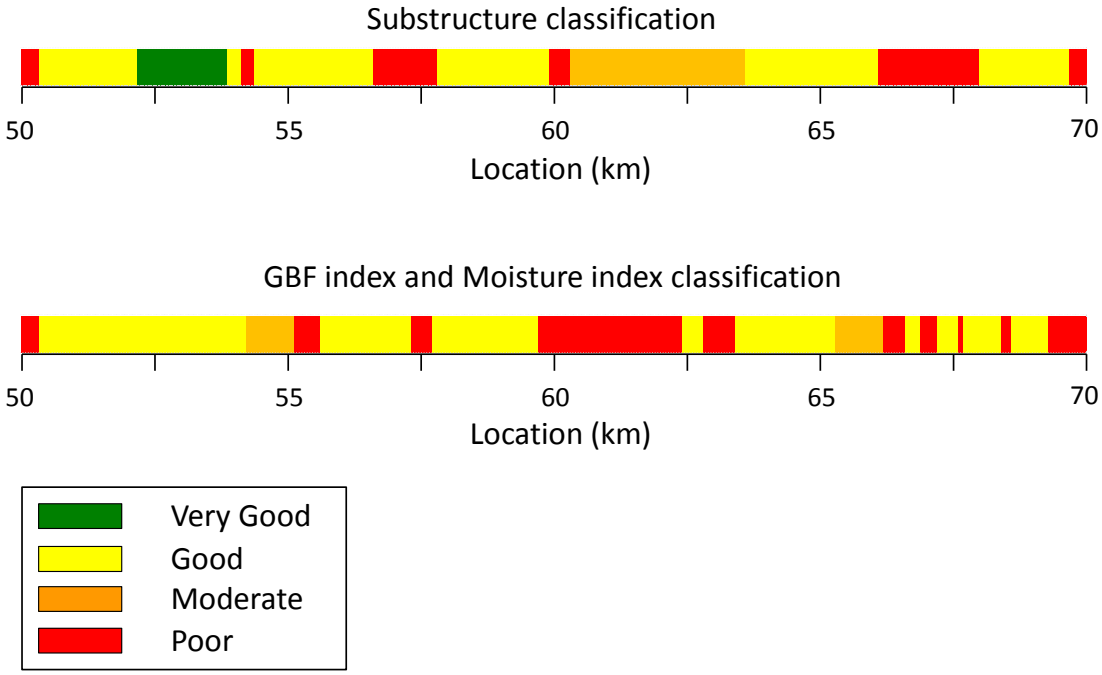

Figure 4.48: KN test section final classification.

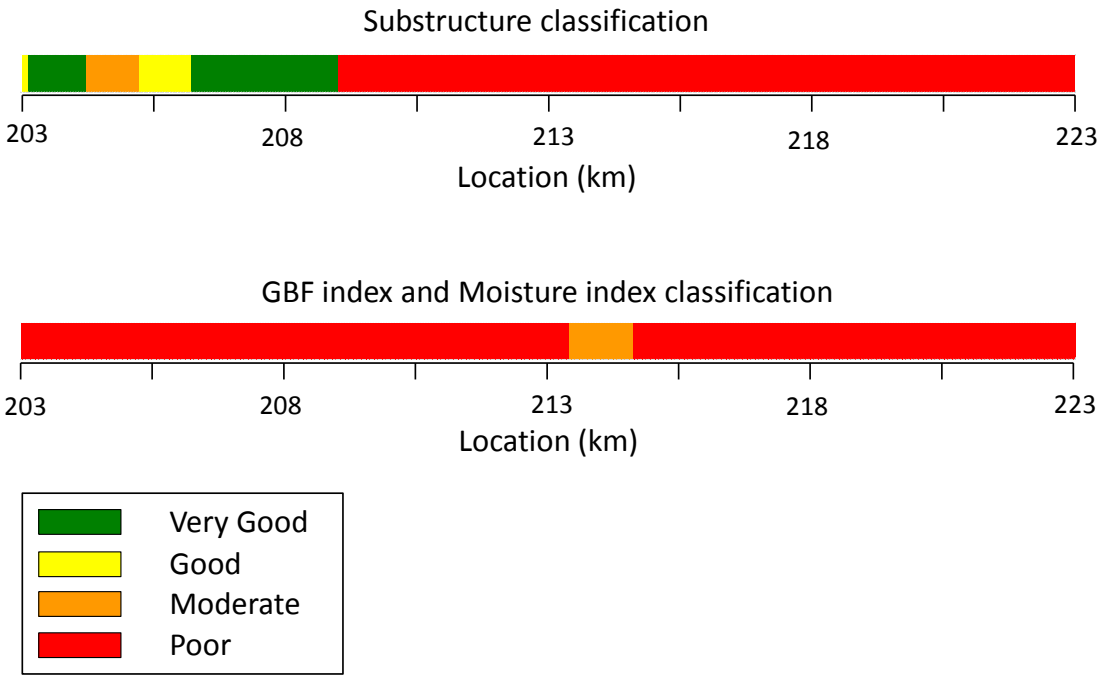

Figure 4.49: NT test section final classification.

When re-evaluating both the substructure classification and the GBF index and moisture classification of the KN test section, it was found that there are now less Class 1 (very good) sections. This was because they were converted to Class 2 as these sections were shorter than a thousand meters. The Class 3 and Class 4 sections were also longer, but they were still shorter than the thousand meter minimum distance. This was done because these sections were predominantly at bridges, tunnels and switches.

With the re-evaluation of the NT test section, it was found that most of the site was converted to Class 4 (poor) with only the first six kilometres being Classes 1, 2 or 3 for the substructure classification. The classification of the GBF index and moisture condition was predominantly Class 4 with only a short section being Class 3.

4.10.2 Evaluation of the characterization model

The evaluation of the GPR substructure characterization model was done by comparing it to a typical railway track substructure investigation. The comparison was done according to the cost per kilometre and the efficiency of each of the two methods for the 40 km long section used in the development of the characterization model.

To fully investigate the track substructure by in situ tests, a test pit needs to be excavated every 200 m. The two test sections comprised a total of 40 km and therefore two hundred test pits would have to be excavated. The tests included at each test pit would be as follows:

- Profiling of the test pit
- Two foundation indicator samples
- Two CBR samples that include Mod. AASHTO testing
- Ballast fouling sample

In situ tests would also be required for the GPR substructure characterization to calibrate the GPR results. Each classification section will need at least one test pit per section and one every 2 km in the section. From this it was determined that twenty two test pits would be required for the GPR survey.

The analysis of the two characterization methods is based on the cost of the items in the year 2011. Average values were taken for the cost of the investigation. The costs of the items within the analysis would all be relative to the cost of the GPR survey per kilometre. It should be noted that this is only a basic analysis of the cost of the investigation. The cost of both the GPR survey and the in situ tests are subject to exchange rates in different countries and are dependent on the pricing of the contractors. A summary of the cost relationship between the two characterization methods is given in Figure 4.50.

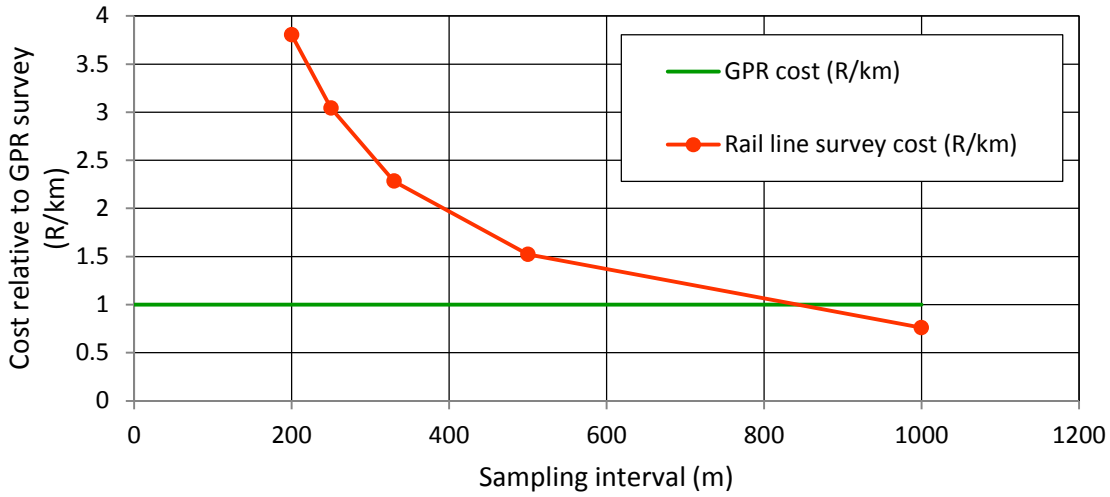

Figure 4.50: Cost relationship of GPR substructure characterization.

The cost analysis shows that characterizing the railway track substructure using GPR is feasible up until one test pit per kilometre is used for the in situ investigation. A typical in situ track substructure investigation is 3.7 times more expensive per kilometre at 200 m sampling interval. At 250 m and 500 m intervals the in situ investigation is 3 times and 1.5 times more expensive per kilometre than the GPR survey. The breakeven point of the two investigation techniques is at a sampling interval between 800 m and 900 m.

The efficiency of the GPR substructure characterization model was evaluated by looking at the time it takes for completion. In comparing it with the in situ investigation, the time taken on site and after will be compared. A GPR survey can be conducted at 40 km/h and needs to be done in both directions with older systems and in one direction for the newer systems. For the test section used in this study, there was approximately one test pit for every two kilometres, amounting to twenty test pits in total. With an average of four test pits excavated per day, the duration of the site survey using GPR would take approximately two weeks. The evaluation of the GPR results and the laboratory test data would further take another four to six weeks. The total time taken for the completion of a GPR substructure characterization would therefore be approximately eight weeks.

Moreover, using only an in situ investigation to characterize the track substructure will require about two hundred test pits. The time taken to complete this will take about ten weeks and including two weeks to complete the evaluation thereof, a total of twelve weeks are needed for an in situ investigation.

Therefore, the GPR substructure characterization for this section would take two thirds of the time that it would take for an in situ investigation. This depends on the type of GPR equipment used and the amount of test pits that can be excavated per day. The length of the surveyed section will also influence the time taken to complete the characterization of the track substructure. The percentage of time taken for the GPR substructure characterization in relation to the in situ investigation will decrease with an increase in length surveyed.

It can therefore be stated from the evaluation above, that a GPR substructure characterization is more cost effective and efficient than a traditional in situ investigation. It should also be noted that the evaluation only considered a basic investigation and that that the cost and time taken for tests like LWD, RVM, MDD and other in situ testing techniques, were not considered.

For the most effective substructure characterization, it is recommended that GPR substructure characterization be used in conjunction with traditional in situ classification. The aim would

then be to obtain a continuous characterization of the substructure from the GPR characterization model and a more in depth characterization from the in situ testing at problematic sections. The LWD, RVM, MDD can be used to evaluate the track performance on a site specific basis. This will allow engineers to make decisions with regards to track substructure rehabilitation with a complete and comprehensive overview and understanding of the condition of the track.

4.11 DISCUSSION

The analyses of the laboratory and field measurements were done to develop a GPR track substructure characterization model. The analyses of the in situ tests were first done, after which the GPR field analyses were completed. The characterization model was then developed and evaluated.

Firstly, the ballast dielectric permittivities were determined for the dolerite (5.23) and quartzite (7.43) and the increase in dielectric permittivity with the addition of moisture was also obtained. These values assisted with the calibration of the GPR field survey.

Following this, the analysis of the soil and ballast parameters indicated that the KN test section had better substructure and ballast quality than the NT test section. The KN test section had a newly constructed substructure (2005), whereas the NT test section's substructure was constructed as early as 1934. The results from the soil parameters (GM, LL, PI, LS) showed that the substructure of the KN test section is in better condition than the NT test section. The gradation showed that the KN test section had more gravel and the NT test section more clay but both sections had similar sand contents.

In addition to the previous findings, the moisture content of the NT test section was higher than that of the KN test section. This can be attributed to the higher clay and silt content and could have influenced the GPR signal due to the higher dielectric permittivity of water. The classification of the soil according to the S410 earthworks specification showed that the KN test section was in accordance with its design and the NT test section was classified as bulk earthworks or worse. The average ballast fouling of the KN test section was 5.8 % and 51.7 % for the NT test section.

Equally, the DCP results indicated that the material at the KN test section had a higher penetration resistance than that of the NT test section. This again shows that the KN test

section had better material quality which can be attributed to the percentage gravel whereas the higher penetration at the NT test section can be attributed to the high clay content.

The RVM and MDD deflection results were firstly compared at one section to evaluate the effectiveness of the RVM system. It was found that RVM is an acceptable investigation tool and it compared well with the MDD results. It was further evaluated by using the results to determine the track stiffness, track modulus and substructure modulus. The classification of these results indicated that the NT test section had moderate to good substructure while the KN test section had very good substructure. The results were approximately three times higher for the KN test section compared to the NT test section. Comparing the LWD modulus to the substructure modulus, a correlation coefficient of 0.864 was obtained. This indicated that the use of the LWD as a substructure tool would be practical.

The laboratory and in situ soil sampling results were then compared to the GPR field survey results. These results were used to verify the accuracy of the GPR results. The field and laboratory dielectric permittivity had a good correlation. The in situ moisture condition did not have any correlation with the GPR moisture condition. The GBF index had a good correlation with the in situ ballast index calculations of all three methods. The correlation coefficients were approximately 0.6 for all three comparisons.

The GPR layer thickness results, GBF index and GPR moisture condition were then used to develop the substructure characterization model. These deliverables were further analysed for the characterization. The subballast and subgrade roughness were obtained from the layer thickness results. The average GBF index and the average GPR moisture content roughness were also used. The length over which the average roughness was calculated was 200 m. This was done to obtain a broad characterization of the ballast and substructure for the ease of maintenance strategies. Each deliverable was classified according to four classes (very good, good, moderate and poor).

The classification was applied to the two test sections and the classification of the subballast and subgrade roughness was combined into one foundation classification. The same was done with the GBF index and the GPR moisture condition roughness for the ballast classification. The GPR classification was then compared to the traditional classification methods. This showed that 73 % of the substructure classification differed by one or less class. The ballast classification showed a 75% match in class with 25 % of the classification differing with one class. The class difference could be rectified by further classification based on the in situ tests.

Lastly, an economic evaluation of the GPR characterization model against a typical rail line investigation was done. A 73 % reduction in cost was obtained and the GPR survey would be completed in a third of the time. It is recommended that a GPR substructure characterization is conducted in conjunction with traditional investigation techniques. Further tests could be conducted in areas where anomalies or differences in the GPR survey data occur.

CHAPTER 5

5. CONCLUSIONS AND RECOMMENDATIONS

The conclusions and recommendations from the investigation and development of a GPR substructure characterization model are discussed in this chapter.

5.1 CONCLUSIONS

In this section the main conclusions reached from the investigation and development of a GPR substructure characterization model are discussed first. The conclusions reached from the other objectives of the study as listed below are also discussed in this section.

- Determining the dielectric permittivity of typical South African ballast materials.
- The comparison of GPR deliverables against in situ investigation techniques.
- The use of remote video monitoring for track and substructure deflection measurements and track modulus determination.

5.1.1 GPR characterization model

The study proved that it was possible to effectively develop a GPR substructure characterization model. This was done by using typical GPR survey deliverables namely layer thickness, GPR ballast fouling and GPR moisture content. These deliverables were analysed further for ease of classification in the model. The use of the subballast and subgrade profile roughness was used for foundation classification and the GBF index and the GPR moisture condition index roughness values were used for the ballast classification. The GPR substructure characterization model was evaluated by comparing the classification thereof to classification of in situ investigation techniques. The classification ranges for the GPR characterization model and the in situ investigation techniques are shown in Table 5.1. The GPR classification ranges was obtained from typical GPR results and then divided into four classes. The classification of the in situ investigation techniques was obtained either from the literature or from typical values used by Transnet in South Africa.

Table 5.1: Summary of track substructure classification methods.

	Class 1	Class 2	Class 3	Class 4
	Very Good	Good	Moderate	Poor
Subballast surface R^2 (x 1 000)	0 to 0.5	0.5 to 1	1 to 1.5	> 1.5
Subgrade surface R^2 (x1 000)	0 to 2	2 to 4	4 to 6	> 6
GBF Index Average	0 to 35	35 to 70	70 to 105	> 105
GPR Moisture R^2	0 to 40	40 to 80	80 to 120	> 120
S410 Subballast Layers	SSB	SB	A	Bulk earthworks and less
S410 Subgrade Layers	SSB, SB, A	B	Bulk earthworks	Less than bulk earthworks
Track Substructure foundation Modulus (MPa/m)	>100	50 to 100	20 to 50	<20
Ballast fouling index	< 1	2 - 20	21 – 40	> 40

Comparing the GPR subballast and subgrade profile roughness classification to the earthworks classification and the track modulus classification, the following conclusions were reached:

- Comparing the GPR classification with the bulk earthworks classification, 37% of the results did not differ in classification, 45% differed with one class and 18% differed with two classes.
- Comparing GPR classification with track substructure foundation modulus classification, 9% did not differ, 73% differed with one class and 18% differed with two classes.
- If large differences occur between the classifications, further sampling can be done for more accurate calibration.

Comparing the GBF index and the GPR moisture condition index roughness classification to the different ballast fouling index classifications, the following conclusions were reached:

- When compared to the Pretorius (1993) classification, 75 % of the classes matched exactly and 25 % differed by one class.

- When compared to the ORE (1991) classification, 67 % of the classes matched exactly and 33 % differed by one class.
- When compared to the Tung (1989) classification, only a third of the classes matched exactly and similarly a third differed by one and two classes.

The comparison of the GPR substructure characterization model with a typical in situ railway track substructure investigation with respect to cost and efficiency produced the following conclusions:

- The cost of a typical in situ investigation will decrease with an increase of the sample interval length. At the proposed sample interval of 200 m, the cost of the in situ investigation will be 3.7 times more than that of the GPR characterization. This will decrease until a breakeven point is reached between the two methods at a sampling interval of between 800 m and 900 m.
- The efficiency of the GPR substructure characterization is dependent on the length of the track and the type of equipment used. For the evaluation of the characterization with the KN test section and the NT test section, the GPR substructure characterization will take two thirds of the time of a typical in situ investigation.

Therefore, the use of a GPR substructure characterization model is possible and is more cost effective and efficient than using only a traditional in situ railway track investigation. The most effective use of the GPR substructure characterization model is to use it in conjunction with in situ investigation techniques. The GPR model will then provide a continuous characterization of the substructure and the in situ tests will provide a more in depth classification of problematic areas.

5.1.2 Dielectric permittivity of South African ballast material

The following conclusions were reached from the evaluation of the dolerite and quartzite ballast material using GPR technology:

- Using a 400 MHz antenna in controlled laboratory conditions, a dielectric permittivity of approximately 5 was obtained for dry quartzite and a dielectric permittivity of approximately 7 for dry dolerite. For moist quartzite and dolerite, dielectric permittivity values of approximately 6 and 8 respectively, were obtained.
- Using the field test results, average dielectric permittivity values of 5.8 and 6.3 for dolerite and quartzite respectively, were obtained.

These values correlate well to that of the literature and can therefore be used effectively for the determination of GPR ballast conditions.

5.1.3 Comparison of GPR and in situ investigation techniques

The comparison of the GPR results with the in situ investigating techniques on the two track sections, by using soil sampling and profiling and DCP testing, produced the following conclusions:

- From the soil sampling and profiling on the test section between Komvoorhoogte and Nhlazatshe, it was found that for the first identifiable layer, the material was in accordance with the Transnet earthworks specification. Similarly, the second identifiable layer was between the expected condition of an A and B layer. The layers of the track section between Northam and Thabazimbi were of poor condition and were classified as bulk earthworks according to the specification.
- The DCP results showed no real correlation to the soil sampling but did however correlate well with the soil profiling done at each of the test locations.

Using the GPR survey results and comparing it to the other substructure investigation tools, the following conclusions were obtained:

- Comparing the GPR moisture condition with in situ moisture sampling showed that they do not correlate, but that the GPR moisture condition is an indicator of moisture accumulation within the structure.
- The GBF index compared relatively well to the in situ ballast fouling index results. By using a linear regression it was found that all three methods had approximate R^2 values of 0.6. It should be noted that the GBF index could be calibrated according to the in situ results.

5.1.4 Track and substructure deflection evaluation against vertical axle load

From the investigation of the track and substructure deflection measurements and the vertical axle loads, the following conclusions were reached:

- The relationship between the vertical deflection and the vertical axle load was logarithmic with a less rapid increase in deflection as the axle load approached 30 tons, thereby indicating strain hardening of this particular material.
- The correlation coefficient for both the RVM track deflection and the MDD substructure deflection was about 0.89 and was 0.63 for the RVM substructure

deflection measurements. The lower correlation coefficient for the RVM substructure deflection measurements can be attributed to the vibration of the rod (driven through the ballast) when the train passes.

- The relationship between the track and substructure deflection also shows that conventional design methods are conservative as they assume a linear relationship between axle load and track deflections. This is only true for materials with good foundation properties.

Furthermore, comparing the deflections of the RVM and MDD systems the following conclusion was reached:

- The RVM substructure deflection also compare well with the MDD deflection that is approximately 80 % of the RVM deflection. The difference could be attributed to the placement of the uppermost MDD and differential movement of the MDDs in the MDD string.

It can therefore be concluded that RVM can be used successfully as a track and substructure deflection tool.

5.1.5 Track modulus determination

Using the RVM deflection measurements for the determination of track modulus and track substructure foundation modulus, the following conclusions were obtained:

- For the Komvoorhoogte to Nhlazatshe section, track modulus values between 58 MPa and 171 MPa and track substructure modulus values between 114 MPa/m and 337MPa/m were obtained. For the Northam to Thabazimbi section, track modulus values between 23 MPa and 79 MPa and track substructure foundation modulus values between 45 MPa/m and 156 MPa/m were obtained. This showed that on average, the KN section had moduli of about three times that of the NT section.
- The LWD modulus measurements also showed that the soil at the Komvoorhoogte to Nhlazatshe section had three times higher moduli than those of the Northam to Thabazimbi section.
- Furthermore, the RVM calculated substructure foundation moduli were on average three times larger than the LWD moduli.

The use of RVM deflection measurements for the determination of track modulus and track substructure foundation modulus can be used for the evaluation of the track.

5.2 RECOMMENDATIONS

The following aspects of the study require further investigation and would be suitable for future research topics:

- The implementation of the GPR substructure characterization model in an infrastructure maintenance model is strongly recommended. This will enable evaluation of the condition of the track substructure over time.
- The testing of more South African ballast and soil materials are recommended for determining their typical GPR parametric deliverables.
- The effect of higher axle loads on track resilient deflections should be investigated for better performance predictions and improved design models. This should be evaluated for good and poor foundation conditions.
- Further research should be done with the LWD to investigate its use as a location specific classification tool.

CHAPTER 6

6. REFERENCES

Adrian, R. J. (1991). Particle imaging techniques for experimental fluid mechanics. *Fluid Mechanics, 23*, 261-304.

Al-Qadi, I. L. Xie, W. and Roberts, R. (2008). Scattering Analysis of Ground Penetrating Radar Data to Quantify Railroad Ballast Contamination. *NDT&E International 41*, 441-447.

Al-Qadi, I. L. Xie, W. and Roberts, R. (2010). Optimization of Antenna Configuration in Multiple-Frequency Ground Penetreating Radar System for Railroad Substructure Assessment. *NDT&E International 43*, 20-28.

Anderson, E. and Harris, W. (1993). Using Technologies for higher axle loads and longer trains. *Fifth international heavy haul railway conference*, (pp. 46-55). Beijing, China.

Arangie, P. B. (1997). The Influence of Ballast Fouling on Resilient Behaviour of the Ballast Pavement Layer. *6th International Heavy Haul Conference* (pp. 241 - 256). Cape Town: IHHA.

Belotsserkovskiy, P. (2006). Interaction between a railway track and uniformly moving tandem wheels. *Journal of sound vibration, 298*, 855-876.

Berggren, E. G. Smekal, A. and Silvast, M. (2006). Monitoring and Substructure Condition Assesment of Existing Railway Lines for Upgrading to Higher Axle Loads and Speeds. *Proceedings of the Sevth World Congress on Railway Research June 4-8,2006.* Montréal, Canada.

Bowness, D. Lock, A. C. Powrie, W. Priest, J. A. and Richards, D. J. (2006). Monitoring the dynamic displacements of railway track. *Rail and Rapid Transit, 221*, 13-22.

Bowness, D. Lock, A. C. Richards, D. J. and Powrie, W. (2005). Innovative Remote video Monitoring of Railway Track Displacements. Trans Tech Publications.

Briaud, J. L. and Shields, D. H. (1979). A Special Pressuremeter and Pressuremeter Test for Pavement Evaluation and Design. *Geotechnical Testing Journal, ASTM, Vol. 2, No. 3*, 143-145.

Briaud, J. L. (1992). *The Pressuremeter.* Balkema, Rotterdam: Balkema.

Brightwell, S. and Thomas, M. (2003). Geophysical Assesment of Railway Assets - a Practical View. *Proceedings of the Sixth International Conference on Railway Engineering, April 30 - May 1.* London, U.K.

Brough, M. Stirling, A. Ghatoara, G. and Madelin, K. (2003). Evaluation of railway trackbed and formation: a case study. *NDT & E International, Vol 36*, 145 - 156.

Burrow, M. P. N. Bowness, D. and Ghataora, G. S. (2006). A comparison of railway track foundation design methods. *Rail and Rapid Transit, Vol 221*, 1-12.

Byrne, G. and Berry, A. D. (2008). *A guide to practical Geotechnical Engineering in Southern Africa* (4th Edition ed.). Johannesburg: FRANKI.

Cai, Z. Raymond, G. P. and Bathurst, R. J. (1994). Estimate of Static Track Modulus Using Elastic Foundation Models. *Transportation REsearch Record 1470*, 65-72.

Carpenter, D. Jackson, P. J. and Jay, A. (2004). Enhancement of the GPR Method of Railway Trackbed Investigation by Installation of Radar Detectable Geosynthetics. *NDT & E International, 37*(2), 95-103.

Carr, G. A. (1999). *Dynamic Response of Railroad Track Induced by High Speed Trains and Vertical Stiffness Transitions With Proposed Method of Measurement.* Tufts University.

Ceney, H. (2001). Selection of track form. *Railway Engineering*.

Clark, M. R. Gillespie, R. Kemp, T. McCann, D. M. and Forde, M. C. (2001). Electromagnetic Properties of Railway Ballast. *NDT&E International 34 (2001)*, 305-311.

Clark, M. R. Gordon, M. O. Giannopoulos, A. and Forde, M. C. (2003). Experimetal and Computer Modelling of GPR to Charactirize Trackbed Ballast. *Proceedings of World Congress on Railway Research*, (p. 16). Scotland.

Clark, M. R. McCann, D. M. and Forde, M. C. (2003). GPR as a Tool for the Characterization of Ballast. *Proceedings of the Sixth International Conference on Railway Engineering, April 30 -May 1.* London, U.K.

Clark, M. R. Gordon, M. and Forde, M. C. (2004). Issues over High-Speed Non-Invasive Monitoring of Railway Trackbed. *NDT&E International 37*, 131-139.

Clayton, C. R. Matthews, M. C. and Simons, N. E. (1995). *Site Investigation* (2nd Edition ed.). Oxford: Blackwell Science.

Craig, R. (2007). *Craig's soil mechanics* (7th ed.). Dundee: Spon Press.

Daniels, D. J. (1996). Surface Penetrating Radar. *Electronics & Communications Engineering Journal*, 165-182.

Daniels, D. J. (2004). *Ground Penetrating Radar* (2nd Edition ed.). London, United Kingdom: The Institution of Electrical Engineers.

Davidson, N. C. and Chase, S. B. (1998). Radar Systems for Topographical Bridge Deck Inspection. *Proceedings of the Seventh International Conference on Ground Pentrating Radar, May 27 - 30, 1998*, *2*, pp. 747-751. Lawrence Kansas, USA.

Davis, D. D. Otter, D. Li, D. and Singh, S. (2003). Bridge Approach Performance in Revenue Service. *Railway Track and Structures, December*, 18-20.

Davis, J. L. and Annan, A. P. (1989). Ground-penetrating radar for high resolution mapping of soil and rock stratigraphy. *Geophisical Prospecting, Vol 37*, 531-551.

Davis, J. L. Rossiter, J. R. Mesher, D. E. and Dawley, C. B. (1994). Quantitive Measurement of Pavement Structures Using Radar. *Proceedings of the fifth International Conference on Ground Penetrating Radar*, (pp. 319-334). Kitchener, Ontario, Canada.

Dunnicliff, J. (1988). *Geotechnical instrumentation for monitoring field performance.* New York: Wiley and Sons.

Ebersöhn, W. Trevizo, M. C. and Selig, E. T. (1993). Effect of Low Track Modulus of Track Performance. *Proceedings of the Fifth Intrernational Heavy Haul Conference* (pp. 379-388). International Heavy Haul Association.

Ebersöhn, W. (1995). *Substructure Influence on Track Maintenance Requirements.* Amherst: University of Massachusetts.

El-Said, M. A. (1956). Geophysical prospection of underground water in the desert by means of electromagnetic interference fringes. *Proc. I.R.E. 44*, pp. 24–30 and 940.

Eriksen, A. Gascoyne, J. and Al-Nuaimy, W. (2004). Improved Productivity and Reliability of Ballast Inspection Using Road-Rail Multi-Channel GPR. *Railway Engineering 2004, 6th -7th July 2004, Commonwealth Institute.* London, U.K.

Esveld, C. (2001). *Modern Railway Track* (Vol. Second Edition). Germany: MRT Productions.

Esveld, C. (2009). *Innovations in Railway Track.* TU Delft, Roads & Railway.

Finish Geotechnical Society. (1992). *Ground Penetrating Radar, Geophysical Survey Methods.* Finland: The Finnish Geotechnical Society and The Finnish Building Centre Ltd.

Gallagher, G. P. Leiper, Q. Williamson, R. Clark, M. R. and Forde, M. C. (1998). Application of Ground Penetrating Radar in the Railway Industry. *Proceedings of the First International Conference in Railway Engineering 98* (pp. 33-36). London, UK: Technical Press.

Gallagher, G. P. Leiper, Q. Williamson, R. Clark, M. R. and Forde, M. C. (1999). The Application of Time Domain Ground Penetrating Radar to Evaluate Railway Track Ballast. *NDT&E International 32*, 463-468.

Göbel, C. Hellman, R. and Petzold, H. (1994). Georadar - Model and In-Situ Investigations for Inspection of Railway Tracks. *Proceedings of the Fifth International Conference on Ground Penetrating Radar, June 12-16*, *Vol 3 of 3*, pp. 1101-1106. Kitchener,Ontario, Canada.

Gräbe, P. J. (1997). *The Use of the Pencel Pressuremeter for the Investigation of Railway Formation.* University of Pretoria.

Gräbe, P. J. (2002). *Resilient and Permanent Deformation of Railway Foundations Under Principal Stress Rotation.* Southampton, Engineering. University of Southampton.

Gräbe, P. J. (2008). *Track deflection measurement using particle image velocimetry (PIV): Report no. PJG0806 version1.* University of Pretoria, Civil engineering . Pretoria: Tubular track.

Gräbe, P. J. and Clayton, C. R. (2009). Effects of Principal Stress Rotation on Permanent Deformation in Rail Track Foundations. *Journal of Geotechnical and Geoenvironmental Engineering ASCE 135(4)*, 555-565.

Gräbe, P. J. and Shaw, F. J. (2010). Design Life Prediction of a Heavy Haul Track Foundation. *Proc. IMechE Vol. 224 Part F: J. Rail and Rapid Transit*, 337-344.

Heath, D. L. Shenton, M. J. Sparrow, R. W. and Waters, J. M. (1972). Design of Conventional Rail Track Foundations. *ICE Proceedings 51(2)*, 251-267.

Heymann, G. (2007). Ground Stiffness Measurement by the Continuous Surface Wave Test. *Journal of the South African Institution of Civil Engineering 49(1)*, 25-31.

Hoekstra, P. and Delaney, A. (1974). Dielectric properties of soils at UHF and microwave frequencies. *Journal of Geophysical Research, Vol 79*, 1699-1708.

Hopman, V. and Beuving, E. (2002). Reapeatability, Rproducubility and Accuracy on GPR Measurements. *Proceedings of the Sixth International Conference on the Bearing Capacity of Roads, Railways and Airfields, 24-26 June,2002*, (pp. 627-645). Lisbon, Portugal.

Hugenschmidt, J. (1998). Railway Track Inspection Using GPR - Some Examples from Switzerland. *Proceedings of the Seventh International Conference on Ground Penetrating Radar, May 27-30*, *Vol 1 of 2*, pp. 197-202. Lawrence, Kansas, USA.

Hugenschmidt, J. (2000). Railway track Inspection using GPR. *Journal of Applied Geophysics 43*, 147-155.

Hyslip, J. P. Smith, S. S. Olhoeft, G. R. and Selig, E. T. (2003). Assesment of railway track substructure condition using ground penetrating radar. *AREMA, 5-7 Oct. 2003.* Chicago.

Jack, R. and Jackson, P. (1999). Imaging Attributes of Railway Track Formation and Ballast Using Ground Probing Radar. *NDT&E International 32*, 457-462.

Jennings, J. E. Brink, A. B. and Williams, A. A. (1973). Revised Guide to Soil Profiling for Civil Engineering Purposes in Southern Africa. *Die Siviele Ingenieur inSuid-Afrika, Januarie*, 3-12.

Jol, H. M. (2009). *Ground Penetrating Radar: Theory and Applications* (1st ed.). Amsterdam, Netherlands: Elsevier Science.

Klassen, M. J., Clifton, A. and Watters, B. R. (1987). *Track Evaluation and Ballast Performance Specification*, TRR 1131, Performance of Aggregates in Railroads and Other Track Performance Issues, Washignton, D.C., 35-44

Kleyn, E. G. (1975). *Die Gebruik van die Dinamiese Kegelpeilstaaf (DKP).* Pretoria: Transvaalse Paaidepertement Tak Materiale.

Kleyn, E. G. (1984). *Aspects of Pavement Evaluation and Design as Determined with the Aid of the Dynamic Cone Penetrometer (In Afrikaans).* MEng Thesis, University of Pretoria.

Korpanec, I. Rebeyrotte, E. Guigon, M. and Tordai, L. (2005). Increasing axle load in Europe: State of the art perspectives. *Eighth international heavy haul conference* (pp. 227-235). Rio de Janeiro, Brazil: The Graphic Owl.

Leng, Z. and Al-Qadi, I. L. (2010). Railroad Ballast Evaluation Using Ground-Penetrating Radar-Laboratory Investigation and Field Validation. *Transport Research Record, No. 2159*, 110-116.

Li, D. and Selig, E. T. (1996). Cumulative Plastic Deformation for Fine Grained Soils. *Journal of Geotechnical Engineering ASCE 122 (12)*, 1006 -1013.

Li, D. Selig, E. T. and Chrismer, S. (1996). Methods for Railway Track Granular Layer Thickness Design. *Technology Digest*, -.

Li, D. and Selig, E. T. (1998). Method for railroad track foundation design I: Development. *Journal of geotechnical and geoenvironmental engineering*, 316-322.

Li, D. and Selig, E. T. (1998). Mehtod for railroad track foundation design II: applications. *Journal of geotechnical and geoenvironmental engineering*, 323 - 329.

Love, A. E. (1927). *A Treatise on the Mathematical Theory of Elasticity* (4th Edition ed.). Cambridge: Cambridge University Press.

Lu, S. Farritor, S. Arnold, R. GeMeiner, W. Clark, D. Fateh, M. et al. (2008). Measurement of Vertical Track Modulus - Field Testing, Reapeatability, and Effects of Track Geometry. *Proccedings of the 2008 IEEE/ASME Joint Rail Conference JRC2008, April 22-23*, (pp. 1-8). Wilmington, Delaware, USA.

Lu, S. Duan, H. Greisen, C. Farritor, S. Arnold, R. Hogan, C. et al. (2010). Case Studies Determining the Effects of Track Stiffness on Vehicle Dynamics. *Proceedings of the 2010 Joint Rail Conference JRC2010, April 27-29*, (pp. 1-10). Urbana, Illinois, USA.

Maierhofer, K. and Kind, T. (2002). Application of Impulse Radar for Non-Destructive Investigation of Concrete Structures. In S. Koppenjan, and H. Lee (Ed.), *Proceedings of the Ninth International Conference on Ground Penetrating Radar, April 29 - May 2, 2002*, *4758*, pp. 382-387. Santa Barbara, California.

Manacorda, G. Morandi, D. Sparri, A. and Staccone, G. (2002). A Custimized GPR System for Railroad Track Verification. *Proceedings of the Ninth International Conference on*

Ground Penetrating Radar, April 29 -May 2, 2002, *4758*, pp. 719-723. Santa Barbara, California, USA.

Maree, J. (1993). Aspects of resilient rail pads. *Fifth international heavy haul railway conference*, (pp. 433-439). Beijing, China.

Maser, K. R. and Scullion, T. (1991). Automated Detection of Pavement Layer Thicknesses and Subsurface Moisture Using Ground Penetrating Radar. *Transport Research Board Paper 1991*.

Mesher, D. E. Dawley, C. B. Davies, J. L. and Rosstier, J. R. (1995). Evaluation of New Ground Penetrating Radar Technology to Quantify Pavement Structures. *Transport Research Record 1505*, 17-26.

Mohammadi, S. D. Nikoudel, M. R. Rahimi, H. and Khamehchiyan, M. (2008). Apllication of the Dynamic Cone Penetrometer (DCP) for Determining of Engineering Parameters of Sandy Soils. *Engineering Geology 101* , 195-203.

Morey, R. (1998). *Ground Penetrating Radar for the Evaluating Subsurfuce Conditions for Transportation Facilities. A Synthesis of Highway Practice.* Washington DC: National Academy Press.

Narayanan, R. M. Jakub, J. W. Li, D. and Elias, S. E. (2004). Railroad Track Modulus Estimation Using Ground Penetrating Radar Measurements. *NDT&E International 37*, 141-151.

Olhoeft, G. R. and Selig, E. T. (2002). Ground Penetrating Radar Evaluation of Railway Track Substructure Conditons. In S. Koppenjan, and H. Lee (Ed.), *Proceedings of the Ninth International Conference on Ground Pentrating Radar, April 29 - May 2*, *Vol 4758*, pp. 48-53. Santa Barbara, California.

Olhoeft, G. R. Smith, I. I. Hyslip, J. P. and Selig, E. T. (2004). GPR in Railroad Investigations. *Proceedings of the Tenth International Conference on Ground Penetrating Radar, 21 -24 June 2004*, (pp. 635-638). Delft, The Netherlands.

Paige-Green, P. and Du Plessis, L. (2009). The Use and Interpretation of the Dynamic Cone Penetrometer (DCP) Test. South Africa: CSIR Built Environmnent Pretoria.

Pretorius, F. J. (1993). *The State of the Art of Ballast Fouling and Screening Maintenance System. Report No 24-864/01/93.* Johannesburg: Track Testing Centre.

Priest, J. A. Powrie, W. Yang, L. A. Grabe, P. J. and Clayton, C. R. I. (2010). Measurement of transient ground movements below a ballasted railway line. *Geotechnique, To be published*.

Rayleigh, L. (1885). On Waves Propogated Along the Plane Surface of an Elastic Solid. *London Mathematical Society Proceedings, 17*, (pp. 4-11).

Raymond, G. P. (1978). Design for Railroad Ballast and Subgrade Support. *Journal of the Geotechnical Engineering Division*, 45-60.

Read, D. Chrismer, S. Ebersohn, W. and Selig, E. T. (1994). Track Modulus Measurement at the Pueblo Soft Subgrade Site. *Transportation Research Record 1470*, 55-64.

Remennikov, A. M. and Kaewunren, S. (2007). A review of the loading conditions for railway track structures due to train and track vertical interaction. *Structural control and health monitoring, 15*, 207-234.

Saarenketo, T. (1998). Electric properties of water in clay and silty soils. *Journal of Applied Geophysics, Vol 40*, 73-88.

Saarenketo, T. Silvast, M. and Noukka, J. (2003). Using GPR on Railways to Identify Frost Susceptible Areas. *Proceedings of the 6th International Conference on Railway Engineering*, (p. 11). London, U.K.

Saarenketo, T. (2006). *Electrical properties of road materials ans subgrade soils and the use of Ground Penetrating Radar in Traffic Infrastructure Surveys.* University of Oula, Faculty of Science, Department of Geosciences. Oulu: Oulu University Press.

Scullion, T. Lau, C. L. and Saarenketo, T. (1996). Performance specifications of Ground Penetrating Radar. *Proceedings of the Sixth International Conference on Ground Penetrating Radar, September 30 - October 3, 1996*, (pp. 341-346). Sendai, Japan.

Selig, E. T. and Li, D. (1994). Track Modulus: Its Meaning and Factors Influencing It. *Tranport Research Record 1022*, 65-71.

Selig, E. T. and Waters, J. M. (1994). *Track Geotechnology and Substructure Management.* Townbridge, England: Thomas Telford.

Shahu, J. T. Yudhbir, and Kameswara Rao, N. S. (2000). A Rational Method for Design of Railroad Track Foundation. *Soils and Foundations, Vol 40, No. 6*, 1-10.

Shaw, F. (2005). *Railway Track Formation Stiffnesses.* Pretoria: University of Pretoria.

Silvast, M. Levomäki, M. Nurmikolu, A. and Noukka, J. (2006). NDT Techniques in Railway Structure Analysis. *Proccedings of the Sevth World Congress on Railway Research June 4-8, 2006.* Montréal, Canada.

Silvast, M. Nurmikolu, A. Wiljanen, B. and Levomaki, M. (2010). An Inspection of Railway Ballast Quality Using Ground Penetrating Radar in Finland. *Proc. IMechE, Part F: J. Rail and Rapid Transit 2010, 224*, 345-351.

Smekal, A. Berggren, A. and Hrubec, K. (2003). Track-Substructure Investigation Using Ground Penetrating Radar. *Proceedings of the Sixth International Conference on Railway Engineering, April 30 -May 1.* London, U. K. .

Staccone, G. and de Haan, E. (2003). Safe Rail Track Bed Investigation by High Speed Radar. *Proceedings of the Sixth International Conference on Railway Engineering, April 30 - May 1.* London, U.K.

Stokoe, K. H. Joh, S. and Woods, R. D. (2004). Some Contributions of In Situ Geophysical Measurements to Solving Geotechnical Engineering Problems. *Proceedings of the Second International Conference on Site Caracterization (ISC-2)* (pp. 97-132). Porto, Portugal, : Roterdam: Millpress.

Sussman, T. R. and Selig, E. T. (2000). Resilient Modulus Backcalculation Techniques for Track. *Proceedings of the ASCE Geo-Institute Specialty Conference on Performance Confirmation of Constructed Geotechnical Facilities* (pp. 401-411). Massachusetts-Amherst: ASCE.

Sussman, T. R. O'Hara, K. R. and Selig, E. T. (2002). Development of Material Properties for Railway Application of Ground Penetrating Radar. In S. Koppenjan, and H. Lee (Ed.), *Proceedings of the Ninth International Conference on Ground Penetrating Radar, April 29 - May 2, 2002*, *4758*, pp. 42-47. Santa Barbara, California.

Sussman, T. R. Selig, E. T. and Hyslip, J. P. (2003). Railway Track Condition Indicators from Ground Penetrating Radar. *NDT & E International, 36*(3), 157-167.

Svensson, M. (2001). *Application of the SASW-technique in Geotechnical In-Situ Testing.* Lund: Lund University.

Thompson, R. and Li, D. (2002). Automated Vertical Track Strength Testing Using TTCI's Track Loading Vehicle. *Technology Digest*.

Transnet. (1998). Technical Specification: Specification for the Supply of Stone S406. Johannesburg. South Africa

Transnet. (2006). Technical Specification: Specification for Railway Earthworks S410. Johannesburg. South Africa

White, D. J. Take, W. A. and Bolton, M. D. (2003). Soil deformation measurement using particle image velocimetry (PIV) and photogrammetry. *Geotechnique, 53*(7), 619-631.

Zarembski, A. M. and Palese, J. (2003). Transitions Eliminate Impact at Crossings. *Railway Track and Structures*, 28-30.

Zorn, G. (2005). Operating manual : Light Drop Weight Tester ZFG 2000 (Light Weight Deflectometer, Portable Falling Weight Deflectometer) for the dynamic plate loading test, corresponding to the German "Technical Specification for Soil and Rock in Road Construction". Stendal, Germany: Zorn company.

APPENDIX A

GPR LABORATORY TESTING

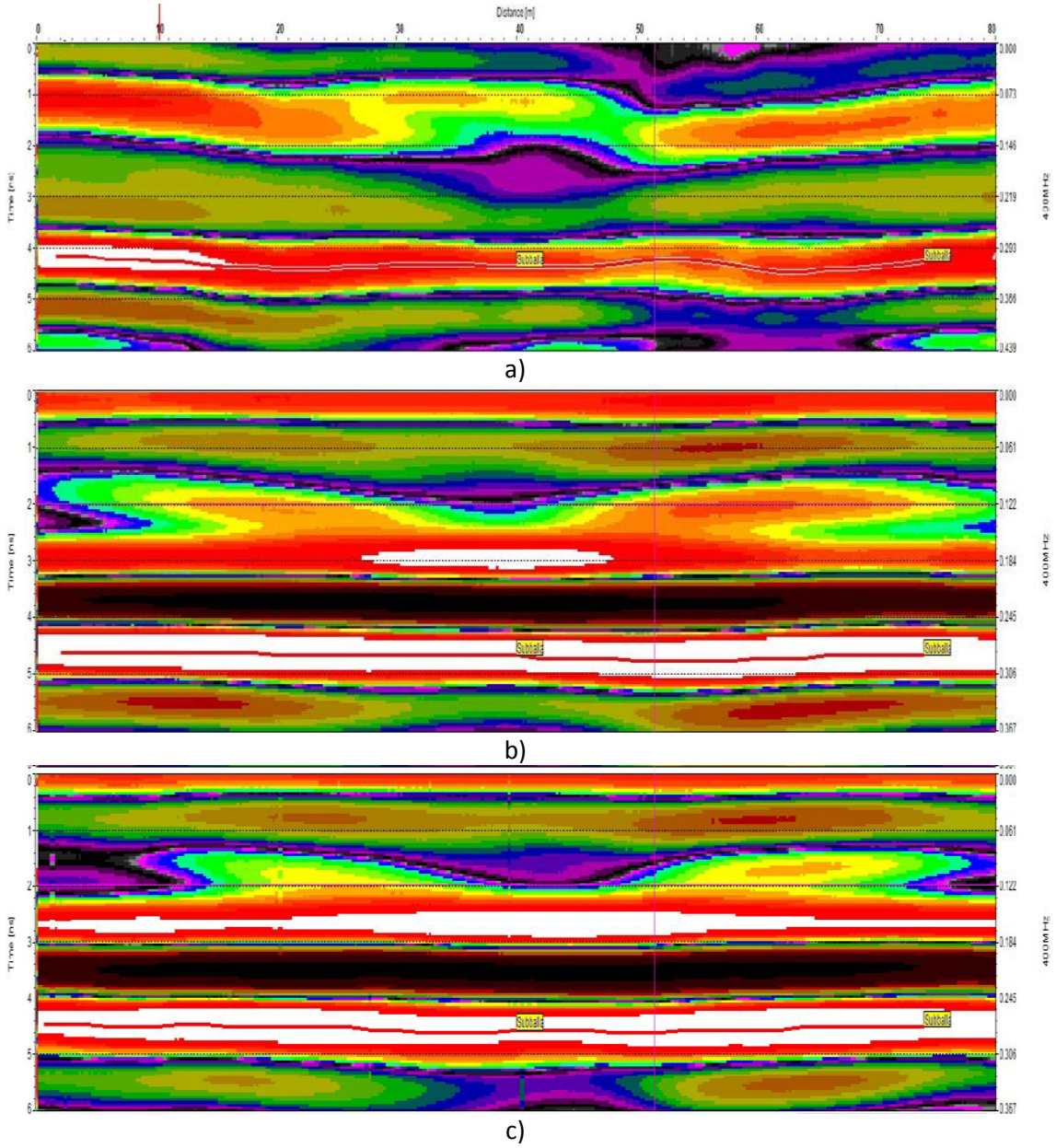

Figure 0-1: GPR Laboratory testing for Box 1 Dolerite a) Dry b) Wet 1 c) Wet 3

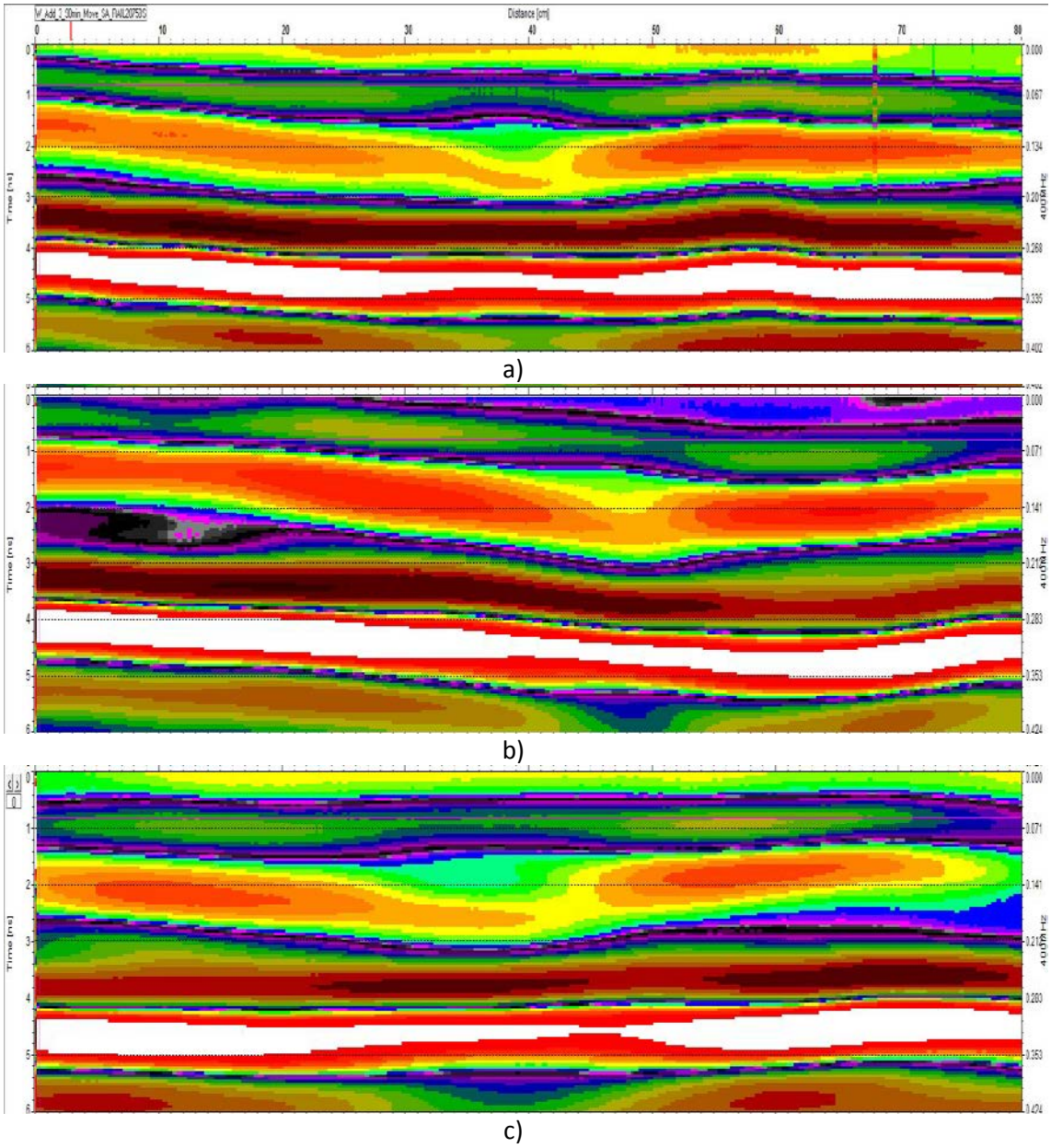

Figure 0-2: GPR Laboratory testing for Box 1 Dolerite a) Wet 3 at 30 minutes b) Wet 3 at 60 minutes c) Wet 3 at 90 minutes

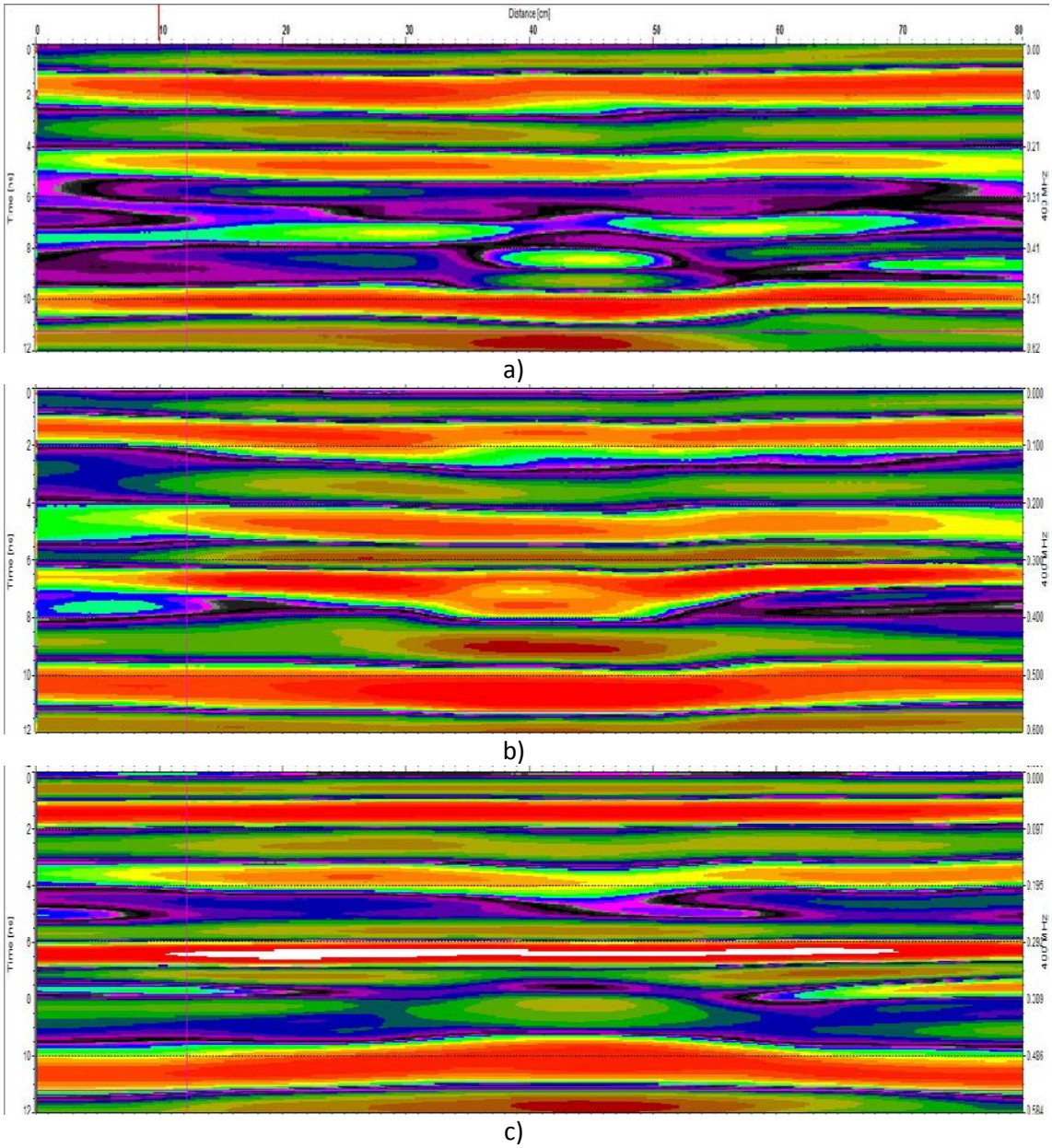

Figure 0-3: GPR Laboratory testing for Box 2 Dolerite a) Dry b) Wet 1 c) Wet 3

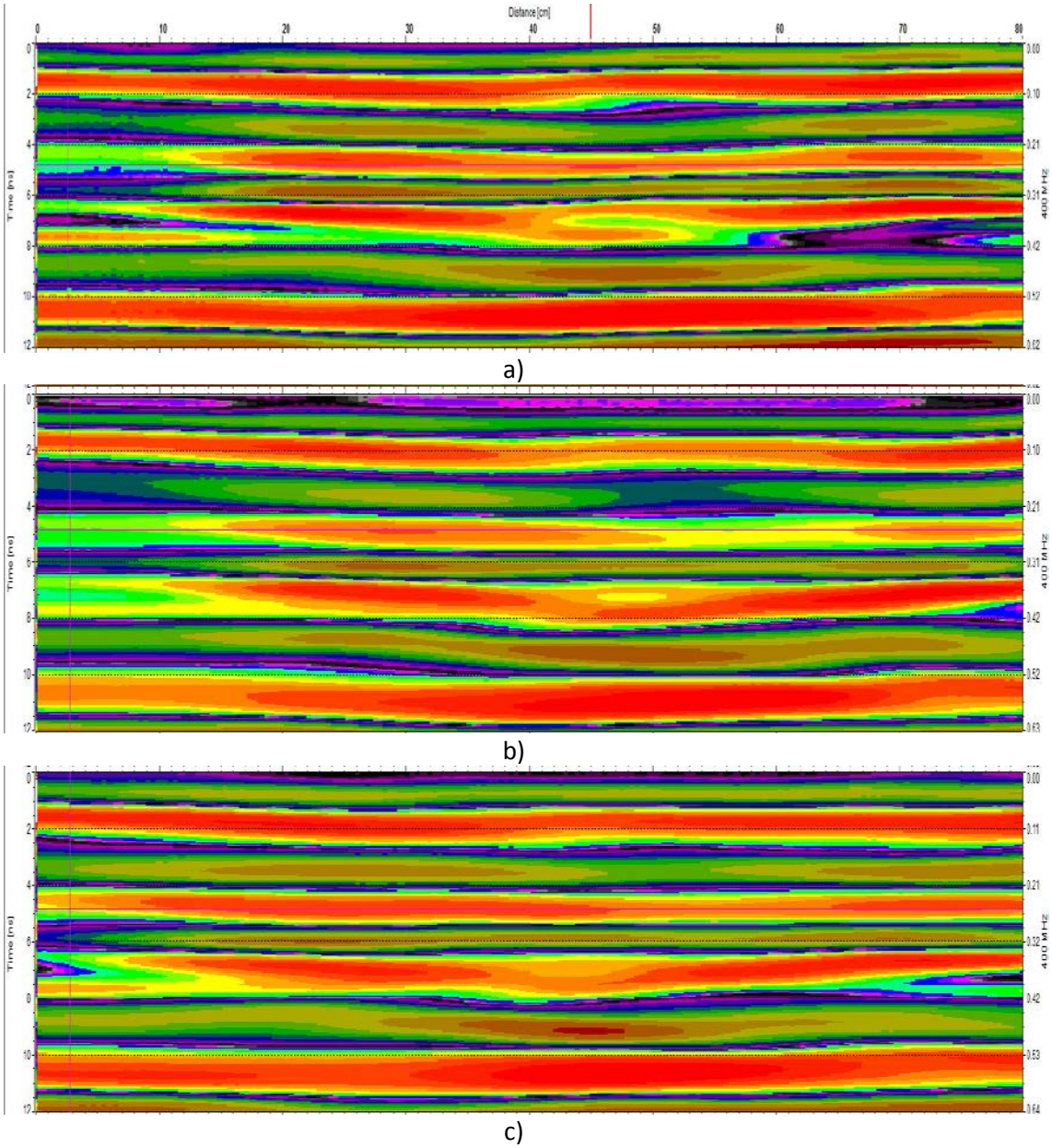

Figure 0-4: GPR Laboratory testing for Box 2 Dolerite a) Wet 3 at 30 minutes b) Wet 3 at 60 minutes c) Wet 3 at 90 minutes

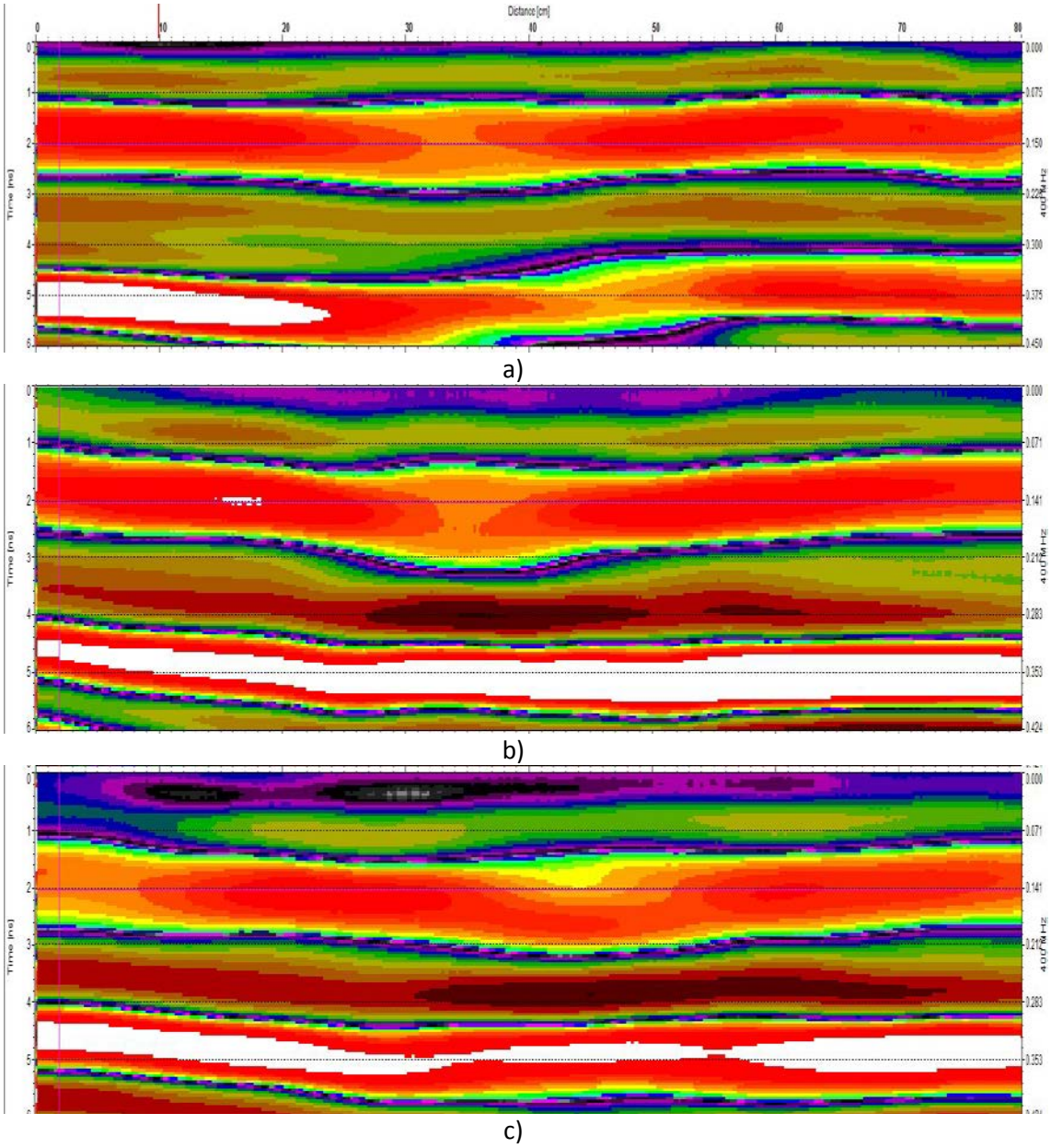

Figure 0-5: GPR Laboratory testing for Box 3 Quartzite a) Dry b) Wet 1 c) Wet 3

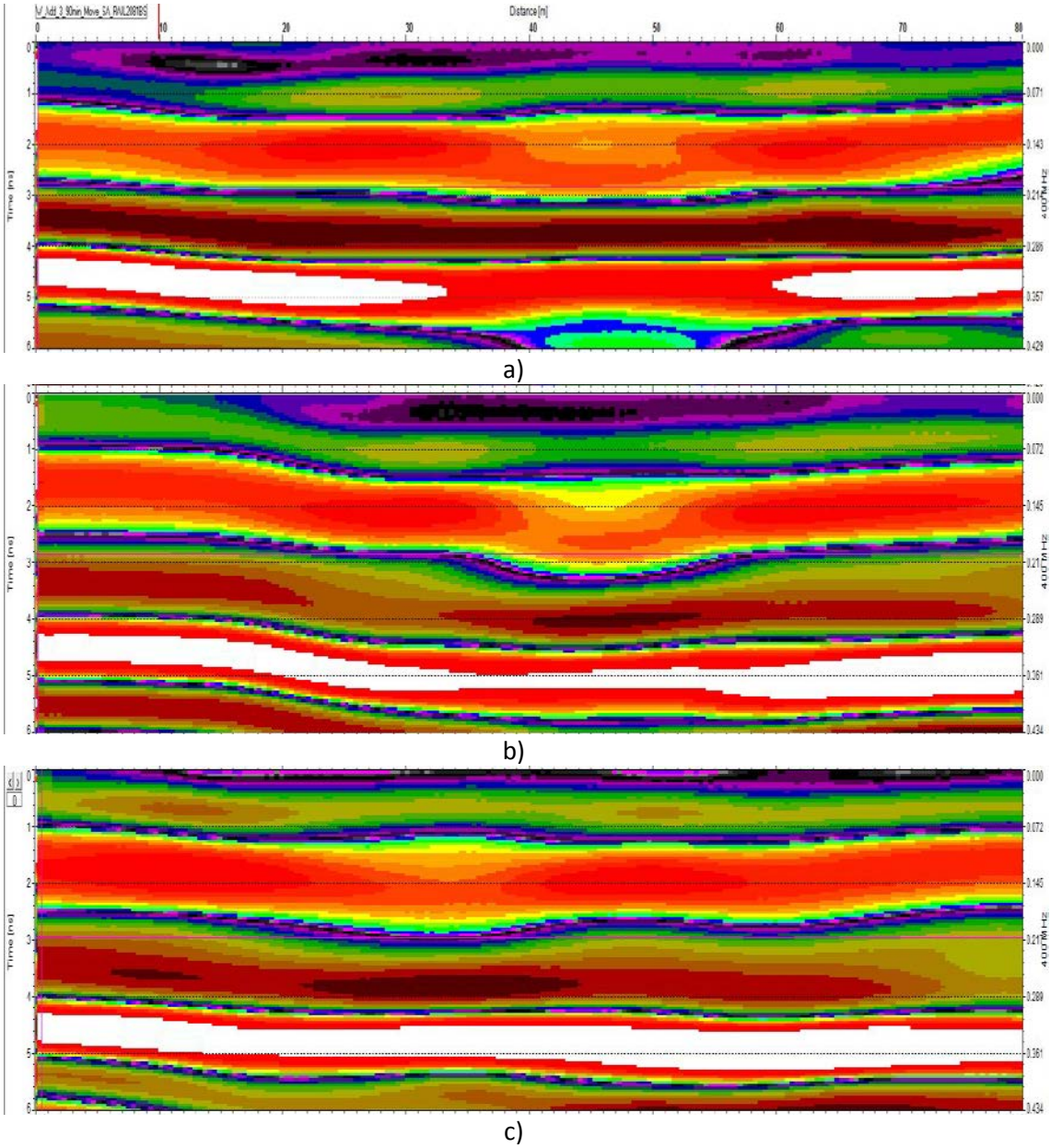

Figure 0-6: GPR Laboratory testing for Box 3 Quartzite a) Wet 3 at 30 minutes b) Wet 3 at 60 minutes c) Wet 3 at 90 minutes

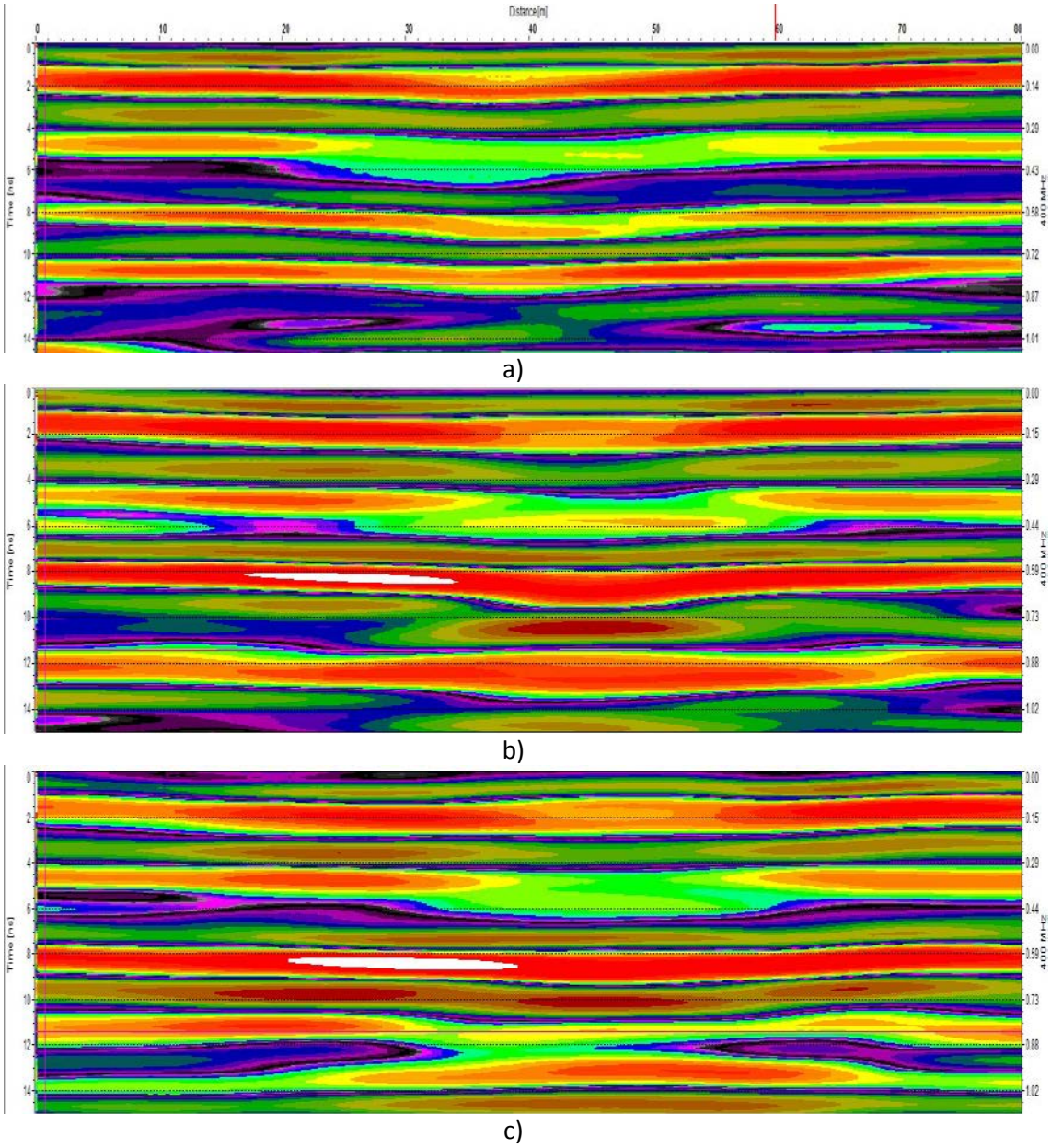

Figure 0-7: GPR Laboratory testing for Box 4 Quartzite a) Dry b) Wet 1 c) Wet 3

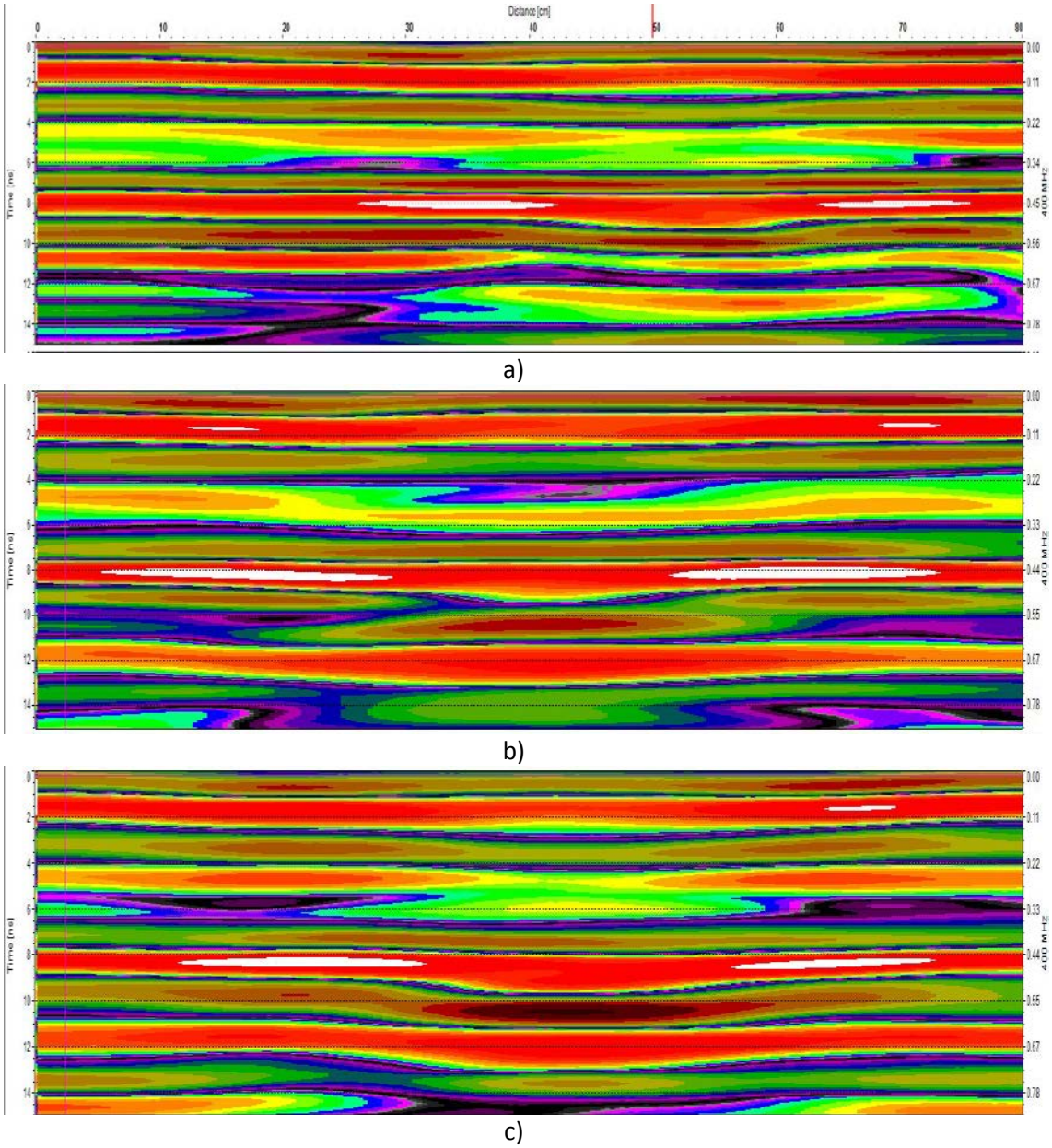

a)

b)

c)

Figure 0-8: GPR Laboratory testing for Box 4 Quartzite a) Wet 3 at 30 minutes b) Wet 3 at 60 minutes c) Wet 3 at 90 minutes

APPENDIX B

GPR FIELD MEASUREMENTS

KOMVOORHOOGTE TO NHLAZATSHE

KM 50 TO KM 70

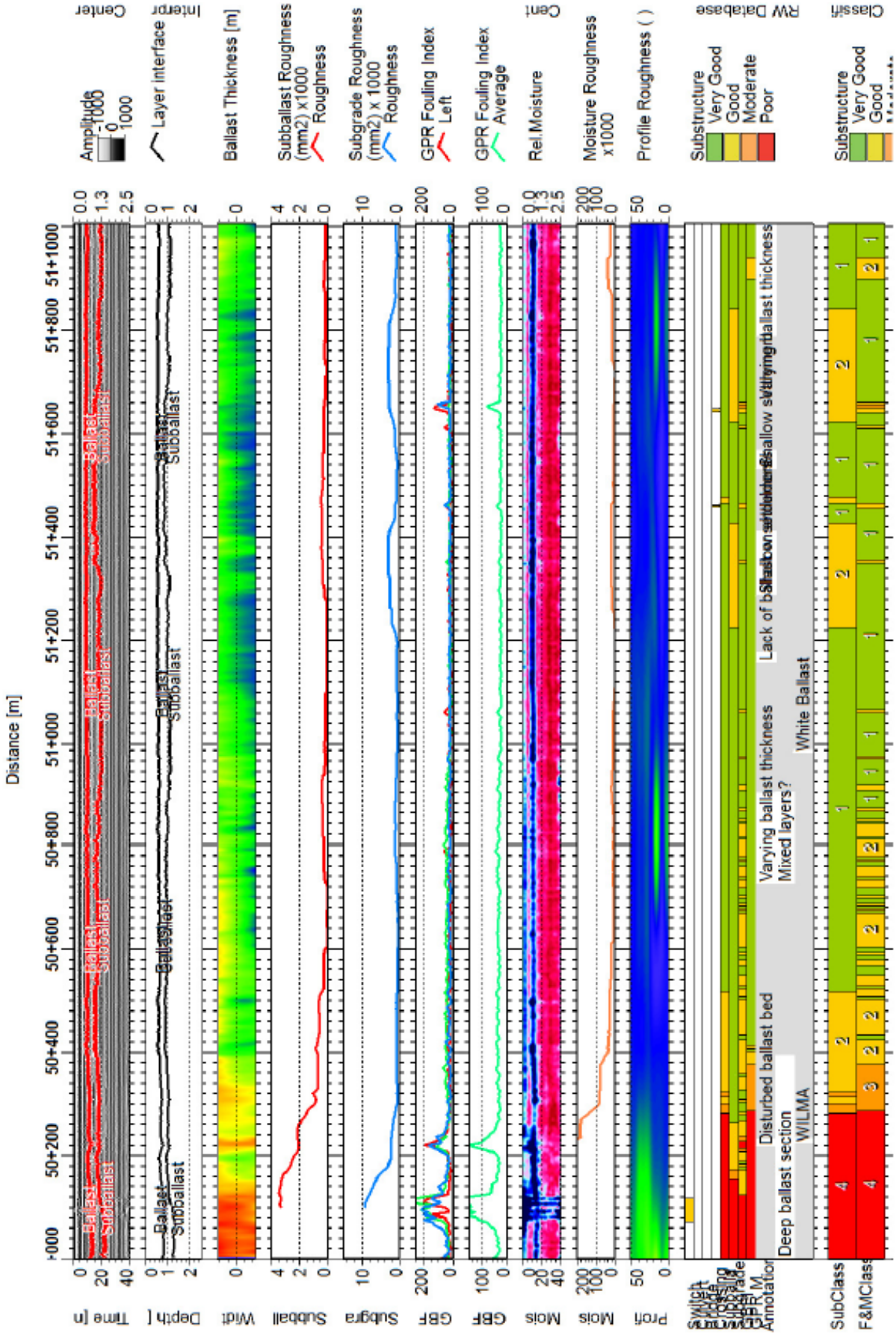
Distance [m]
Amplitude
Layer interface
Ballast Thickness [m]
Subballast Roughness (mm2) x1000 Roughness
Subgrade Roughness (mm2) x 1000 Roughness
GPR Fouling Index Left
GPR Fouling Index Average
Rel.Moisture
Moisture Roughness x1000
Profile Roughness ( )
RW Database
Substructure
Very Good
Good
Moderate
Poor
Ballast
Subballast
Deep ballast section
WILMA
Disturbed ballast bed
Varying ballast thickness
Mixed layers?
White Ballast
Lack of ballast thickness
SubClass
F&MClass

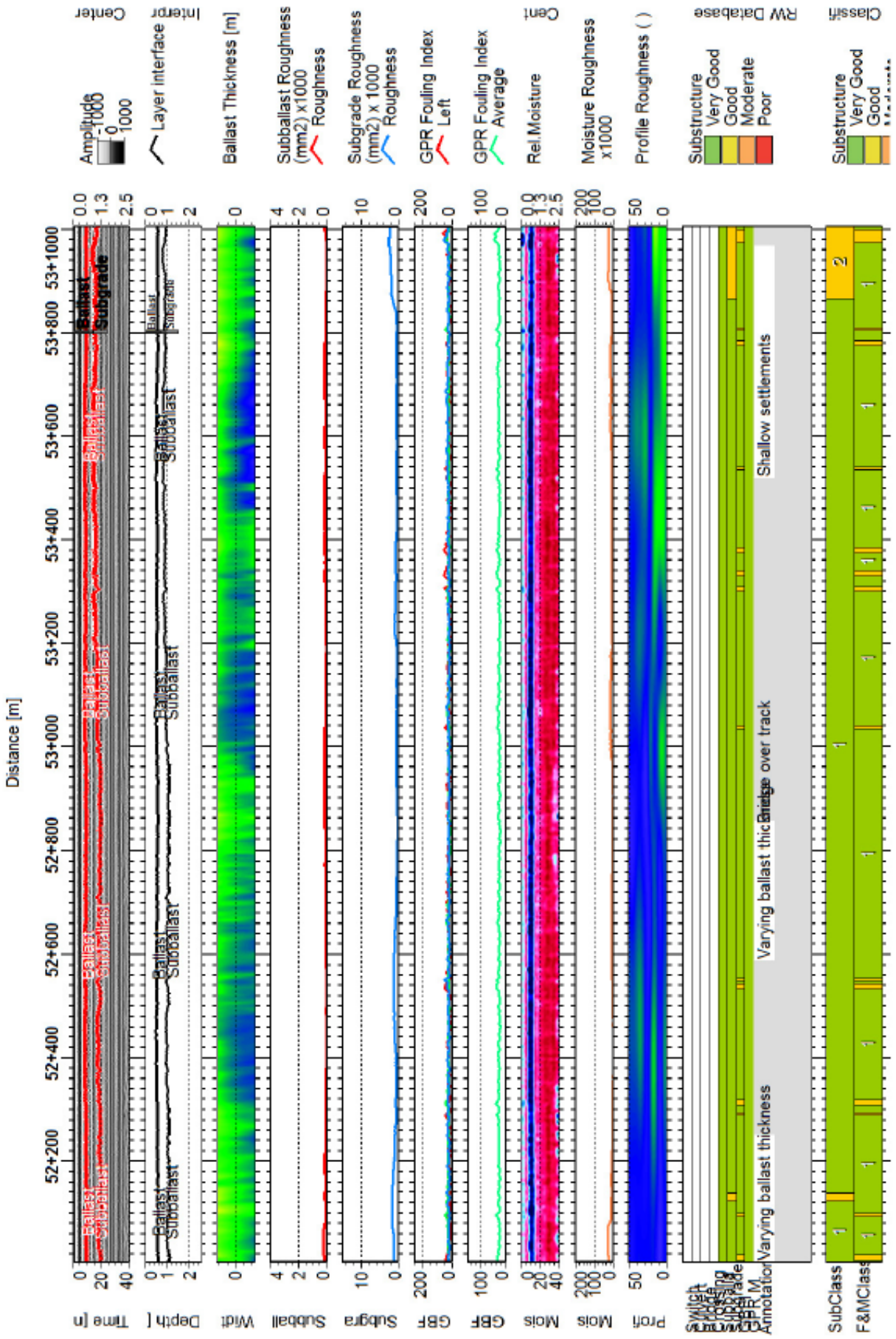
Distance [m]
Time [n
Depth [
Widt
Subbal
Subgra
GBF
GBF
Mois
Mois
Profi
SubClass
F&MClass
Center
Amplitude
-1000
0
1000
Interpr
Layer interface
Ballast Thickness [m]
Subballast Roughness (mm2) x1000 Roughness
Subgrade Roughness (mm2) x 1000 Roughness
GPR Fouling Index Left
GPR Fouling Index Average
Cent
Rel.Moisture
Moisture Roughness x1000
Profile Roughness ( )
RW Database
Substructure
Very Good
Good
Moderate
Poor
Classifi
Substructure
Very Good
Good
Ballast
Subballast
Subgrade
Varying ballast thickness
Varying ballast thic
over track
Shallow settlements

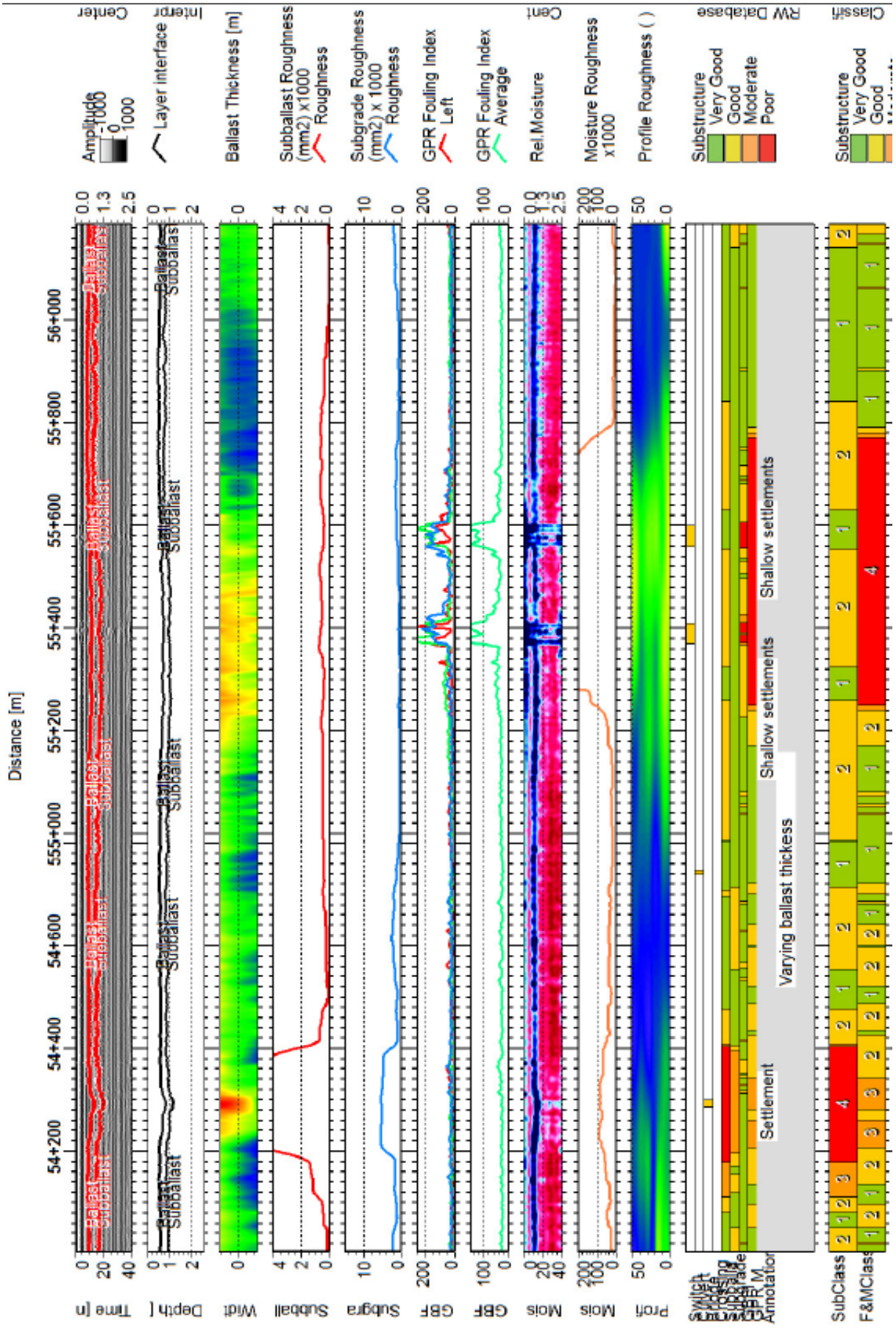
Distance [m]
54+200
54+400
54+600
555+000
55+200
55+400
55+600
55+800
56+000
Time [n
Depth [
Widt
Subball
Subgra
GBF
GBF
Mois
Mois
Profi
SubClass
F&MClass
Center
Amplitude
-1000
0
1000
Interpr
Layer interface
Ballast
Subballast
Ballast Thickness [m]
Subballast Roughness (mm2) x1000
Roughness
Subgrade Roughness (mm2) x 1000
Roughness
GPR Fouling Index
Left
GPR Fouling Index
Average
Cent
Rel.Moisture
Moisture Roughness x1000
Profile Roughness ( )
RW Database
Substructure
Very Good
Good
Moderate
Poor
Classifi
Substructure
Very Good
Good
Settlement
Varying ballast thickess
Shallow settlements
Shallow settlements

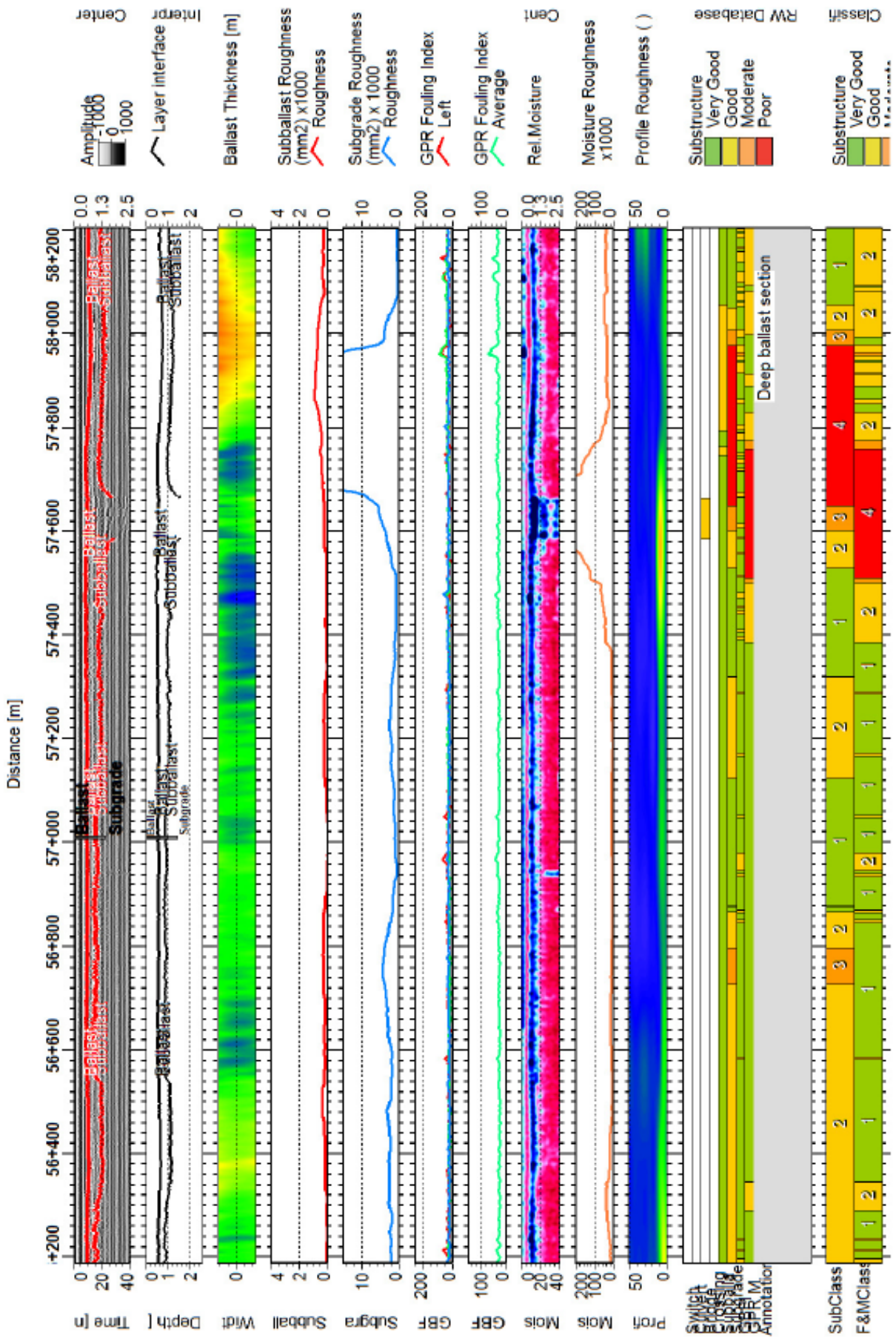
Distance [m]
Time [n
Depth [
Wat
Subbal
Subgra
GBF
GBF
Mois
Mois
Profi
SubClass
F&MClass
Center
Amplitude
Interpr
Layer interface
Ballast Thickness [m]
Subballast Roughness (mm2) x1000
Roughness
Subgrade Roughness (mm2) x 1000
Roughness
GPR Fouling Index
Left
GPR Fouling Index
Average
Cent
Rel.Moisture
Moisture Roughness x1000
Profile Roughness ( )
RW Database
Substructure
Very Good
Good
Moderate
Poor
Deep ballast section
Classifi
Substructure
Very Good
Good

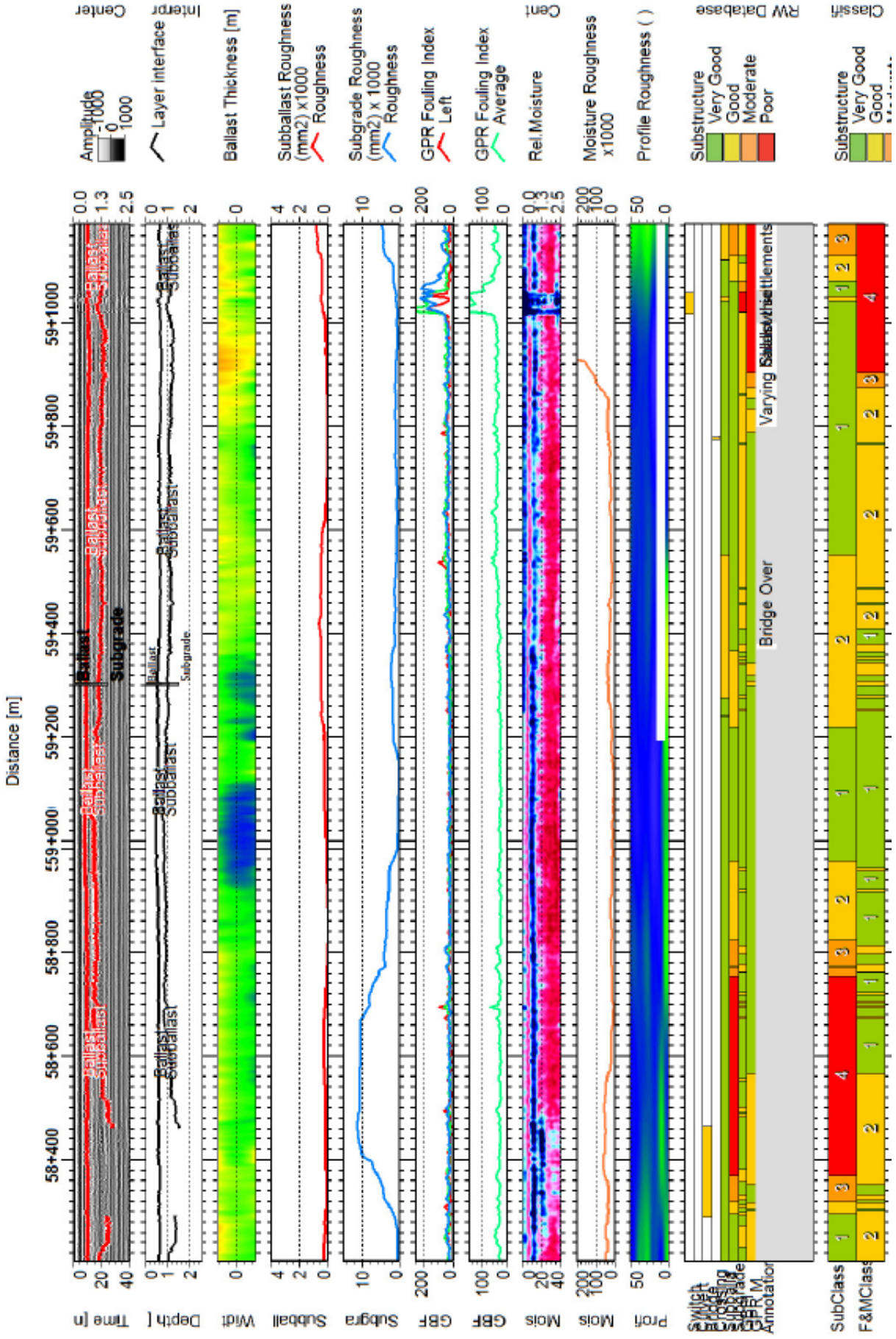
Distance [m]
58+400
58+600
58+800
59+000
59+200
59+400
59+600
59+800
59+1000
Ballast
Subballast
Subgrade
Bridge Over
Varying
Amplitude
Layer Interface
Ballast Thickness [m]
Subballast Roughness (mm2) x1000
Roughness
Subgrade Roughness (mm2) x 1000
Roughness
GPR Fouling Index
Left
GPR Fouling Index
Average
Rel.Moisture
Moisture Roughness x1000
Profile Roughness ( )
RW Database
Substructure
Very Good
Good
Moderate
Poor
SubClass
F&MClass

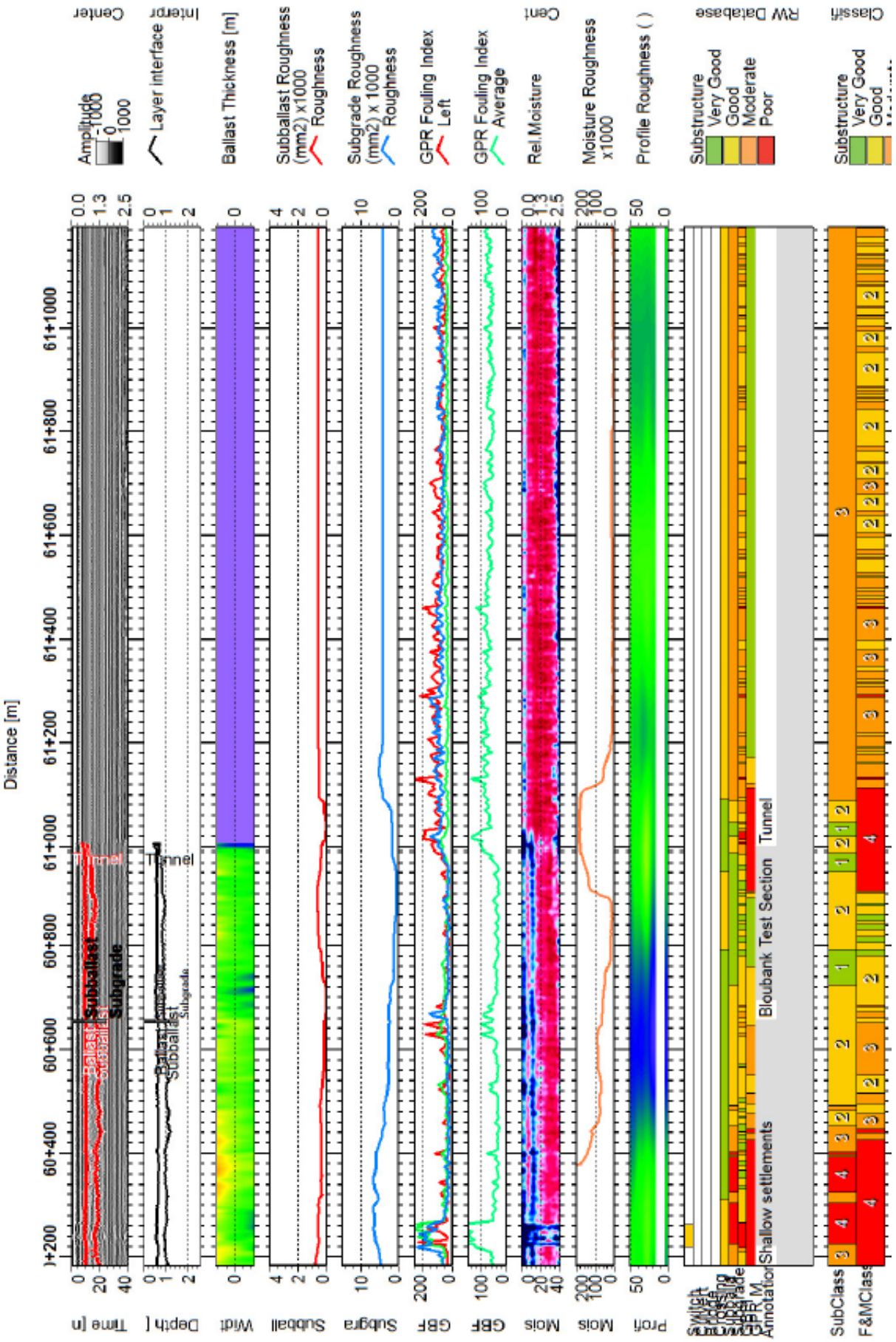
Distance [m]
Time [n
Depth [
Wdt
Subbal
Subgra
GBF
GBF
Mois
Mois
Profi
Switch
GPR M
Annotation
SubClass
F&MClass
Center
Amplitude
Layer interface
Interpr
Ballast Thickness [m]
Subballast Roughness (mm2) x1000
Roughness
Subgrade Roughness (mm2) x 1000
Roughness
GPR Fouling Index
Left
GPR Fouling Index
Average
Cent
Rel.Moisture
Moisture Roughness x1000
Profile Roughness ( )
RW Database
Substructure
Very Good
Good
Moderate
Poor
Classifi
Substructure
Very Good
Good
Ballast
Subballast
Subgrade
Tunnel
Bloubank Test Section
Shallow settlements

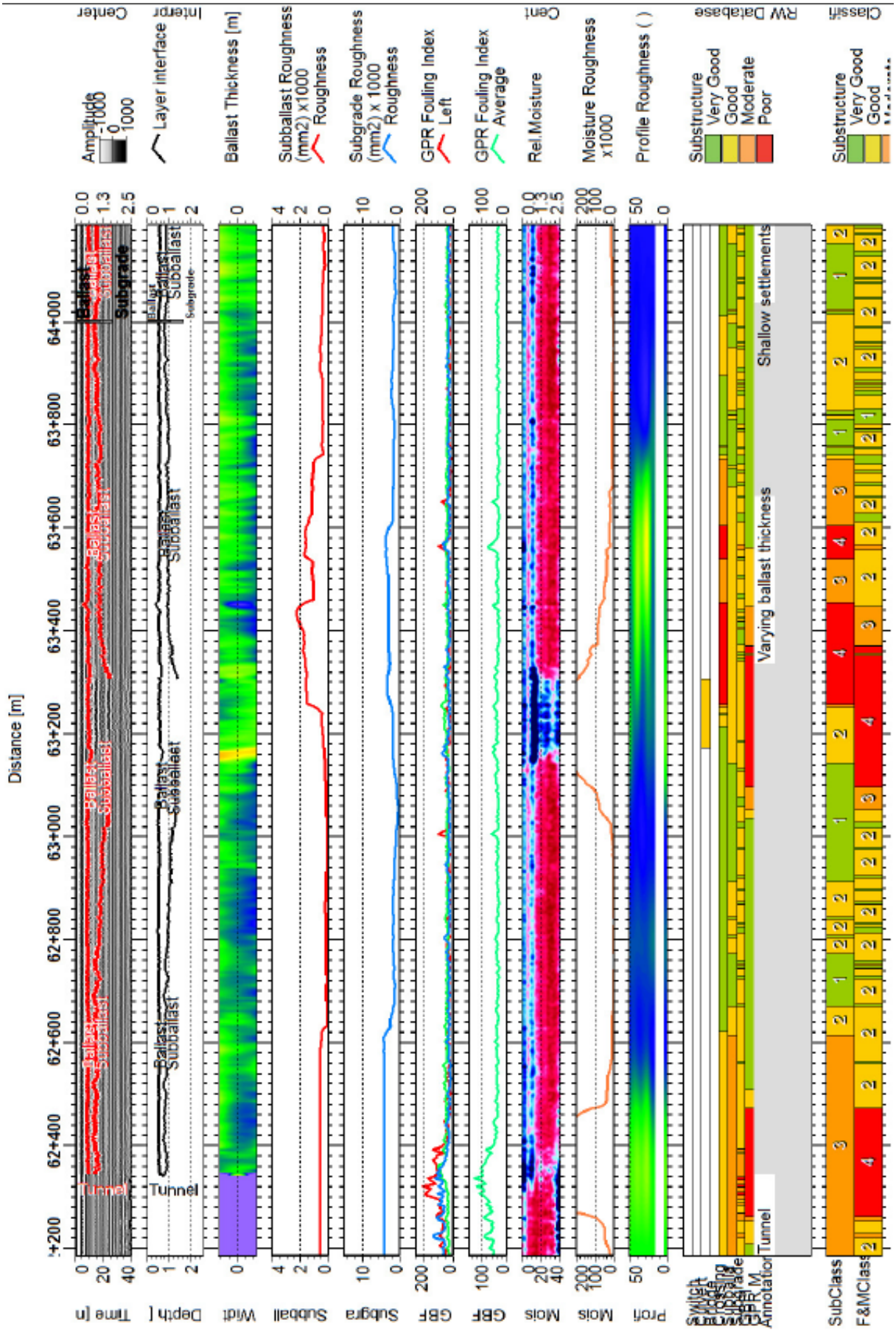
Distance [m]
Time [n
Depth [
Wdt
Subbal
Subgra
GBF
GBF
Mois
Mois
Profi
SubClass
F&MClass
Annotation
Tunnel
Varying ballast thickness
Shallow settlements
Ballast
Subballast
Subgrade
Amplitude
Layer interface
Ballast Thickness [m]
Subballast Roughness (mm2) x1000
Roughness
Subgrade Roughness (mm2) x 1000
Roughness
GPR Fouling Index
Left
GPR Fouling Index
Average
Rel.Moisture
Moisture Roughness x1000
Profile Roughness ( )
RW Database
Substructure
Very Good
Good
Moderate
Poor
Classifi
Substructure
Very Good
Good

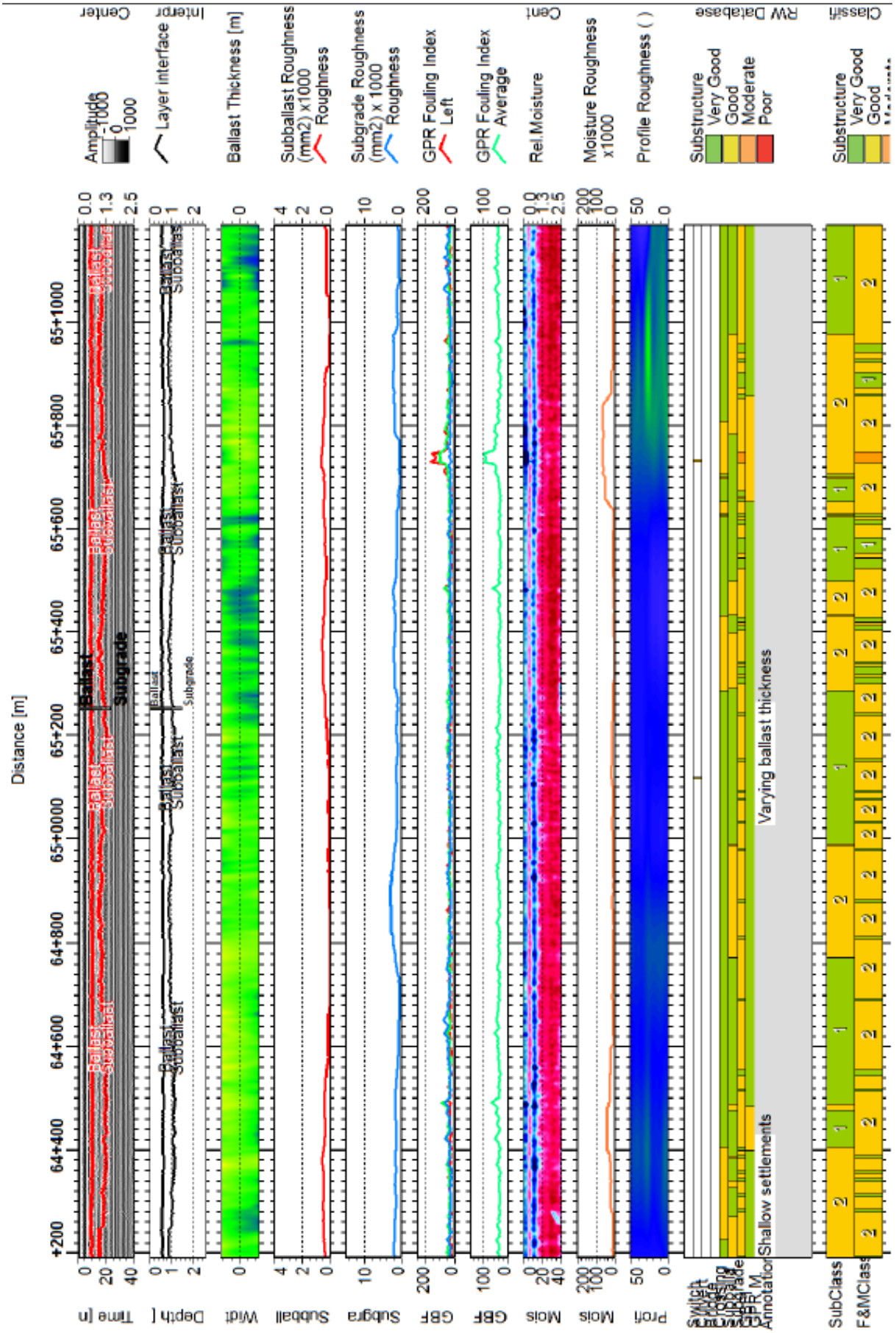
Distance [m]
+200
64+400
64+600
64+800
65+0000
65+200
65+400
65+600
65+800
65+1000
Ballast
Subballast
Subgrade
Varying ballast thickness
Shallow settlements
Amplitude
Layer interface
Ballast Thickness [m]
Subballast Roughness (mm2) x1000
Roughness
Subgrade Roughness (mm2) x 1000
Roughness
GPR Fouling Index
Left
GPR Fouling Index
Average
Rel.Moisture
Moisture Roughness x1000
Profile Roughness ( )
RW Database
Substructure
Very Good
Good
Moderate
Poor
Classifi
Substructure
Very Good
Good
SubClass
F&MClass

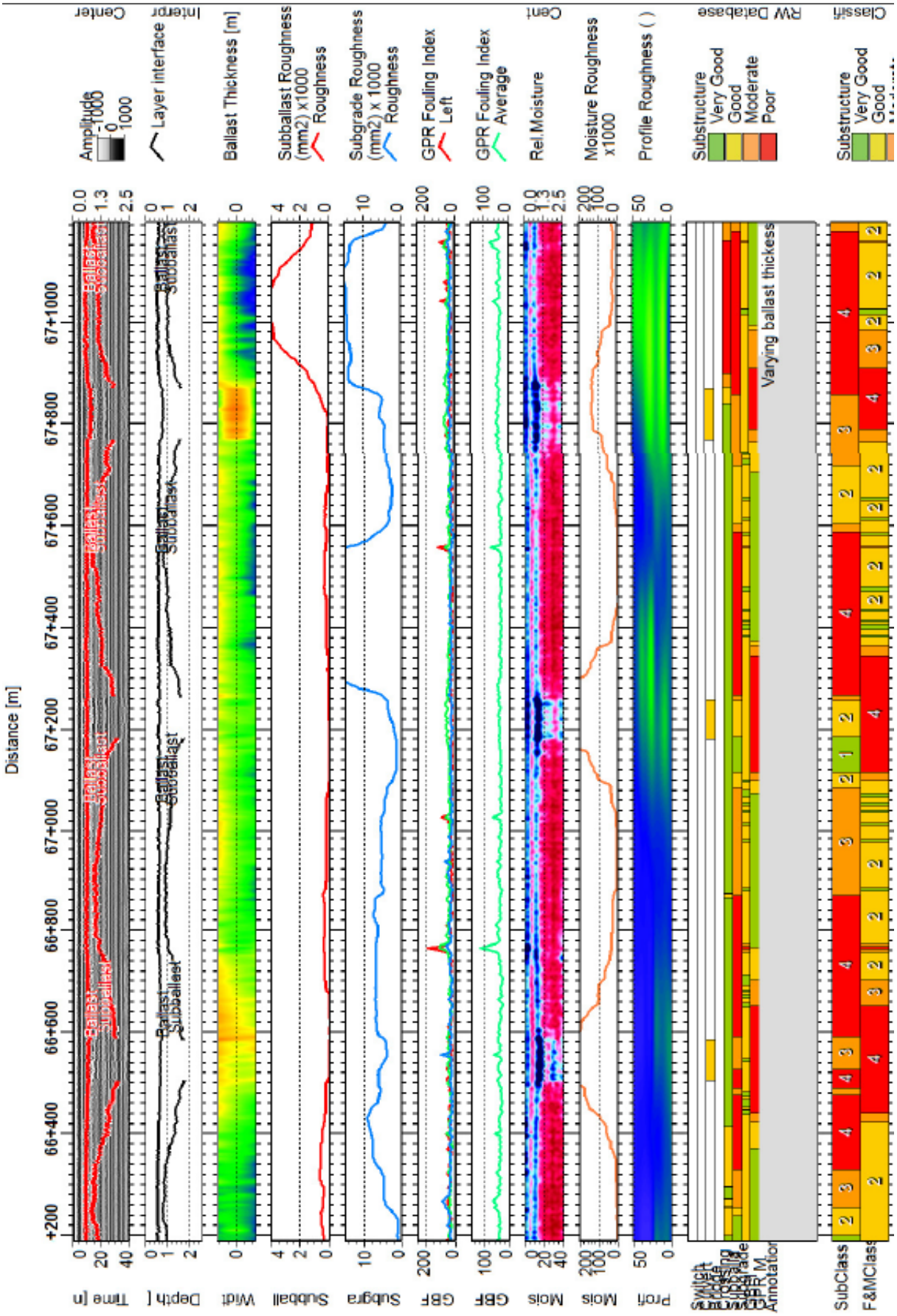
Distance [m]
+200
66+400
66+600
66+800
67+000
67+200
67+400
67+600
67+800
67+1000
Time [n
Depth [
Wat
Subbal
Subgra
GBF
GBF
Mois
Mois
Profi
SubClass
F&MClass
Center
Amplitude
-1000
0
1000
Interpr
Layer interface
Ballast
Subballast
Ballast Thickness [m]
Subballast Roughness (mm2) x1000
Roughness
Subgrade Roughness (mm2) x 1000
Roughness
GPR Fouling Index
Left
GPR Fouling Index
Average
Cent
Rel.Moisture
Moisture Roughness x1000
Profile Roughness ( )
RW Database
Substructure
Very Good
Good
Moderate
Poor
Varying ballast thickness
Classifi
Substructure
Very Good
Good

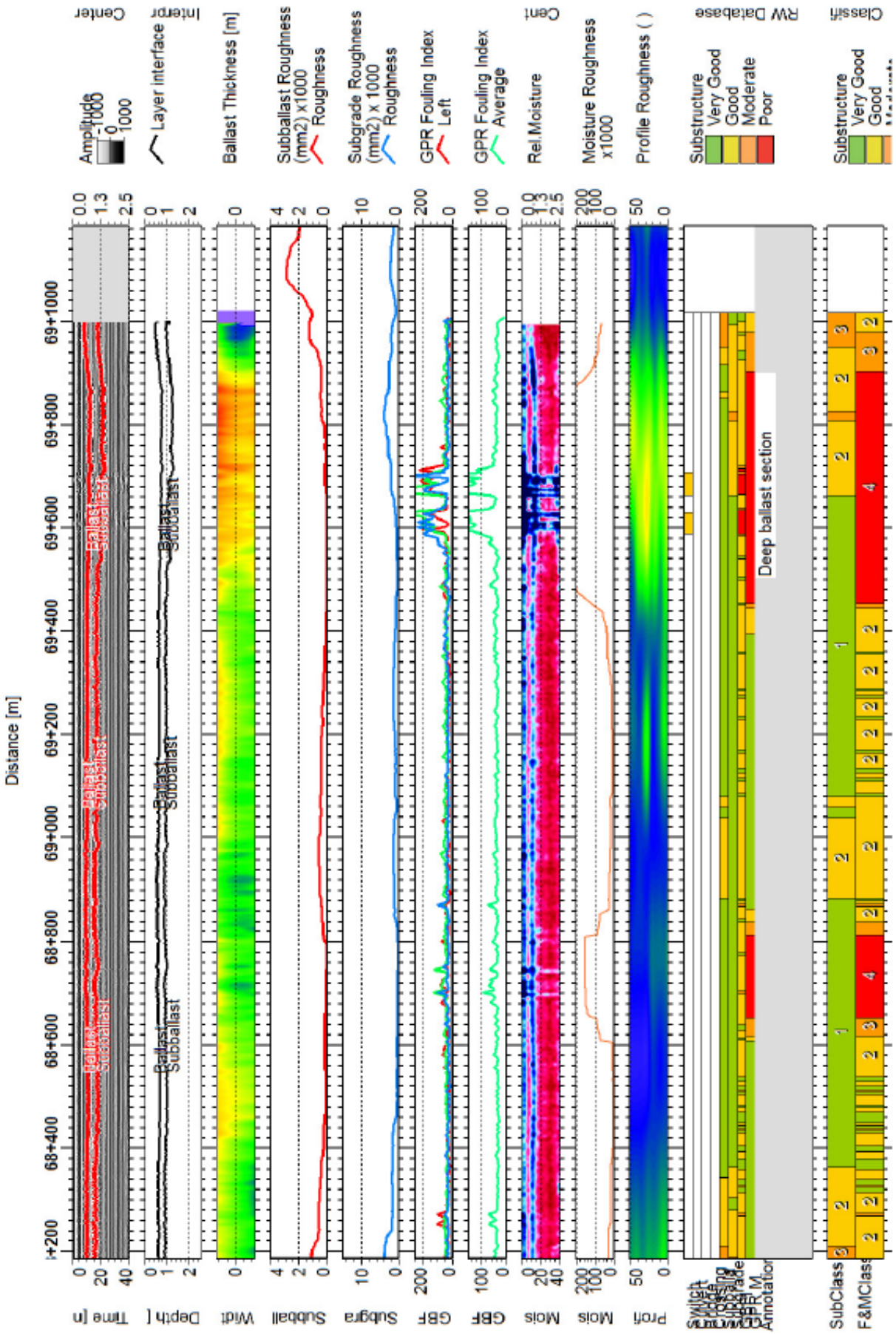
Distance [m]
Amplitude
Layer interface
Ballast Thickness [m]
Subballast Roughness (mm2) x1000
Roughness
Subgrade Roughness (mm2) x 1000
Roughness
GPR Fouling Index
Left
GPR Fouling Index
Average
Rel.Moisture
Moisture Roughness x1000
Profile Roughness ( )
RW Database
Substructure
Very Good
Good
Moderate
Poor
Deep ballast section
Ballast
Subballast
SubClass
F&MClass

NORTHAM TO THABAZIMBI

KM 203 TO KM 223

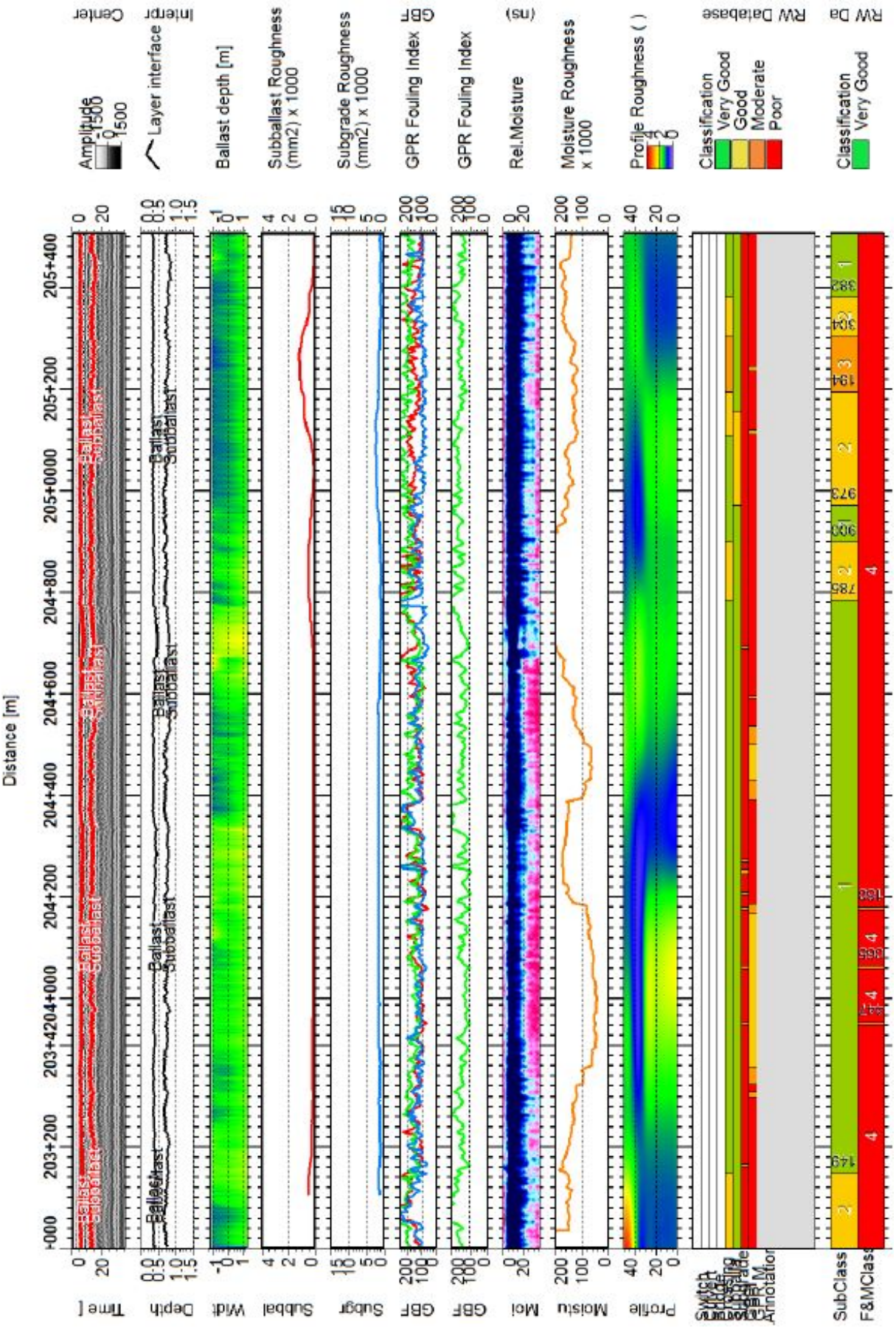
Distance [m]
Amplitude
Layer interface
Ballast depth [m]
Subballast Roughness (mm2) x 1000
Subgrade Roughness (mm2) x 1000
GPR Fouling Index
GPR Fouling Index
Rel.Moisture (ns)
Moisture Roughness x 1000
Profile Roughness ( )
Classification
Very Good
Good
Moderate
Poor
Classification
Very Good
Ballast
Subballast
SubClass
F&MClass

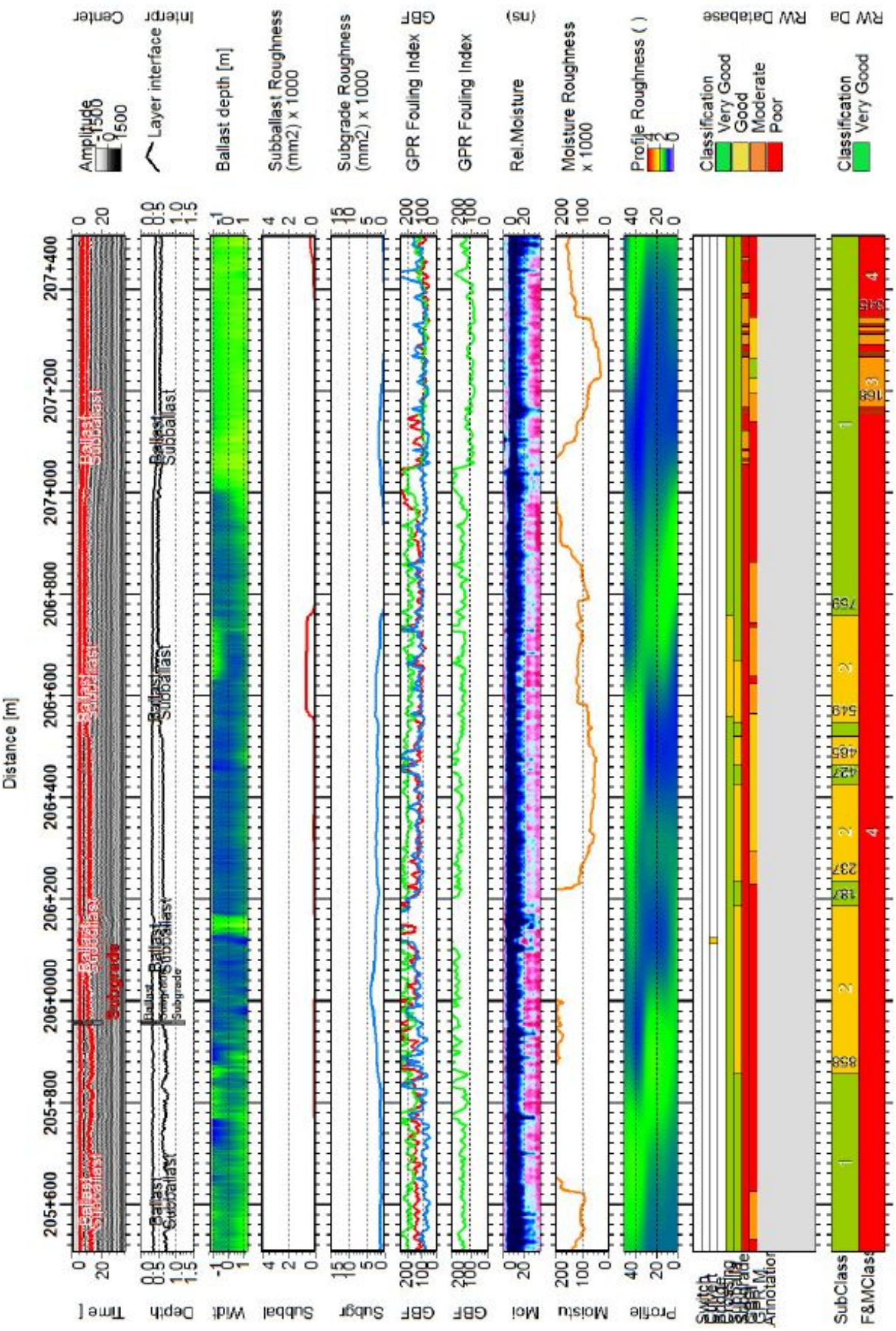
Distance [m]
205+600
205+800
206+0000
206+200
206+400
206+600
206+800
207+000
207+200
207+400
207+400
Amplitude
Center
Layer interface
Interpr
Ballast depth [m]
Subballast Roughness (mm2) x 1000
Subgrade Roughness (mm2) x 1000
GPR Fouling Index
GBF
GPR Fouling Index
Rel.Moisture
(ns)
Moisture Roughness x 1000
Profile Roughness ( )
Classification
Very Good
Good
Moderate
Poor
RW Database
Classification
Very Good
RW Da
Ballast
Subballast
Subgrade
SubClass
F&MClass

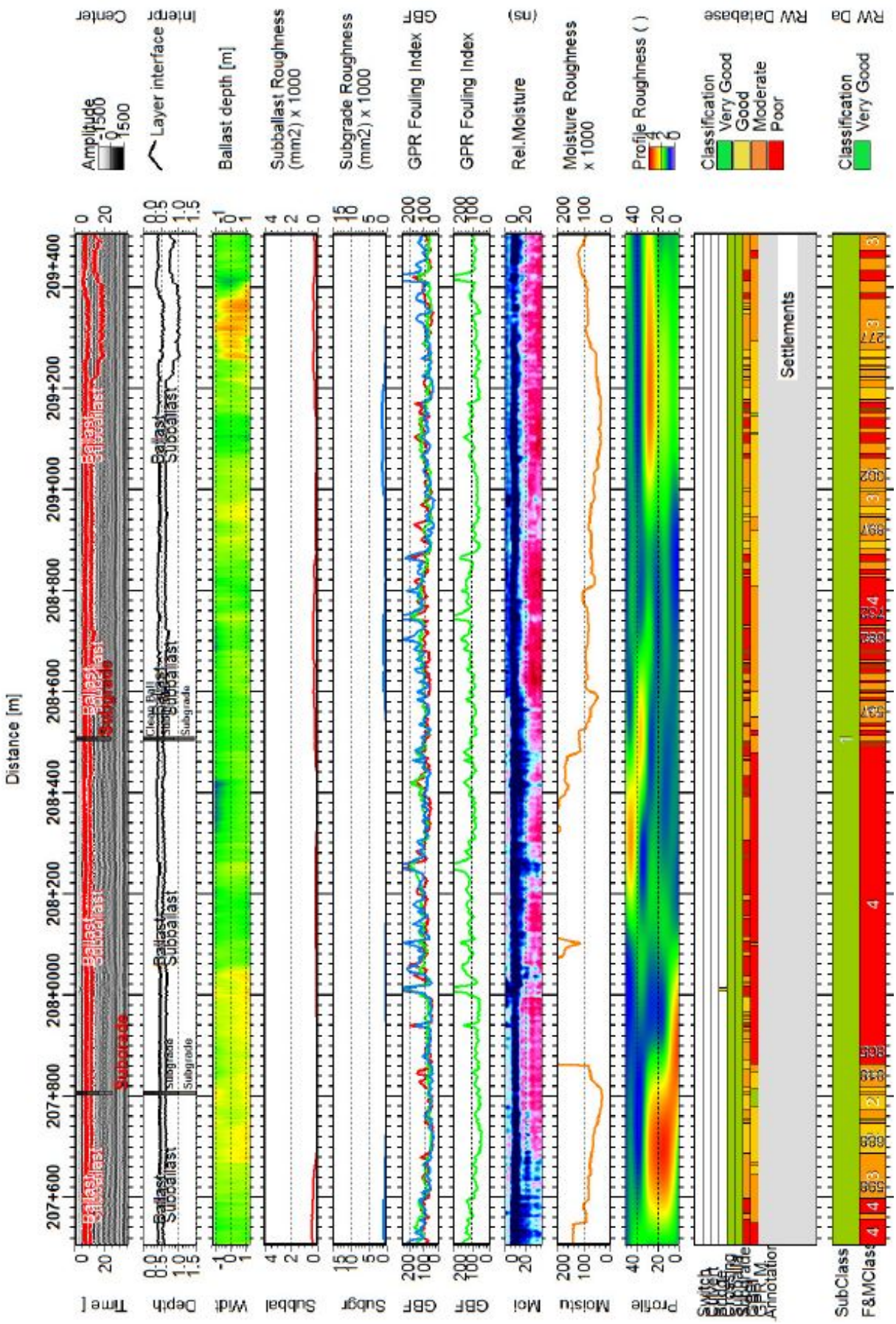
Distance [m]
207+600
207+800
208+0000
208+200
208+400
208+600
208+800
209+000
209+200
209+400
Ballast
Subballast
Subgrade
Ballast depth [m]
Subballast Roughness (mm2) x 1000
Subgrade Roughness (mm2) x 1000
GPR Fouling Index
GPR Fouling Index
Rel.Moisture
Moisture Roughness x 1000
Profile Roughness ( )
Classification
Very Good
Good
Moderate
Poor
Settlements
SubClass
F&MClass

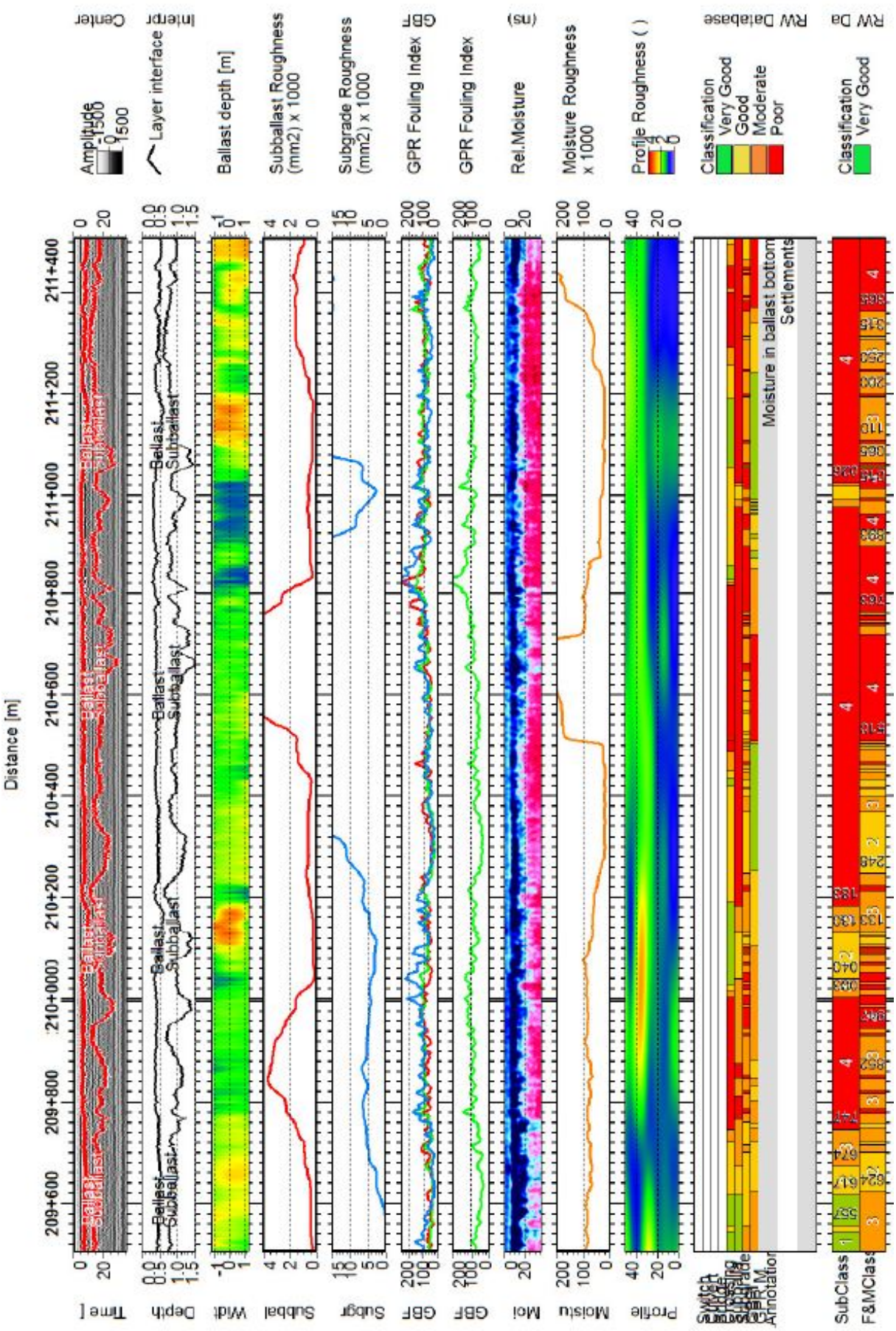
Distance [m]
209+600
209+800
210+000
210+200
210+400
210+600
210+800
211+000
211+200
211+400
Amplitude
Layer interface
Ballast depth [m]
Subballast Roughness (mm2) x 1000
Subgrade Roughness (mm2) x 1000
GPR Fouling Index
GPR Fouling Index
Rel.Moisture (ns)
Moisture Roughness x 1000
Profile Roughness ( )
Classification
Very Good
Good
Moderate
Poor
Classification
Very Good
Moisture in ballast bottom
Settlements
Ballast
Subballast
SubClass
F&MClass

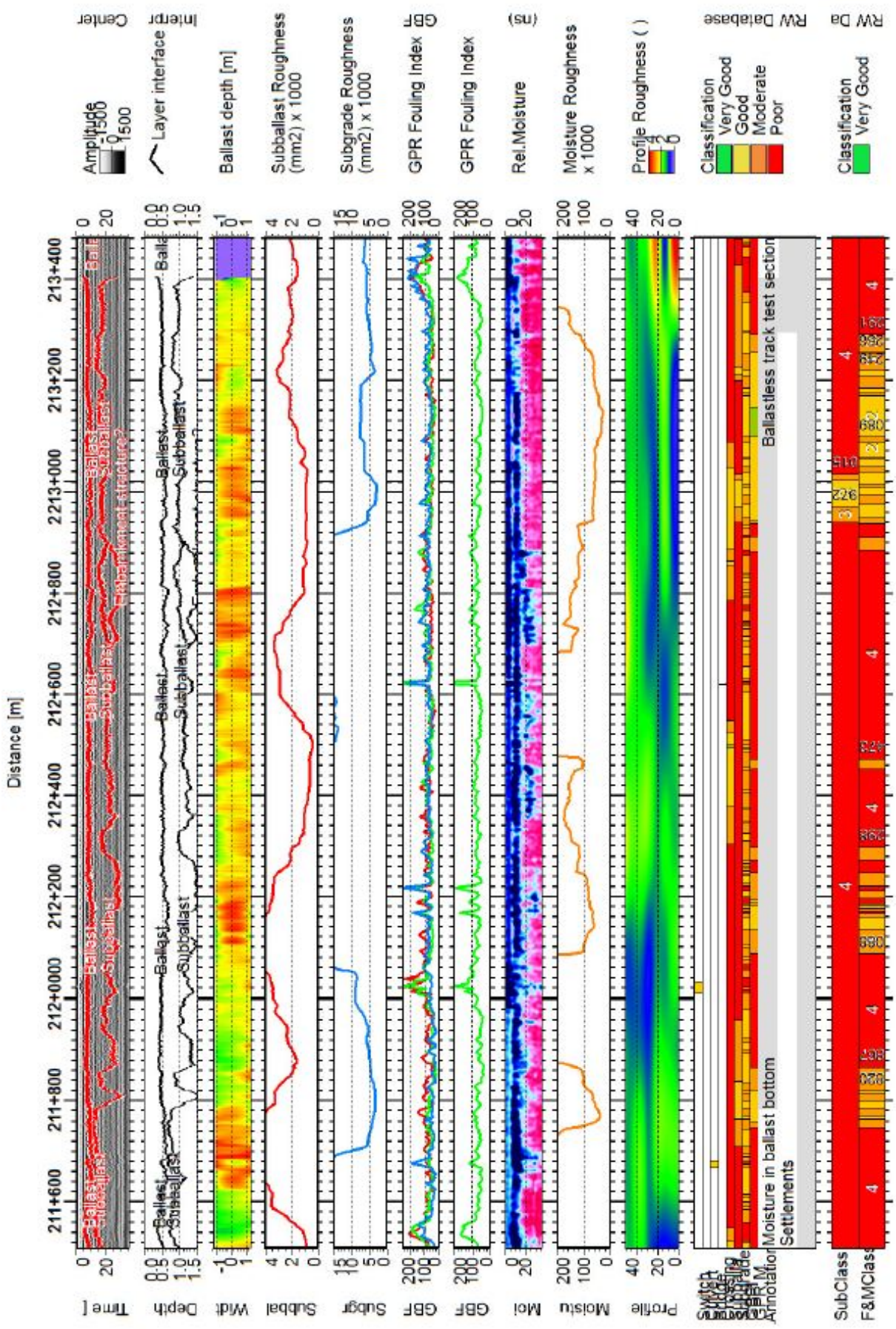
Distance [m]
211+600
211+800
212+0000
212+200
212+400
212+600
212+800
2213+000
213+200
213+400
Amplitude
Layer interface
Ballast depth [m]
Subballast Roughness (mm2) x 1000
Subgrade Roughness (mm2) x 1000
GPR Fouling Index
GPR Fouling Index
Rel.Moisture
Moisture Roughness x 1000
Profile Roughness ( )
Classification
Very Good
Good
Moderate
Poor
Classification
Very Good
Ballastless track test section
Moisture in ballast bottom
Settlements
SubClass
F&MClass

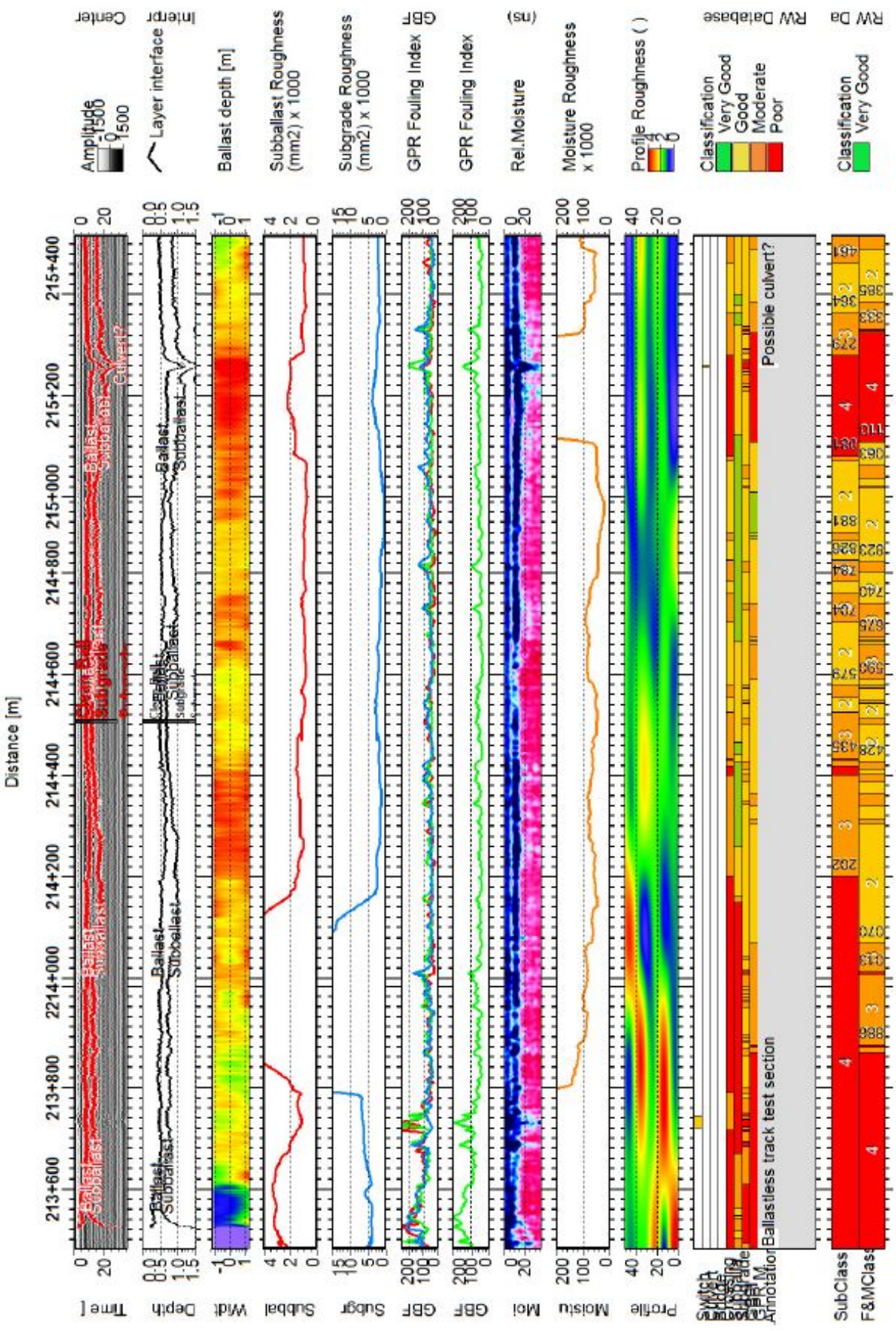
Distance [m]
213+600
213+800
214+000
214+200
214+400
214+600
214+800
215+000
215+200
215+400
Ballastless track test section
Possible culvert?
Ballast
Subballast
Subgrade
Amplitude
Layer interface
Ballast depth [m]
Subballast Roughness (mm2) x 1000
Subgrade Roughness (mm2) x 1000
GPR Fouling Index
GPR Fouling Index
Rel.Moisture
Moisture Roughness x 1000
Profile Roughness ( )
Classification
Very Good
Good
Moderate
Poor
Classification
Very Good
SubClass
F&MClass

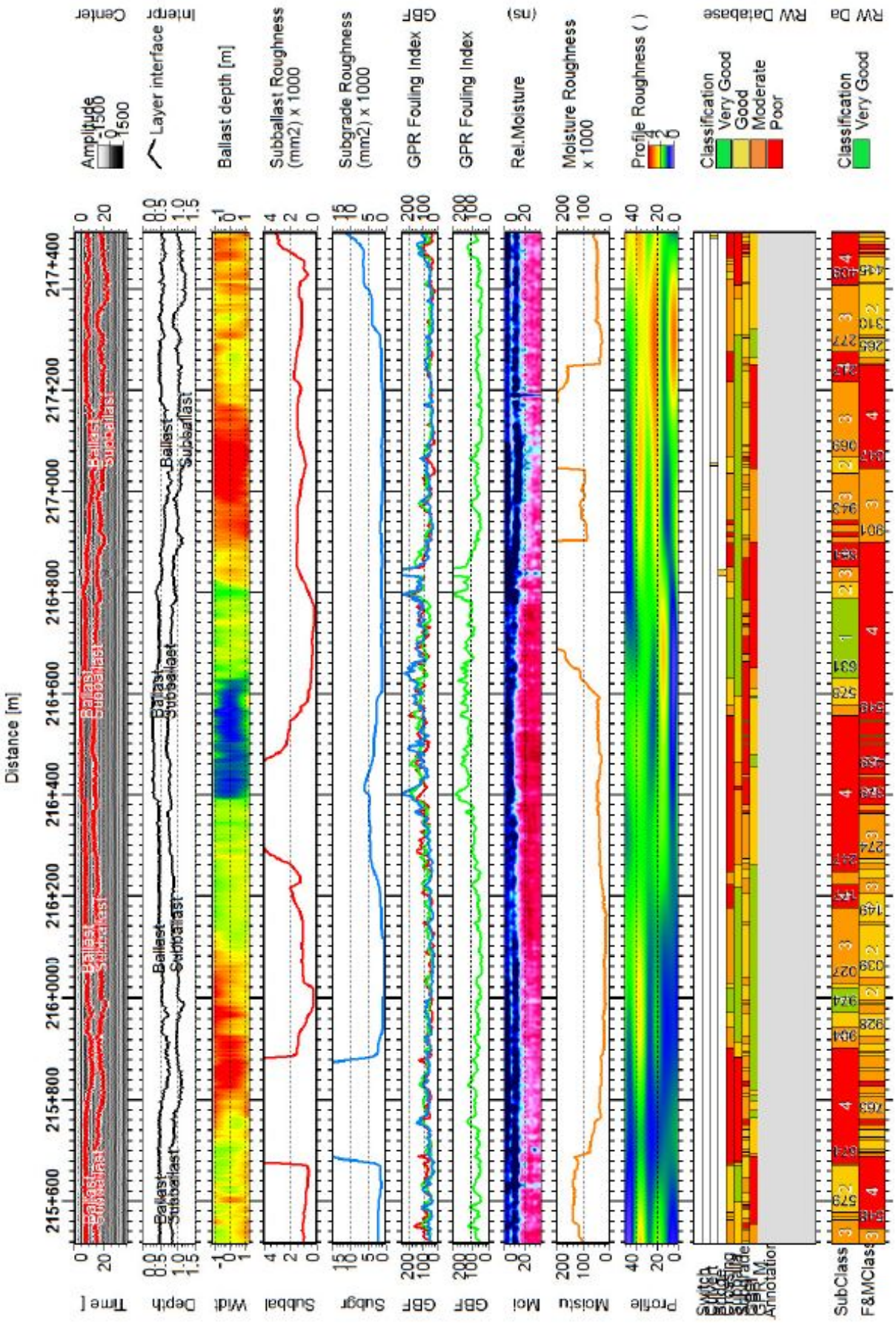
Distance [m]
215+600
215+800
216+000
216+200
216+400
216+600
216+800
217+000
217+200
217+400
Amplitude
Layer interface
Ballast depth [m]
Subballast Roughness (mm2) x 1000
Subgrade Roughness (mm2) x 1000
GPR Fouling Index
GPR Fouling Index
Rel.Moisture
Moisture Roughness x 1000
Profile Roughness ( )
Classification
Very Good
Good
Moderate
Poor
Classification
Very Good
Ballast
Subballast
SubClass
F&MClass

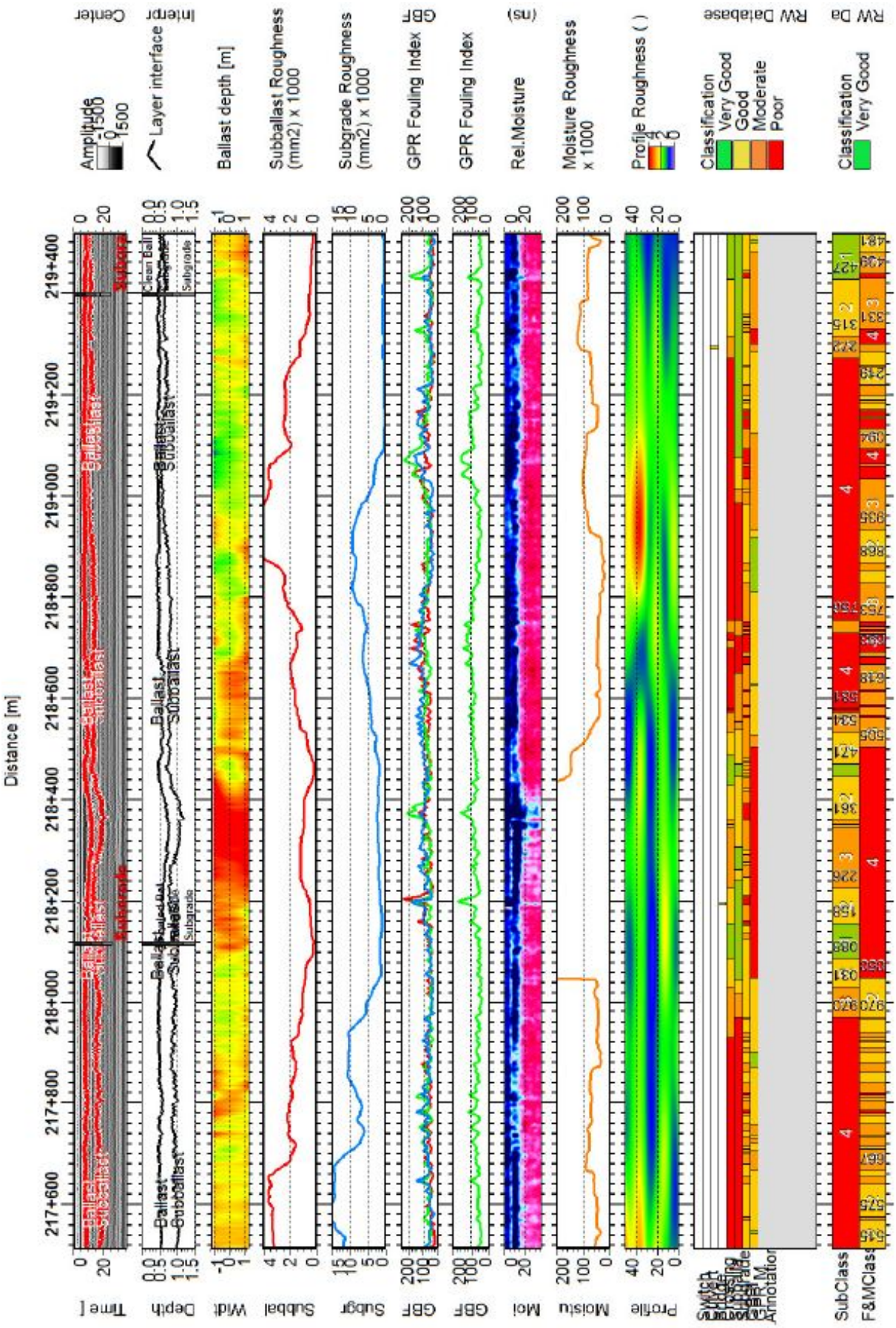
Distance [m]
Amplitude
Layer interface
Ballast depth [m]
Subballast Roughness (mm2) x 1000
Subgrade Roughness (mm2) x 1000
GPR Fouling Index
GPR Fouling Index
Rel.Moisture
Moisture Roughness x 1000
Profile Roughness ( )
Classification
Very Good
Good
Moderate
Poor
Classification
Very Good
Ballast
Subballast
Subgrade
Clean Ballast
SubClass
F&MClass

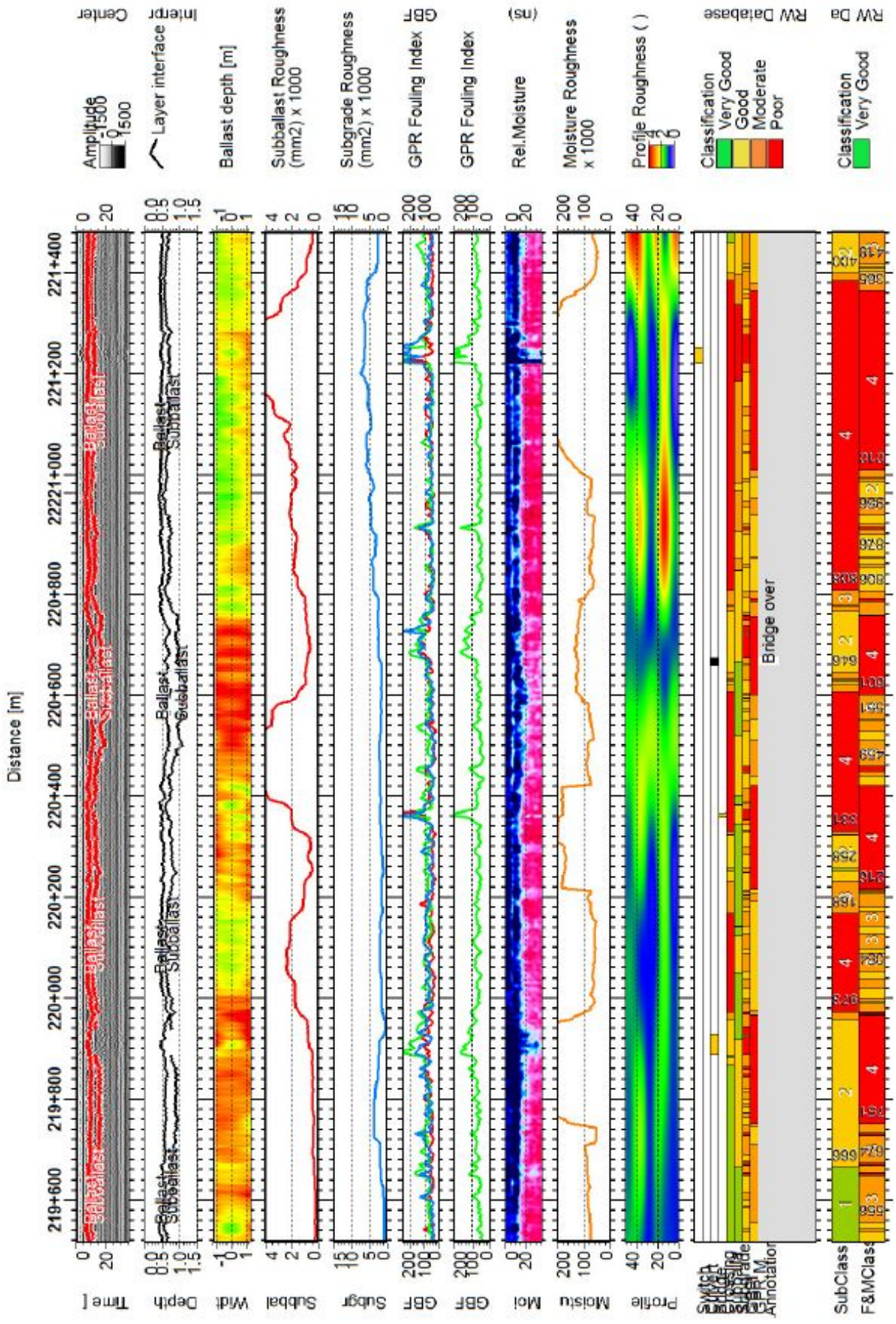
Distance [m]
Amplitude
Layer interface
Ballast depth [m]
Subballast Roughness (mm2) x 1000
Subgrade Roughness (mm2) x 1000
GPR Fouling Index
GPR Fouling Index
Rel.Moisture
Moisture Roughness x 1000
Profile Roughness ( )
Classification
Very Good
Good
Moderate
Poor
Classification
Very Good
Ballast
Subballast
Bridge over
SubClass
F&MClass

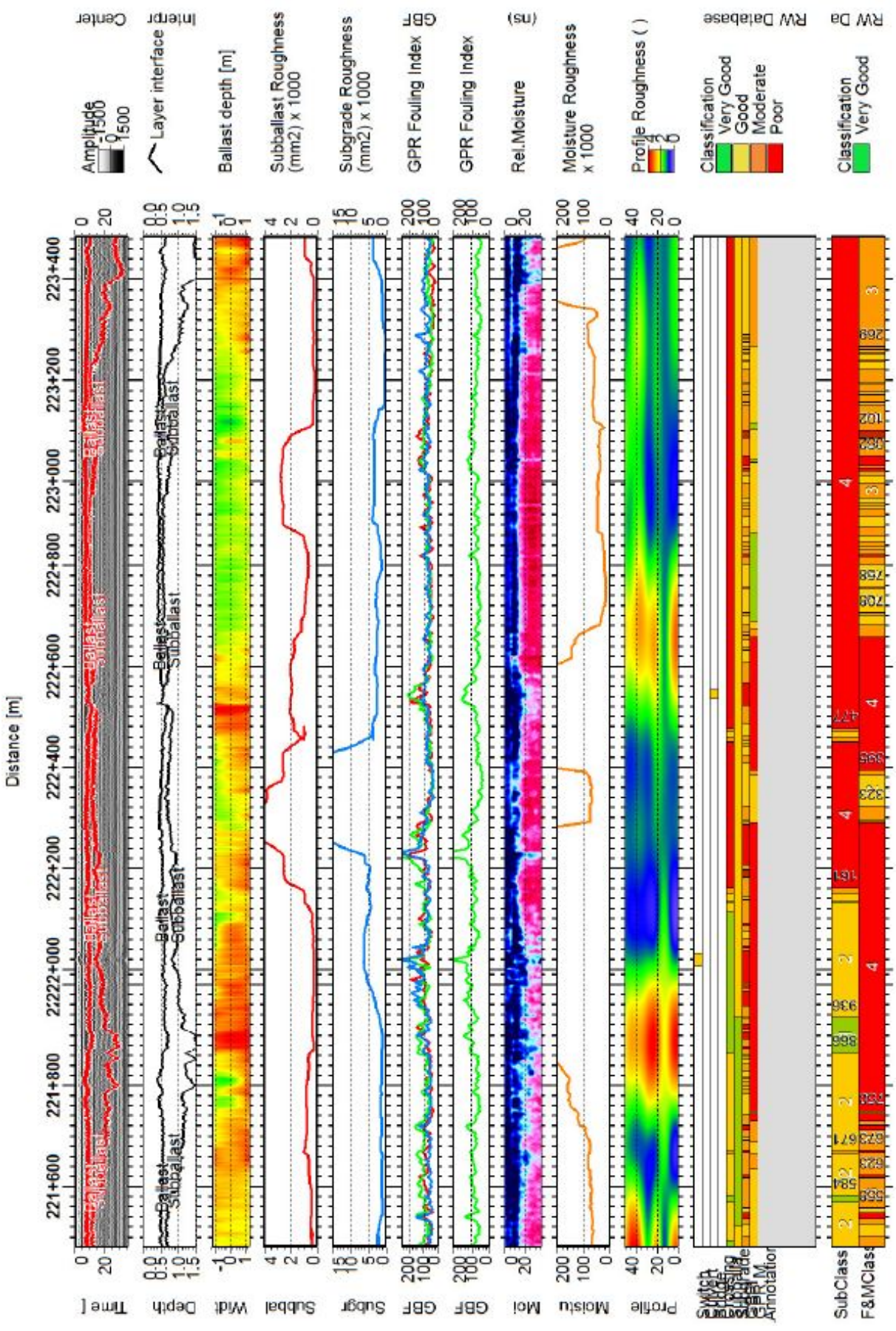
Distance [m]
Amplitude
Layer interface
Ballast depth [m]
Subballast Roughness (mm2) x 1000
Subgrade Roughness (mm2) x 1000
GPR Fouling Index
GPR Fouling Index
Rel.Moisture
Moisture Roughness x 1000
Profile Roughness ( )
Classification
Very Good
Good
Moderate
Poor
Classification
Very Good
Ballast
Subballast
SubClass
F&MClass

APPENDIX C

SOIL LABORATORY RESULTS

SIEVE AND HYDROMETER ANALYSIS

GEOSTRADA

SIEVE AND HYDROMETER ANALYSIS

LAB/G9

Tests done according to TMH1& MT 1 Methods

☑ A1a ☑ A2 ☑ A3 ☑ A4 ☑ A5 ☑ A6

Client : UNIVERSITY OF PRETORIA **Contract :** KOMVOORHOOGTE - NHLAZATSHE **Job No :** 2011-C-279

Date : 2011-07-14

Sample No	Hole No/km	Depth (m)	Description Material	Classification Material	GM	Percentage passing sieves															Atterberg Limits		
						53,0 mm	37,5 mm	26,5 mm	19,0 mm	13,2 mm	9,5 mm	4,75 mm	2,00 mm	0,425 mm	0,075 mm	0.060 mm	0.050 mm	0.020 mm	0.005 mm	0.002 mm	Liquid limit	Plasticity index	Linear shrinkage
1/1448	km53+800	0 - 220		Silty sand	1.89	100	93	87	79	72	69	62	54	40	17	14	13	9	4	3	25	10	3.5
1/1449	km53+800	220 - 800		Silty sand	1.65		100	96	89	83	80	73	65	45	25	21	20	14	9	6	30	14	6.5
1/1450	km57+000	0 - 400		Silty sand	1.85			100	99	89	79	63	53	40	22	14	13	8	4	3	16	3	1.0
1/1451	km57+000	400 - 800		Silty sand	1.45		100	98	98	98	97	93	79	52	24	20	19	14	9	6	27	12	4.5
1/1452	km59+300	0 - 400		Sand	2.43			100	97	84	65	45	31	18	8	6	6	3	2	1		NP	0.0
1/1453	km59+300	400 - 800		Silty sand	1.47				100	99	98	93	79	52	22	19	17	12	10	5	27	10	3.5
1/1454	km60+650	0 - 580		Silty sand	2.32			100	99	88	73	51	37	21	10	8	8	5	2	2		NP	0.0
1/1455	km60+650	580 - 950		Sand	1.71				100	99	98	94	77	36	16	14	14	10	6	4	30	14	5.5
1/1456	km64+000	0 - 460		Silty sand	2.24			100	95	82	70	54	40	24	12	10	9	6	3	2	19	5	2.0
1/1457	km64+000	460 - 1000		Silty sand	1.33					100	99	96	84	57	26	23	23	17	10	7	28	15	4.0
1/1458	km65+250	0 - 400		Sand	2.30			100	97	81	67	49	37	23	10	7	7	5	2	2	20	8	2.0
1/1459	km65+250	400 - 800		Silty sand	1.50	100	96	94	93	92	91	88	76	51	23	20	20	14	9	6	27	14	3.5

GEOSTRADA

SIEVE AND HYDROMETER ANALYSIS

LAB/G9

Tests done according to TMH1& MT 1 Methods

☑ A1a ☑ A2 ☑ A3 ☑ A4 ☑ A5 ☑ A6

Client : UNIVERSITY OF PRETORIA **Contract :** NORTHAM - THABAZIMBE **Job No :** 2011-C-279

Date : 2011-07-14

Sample No	Hole No/km	Depth (m)	Description Material	Classification Material	GM	Percentage passing sieves															Atterberg Limits		
						53,0 mm	37,5 mm	26,5 mm	19,0 mm	13,2 mm	9,5 mm	4,75 mm	2,00 mm	0,425 mm	0,075 mm	0.060 mm	0.050 mm	0.020 mm	0.005 mm	0.002 mm	Liquid limit	Plasticity index	Linear shrinkage
1/1460	km207+800	0 - 1000	NT 004.1	Clayey sand	0.83							100	95	72	50	43	42	38	28	20	32	18	7.0
1/1446	Km208-500	450 - 1000		Sandy clay	0.69		100	93	92	92	91	91	89	78	64	57	55	50	35	27	41	21	10.5
1/1461	km208+500	0 - 450	NT 006	Silty sand	2.07	100	86	86	73	65	60	49	41	31	21	17	16	11	8	6	27	14	4.5
1/1462	km208+500	450 - 1000	NT 006	Sandy clay	0.72		100	94	94	93	92	91	89	76	63	57	56	49	39	30	41	26	9.5
1/1440	Km 214-500	000 - 600	NT 007.1	Silty sand	2.16	100	94	77	65	58	54	46	40	28	16	13	13	9	6	5	29	15	7.0
1/1441	Km214-500	600 - 1000	NT 007.1	Sandy clay	0.17							100	99	97	87	68	68	68	49	40	82	53	17.0
1/1463	km214+500	0 - 600	NT 007.1	Silty sand	2.62	100	83	66	50	40	34	27	20	12	6	5	5	4	2	1	25	9	3.5
1/1464	km214+500	600 - 1000	NT 007.1	Clay	0.13								100	98	89	80	78	70	52	42	82	56	16.5
1/1443	Km218/2	400 - 800	NT 010	Sandy clay	0.41						100	99	98	95	66	56	56	47	37	30	57	35	12.0
1/1465	km218+120	400 - 800	NT 010	Sandy clay	0.50						100	99	97	90	63	56	54	44	34	28	56	35	14.5
1/1439	Km 219-400	400 - 600		Sandy clay	0.46					100	99	98	96	89	69	58	56	49	35	26	66	41	19.0
1/1444	Km219-400	100 - 400		Clayey sand	1.35	100	93	90	84	81	78	73	68	62	35	33	31	22	16	12	33	18	8.5
1/1445	Km219-400	900 - 1100		Sand	1.80			100	99	99	98	87	69	37	14	12	10	8	4	3	27	10	4.5
1/1466	km219+400	100 - 400	Northern Thabazimbi	Silty sand	1.95	100	95	90	79	73	67	57	47	36	22	18	17	12	8	7	29	15	7.0
1/1467	km219+400	400 - 600	Northern Thabazimbi	Sandy clay	0.97		100	90	86	84	82	81	78	70	55	50	49	40	30	23	66	42	17.0
1/1468	km219+400	600 - 1000	Northern Thabazimbi	Sand	2.14			100	99	98	97	82	53	24	9	7	7	5	3	2	25	8	3.5

FOUNDATION INDICATOR TEST RESULTS

FOUNDATION INDICATOR TEST RESULTS

GEOSTRADA

TEST LOCATION	km53+800	PROJECT	KOMVOORHOOGTE - NHLAZATSHE
SAMPLE NO.	1/1448	PROJECT NUMBER	2011-C-279
DEPTH	0 - 220 m	CLIENT	UNIVERSITY OF PRETORIA

SIEVE ANALYSIS				ATTERBERG LIMITS			SOIL CLASSIFICATION	
Sieve (mm)	% Passing	Sieve (mm)	% Passing					
53.000	100	0.425	40	Liquid limit	(%)	25	% Gravel	46
37.500	93	0.075	17	Plastic limit	(%)	15	% Sand	40
26.500	87	0.060	14	Plasticity Index	(%)	10	% Silt	11
19.000	79	0.050	13	Weighted PI	(%)	4	% Clay	3
13.200	72	0.020	9	Linear Shrinkage	(%)	3.5	Activity	3.3
9.500	69	0.005	4	Grading Modulus		1.89	Unified Classification	SC
4.750	62	0.002	3	Uniformity coefficient		138	TRB Classification	A - 2 - 4
2.000	54			Coefficient of curvature		0.6		

PARTICLE SIZE DISTRIBUTION

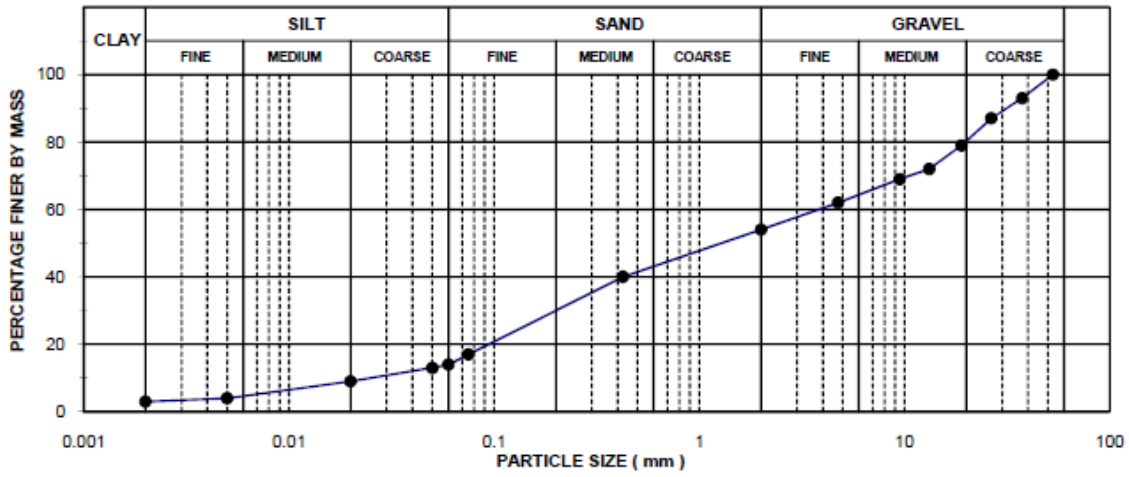

POTENTIAL EXPANSIVENESS
Van der Merwe's Activity Chart

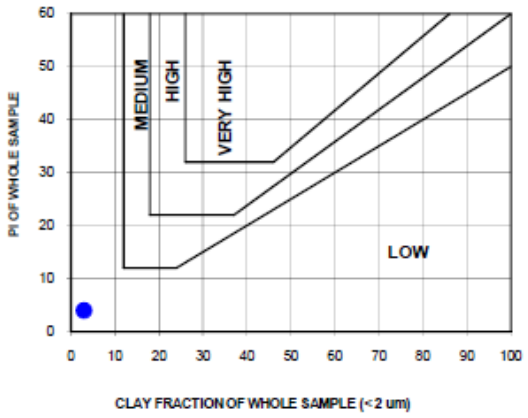

CASAGRANDE 'A' LINE

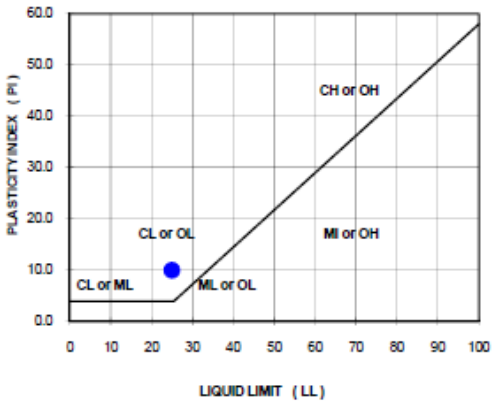

FOUNDATION INDICATOR TEST RESULTS

TEST LOCATION	km53+800	PROJECT	KOMVOORHOOGTE - NHLAZATSHE
SAMPLE NO.	1/1449	PROJECT NUMBER	2011-C-279
DEPTH	220 - 800 m	CLIENT	UNIVERSITY OF PRETORIA

SIEVE ANALYSIS				ATTERBERG LIMITS			SOIL CLASSIFICATION	
Sieve (mm)	% Passing	Sieve (mm)	% Passing					
53.000	100	0.425	45	Liquid limit	(%)	30	% Gravel	35
37.500	100	0.075	25	Plastic limit	(%)	16	% Sand	44
26.500	96	0.060	21	Plasticity Index	(%)	14	% Silt	15
19.000	89	0.050	20	Weighted PI	(%)	6	% Clay	6
13.200	83	0.020	14	Linear Shrinkage	(%)	6.5	Activity	2.3
9.500	80	0.005	9	Grading Modulus		1.65	Unified Classification	SC
4.750	73	0.002	6	Uniformity coefficient		161	TRB Classification	A - 2 - 6
2.000	65			Coefficient of curvature		1.7		

PARTICLE SIZE DISTRIBUTION

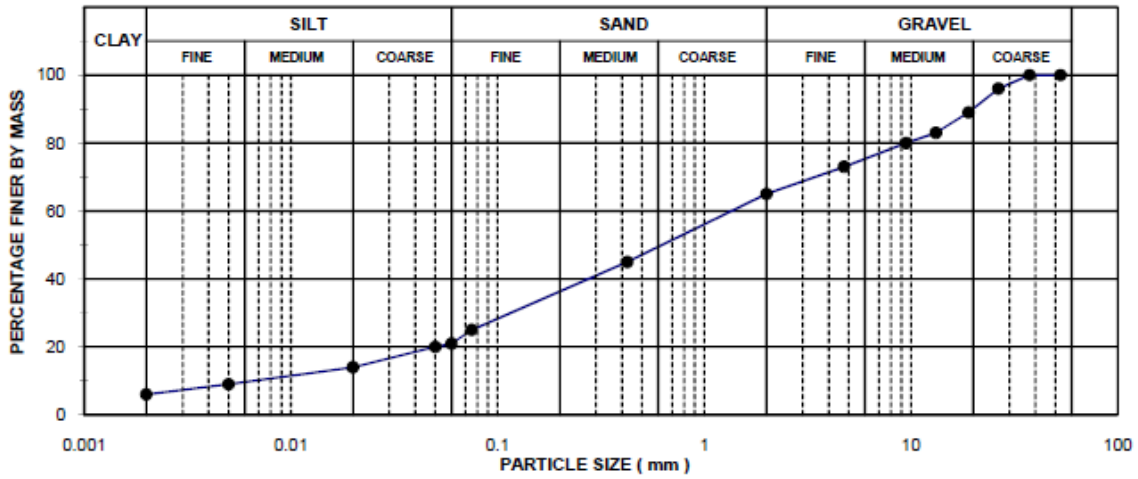

POTENTIAL EXPANSIVENESS
Van der Merwe's Activity Chart

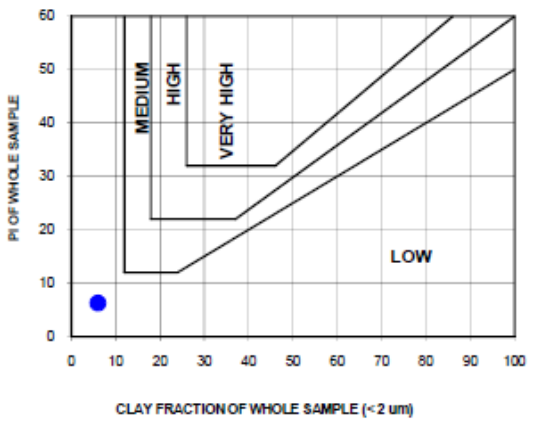

CASAGRANDE 'A' LINE

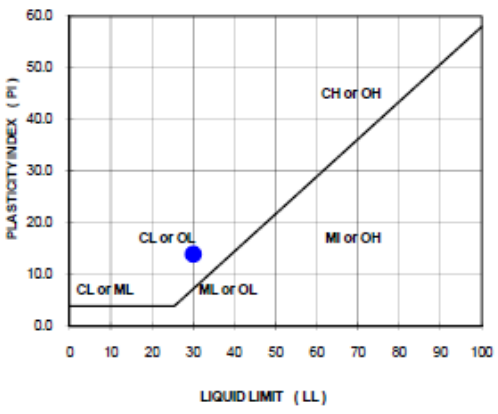

FOUNDATION INDICATOR TEST RESULTS

TEST LOCATION	km57+000	PROJECT	KOMVOORHOOGTE - NHLAZATSHE
SAMPLE NO.	1/1450	PROJECT NUMBER	2011-C-279
DEPTH	0 - 400 m	CLIENT	UNIVERSITY OF PRETORIA

SIEVE ANALYSIS				ATTERBERG LIMITS			SOIL CLASSIFICATION	
Sieve (mm)	% Passing	Sieve (mm)	% Passing					
53.000	100	0.425	40	Liquid limit	(%)	16	% Gravel	47
37.500	100	0.075	22	Plastic limit	(%)	13	% Sand	39
26.500	100	0.060	14	Plasticity Index	(%)	3	% Silt	11
19.000	99	0.050	13	Weighted PI	(%)	1	% Clay	3
13.200	89	0.020	8	Linear Shrinkage	(%)	1.0	Activity	1.0
9.500	79	0.005	4	Grading Modulus		1.85	Unified Classification	SM
4.750	63	0.002	3	Uniformity coefficient		115	TRB Classification	A-- 1 - b
2.000	53			Coefficient of curvature		0.4		

PARTICLE SIZE DISTRIBUTION

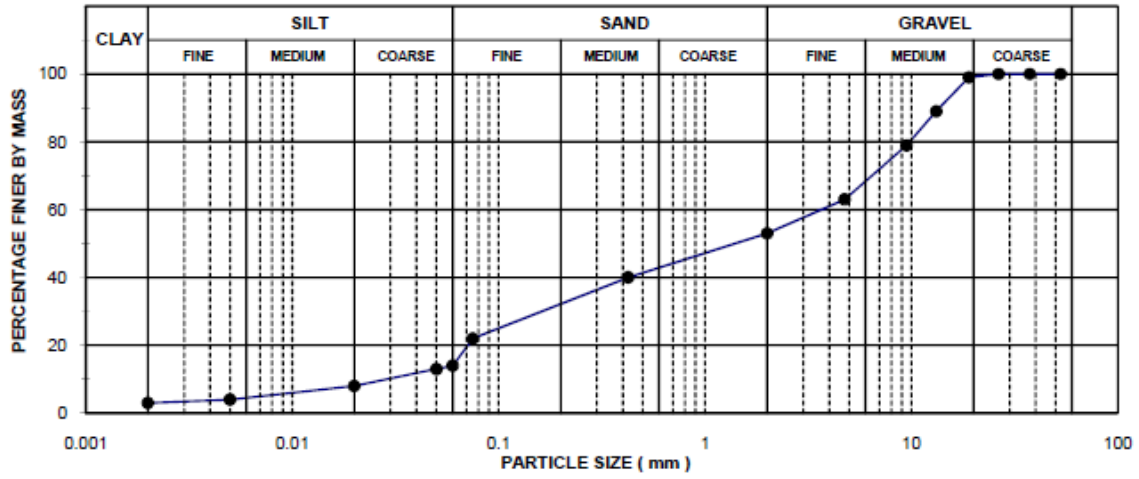

POTENTIAL EXPANSIVENESS
Van der Merwe's Activity Chart

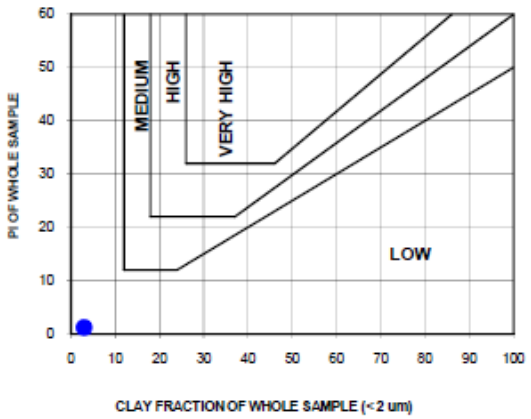

CASAGRANDE 'A' LINE

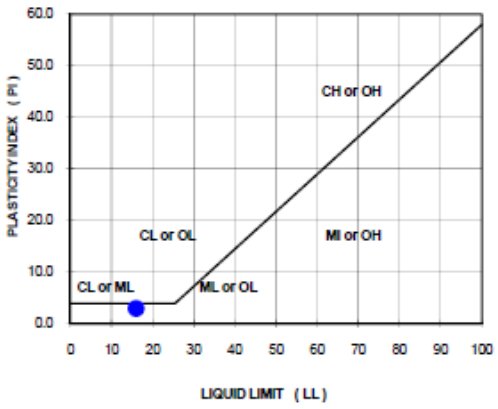

FOUNDATION INDICATOR TEST RESULTS

TEST LOCATION	km57+000	PROJECT	KOMVOORHOOGTE - NHLAZATSHE
SAMPLE NO.	1/1451	PROJECT NUMBER	2011-C-279
DEPTH	400 - 800 m	CLIENT	UNIVERSITY OF PRETORIA

SIEVE ANALYSIS				ATTERBERG LIMITS			SOIL CLASSIFICATION	
Sieve (mm)	% Passing	Sieve (mm)	% Passing					
53.000	100	0.425	52	Liquid limit	(%)	27	% Gravel	21
37.500	100	0.075	24	Plastic limit	(%)	15	% Sand	59
26.500	98	0.060	20	Plasticity Index	(%)	12	% Silt	14
19.000	98	0.050	19	Weighted PI	(%)	6	% Clay	6
13.200	98	0.020	14	Linear Shrinkage	(%)	4.5	Activity	2.0
9.500	97	0.005	9	Grading Modulus		1.45	Unified Classification	SC
4.750	93	0.002	6	Uniformity coefficient		89	TRB Classification	A - 2 - 6
2.000	79			Coefficient of curvature		2.6		

PARTICLE SIZE DISTRIBUTION

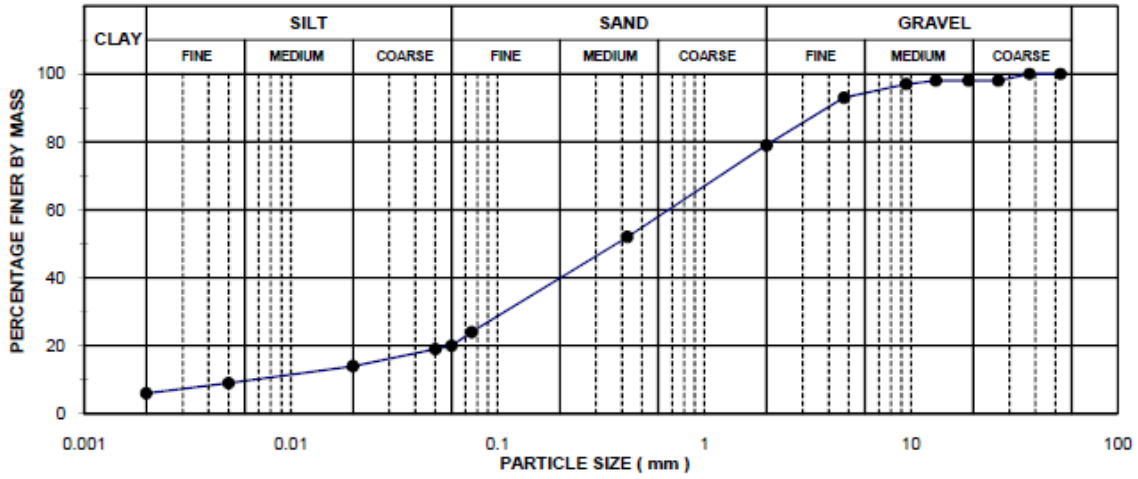

POTENTIAL EXPANSIVENESS
Van der Merwe's Activity Chart

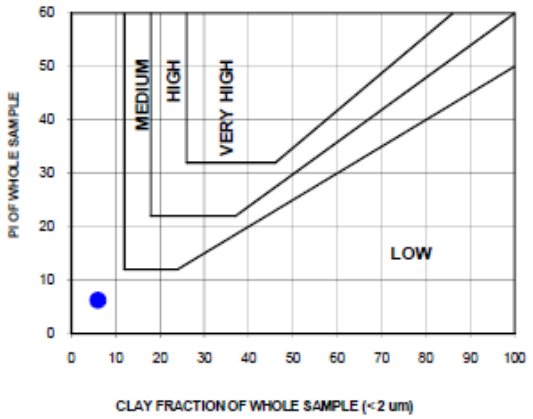

CASAGRANDE 'A' LINE

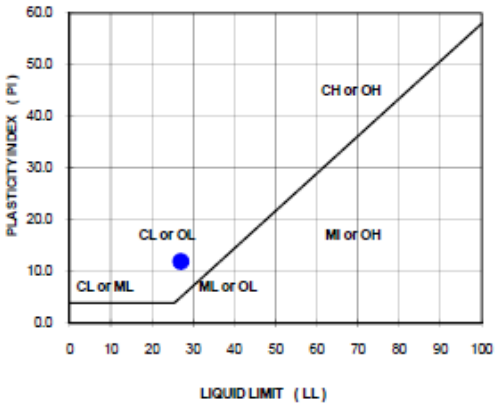

FOUNDATION INDICATOR TEST RESULTS

GEOSTRADA

TEST LOCATION	km59+300	PROJECT	KOMVOORHOOGTE - NHLAZATSHE
SAMPLE NO.	1/1452	PROJECT NUMBER	2011-C-279
DEPTH	0 - 400 m	CLIENT	UNIVERSITY OF PRETORIA

SIEVE ANALYSIS			
Sieve (mm)	% Passing	Sieve (mm)	% Passing
53.000	100	0.425	18
37.500	100	0.075	8
26.500	100	0.060	6
19.000	97	0.050	6
13.200	84	0.020	3
9.500	65	0.005	2
4.750	45	0.002	1
2.000	31		

ATTERBERG LIMITS		
Liquid limit (%)	0	
Plastic limit (%)	0	
Plasticity Index (%)	NP	
Weighted PI (%)	0	
Linear Shrinkage (%)	0.0	
Grading Modulus	2.43	
Uniformity coefficient	57	
Coefficient of curvature	2.9	

SOIL CLASSIFICATION	
% Gravel	69
% Sand	25
% Silt	5
% Clay	1
Activity	0.0
Unified Classification	GW
TRB Classification	A - 2 - 6

PARTICLE SIZE DISTRIBUTION

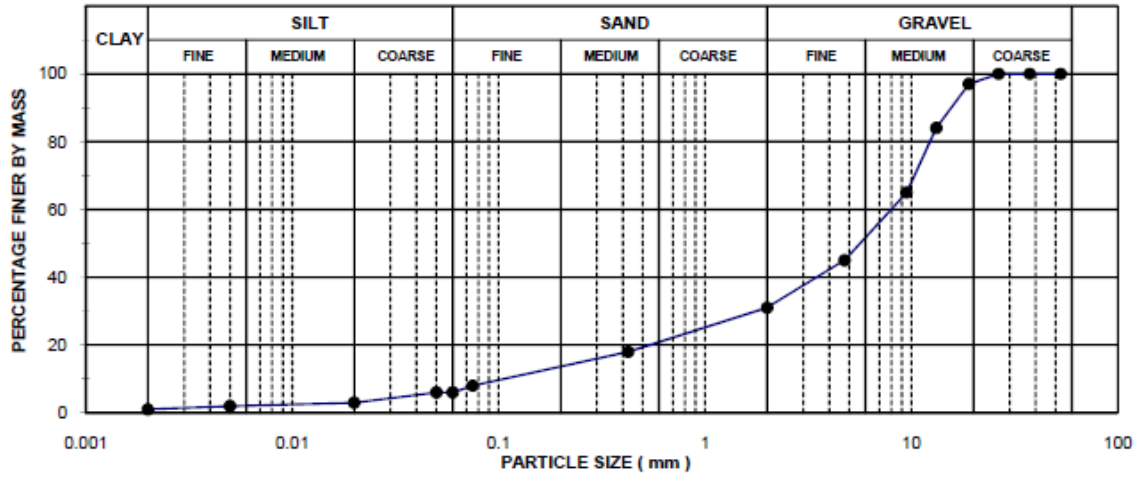

POTENTIAL EXPANSIVENESS
Van der Merwe's Activity Chart

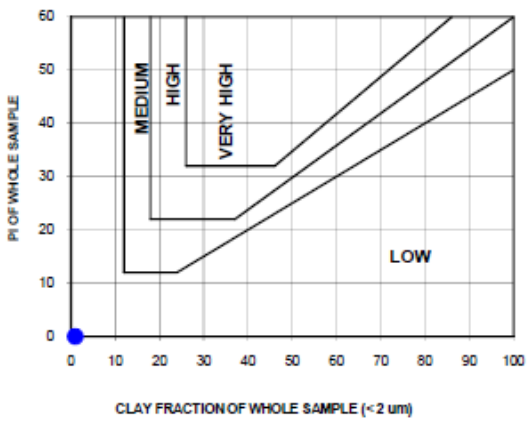

CASAGRANDE 'A' LINE

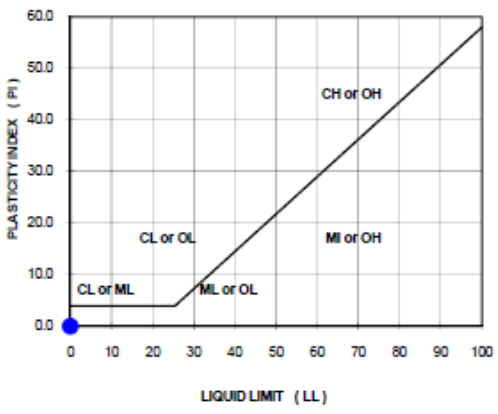

FOUNDATION INDICATOR TEST RESULTS

GEOSTRADA

TEST LOCATION	km59+300	PROJECT	KOMVOORHOOGTE - NHLAZATSHE
SAMPLE NO.	1/1453	PROJECT NUMBER	2011-C-279
DEPTH	400 - 800 m	CLIENT	UNIVERSITY OF PRETORIA

SIEVE ANALYSIS				ATTERBERG LIMITS			SOIL CLASSIFICATION	
Sieve (mm)	% Passing	Sieve (mm)	% Passing					
53.000	100	0.425	52	Liquid limit	(%)	27	% Gravel	21
37.500	100	0.075	22	Plastic limit	(%)	17	% Sand	60
26.500	100	0.060	19	Plasticity Index	(%)	10	% Silt	14
19.000	100	0.050	17	Weighted PI	(%)	5	% Clay	5
13.200	99	0.020	12	Linear Shrinkage	(%)	3.5	Activity	2.0
9.500	98	0.005	10	Grading Modulus		1.47	Unified Classification	SC
4.750	93	0.002	5	Uniformity coefficient		127	TRB Classification	A - 2 - 4
2.000	79			Coefficient of curvature		4.6		

PARTICLE SIZE DISTRIBUTION

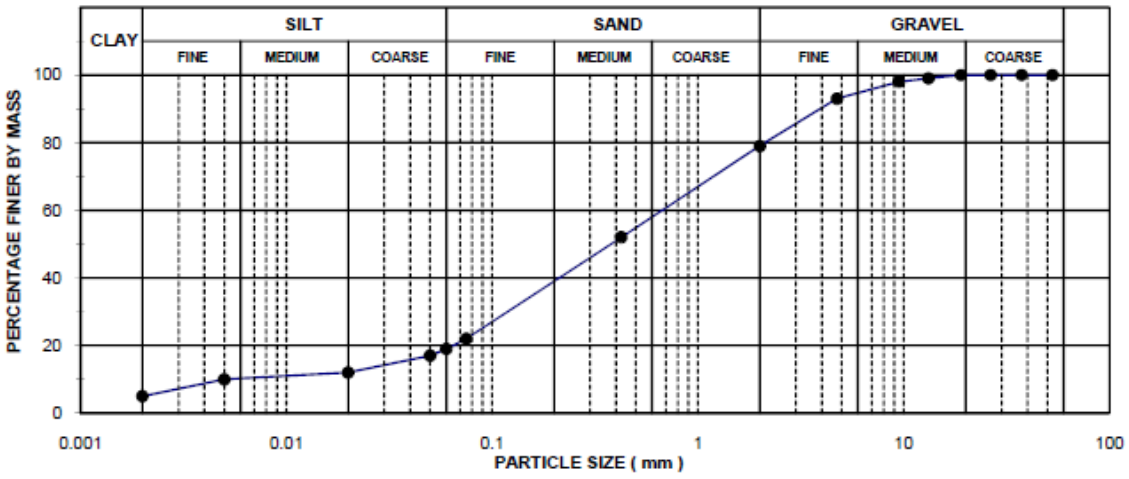

POTENTIAL EXPANSIVENESS
Van der Merwe's Activity Chart

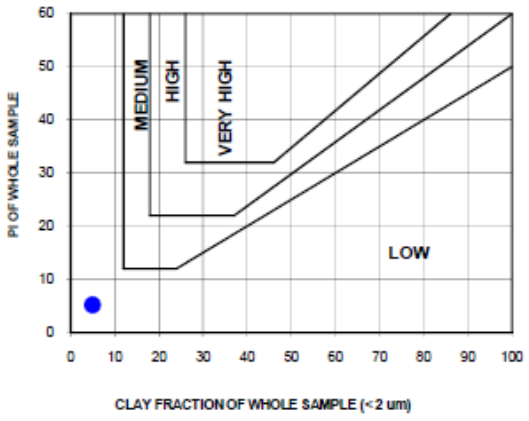

CASAGRANDE 'A' LINE

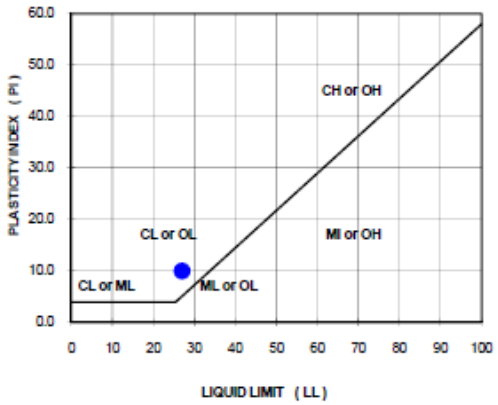

FOUNDATION INDICATOR TEST RESULTS

TEST LOCATION	km60+650	PROJECT	KOMVOORHOOGTE - NHLAZATSHE
SAMPLE NO.	1/1454	PROJECT NUMBER	2011-C-279
DEPTH	0 - 580 m	CLIENT	UNIVERSITY OF PRETORIA

SIEVE ANALYSIS				ATTERBERG LIMITS			SOIL CLASSIFICATION	
Sieve (mm)	% Passing	Sieve (mm)	% Passing					
53.000	100	0.425	21	Liquid limit	(%)	0	% Gravel	63
37.500	100	0.075	10	Plastic limit	(%)	0	% Sand	29
26.500	100	0.060	8	Plasticity Index	(%)	NP	% Silt	6
19.000	99	0.050	8	Weighted PI	(%)	0	% Clay	2
13.200	88	0.020	5	Linear Shrinkage	(%)	0.0	Activity	0.0
9.500	73	0.005	2	Grading Modulus		2.32	Unified Classification	0
4.750	51	0.002	2	Uniformity coefficient		87	TRB Classification	A - 2 - 6
2.000	37			Coefficient of curvature		3.3		

PARTICLE SIZE DISTRIBUTION

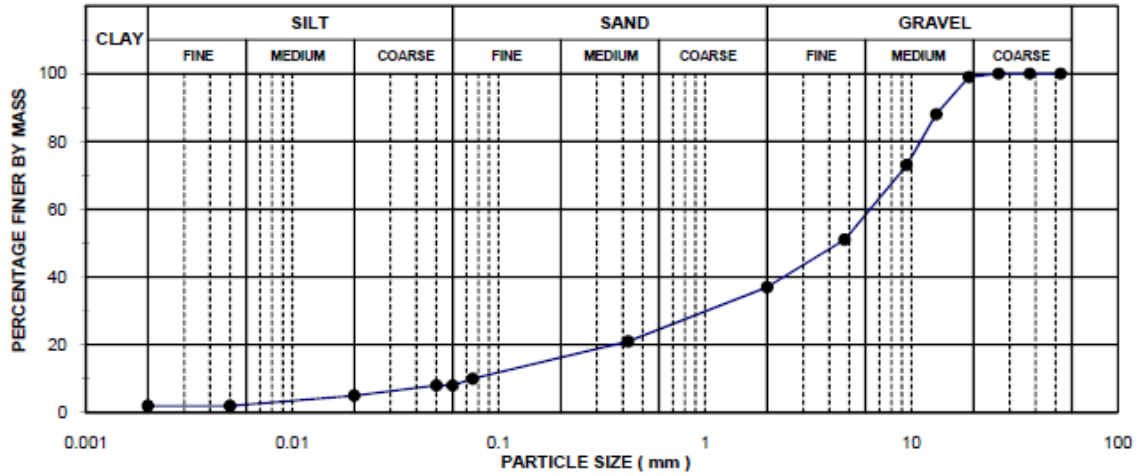

POTENTIAL EXPANSIVENESS
Van der Merwe's Activity Chart

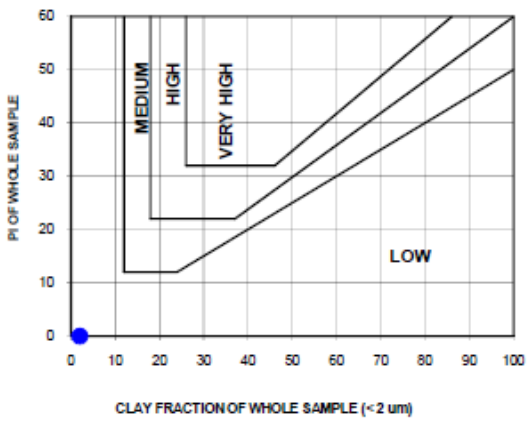

CASAGRANDE 'A' LINE

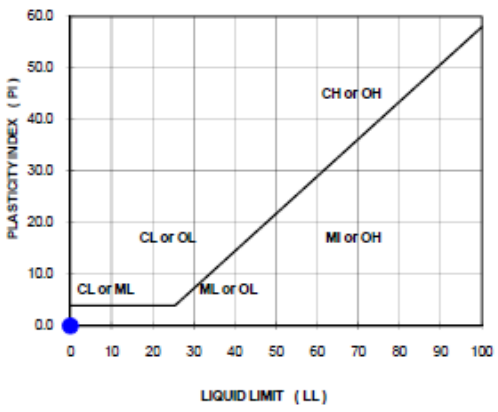

FOUNDATION INDICATOR TEST RESULTS

TEST LOCATION	km60+650	PROJECT	KOMVOORHOOGTE - NHLAZATSHE
SAMPLE NO.	1/1455	PROJECT NUMBER	2011-C-279
DEPTH	580 - 950 m	CLIENT	UNIVERSITY OF PRETORIA

SIEVE ANALYSIS				ATTERBERG LIMITS			SOIL CLASSIFICATION	
Sieve (mm)	% Passing	Sieve (mm)	% Passing					
53.000	100	0.425	36	Liquid limit	(%)	30	% Gravel	23
37.500	100	0.075	16	Plastic limit	(%)	16	% Sand	63
26.500	100	0.060	14	Plasticity Index	(%)	14	% Silt	10
19.000	100	0.050	14	Weighted PI	(%)	5	% Clay	4
13.200	99	0.020	10	Linear Shrinkage	(%)	5.5	Activity	3.5
9.500	98	0.005	6	Grading Modulus		1.71	Unified Classification	SC
4.750	94	0.002	4	Uniformity coefficient		61	TRB Classification	A - 2 - 6
2.000	77			Coefficient of curvature		3.5		

PARTICLE SIZE DISTRIBUTION

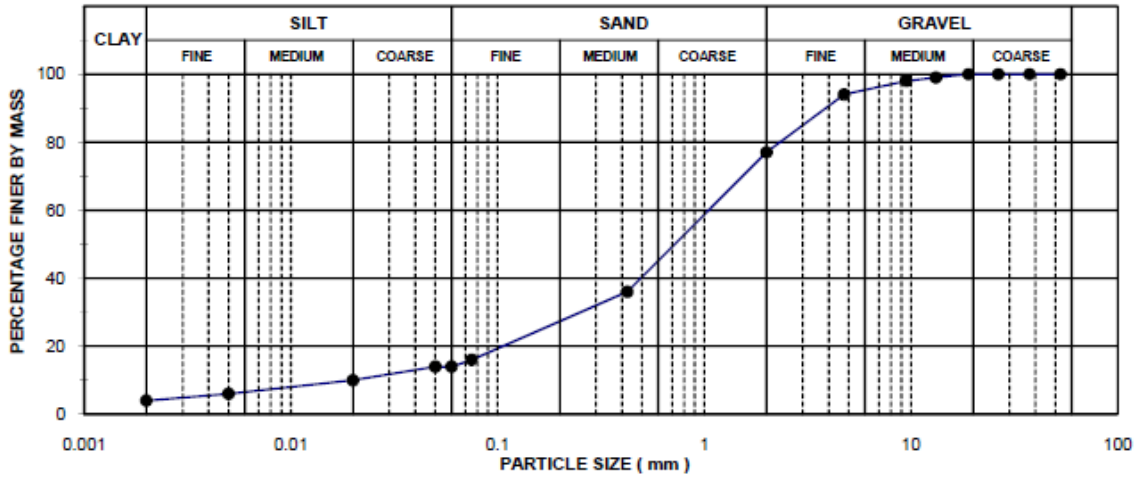

POTENTIAL EXPANSIVENESS
Van der Merwe's Activity Chart

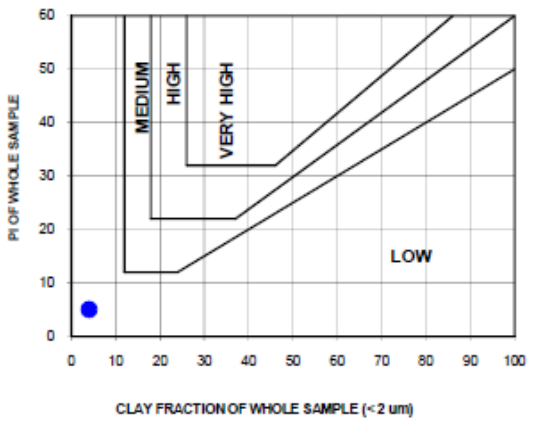

CASAGRANDE 'A' LINE

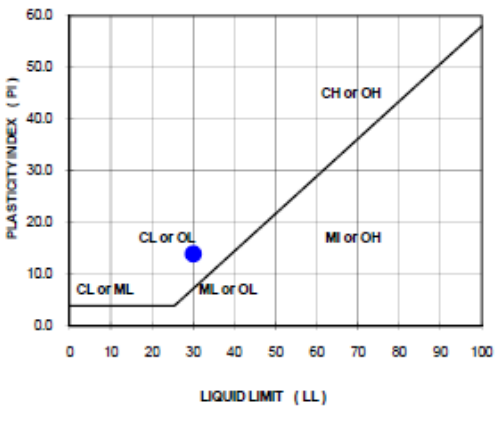

FOUNDATION INDICATOR TEST RESULTS

TEST LOCATION	km64+000	PROJECT	KOMVOORHOOGTE - NHLAZATSHE
SAMPLE NO.	1/1456	PROJECT NUMBER	2011-C-279
DEPTH	0 - 460 m	CLIENT	UNIVERSITY OF PRETORIA

SIEVE ANALYSIS				ATTERBERG LIMITS			SOIL CLASSIFICATION	
Sieve (mm)	% Passing	Sieve (mm)	% Passing					
53.000	100	0.425	24	Liquid limit	(%)	19	% Gravel	60
37.500	100	0.075	12	Plastic limit	(%)	14	% Sand	30
26.500	100	0.060	10	Plasticity Index	(%)	5	% Silt	8
19.000	95	0.050	9	Weighted PI	(%)	1	% Clay	2
13.200	82	0.020	6	Linear Shrinkage	(%)	2.0	Activity	2.5
9.500	70	0.005	3	Grading Modulus		2.24	Unified Classification	0
4.750	54	0.002	2	Uniformity coefficient		105	TRB Classification	A - 1 - a
2.000	40			Coefficient of curvature		2.6		

PARTICLE SIZE DISTRIBUTION

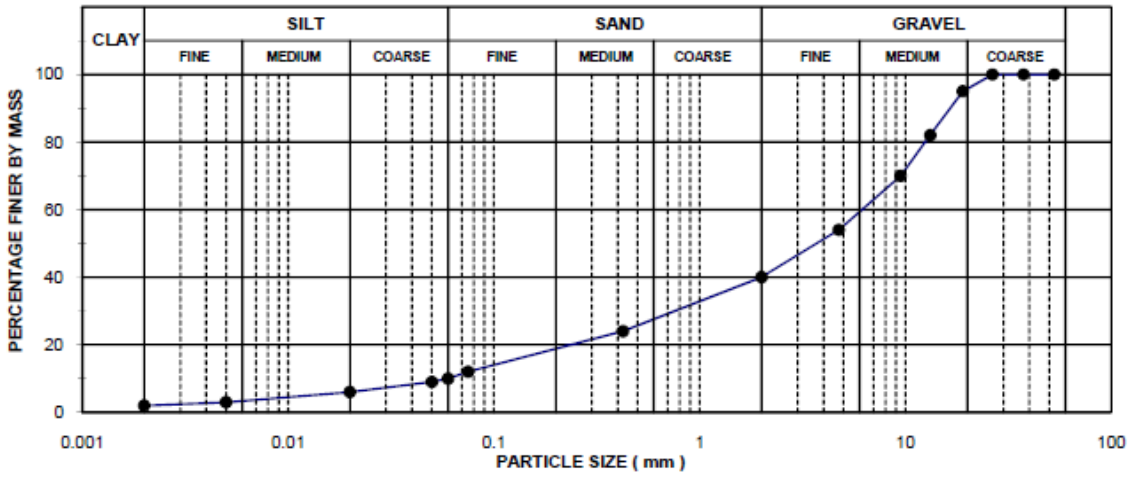

POTENTIAL EXPANSIVENESS
Van der Merwe's Activity Chart

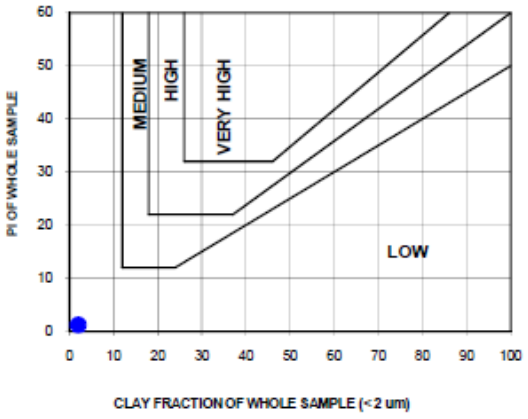

CASAGRANDE 'A' LINE

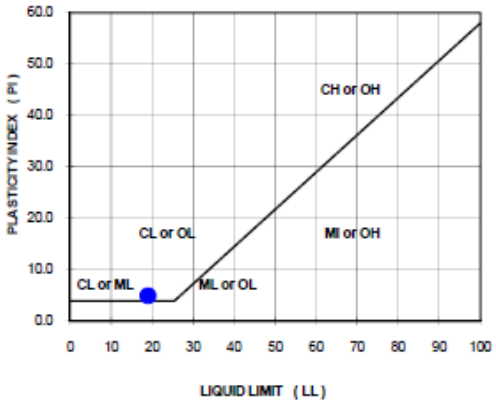

FOUNDATION INDICATOR TEST RESULTS

GEOSTRADA

TEST LOCATION	km64+000	PROJECT	KOMVOORHOOGTE - NHLAZATSHE
SAMPLE NO.	1/1457	PROJECT NUMBER	2011-C-279
DEPTH	460 - 1000 m	CLIENT	UNIVERSITY OF PRETORIA

SIEVE ANALYSIS			
Sieve (mm)	% Passing	Sieve (mm)	% Passing
53.000	100	0.425	57
37.500	100	0.075	26
26.500	100	0.060	23
19.000	100	0.050	23
13.200	100	0.020	17
9.500	99	0.005	10
4.750	96	0.002	7
2.000	84		

ATTERBERG LIMITS		
Liquid limit	(%)	28
Plastic limit	(%)	13
Plasticity Index	(%)	15
Weighted PI	(%)	9
Linear Shrinkage	(%)	4.0
Grading Modulus		1.33
Uniformity coefficient		86
Coefficient of curvature		3.6

SOIL CLASSIFICATION	
% Gravel	16
% Sand	61
% Silt	16
% Clay	7
Activity	2.1
Unified Classification	SC
TRB Classification	A - 2 - 6

PARTICLE SIZE DISTRIBUTION

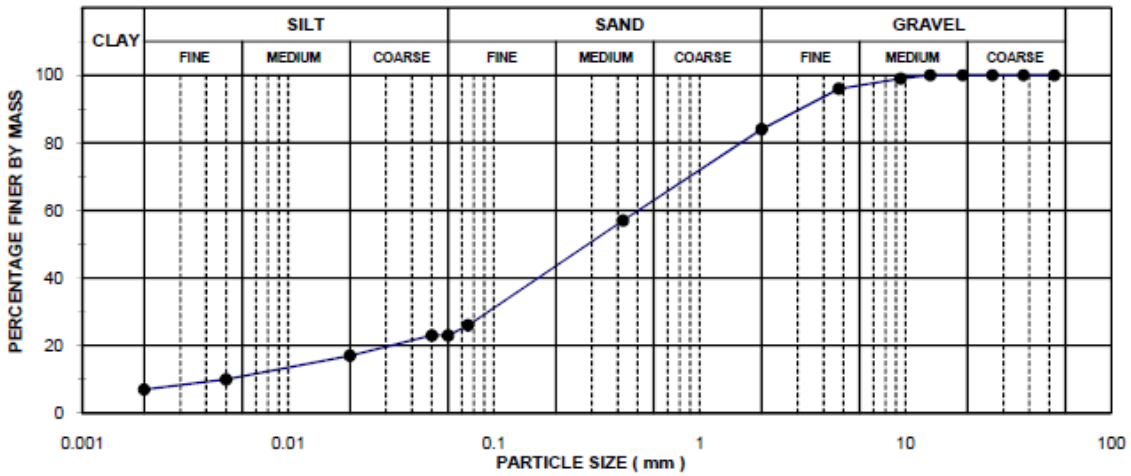

POTENTIAL EXPANSIVENESS
Van der Merwe's Activity Chart

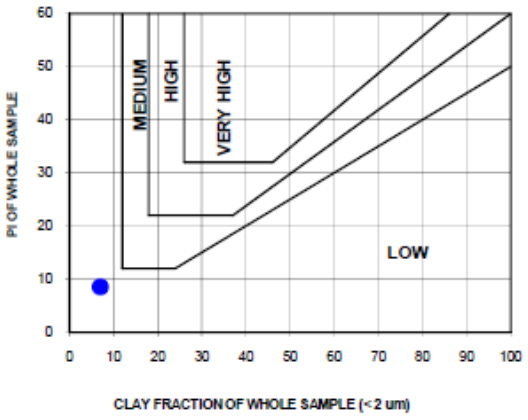

CASAGRANDE 'A' LINE

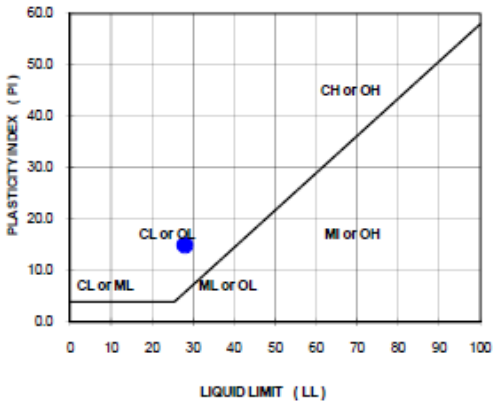

FOUNDATION INDICATOR TEST RESULTS

GEOSTRADA

TEST LOCATION	km65+250	PROJECT	KOMVOORHOOGTE - NHLAZATSHE
SAMPLE NO.	1/1458	PROJECT NUMBER	2011-C-279
DEPTH	0 - 400 m	CLIENT	UNIVERSITY OF PRETORIA

SIEVE ANALYSIS				ATTERBERG LIMITS			SOIL CLASSIFICATION	
Sieve (mm)	% Passing	Sieve (mm)	% Passing					
53.000	100	0.425	23	Liquid limit	(%)	20	% Gravel	63
37.500	100	0.075	10	Plastic limit	(%)	12	% Sand	30
26.500	100	0.060	7	Plasticity Index	(%)	8	% Silt	5
19.000	97	0.050	7	Weighted PI	(%)	2	% Clay	2
13.200	81	0.020	5	Linear Shrinkage	(%)	2.0	Activity	4.0
9.500	67	0.005	2	Grading Modulus		2.30	Unified Classification	GW
4.750	49	0.002	2	Uniformity coefficient		99	TRB Classification	A - 2 - 4
2.000	37			Coefficient of curvature		2.5		

PARTICLE SIZE DISTRIBUTION

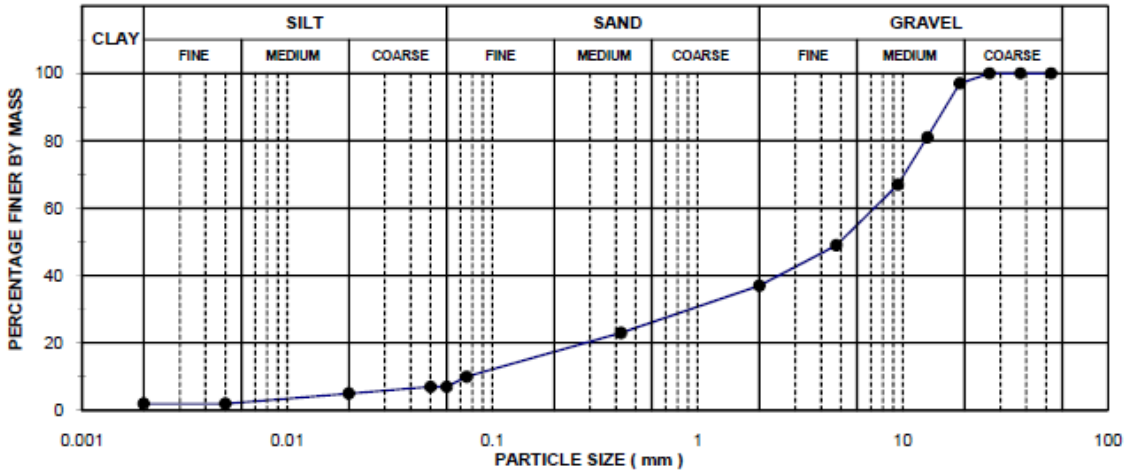

POTENTIAL EXPANSIVENESS
Van der Merwe's Activity Chart

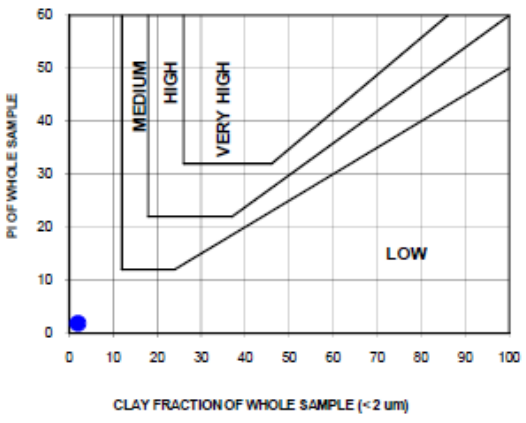

CASAGRANDE 'A' LINE

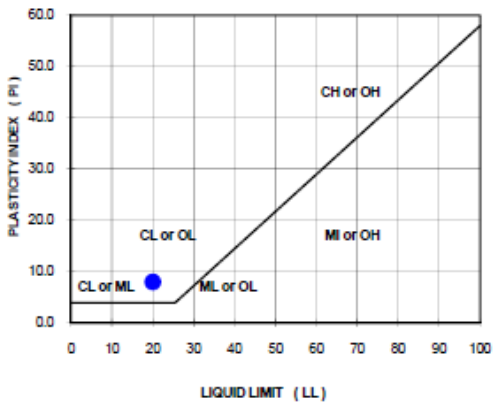

FOUNDATION INDICATOR TEST RESULTS

GEOSTRADA

TEST LOCATION	km65+250	PROJECT	KOMVOORHOOGTE - NHLAZATSHE
SAMPLE NO.	1/1459	PROJECT NUMBER	2011-C-279
DEPTH	400 - 800 m	CLIENT	UNIVERSITY OF PRETORIA

SIEVE ANALYSIS				ATTERBERG LIMITS			SOIL CLASSIFICATION	
Sieve (mm)	% Passing	Sieve (mm)	% Passing					
53.000	100	0.425	51	Liquid limit	(%)	27	% Gravel	24
37.500	96	0.075	23	Plastic limit	(%)	13	% Sand	56
26.500	94	0.060	20	Plasticity Index	(%)	14	% Silt	14
19.000	93	0.050	20	Weighted PI	(%)	7	% Clay	6
13.200	92	0.020	14	Linear Shrinkage	(%)	3.5	Activity	2.3
9.500	91	0.005	9	Grading Modulus		1.50	Unified Classification	SC
4.750	88	0.002	6	Uniformity coefficient		99	TRB Classification	A - 2 - 6
2.000	76			Coefficient of curvature		2.7		

PARTICLE SIZE DISTRIBUTION

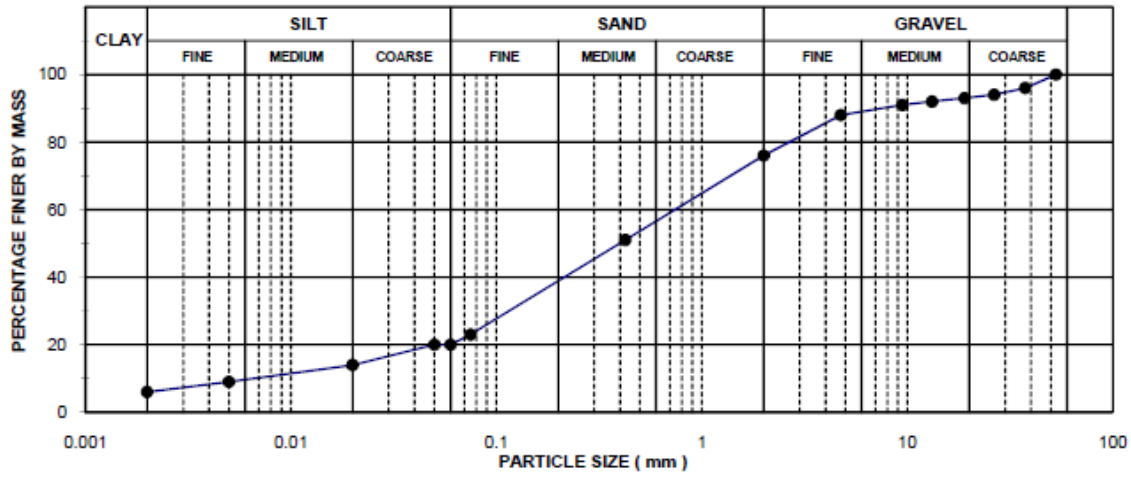

POTENTIAL EXPANSIVENESS
Van der Merwe's Activity Chart

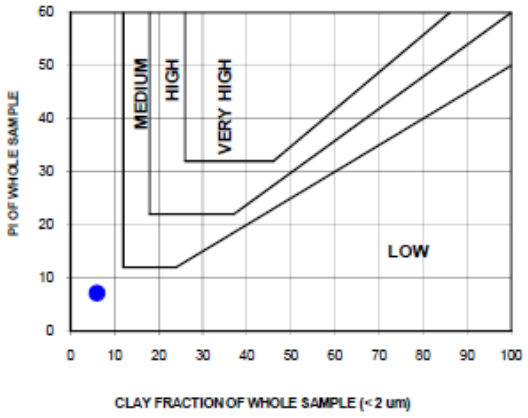

CASAGRANDE 'A' LINE

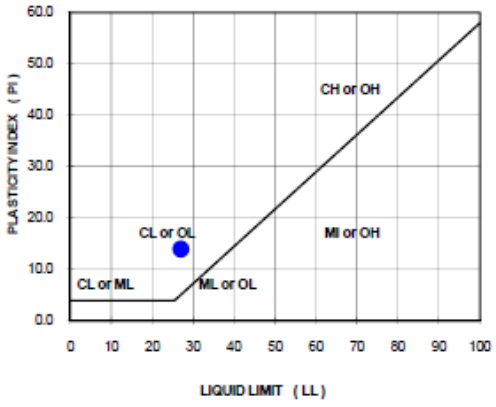

FOUNDATION INDICATOR TEST RESULTS

GEOSTRADA

TEST LOCATION	Km219-400	PROJECT	NORTHAM - THABAZIMBE
SAMPLE NO.	1/1439	PROJECT NUMBER	2011-C-279
DEPTH	400 - 600 m	CLIENT	UNIVERSITY OF PRETORIA

SIEVE ANALYSIS			
Sieve (mm)	% Passing	Sieve (mm)	% Passing
53.000	100	0.425	89
37.500	100	0.075	69
26.500	100	0.060	58
19.000	100	0.050	56
13.200	100	0.020	49
9.500	99	0.005	35
4.750	98	0.002	26
2.000	96		

ATTERBERG LIMITS		
Liquid limit	(%)	66
Plastic limit	(%)	25
Plasticity Index	(%)	41
Weighted PI	(%)	36
Linear Shrinkage	(%)	19.0
Grading Modulus		0.46
Uniformity coefficient		31
Coefficient of curvature		0.1

SOIL CLASSIFICATION	
% Gravel	4
% Sand	38
% Silt	32
% Clay	26
Activity	1.6
Unified Classification	CH
TRB Classification	A - 7 - 6

PARTICLE SIZE DISTRIBUTION

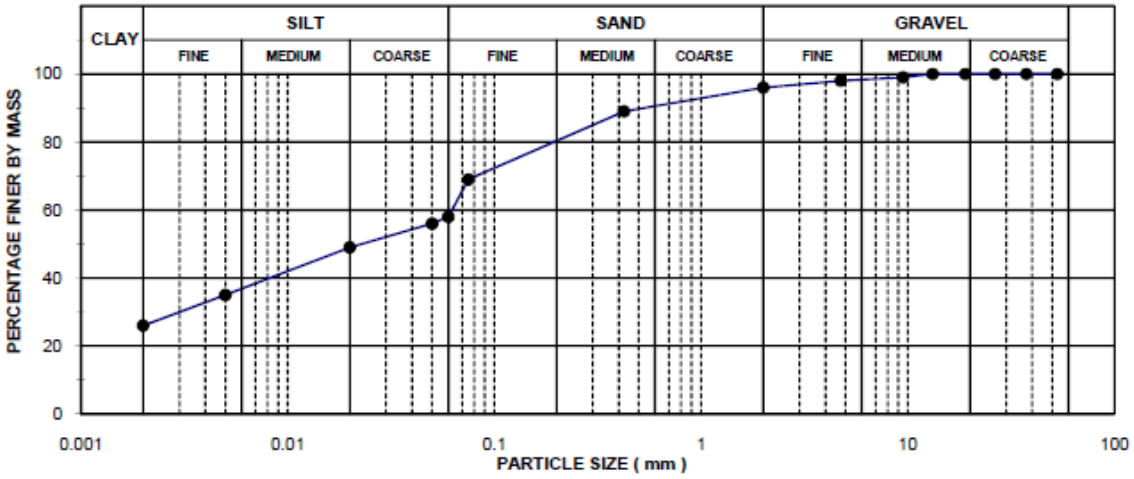

POTENTIAL EXPANSIVENESS
Van der Merwe's Activity Chart

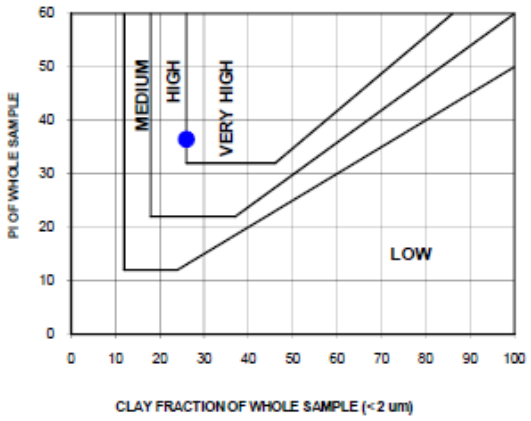

CASAGRANDE 'A' LINE

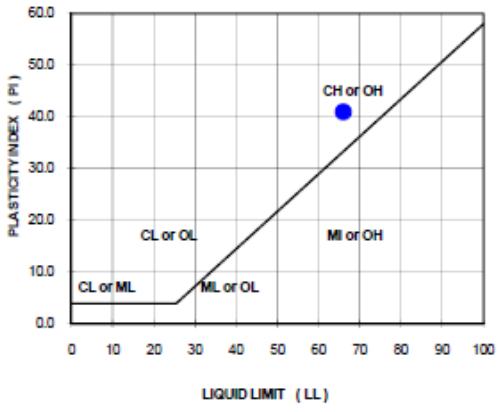

FOUNDATION INDICATOR TEST RESULTS

TEST LOCATION	Km214-500	PROJECT	NORTHAM - THABAZIMBE
SAMPLE NO.	1/1440	PROJECT NUMBER	2011-C-279
DEPTH	0 - 600 m	CLIENT	UNIVERSITY OF PRETORIA

SIEVE ANALYSIS			
Sieve (mm)	% Passing	Sieve (mm)	% Passing
53.000	100	0.425	28
37.500	94	0.075	16
26.500	77	0.060	13
19.000	65	0.050	13
13.200	58	0.020	9
9.500	54	0.005	6
4.750	46	0.002	5
2.000	40		

ATTERBERG LIMITS		
Liquid limit	(%)	29
Plastic limit	(%)	14
Plasticity Index	(%)	15
Weighted PI	(%)	4
Linear Shrinkage	(%)	7.0
Grading Modulus		2.16
Uniformity coefficient		504
Coefficient of curvature		1.1

SOIL CLASSIFICATION	
% Gravel	60
% Sand	27
% Silt	8
% Clay	5
Activity	3.0
Unified Classification	GC
TRB Classification	A - 2 - 6

PARTICLE SIZE DISTRIBUTION

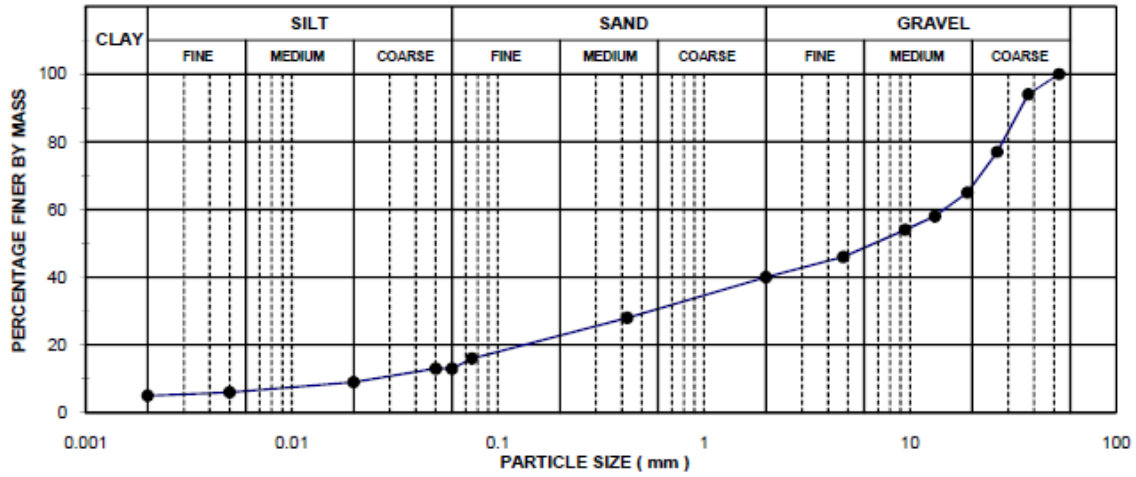

POTENTIAL EXPANSIVENESS
Van der Merwe's Activity Chart

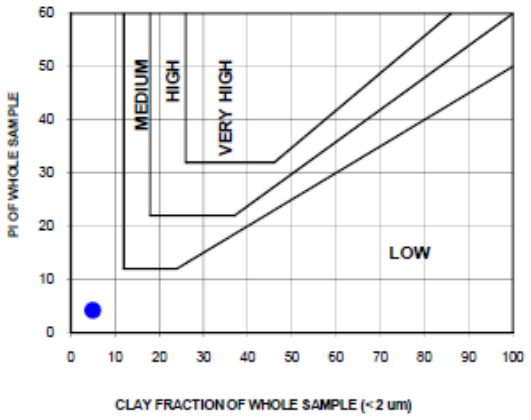

CASAGRANDE 'A' LINE

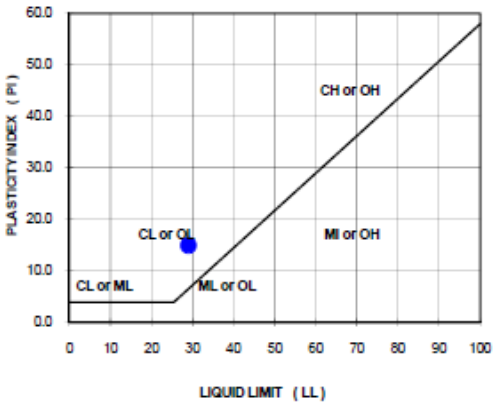

FOUNDATION INDICATOR TEST RESULTS

GEOSTRADA

TEST LOCATION	Km214-500	PROJECT	NORTHAM - THABAZIMBE
SAMPLE NO.	1/1441	PROJECT NUMBER	2011-C-279
DEPTH	600 - 1000 m	CLIENT	UNIVERSITY OF PRETORIA

SIEVE ANALYSIS			
Sieve (mm)	% Passing	Sieve (mm)	% Passing
53.000	100	0.425	97
37.500	100	0.075	87
26.500	100	0.060	68
19.000	100	0.050	68
13.200	100	0.020	68
9.500	100	0.005	49
4.750	100	0.002	40
2.000	99		

ATTERBERG LIMITS		
Liquid limit	(%)	83
Plastic limit	(%)	27
Plasticity Index	(%)	56
Weighted PI	(%)	54
Linear Shrinkage	(%)	17.0
Grading Modulus		0.17
Uniformity coefficient		7
Coefficient of curvature		0.1

SOIL CLASSIFICATION	
% Gravel	1
% Sand	31
% Silt	28
% Clay	40
Activity	1.4
Unified Classification	CH
TRB Classification	A - 7 - 6

PARTICLE SIZE DISTRIBUTION

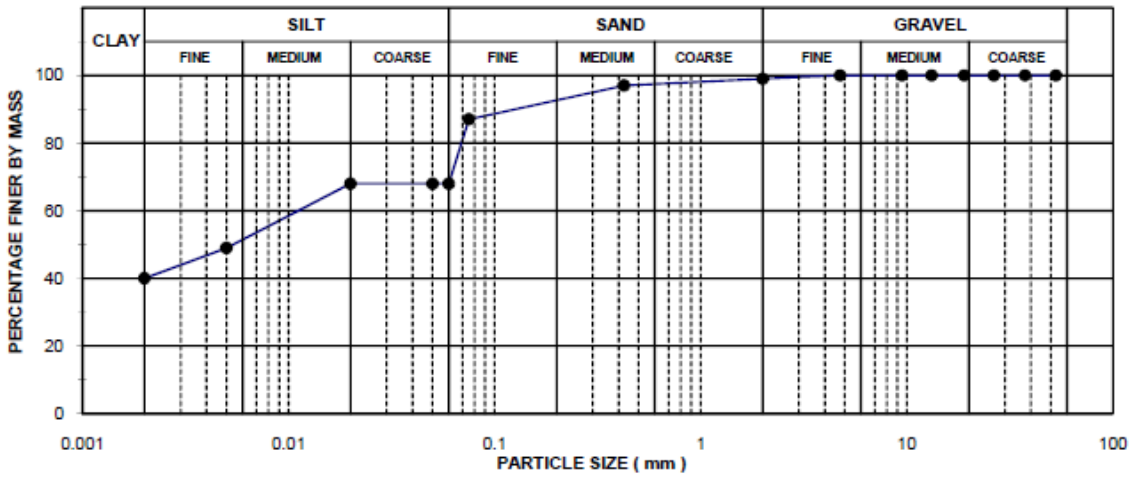

POTENTIAL EXPANSIVENESS
Van der Merwe's Activity Chart

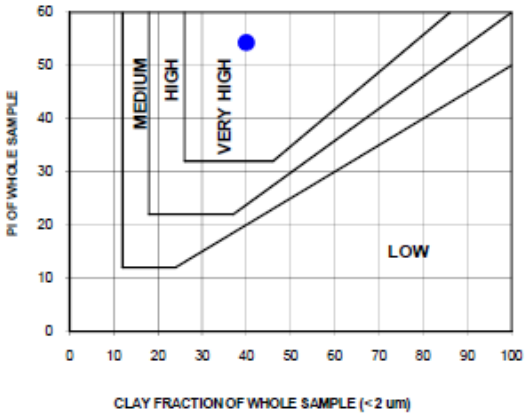

CASAGRANDE 'A' LINE

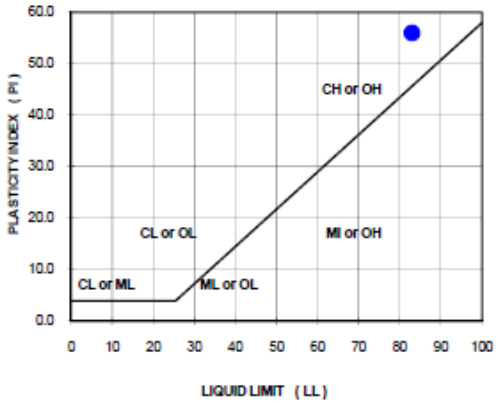

GEOSTRADA

FOUNDATION INDICATOR TEST RESULTS

TEST LOCATION	Km218/2	PROJECT	NORTHAM - THABAZIMBE
SAMPLE NO.	1/1443	PROJECT NUMBER	2011-C-279
DEPTH	400 - 800 m	CLIENT	UNIVERSITY OF PRETORIA

SIEVE ANALYSIS			
Sieve (mm)	% Passing	Sieve (mm)	% Passing
53.000	100	0.425	95
37.500	100	0.075	66
26.500	100	0.060	56
19.000	100	0.050	56
13.200	100	0.020	47
9.500	100	0.005	37
4.750	99	0.002	30
2.000	98		

ATTERBERG LIMITS		
Liquid limit	(%)	57
Plastic limit	(%)	22
Plasticity Index	(%)	35
Weighted PI	(%)	33
Linear Shrinkage	(%)	12.0
Grading Modulus		0.41
Uniformity coefficient		33
Coefficient of curvature		0.0

SOIL CLASSIFICATION	
% Gravel	2
% Sand	42
% Silt	26
% Clay	30
Activity	1.2
Unified Classification	CH
TRB Classification	A - 7 - 6

PARTICLE SIZE DISTRIBUTION

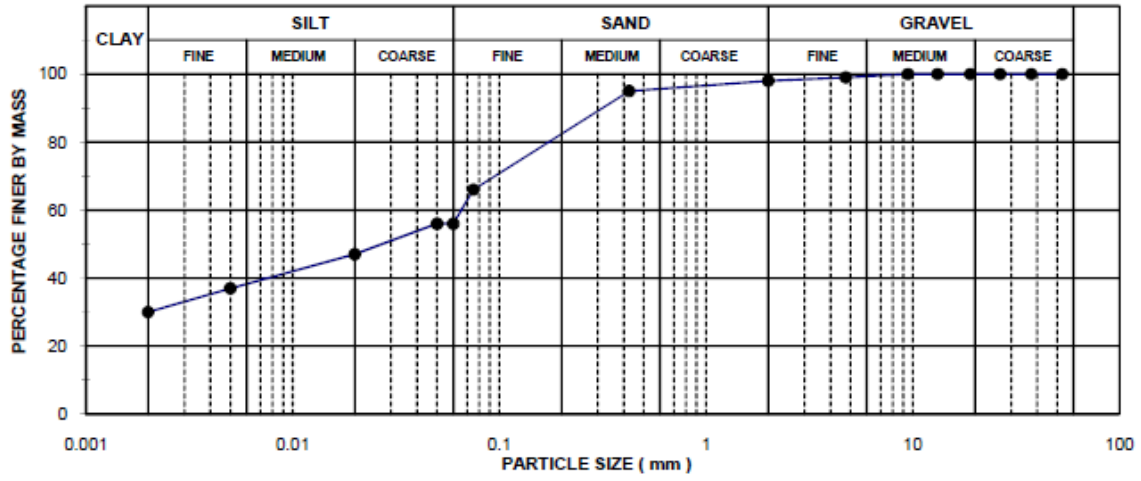

POTENTIAL EXPANSIVENESS
Van der Merwe's Activity Chart

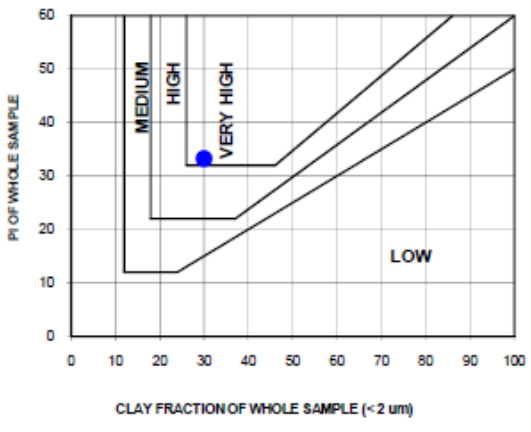

CASAGRANDE 'A' LINE

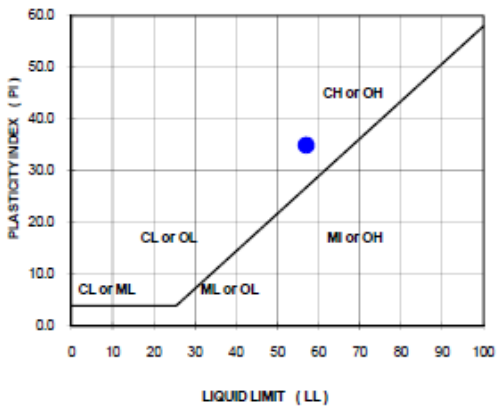

FOUNDATION INDICATOR TEST RESULTS

TEST LOCATION	Km219-400	PROJECT	NORTHAM - THABAZIMBE
SAMPLE NO.	1/1444	PROJECT NUMBER	2011-C-279
DEPTH	100 - 400 m	CLIENT	UNIVERSITY OF PRETORIA

SIEVE ANALYSIS				ATTERBERG LIMITS			SOIL CLASSIFICATION	
Sieve (mm)	% Passing	Sieve (mm)	% Passing					
53.000	100	0.425	62	Liquid limit	(%)	33	% Gravel	32
37.500	93	0.075	35	Plastic limit	(%)	15	% Sand	35
26.500	90	0.060	33	Plasticity Index	(%)	18	% Silt	21
19.000	84	0.050	31	Weighted PI	(%)	11	% Clay	12
13.200	81	0.020	22	Linear Shrinkage	(%)	8.5	Activity	1.5
9.500	78	0.005	16	Grading Modulus		1.35	Unified Classification	SC
4.750	73	0.002	12	Uniformity coefficient		200	TRB Classification	A - 2 - 6
2.000	68			Coefficient of curvature		3.0		

PARTICLE SIZE DISTRIBUTION

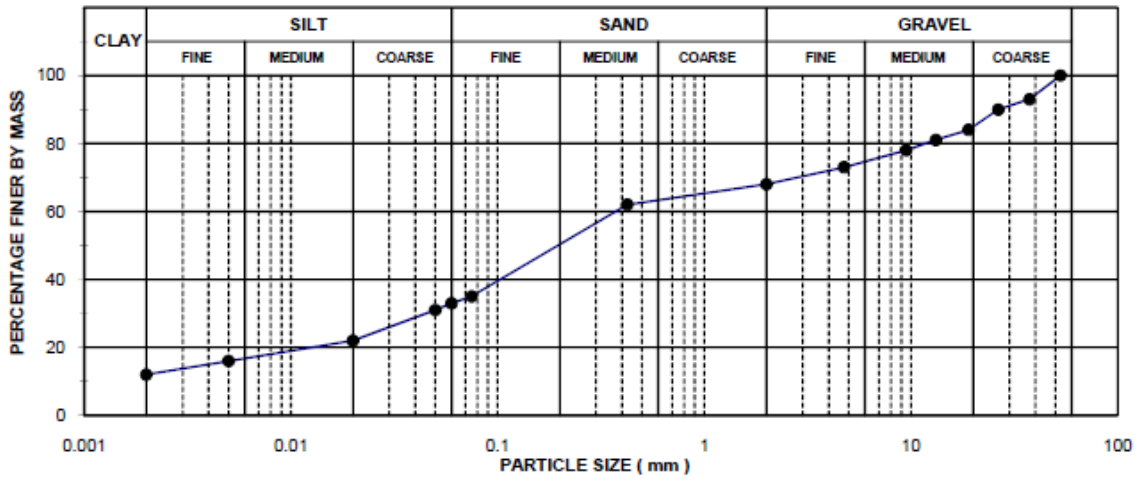

POTENTIAL EXPANSIVENESS
Van der Merwe's Activity Chart

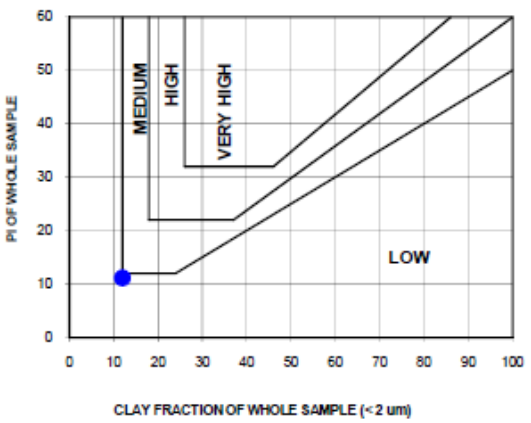

CASAGRANDE 'A' LINE

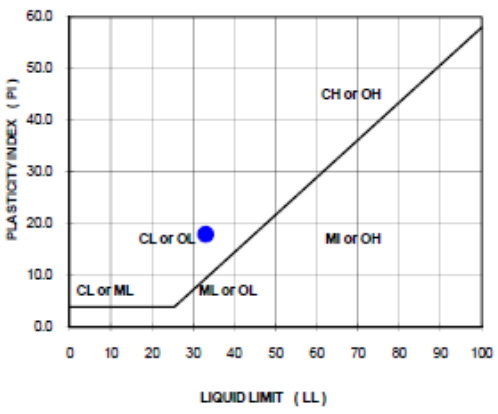

FOUNDATION INDICATOR TEST RESULTS

TEST LOCATION	Km219-400	PROJECT	NORTHAM - THABAZIMBE
SAMPLE NO.	1/1445	PROJECT NUMBER	2011-C-279
DEPTH	900 - 1100 m	CLIENT	UNIVERSITY OF PRETORIA

SIEVE ANALYSIS			
Sieve (mm)	% Passing	Sieve (mm)	% Passing
53.000	100	0.425	37
37.500	100	0.075	14
26.500	100	0.060	12
19.000	99	0.050	10
13.200	99	0.020	8
9.500	98	0.005	4
4.750	87	0.002	3
2.000	69		

ATTERBERG LIMITS		
Liquid limit	(%)	27
Plastic limit	(%)	17
Plasticity Index	(%)	10
Weighted PI	(%)	4
Linear Shrinkage	(%)	4.5
Grading Modulus		1.80
Uniformity coefficient		30
Coefficient of curvature		1.3

SOIL CLASSIFICATION	
% Gravel	31
% Sand	57
% Silt	9
% Clay	3
Activity	3.3
Unified Classification	SC
TRB Classification	A - 2 - 4

PARTICLE SIZE DISTRIBUTION

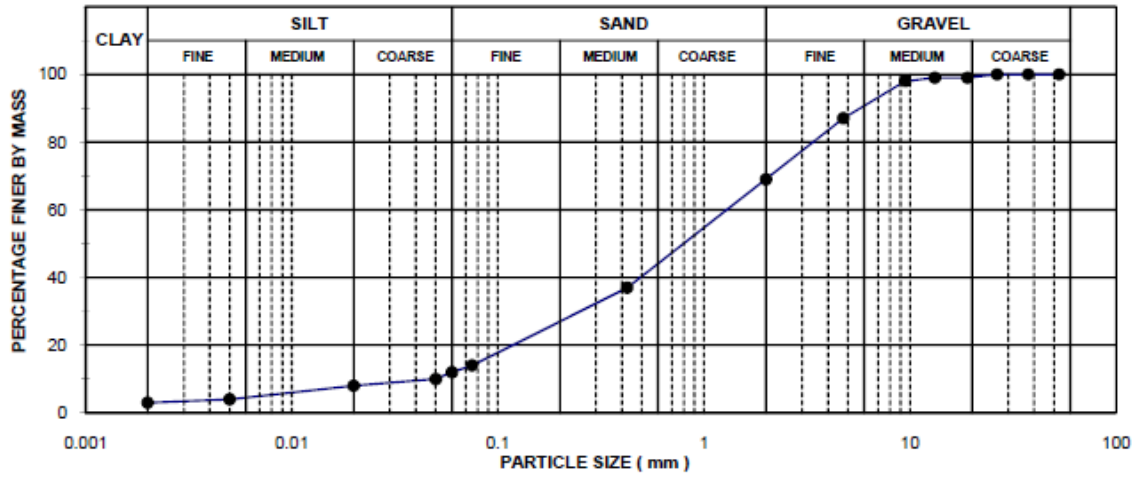

POTENTIAL EXPANSIVENESS
Van der Merwe's Activity Chart

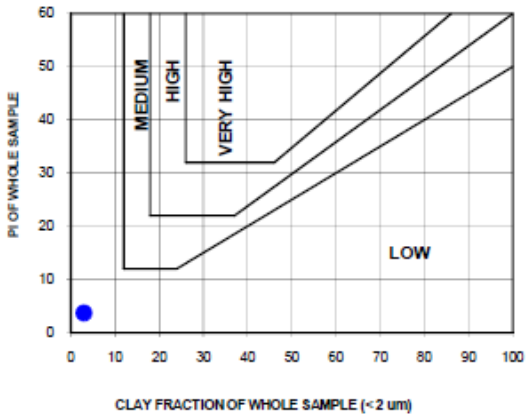

CASAGRANDE 'A' LINE

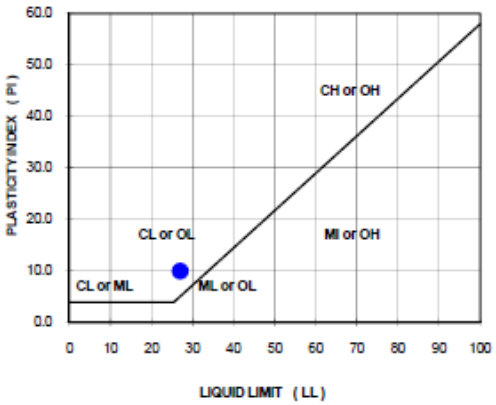

FOUNDATION INDICATOR TEST RESULTS

TEST LOCATION	Km208-500	PROJECT	NORTHAM - THABAZIMBE
SAMPLE NO.	1/1446	PROJECT NUMBER	2011-C-279
DEPTH	450 - 1000 m	CLIENT	UNIVERSITY OF PRETORIA

SIEVE ANALYSIS			
Sieve (mm)	% Passing	Sieve (mm)	% Passing
53.000	100	0.425	78
37.500	100	0.075	64
26.500	93	0.060	57
19.000	92	0.050	55
13.200	92	0.020	50
9.500	91	0.005	35
4.750	91	0.002	27
2.000	89		

ATTERBERG LIMITS		
Liquid limit	(%)	41
Plastic limit	(%)	20
Plasticity Index	(%)	21
Weighted PI	(%)	16
Linear Shrinkage	(%)	10.5
Grading Modulus		0.69
Uniformity coefficient		33
Coefficient of curvature		0.1

SOIL CLASSIFICATION	
% Gravel	11
% Sand	32
% Silt	30
% Clay	27
Activity	0.8
Unified Classification	CL
TRB Classification	A - 7 - 6

PARTICLE SIZE DISTRIBUTION

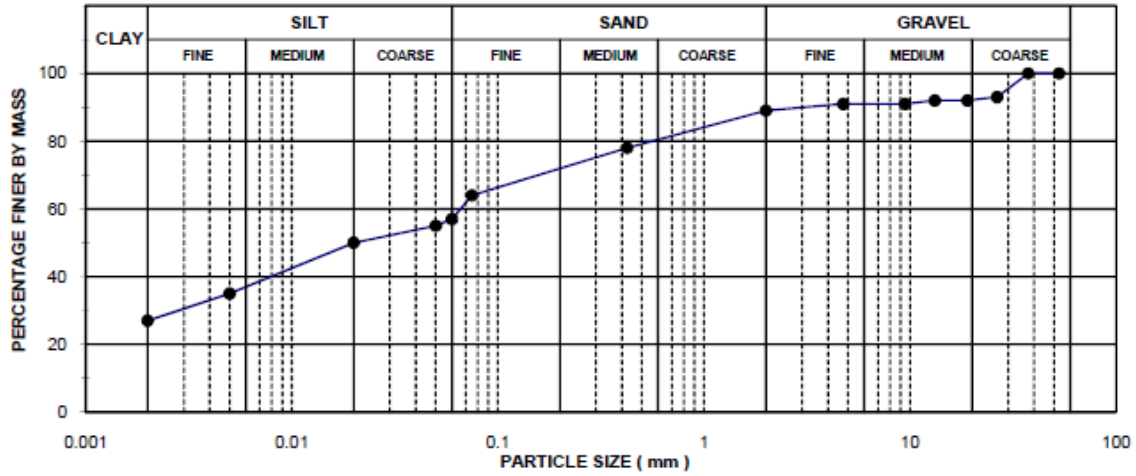

POTENTIAL EXPANSIVENESS
Van der Merwe's Activity Chart

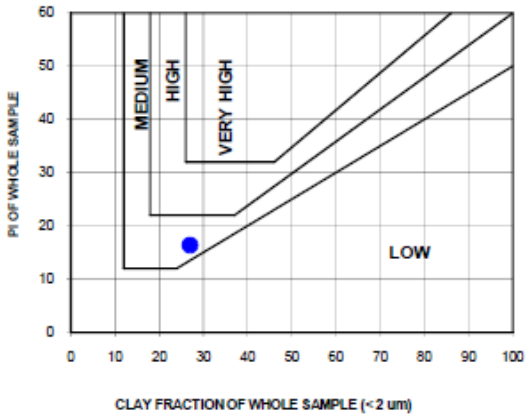

CASAGRANDE 'A' LINE

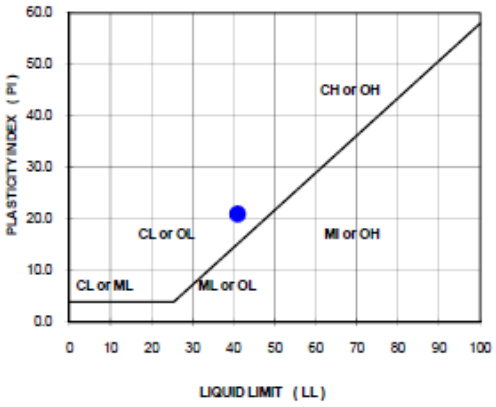

FOUNDATION INDICATOR TEST RESULTS

GEOSTRADA

TEST LOCATION	km207+800	PROJECT	NORTHAM - THABAZIMBE
SAMPLE NO.	1/1460	PROJECT NUMBER	2011-C-279
DEPTH	0 - 1000 m	CLIENT	UNIVERSITY OF PRETORIA

SIEVE ANALYSIS			
Sieve (mm)	% Passing	Sieve (mm)	% Passing
53.000	100	0.425	72
37.500	100	0.075	50
26.500	100	0.060	43
19.000	100	0.050	42
13.200	100	0.020	38
9.500	100	0.005	28
4.750	100	0.002	20
2.000	95		

ATTERBERG LIMITS		
Liquid limit	(%)	32
Plastic limit	(%)	14
Plasticity Index	(%)	18
Weighted PI	(%)	13
Linear Shrinkage	(%)	7.0
Grading Modulus		0.83
Uniformity coefficient		117
Coefficient of curvature		0.2

SOIL CLASSIFICATION	
% Gravel	5
% Sand	52
% Silt	23
% Clay	20
Activity	0.9
Unified Classification	SC
TRB Classification	A - 6

PARTICLE SIZE DISTRIBUTION

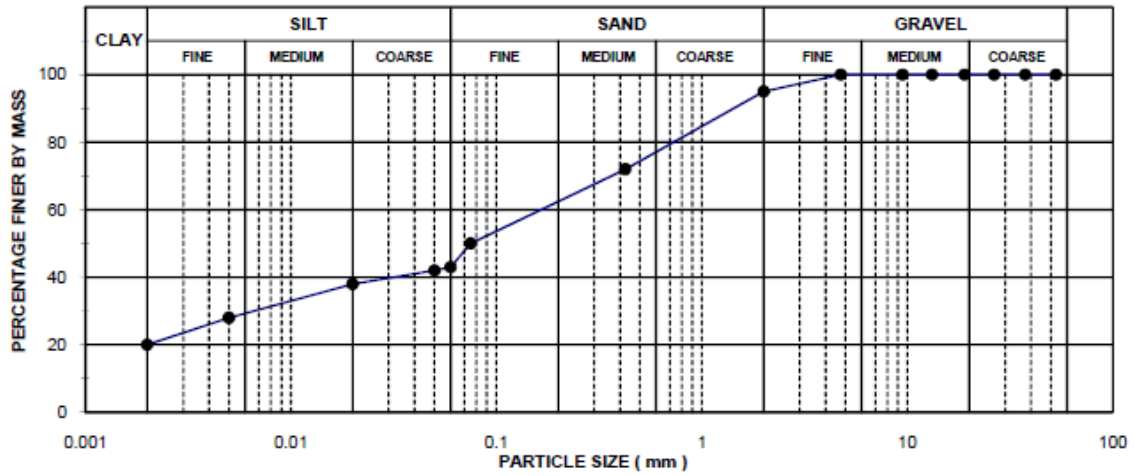

POTENTIAL EXPANSIVENESS
Van der Merwe's Activity Chart

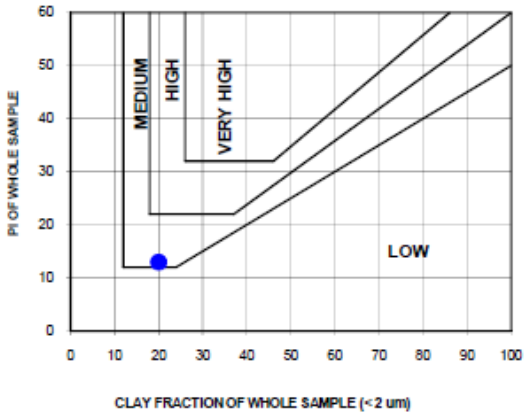

CASAGRANDE 'A' LINE

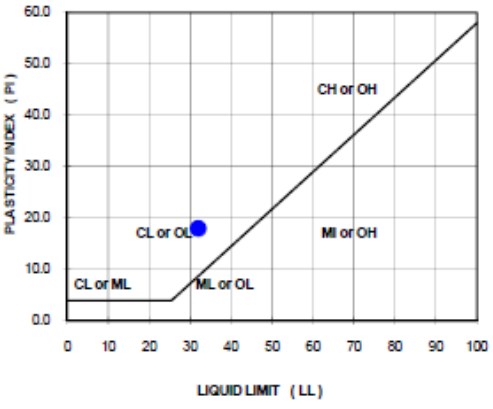

FOUNDATION INDICATOR TEST RESULTS

TEST LOCATION	km208+500	PROJECT	NORTHAM - THABAZIMBE
SAMPLE NO.	1/1461	PROJECT NUMBER	2011-C-279
DEPTH	0 - 450 m	CLIENT	UNIVERSITY OF PRETORIA

SIEVE ANALYSIS				ATTERBERG LIMITS			SOIL CLASSIFICATION	
Sieve (mm)	% Passing	Sieve (mm)	% Passing					
53.000	100	0.425	31	Liquid limit	(%)	27	% Gravel	59
37.500	86	0.075	21	Plastic limit	(%)	13	% Sand	24
26.500	86	0.060	17	Plasticity Index	(%)	14	% Silt	11
19.000	73	0.050	16	Weighted PI	(%)	4	% Clay	6
13.200	65	0.020	11	Linear Shrinkage	(%)	4.5	Activity	2.3
9.500	60	0.005	8	Grading Modulus		2.07	Unified Classification	GC
4.750	49	0.002	6	Uniformity coefficient		559	TRB Classification	A - 2 - 6
2.000	41			Coefficient of curvature		1.0		

PARTICLE SIZE DISTRIBUTION

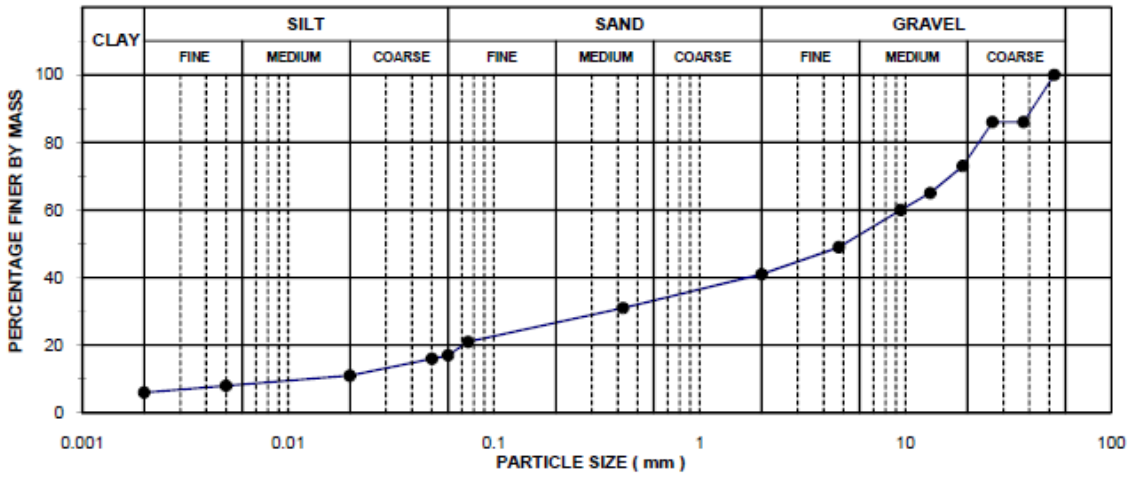

POTENTIAL EXPANSIVENESS
Van der Merwe's Activity Chart

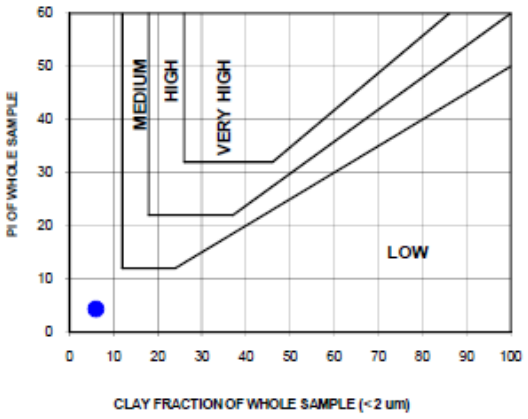

CASAGRANDE 'A' LINE

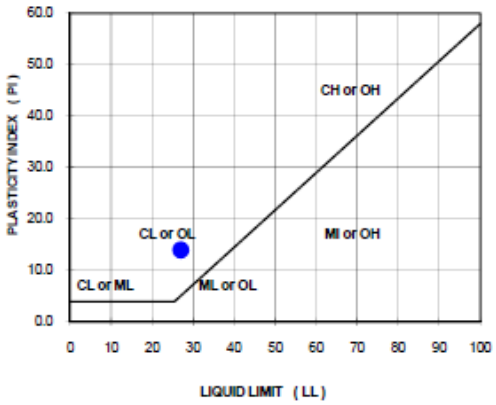

FOUNDATION INDICATOR TEST RESULTS

GEOSTRADA

TEST LOCATION	km208+500	PROJECT	NORTHAM - THABAZIMBE
SAMPLE NO.	1/1462	PROJECT NUMBER	2011-C-279
DEPTH	450 - 1000 m	CLIENT	UNIVERSITY OF PRETORIA

SIEVE ANALYSIS			
Sieve (mm)	% Passing	Sieve (mm)	% Passing
53.000	100	0.425	76
37.500	100	0.075	63
26.500	94	0.060	57
19.000	94	0.050	56
13.200	93	0.020	49
9.500	92	0.005	39
4.750	91	0.002	30
2.000	89		

ATTERBERG LIMITS		
Liquid limit	(%)	41
Plastic limit	(%)	15
Plasticity Index	(%)	26
Weighted PI	(%)	20
Linear Shrinkage	(%)	9.5
Grading Modulus		0.72
Uniformity coefficient		34
Coefficient of curvature		0.0

SOIL CLASSIFICATION	
% Gravel	11
% Sand	32
% Silt	27
% Clay	30
Activity	0.9
Unified Classification	CL
TRB Classification	A - 7 - 6

PARTICLE SIZE DISTRIBUTION

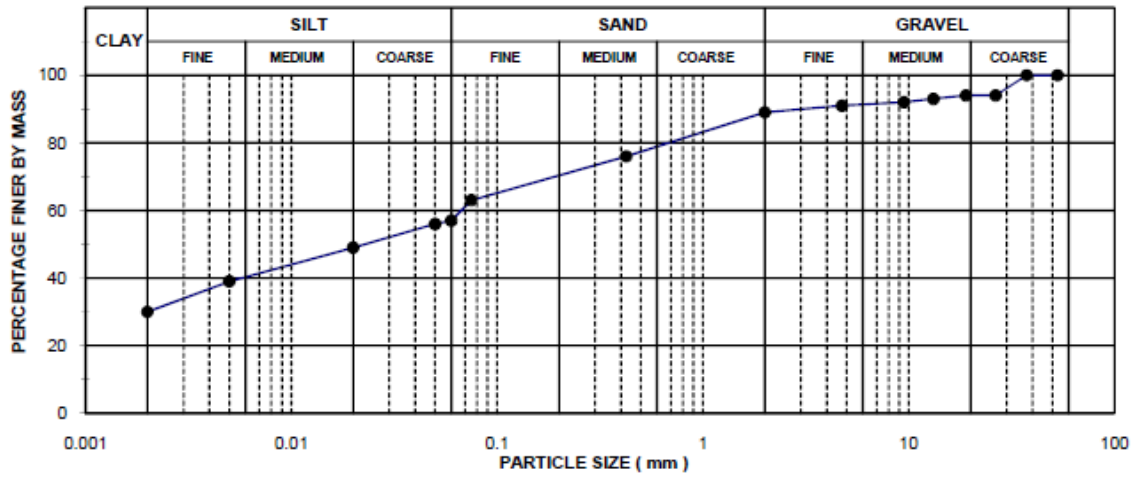

POTENTIAL EXPANSIVENESS
Van der Merwe's Activity Chart

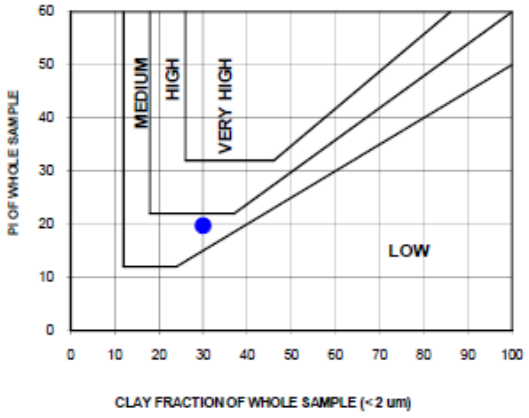

CASAGRANDE 'A' LINE

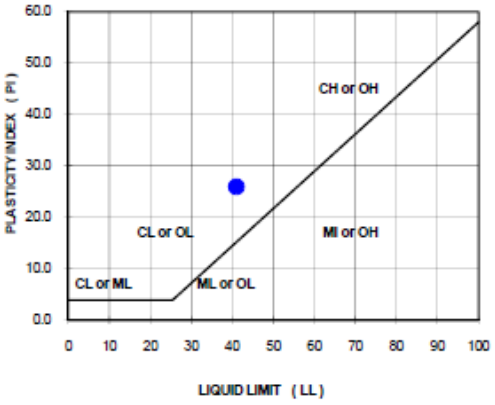

FOUNDATION INDICATOR TEST RESULTS

GEOSTRADA

TEST LOCATION	km214+500	PROJECT	NORTHAM - THABAZIMBE
SAMPLE NO.	1/1463	PROJECT NUMBER	2011-C-279
DEPTH	0 - 600 m	CLIENT	UNIVERSITY OF PRETORIA

SIEVE ANALYSIS			
Sieve (mm)	% Passing	Sieve (mm)	% Passing
53.000	100	0.425	12
37.500	83	0.075	6
26.500	66	0.060	5
19.000	50	0.050	5
13.200	40	0.020	4
9.500	34	0.005	2
4.750	27	0.002	1
2.000	20		

ATTERBERG LIMITS		
Liquid limit	(%)	25
Plastic limit	(%)	16
Plasticity Index	(%)	9
Weighted PI	(%)	1
Linear Shrinkage	(%)	3.5
Grading Modulus		2.62
Uniformity coefficient		76
Coefficient of curvature		6.3

SOIL CLASSIFICATION	
% Gravel	80
% Sand	15
% Silt	4
% Clay	1
Activity	9.0
Unified Classification	0
TRB Classification	A - 2 - 4

PARTICLE SIZE DISTRIBUTION

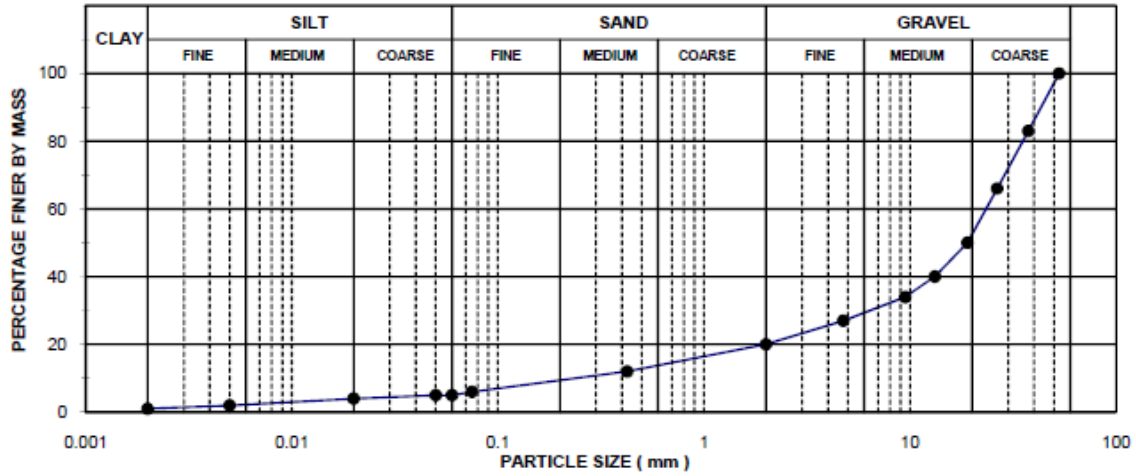

POTENTIAL EXPANSIVENESS
Van der Merwe's Activity Chart

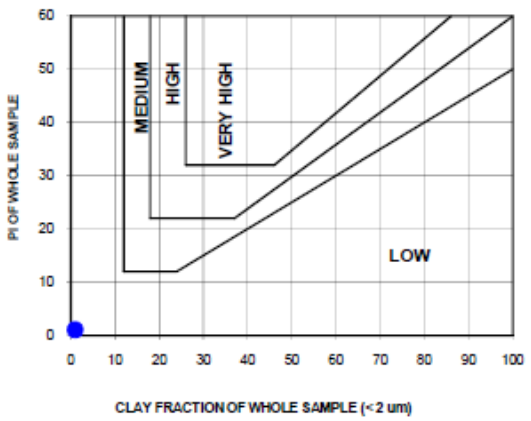

CASAGRANDE 'A' LINE

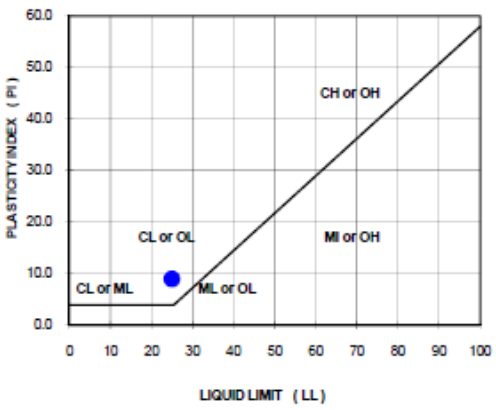

FOUNDATION INDICATOR TEST RESULTS

TEST LOCATION	km214+500	PROJECT	NORTHAM - THABAZIMBE
SAMPLE NO.	1/1464	PROJECT NUMBER	2011-C-279
DEPTH	600 - 1000 m	CLIENT	UNIVERSITY OF PRETORIA

SIEVE ANALYSIS			
Sieve (mm)	% Passing	Sieve (mm)	% Passing
53.000	100	0.425	98
37.500	100	0.075	89
26.500	100	0.060	80
19.000	100	0.050	78
13.200	100	0.020	70
9.500	100	0.005	52
4.750	100	0.002	42
2.000	100		

ATTERBERG LIMITS		
Liquid limit	(%)	82
Plastic limit	(%)	26
Plasticity Index	(%)	56
Weighted PI	(%)	55
Linear Shrinkage	(%)	16.5
Grading Modulus		0.13
Uniformity coefficient		6
Coefficient of curvature		0.2

SOIL CLASSIFICATION	
% Gravel	0
% Sand	20
% Silt	38
% Clay	42
Activity	1.3
Unified Classification	CH
TRB Classification	A - 7 - 6

PARTICLE SIZE DISTRIBUTION

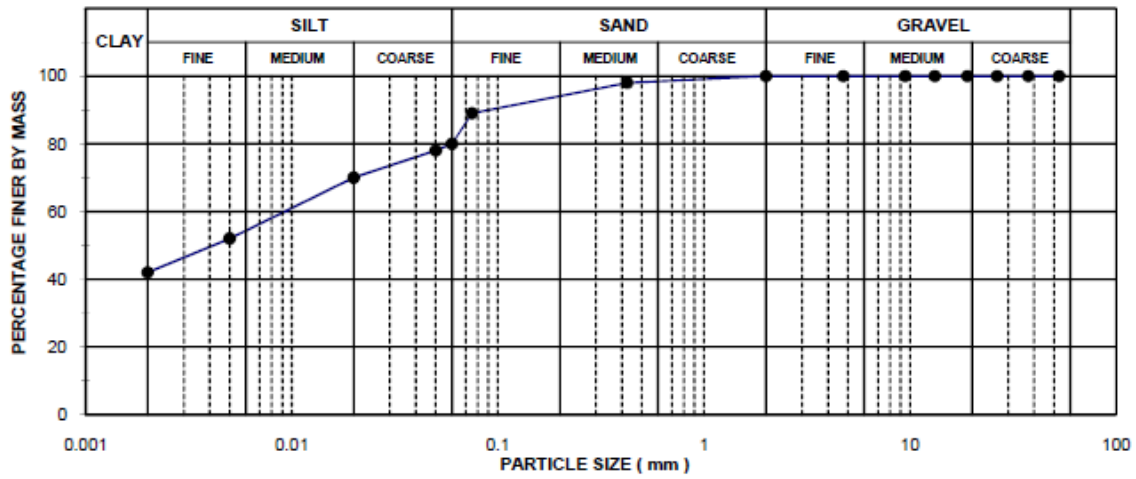

POTENTIAL EXPANSIVENESS
Van der Merwe's Activity Chart

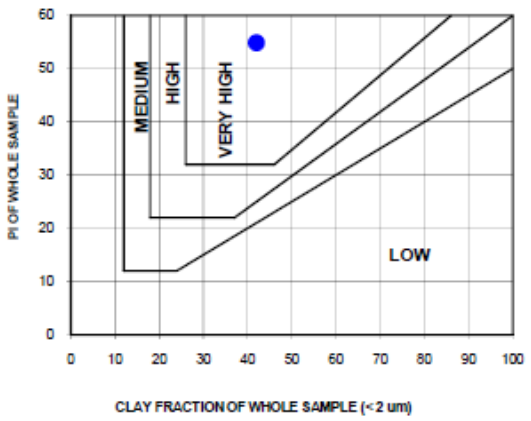

CASAGRANDE 'A' LINE

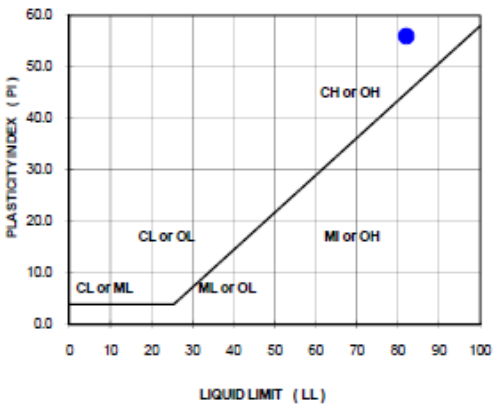

FOUNDATION INDICATOR TEST RESULTS

TEST LOCATION	km218+120	PROJECT	NORTHAM - THABAZIMBE
SAMPLE NO.	1/1465	PROJECT NUMBER	2011-C-279
DEPTH	400 - 800 m	CLIENT	UNIVERSITY OF PRETORIA

SIEVE ANALYSIS			
Sieve (mm)	% Passing	Sieve (mm)	% Passing
53.000	100	0.425	90
37.500	100	0.075	63
26.500	100	0.060	56
19.000	100	0.050	54
13.200	100	0.020	44
9.500	100	0.005	34
4.750	99	0.002	28
2.000	97		

ATTERBERG LIMITS		
Liquid limit	(%)	56
Plastic limit	(%)	21
Plasticity Index	(%)	35
Weighted PI	(%)	32
Linear Shrinkage	(%)	14.5
Grading Modulus		0.50
Uniformity coefficient		34
Coefficient of curvature		0.1

SOIL CLASSIFICATION	
% Gravel	3
% Sand	41
% Silt	28
% Clay	28
Activity	1.3
Unified Classification	CH
TRB Classification	A - 7 - 6

PARTICLE SIZE DISTRIBUTION

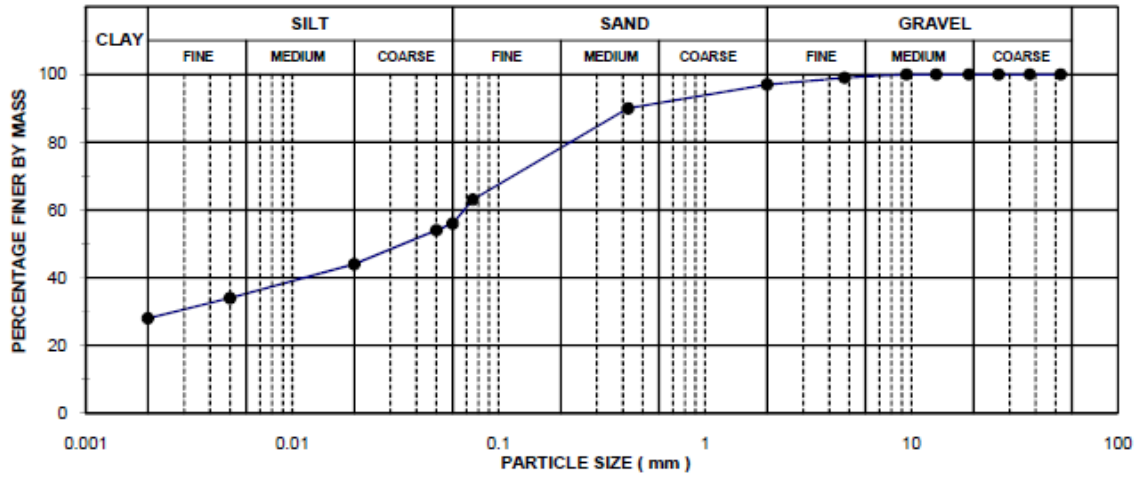

POTENTIAL EXPANSIVENESS
Van der Merwe's Activity Chart

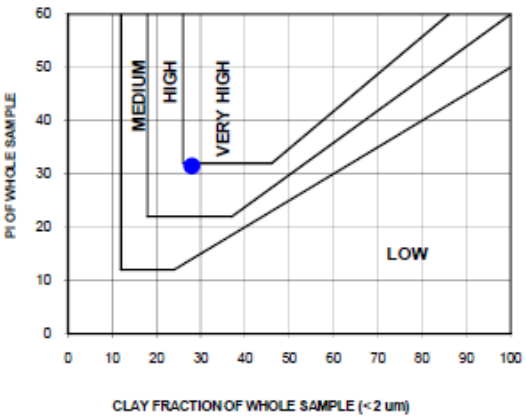

CASAGRANDE 'A' LINE

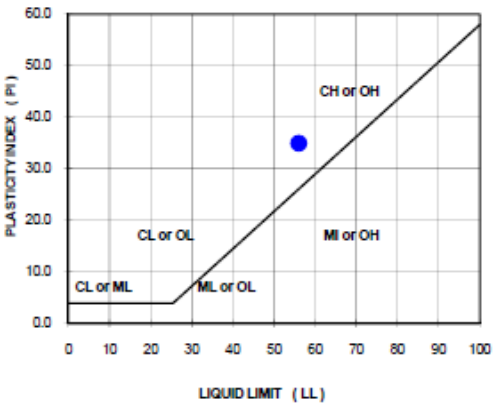

FOUNDATION INDICATOR TEST RESULTS

GEOSTRADA

TEST LOCATION	km219+400	PROJECT	NORTHAM - THABAZIMBE
SAMPLE NO.	1/1466	PROJECT NUMBER	2011-C-279
DEPTH	100 - 400 m	CLIENT	UNIVERSITY OF PRETORIA

SIEVE ANALYSIS			
Sieve (mm)	% Passing	Sieve (mm)	% Passing
53.000	100	0.425	36
37.500	95	0.075	22
26.500	90	0.060	18
19.000	79	0.050	17
13.200	73	0.020	12
9.500	67	0.005	8
4.750	57	0.002	7
2.000	47		

ATTERBERG LIMITS		
Liquid limit	(%)	29
Plastic limit	(%)	14
Plasticity Index	(%)	15
Weighted PI	(%)	5
Linear Shrinkage	(%)	7.0
Grading Modulus		1.95
Uniformity coefficient		426
Coefficient of curvature		0.9

SOIL CLASSIFICATION	
% Gravel	53
% Sand	29
% Silt	11
% Clay	7
Activity	2.1
Unified Classification	GC
TRB Classification	A - 2 - 6

PARTICLE SIZE DISTRIBUTION

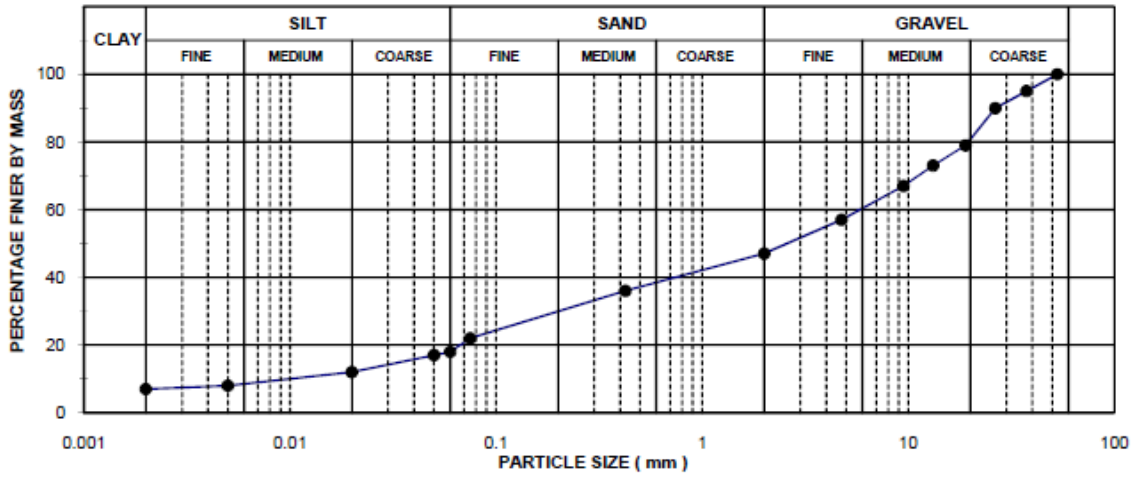

POTENTIAL EXPANSIVENESS
Van der Merwe's Activity Chart

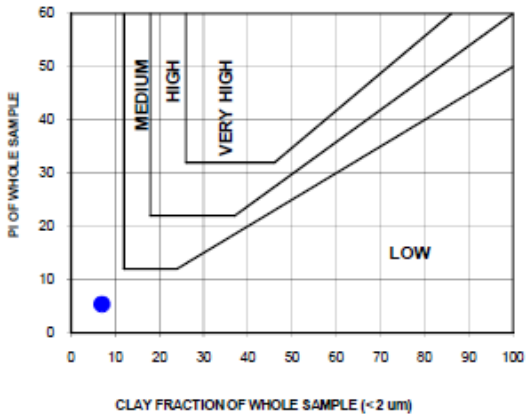

CASAGRANDE 'A' LINE

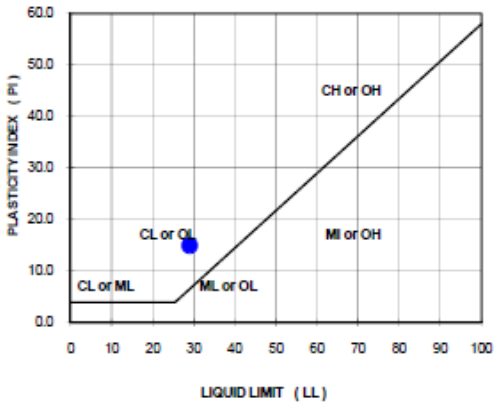

FOUNDATION INDICATOR TEST RESULTS

GEOSTRADA

TEST LOCATION	km219+400	PROJECT	NORTHAM - THABAZIMBE
SAMPLE NO.	1/1467	PROJECT NUMBER	2011-C-279
DEPTH	400 - 600 m	CLIENT	UNIVERSITY OF PRETORIA

SIEVE ANALYSIS			
Sieve (mm)	% Passing	Sieve (mm)	% Passing
53.000	100	0.425	70
37.500	100	0.075	55
26.500	90	0.060	50
19.000	86	0.050	49
13.200	84	0.020	40
9.500	82	0.005	30
4.750	81	0.002	23
2.000	78		

ATTERBERG LIMITS		
Liquid limit	(%)	66
Plastic limit	(%)	24
Plasticity Index	(%)	42
Weighted PI	(%)	29
Linear Shrinkage	(%)	17.0
Grading Modulus		0.97
Uniformity coefficient		96
Coefficient of curvature		0.1

SOIL CLASSIFICATION	
% Gravel	22
% Sand	28
% Silt	27
% Clay	23
Activity	1.8
Unified Classification	CH
TRB Classification	A - 7 - 6

PARTICLE SIZE DISTRIBUTION

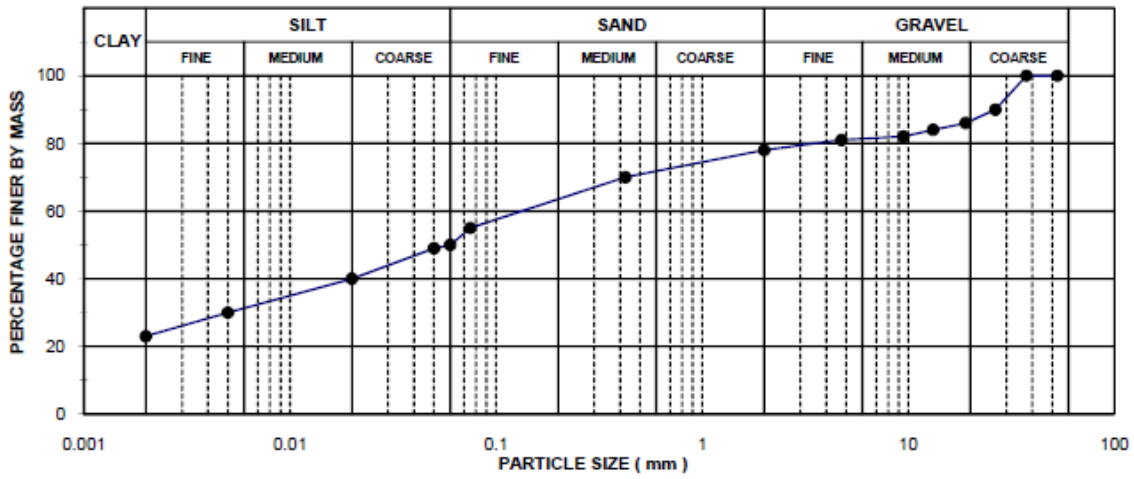

POTENTIAL EXPANSIVENESS
Van der Merwe's Activity Chart

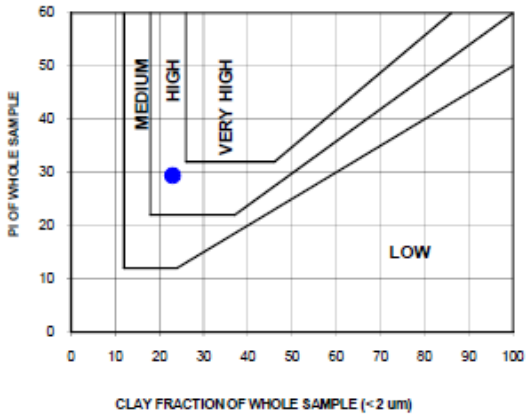

CASAGRANDE 'A' LINE

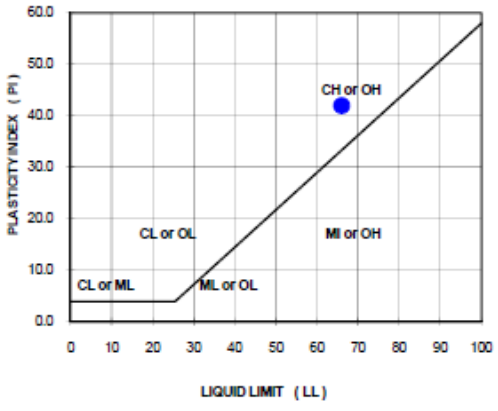

SUMMARY OF CBR RESULTS

SUMMARY OF CBR RESULTS

LAB/G15

Tests done according to TMH1 Methods

☑ A7 ☑ A8 ☐ A9

Client : UNIVERSITY OF PRETORIA **Contract:** KOMVOORHOOGTE - NHLAZATSHE **Date:** 2011-07-14

Job No: 2011-C-279

Sample No / Hole No / Depth (mm)		California bearing ratio at 2.54 mm	5.08 mm	7.62 mm	100% / 97% / 93%	98% / 95% / 90%	Swell after soaking %	Modified AASHTO data: Max dry density kg/m³	Optimum moisture content %	Laboratory compaction data: Dry density kg/m³	Percentage of modified AASHTO density	Average moulding moisture content %
1/1448	a	100	121	133	107	85	0.0			2302	99.4	
53.8	b	71	80	84	76	69	0.0	2322	7.6	2241	96.5	7.5
0 - 220	c	63	74	73	66	62	0.0			2106	90.7	
1/1449	a	113	119	118	130	87	0.0			2256	99.3	
53.8	b	47	50	52	71	47	0.0	2272	9.3	2159	95.0	9.4
220 - 800	c	40	45	48	44	39	0.0			2060	90.7	
1/1452	a	225	297	341	235	187	0.0			2500	99.6	
59.3	b	159	207	238	166	101	0.0	2510	5.9	2426	96.6	5.9
0 - 400	c	110	157	179	57	24	0.0			2392	95.3	
1/1455	a	125	154	168	93	65	0.0			2181	101.7	
60.65	b	45	50	49	55	39	0.0	2144	6.5	2056	95.9	6.5
580 - 950	c	28	28	28	29	18	0.0			1992	92.9	

a - Modified AASHTO b - NRB c - Proctor

GEOSTRADA

SUMMARY OF CBR RESULTS

LAB/G15

Tests done according to TMH1 Methods

☑ A7 ☑ A8 ☐ A9

Client : UNIVERSITY OF PRETORIA **Contract:** KOMVOORHOOGTE - NHLAZATSHE **Date:** 2011-07-14

Job No: 2011-C-279

Sample No / Hole No / Depth (mm)		California bearing ratio at 2.54 mm	5.08 mm	7.62 mm	100% / 97% / 93%	98% / 95% / 90%	Swell after soaking %	Modified AASHTO data: Max dry density kg/m³	Optimum moisture content %	Laboratory compaction data: Dry density kg/m³	Percentage of modified AASHTO density	Average moulding moisture content %
1/1457	a	121	143	143	126	81	0.0			2155	99.8	
64	b	42	49	51	65	42	0.0	2158	5.8	2049	95.0	5.7
460 - 1000	c	30	34	37	30	19	0.0			2020	93.6	
1/1458	a	178	236	282	168	134	0.0			2500	100.5	
65.25	b	102	129	142	119	91	0.0	2488	5.4	2379	95.6	5.4
0 - 400	c	69	79	90	62	35	0.0			2328	93.6	
1/1459	a	69	91	124	86	55	0.0			2153	99.0	
65.25	b	42	64	72	44	32	0.0	2175	7.0	2105	96.8	6.9
400 - 800	c	31	41	45	23	14	0.0			2065	94.9	
	a											
	b											
	c											

a - Modified AASHTO b - NRB c - Proctor

GEOSTRADA

SUMMARY OF CBR RESULTS

LAB/G15

Tests done according to TMH1 Methods

☑ A7 ☑ A8 ☐ A9

Client : UNIVERSITY OF PRETORIA **Contract:** NORTHAM - THABAZIMBE **Date:** 2011-07-14

Job No: 2011-C-279

Sample No / Hole No / Depth (mm)		California bearing ratio at 2.54 mm	5.08 mm	7.62 mm	100% / 97% / 93%	98% / 95% / 90%	Swell after soaking %	Modified AASHTO data: Max dry density kg/m³	Optimum moisture content %	Laboratory compaction data: Dry density kg/m³	Percentage of modified AASHTO density	Average moulding moisture content %
1/1446	a	4	3	3	4.2	3.5	0.6			1734	98.2	
Km208-500	b	2	2	2	3.1	2.6	0.8	1765	15.9	1651	93.5	16.0
450 - 1000	c	2	2	2	2.2	2.2	0.9			1540	87.2	
1/1440	a	112	128	137	120	95	0.0			2402	99.4	
Km214-500	b	74	81	83	84	65	0.0	2416	4.9	2320	96.0	4.9
000 - 600	c	37	36	36	49	32	0.0			2197	90.9	
1/1441	a	No reading	No reading	No reading	No readings					1601	98.0	
Km214-500	b	No reading	No reading	No reading				1633	21.8	1512	92.6	21.6
600 - 1000	c	No reading	No reading	No reading						1454	89.0	
1/1443	a	No reading	No reading	No reading	No readings					1674	101.3	
Km218/2	b	No reading	No reading	No reading				1652	18.2	1589	96.2	18.3
400 - 800	c	No reading	No reading	No reading						1511	91.4	

a - Modified AASHTO b - NRB c - Proctor

GEOSTRADA

SUMMARY OF CBR RESULTS

LAB/G15

Tests done according to TMH1 Methods

☑ A7 ☑ A8 ☐ A9

Client : UNIVERSITY OF PRETORIA **Contract:** NORTHAM - THABAZIMBE **Date:** 2011-07-14

Job No: 2011-C-279

Sample No / Hole No / Depth (mm)		California bearing ratio at 2.54 mm	5.08 mm	7.62 mm	100% / 97% / 93%	98% / 95% / 90%	Swell after soaking %	Modified AASHTO data: Max dry density kg/m³	Optimum moisture content %	Laboratory compaction data: Dry density kg/m³	Percentage of modified AASHTO density	Average moulding moisture content %
1/1439	a	No reading	No reading	No reading	No readings					1538	99.2	
Km219-400	b	No reading	No reading	No reading				1550	21.0	1466	94.6	20.1
400 - 600	c	No reading	No reading	No reading						1388	89.5	
1/1444	a	66	75	75	70	48	0.0			2196	99.7	
Km219-400	b	29	31	30	40	29	0.0	2202	7.1	2102	95.4	7.3
100 - 400	c	23	20	18	25	21	0.0			2005	91.0	
1/1445	a	29	31	27	28	26	0.0			2195	101.9	
Km219-400	b	25	23	21	25	24	0.0	2154	6.0	2083	96.7	6.0
900 - 1100	c	23	22	21	23	21	0.0			1984	92.1	
	a											
	b											
	c											

a - Modified AASHTO b - NRB c - Proctor